DISS. ETH NO. 20053

Source apportionment of ambient submicron aerosol using stationary and mobile aerosol mass spectrometer data

A dissertation submitted to

ETH ZURICH

for the degree of

Doctor of Sciences

presented by

CLAUDIA MOHR
Dipl. Umwelt-Natw. ETH
born on 21 April 1982
citizen of Basel BS and Dürrenroth BE

accepted on the recommendation of

Prof. Dr. U. Baltensperger, examiner
Prof. Dr. U. Lohmann, co-examiner
Dr. A. S. H. Prévôt, co-examiner
Dr. A. Kiendler-Scharr, co-examiner

2011

CONTENTS

ABSTRACT

Atmospheric aerosols are liquid, solid, or mixed-phase particles suspended in air. Their impact on climate, human health, visibility, and ecosystems has made them the focus of many research activities. Numerous natural or anthropogenic sources directly emit particles into the air (primary aerosol), or release gas-phase precursors whose oxidation products can partition into the particle phase (secondary aerosol). Consequently, the chemical composition of ambient particulate matter (PM) varies considerably with location and time. Our knowledge about sources, fate, and mutual interaction of gas-phase and aerosol compounds is still limited; however it is the basis for all mitigation strategies. This thesis contributes to this knowledge by investigating sources of ambient aerosol using aerosol mass spectrometry, with a particular focus on the organic fraction.

Mobile measurements of the chemical composition of submicron PM (PM_1) were performed using the PSI mobile laboratory during winter 2007/2008 and December 2008 in the metropolitan area of Zurich, Switzerland. Source components of the organic aerosol (OA) fraction measured by an aerosol mass spectrometer (AMS) were investigated using positive matrix factorization (PMF), a factor analytical model which outputs a number of constant source profiles (factors) and their varying contributions over time. Three factors were identified: hydrocarbon-like OA (HOA) related to traffic emissions; wood burning OA from domestic heating sources (WBOA); and oxygenated OA (OOA), assigned to secondary OA. The simultaneous assessment of the chemical composition of PM_1 for an urban background site and various sites throughout the city allowed the separation and quantification of the locally emitted or formed fraction of PM_1, and the fraction of PM_1 originating from the urban background. Small-scale meteorological effects were corrected using a newly developed method based on the ratio of local sulfate to background sulfate. Especially during thermal inversions over the Swiss plateau, urban background concentrations contribute substantially to the on-road mass concentrations of PM_1 components in downtown Zurich (between 30 and 100%).

Ambient measurements of the PM_1 chemical composition were also conducted in March 2009 in Barcelona, Spain. Two AMS instruments were deployed simultaneously, with one at an urban background site and one in the PSI mobile laboratory. For both instruments, PMF resolved five OA factors: LV-OOA (low-volatility OOA), related to regional, highly photochemically aged OOA; SV-OOA (semi-volatile OOA), a less aged OOA; HOA, BBOA from domestic heating or

agricultural biomass burning activities, and COA (cooking OA). At the urban background site, COA contributes 17% to OA. The importance of cooking activities for ambient urban air quality is only now beginning to be assessed as high-resolution AMS spectra become available. Methods to detect and estimate COA in ambient datasets based on the fractions of organic mass fragments at *m/z* 55, 57, and 44 were developed. The mobile AMS measurements were conducted in the Barcelona region to asses the spatial variation of emissions and PM_1 components and their evolution in the city plume. High concentrations of HOA and other traffic-related species were found in the city center. In the harbor area upwind of the city center, substantial contributions from secondary aerosol components advected by the sea breeze were measured. Downwind of the city center, photochemical aging of the air masses and additional primary aerosol sources (industrial areas, the airport, and agricultural open fires) lead to an increase in aerosol mass and oxidation state with increasing distance from the city center.

The results emphasize the advantage of mobile measurements for distinguishing local from regional aerosol sources and confirm the importance of chemical composition measurements with a high mass and time resolution for insights into atmospheric aerosol sources and processes.

ZUSAMMENFASSUNG

Atmosphärische Aerosole sind eine Suspension flüssiger, fester oder gemischtphasiger Partikel in Luft. Ihre Auswirkungen auf das Klima, die menschliche Gesundheit, Sichtverhältnisse und Ökosysteme machen sie zum Fokus vieler Forschungsaktivitäten. Zahlreiche natürliche oder anthropogene Quellen emittieren Partikel direkt in die Luft oder stossen gasförmige Vorläufersubstanzen aus, deren Oxidationsprodukte in die Partikelphase übergehen können. Die chemische Zusammensetzung von Feinstaub variiert deshalb beträchtlich. Sinnvolle Strategien zur Begrenzung von Feinstaub in der Luft bedingen genaue Kenntnisse über Quellen, Abbauverhalten und gegenseitige Wechselwirkungen gas- und partikelförmiger Komponenten. Diese Kenntnisse aber sind bisher nur begrenzt vorhanden; gerade im Bezug auf organisches Material, einen der Hauptbestandteile im atmosphärischen Aerosol. Die vorliegende Dissertation hilft, diese Lücke zu schliessen, indem sie mittels Aerosol-Massenspektrometrie Quellen atmosphärischen Feinstaubs – insbesondere organischen Materials - untersucht.

Im Winter 2007/2008 und im Dezember 2009 wurden in Zürich mit dem PSI-Messfahrzeug mobile Messungen der chemischen Zusammensetzung von PM_1 (Feinstaub mit einem Durchmesser < 1 µm) durchgeführt. Die mit einem Aerosol-Massenspektrometer (AMS) gemessenen organischen Bestandteile wurden mit positiver Matrizenzerlegung (PMF) analysiert. PMF ist ein Faktoranalyse-Modell, das eine bestimmte Anzahl konstanter Quellenprofile (Faktoren) und deren variierende Beiträge pro Zeit ermittelt. Drei Faktoren organischen Aerosols (OA) wurden so identifiziert: Kohlenwasserstoff-ähnliches OA (HOA) aus Verkehrsemissionen; OA aus Holzheizungen (WBOA); und oxidiertes (sekundäres) OA (OOA), gebildet aus der Oxidation gasförmiger Vorläuferstoffe. Die chemische Zusammensetzung von PM_1 wurde gleichzeitig für einen städtischen Hintergrundstandort und verschiedenen Standorte in der Stadt bestimmt. Dies erlaubte die Unterscheidung und Quantifizierung zwischen lokal (in der Stadt) und regional emittiertem oder gebildetem Feinstaub. Kleinskalige meteorologische Effekte wurden mittels einer neu entwickelten Methode eliminiert, welche auf dem Sulfat-Verhältnis zwischen Hintergrundstandort und lokalem Standort beruht. Vor allem während winterlichen Inversionslagen

über dem Schweizerischen Mittelland tragen regionale Hintergrundkonzentrationen substantiell zu den PM_1-Konzentrationen in der Stadt bei (zwischen 30 und 100%).

Die chemische Zusammensetzung von PM_1 wurde auch in Barcelona, Spanien, im März 2009 gemessen. Zwei AMS wurden dabei simultan eingesetzt, eines an einem städtischen Hintergrundstandort, das andere im PSI-Messfahrzeug. Fünf OA-Faktoren konnten mittels PMF ermittelt werden: Regionales, photochemisch gealtertes OOA (schwerflüchtig, LV-OOA) und halbflüchtiges, weniger gealtertes OOA (SV-OOA), HOA, OA aus Holzheizungen oder landwirtschaftlichen Feuern (BBOA) und OA aus Kochemissionen (COA). Am städtischen Hintergrundstandort macht COA 17% von OA aus; seine Bedeutung für die städtische Luftqualität wird erst in jüngster Zeit und dank der Verfügbarkeit hoch aufgelöster Massenspektren nach und nach deutlich. Methoden zur Entdeckung und Abschätzung von COA, basierend auf den Anteilen der organischen Massenfragmente bei *m/z* 55, 57, und 44, wurden entwickelt. Zur Abschätzung der räumlichen Variation der Emissionen und PM_1-Komponenten und ihrer Entwicklung in der Abluftfahne der Stadt wurden mobile Messungen in der Stadt Barcelona sowie in ihrem Umland durchgeführt. Im Stadtzentrum wurden hohe Konzentrationen von HOA und anderer verkehrsbedingter Spezies gemessen. In der Hafengegend wurden substantielle Konzentrationen sekundärer Aerosolkomponenten gemessen, welche durch den Meerwind transportiert wurden. In der Abluftfahne der Stadt führen die photochemische Alterung der Luftmassen und zusätzliche primäre Feinstaubquellen (Industriezonen, Flughafen, und landwirtschaftliche Feuer) zu einer Zunahme der Masse und des Grads der Oxidierung des Feinstaubs mit zunehmendem Abstand vom Stadtzentrum.

Diese Resultate unterstreichen die Vorteile mobiler Messungen für die Unterscheidung lokaler und regionaler Feinstaubquellen und bestätigen die Bedeutung von Messungen mit hoher Zeit- und Massenauflösung für neue Erkenntnisse über atmosphärische Feinstaubquellen und -prozesse.

PREFACE

"In a decade, urban dwellers will have to wear gas masks to survive air pollution […] By 1985, air pollution will have reduced the amount of sunlight reaching Earth by one half."

(Life, 1970)

Air pollution has been a consequence of human activities since the beginning of the domestic use of fire (Bowman et al., 2009). Ancient civilizations in Greece and Rome were troubled by emissions from burning coal or smelting of ores (Hong et al., 1994). In medieval London, the pollution from coal burnt in limestone kilns, for other industries and heating was regarded as such a serious issue that a commission was set up to investigate the problem (Brimblecome, 1987). The development of the steam engine marked the beginning of the industrial revolution and led to a vast increase in coal combustion. Industries based on coal combustion developed on all continents. Consequently, the (urban) air quality deteriorated rapidly. Extreme pollution episodes like the London fog event in 1952 (Wilkins, 1954) or persistent smog layers in sunny regions such as California (Middleton et al., 1950) followed. Nowadays, the world's growing population brings about a similarly growing demand for energy. This energy is mostly provided by the combustion of fossil fuel, which involves emissions of harmful pollutants into the urban air (Gurjar et al., 2010).

Common to all these effects is the fact that aerosols play a major role. Therefore, a detailed knowledge on aerosols is essential for improving air quality.

1

INTRODUCTION

1.1 Atmospheric aerosols

1.1.1 Definition and properties

Atmospheric aerosols are suspensions of liquid, solid or mixed-phase particles in air. Phenomena such as e. g. dust, fume, smog, or smoke all describe forms of aerosols. The particles can be directly emitted into the air (primary aerosols) as e. g. pollen, dust, and sea salt, or by anthropogenic sources such as fossil fuel and wood combustion. In addition, gas phase precursors, again from a wide variety of anthropogenic and natural sources, can undergo photochemical reactions that produce more highly oxidized species that are less volatile. Nucleation or condensation of these species leads to the formation of secondary aerosols. Aerosols are removed from the atmosphere by wet or dry deposition (see Fig. 1). Their impacts on ecosystems (Grantz et al., 2003), visibility (Watson, 2002), climate (section 1.1.2), and human health (section 1.1.3) have made atmospheric aerosols the focus of numerous research activities.

Aerosol sources are abundant and vary greatly with time and space, and so do the particles' physicochemical properties. They span a size range from a few nm to more than 100 μm (Fig. 1). Ambient size distributions based on number concentrations (cm^{-3}) are usually dominated by two modes: A nucleation mode comprising particles with a diameter up to 10 nm, and an Aitken mode around 30 – 50 nm. Since those very small particles do not substantially contribute to particle mass, the typical ambient mass size distribution exhibits a different form: As well bimodal, it is made up by an accumulation mode (comprising particles with a diameter of a few hundred nm), and a coarse mode with particles up to 10 μm (Seinfeld and Pandis, 2006). Particles with a diameter up to 2.5 μm are referred to as fine particles; larger particles are classified as coarse particles.

Common classifications of particulate matter (PM) are based on the aerodynamic diameter: PM_{10} refers to particles with an aerodynamic diameter d_a of 10 μm or less; $PM_{2.5}$ to particles with a d_a of 2.5 μm or less; and PM_1 to particles with a d_a of 1 μm or less.

Atmospheric particles also vary in shape, density and chemical composition, all of which determines their life time in the atmosphere (spanning from minutes to weeks, Seinfeld and Pandis, 2006). Their atmospheric concentrations are usually given in the mass space and can range from 10^{-7} to 10^{9} µg m^{-3} (Hinds, 1999).
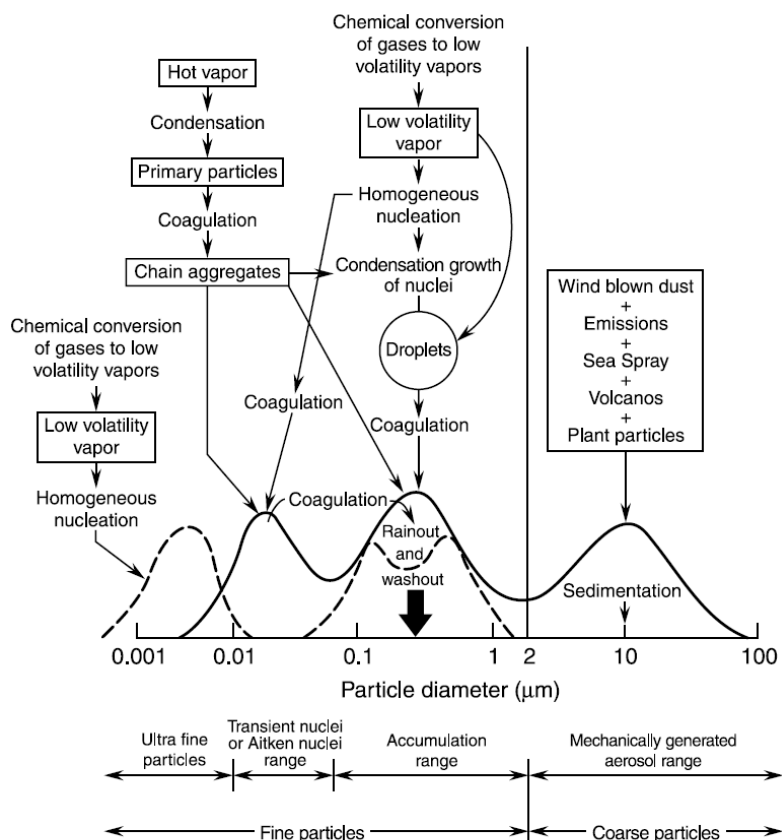

Figure 1: Schematic of typical atmospheric aerosol size distributions and sources adding to the different modes. The solid and the dashed lines represent the original and revised version of the size distribution model, respectively (Finlayson-Pitts and Pitts, 2000).

1.1.2 Climate effects

Aerosols have an influence on the climate system by influencing the Earth's global mean energy balance: They are radiative forcing components. The net radiative forcing of aerosols is negative; they have a cooling effect on the atmosphere (IPCC, 2007). The physical mechanisms by which aerosols affect the climate system are divided into direct effects and indirect effects.

The direct effects include the scattering and absorption of solar radiation and the scattering, absorption and emission of thermal radiation by aerosol particles (Lohmann and Feichter, 2005). They are dependent on the temporal and spatial distribution of the aerosol in the troposphere and its optical properties, which in turn are highly influenced by size and chemical composition. Externally mixed sulfate, nitrate, mineral dust, and organic carbon (OC) aerosols mainly scatter

light and therefore have a negative radiative forcing; the radiative forcing due to black carbon (BC) is positive because BC strongly absorbs light, which is then transformed into heat. Internally mixed particles are less well understood; however, it is unlikely that the radiative forcing from different components will add up linearly (Haywood and Boucher, 2000).

Aerosol particles act as cloud condensation and ice nuclei (CCN and IN, respectively); their number concentration influences the cloud droplet size and thus the cloud albedo and lifetime. These mechanisms are referred to as indirect effects or cloud effects (Lohmann and Feichter, 2005). Figure 2 presents a schematic overview of the radiative mechanisms associated with the direct and indirect effects (IPCC, 2007). The cloud effects will briefly be explained in the following (Lohmann and Feichter, 2005):

- 1st indirect effect or cloud albedo/Twomey effect: For clouds with constant liquid water content (LWC), an increase in the number of cloud condensation nuclei will lead to a higher cloud droplet number concentration (CDNC) with smaller cloud droplets, and thus enhanced reflection of solar radiation.

- 2nd indirect effect or cloud lifetime/Albrecht effect: More and smaller cloud droplets reduce the precipitation efficiency of the cloud and therefore prolong its lifetime.

- Semi-direct effect: Absorption of solar radiation by black carbon leads to a heating of the air and thus evaporation of cloud droplets.

- For mixed-phase clouds, an increasing aerosol concentration may lead to a decrease in cloud water content.

Global mean aerosol radiative forcings (best estimates and 5 to 95% uncertainty ranges) in 2005 with respect to 1750 were estimated to be -0.5 (-0.9 to -0.1) W m^{-2} for the direct effects and -0.7 (-1.8 to -0.3) W m^{-2} for the indirect effects (IPCC, 2007).
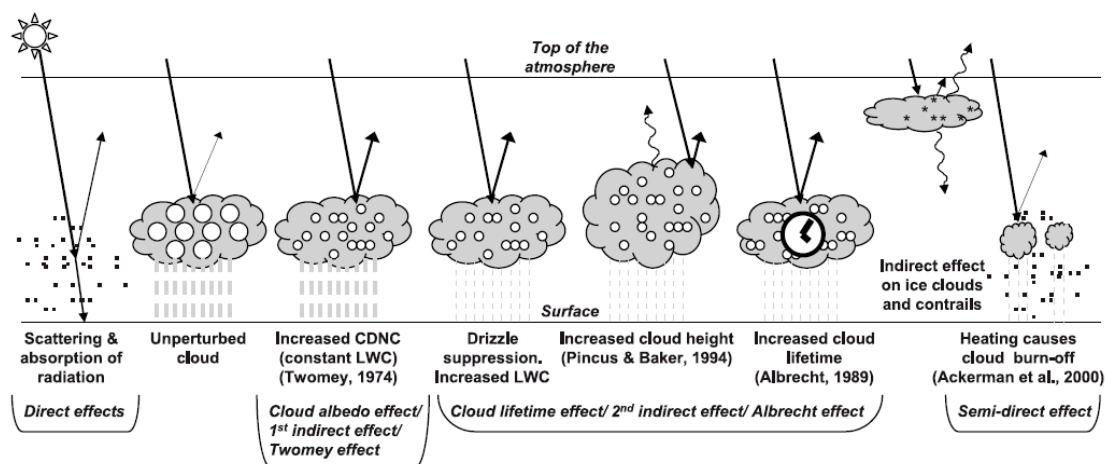
Figure 2: Schematic of the various radiative mechanisms associated with aerosols and clouds. Dots represent aerosol particles; open circles cloud droplets; straight lines the incident and reflected solar radiation, and wavy lines the terrestrial radiation (IPCC, 2007).

1.1.3 Health effects and legal regulations

The negative effects of atmospheric aerosols on human health have been assessed in numerous epidemiological studies worldwide: The London winter smog episode in December 1952 was shown to have increased the number of deaths per day by a factor of ~3 (Wilkins, 1954). Long-term exposure to PM_{10} and $PM_{2.5}$ was associated with increased risks of all-cause, cardiopulmonary and respiratory morbidity and mortality (Dockery et al., 1993; Samet et al., 2000; Pope et al., 2002; Brook et al., 2004; Laden et al., 2006). Physiological effects of PM include inflammation in the smaller airways and interferences with the mucociliary clearance and inactivation mechanisms of bacteria in lung tissue (Nel, 2005).

In addition to concentrations levels, particle size (see section 1.1.1), surface area, morphology, and chemical composition determine the health risk of PM. Figure 3 shows the deposition probability of inhaled particle mass and the particles' penetration depth into the human respiratory tract as a function of particle size. The behavior of larger particles (with a diameter above 1 μm, UGZ, 2004) is dominated by sedimentation and inertial impaction at the surface of the upper airways, in the nasopharyngeal and the tracheobronchial region. For ultrafine particles (with a diameter below 100 nm, UGZ, 2004), Brownian diffusion governs the deposition, and they can penetrate deep into the alveolar region of the lung. The deposition probability reaches a minimum between 100 nm and 1 μm at the intersection between the two mechanisms. Particles smaller than a few tens of nm are removed by diffusion in the upper airways (Maynard and Kuempel, 2005).
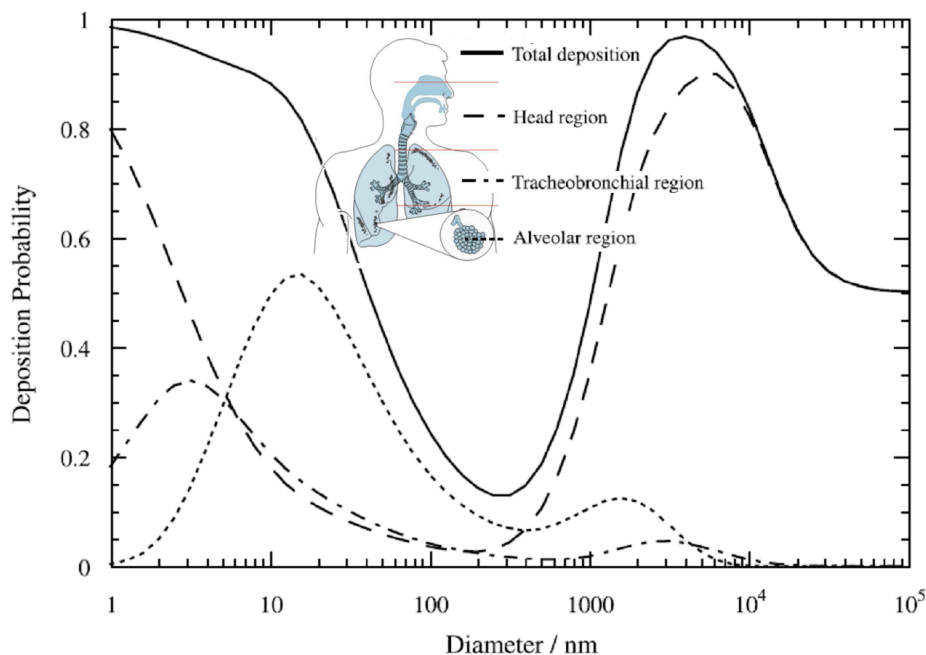
Figure 3: Deposition probability and penetration depth of particles in the respiratory tract as a function of size. Montage based on graphs by Maynard and Kuempel, (2005), and UGZ (2004).

Ultrafine particles are potentially the most dangerous, since they have the largest surface area, may gain access to the systemic circulation by penetrating alveolar membranes, and have the highest content of potentially toxic hydrocarbons (Nel, 2005). Soot and organic particles from incomplete combustion, especially of Diesel fuel and wood, the two most important sources of submicron particles in Switzerland, were shown to be highly cytotoxic (Nussbaumer et al., 2005). In addition, volatile organic compounds from incomplete combustion such as polycyclic aromatic hydrocarbons (PAHs, many of them carcinogenic, Li et al., 2003) can be adsorbed on the surface of these particles (Nussbaumer et al., 2005). First tests indicate distinct effects of secondary organic aerosol in lung cells (Baltensperger et al., 2008).

PM air quality standards only exist for PM_{10} in Switzerland. The 1-day average limit value is 50 ug m^{-3} and may only be exceeded once per year; the limit value for the annual average is 20 ug m^{-3} (BAFU and UVEK, 2011). In the European Union, the 1-day average limit value is the same as in Switzerland, but may be exceeded up to 35 times per year; the limit value for the annual average is 40 ug m^{-3}. In addition, there are also regulations for $PM_{2.5}$, with a limit value for the annual average of 25 ug m^{-3} (European Parliament and the Council, 2008).

1.1.4 Chemical composition

Depending on sources and meteorological conditions, tropospheric aerosols can contain sulfate, ammonium, nitrate, sodium, chloride, trace metals, crustal elements, water, and carbonaceous material. Carbonaceous material can be further divided into black or elemental carbon (BC or EC, depending on whether its optical or chemical properties are measured) and organic matter (OM, often referred to as organic aerosol OA).

The sources and formation mechanisms of the inorganic compounds and BC are rather well understood. Secondary inorganics are formed from gas phase pollutants: Ammonia (NH_3), emitted into the atmosphere by activities related to agriculture (livestock farming, fertilizers), combustion, or biological decay, is the dominant base in the atmosphere and reacts with nitric acid (HNO_3), sulfuric acid (H_2SO_4) and hydrogen chloride (HCl) to form particulate ammonium nitrate (NH_4NO_3), ammonium sulfate (($NH_4)_2SO_4$), and ammonium chloride (NH_4Cl) (Bouwman et al., 1997). Nitric acid and sulfuric acid are the oxidation products of NO_x, mostly emitted from fossil fuel combustion from traffic, but also from households, industry, and agriculture, and SO_2 from sulfur-containing fuel combustion, respectively. Chloride (Cl^-) sources in Switzerland are HCl emissions or suspension of de-icing salt (NaCl) (BAFU, 2009), in marine environments NaCl from sea salt aerosols (Smolík et al., 2003). Trace metals in ambient air can be due to natural processes such as volcanic eruptions, dust storms, and rock weathering; or anthropogenic activities such as fossil hydrocarbon combustion and metallurgical industries. Metalliferous particles tend to be in the Aitken or accumulation mode (Moreno et al., 2011). Mechanical processes are responsible for coarse particles containing crustal elements, among others (compare Fig. 1). The water content of atmospheric particles depends on the chemical composition and the relative humidity (Engelhart et al., 2011). BC is emitted largely from incomplete combustion processes of fossil fuel or biomass.
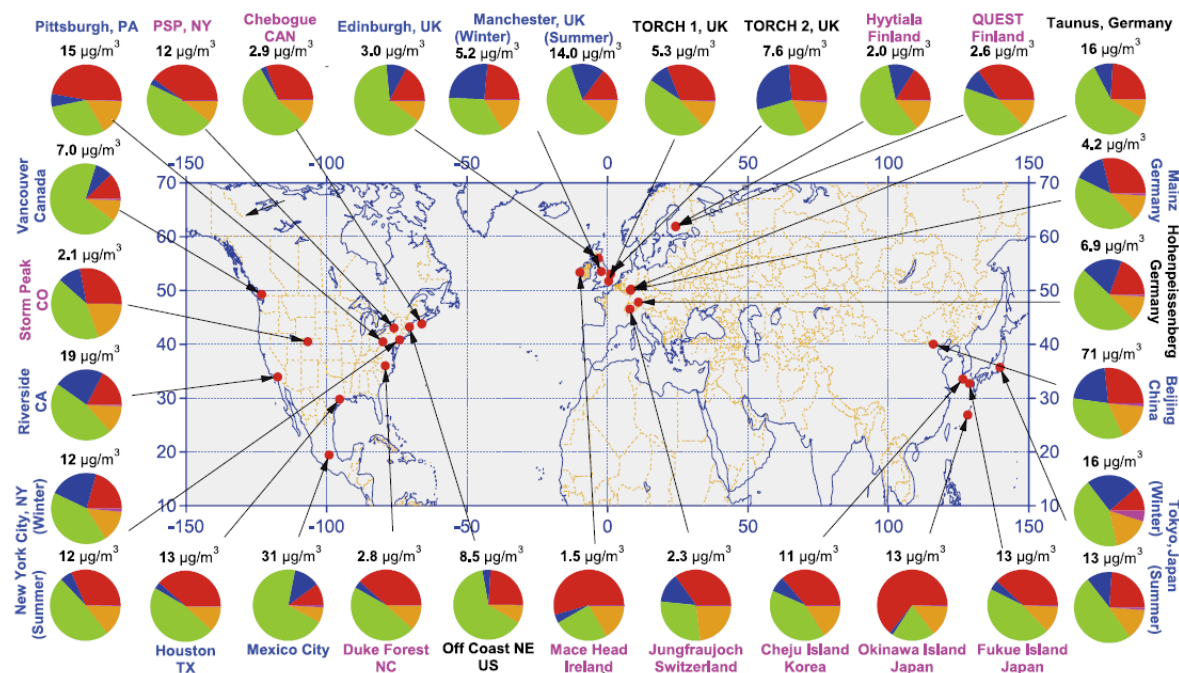
Figure 4: Chemical composition of PM_1. Colors for the study labels indicate the type of sampling location: urban areas (blue), <100 miles downwind of major cites (black), and rural/remote areas >100 miles downwind (pink). Pie charts show the average mass concentration and chemical composition: organics (green), sulfate (red), nitrate (blue), ammonium (orange), and chloride (purple), of non-refractory PM_1 (Zhang et al., 2007).

Organic compounds can make up as much as 20-90% of total aerosol mass depending on location and/or season (Jimenez et al., 2009). Figure 4 shows the chemical composition of PM_1 in 25 locations in the Northern hemisphere based on aerosol mass spectrometer (AMS) data. Numerous sources emit organic aerosol; in addition, secondary organic aerosol (SOA) is formed from atmospheric oxidation products of volatile organic compounds (VOCs), of which it is estimated that there are between 10 000 and 100 000 different compounds (Goldstein and Galbally, 2007). Knowledge about sources, fate and mutual interaction of gas-phase and aerosol compounds is thus still limited. Organic aerosol will be addressed separately in the next chapter.

1.2 Organic aerosols

1.2.1 Sources and evolution in the atmosphere

Primary organic aerosol (OA) sources were the first OA sources to be identified and quantified: Fossil fuel combustion in diesel and gasoline cars, aircrafts, etc., forest fires and wood burning, coal burning, cigarette smoke, meat cooking, but also tire wear and brake lining (Hildemann et al., 1991).

Secondary organic aerosol (SOA) formation, the gas-to-particle conversion of oxidation products of volatile organic compounds (VOCs), has been investigated since the 1970s (Jacobson et al., 2000). Discrepancies between modeled and measured organic aerosol concentrations indicated the importance of SOA for ambient mass concentrations and implied that not only biogenic, but also anthropogenic VOCs must play a major role in SOA formation (Volkamer et al., 2006). The deconvolution of OA measured with an aerosol mass spectrometer (AMS, Canagaratna et al., 2007, and references therein) into a hydrocarbon-like OA (HOA) corresponding to primary OA emissions from traffic or cooking, and an oxygenated OA (OOA) related to SOA (Zhang et al., 2005a) showed that even in urban environments, where primary emissions are abundant, OOA is the dominant component of OA (Zhang et al., 2007).

The application of positive matrix factorization (PMF, Paatero and Tapper, 1994; Paatero and Tapper, 1993) to the organic data matrix measured by AMS (Lanz et al., 2007) made the identification and quantification of further OA source factors such as biomass burning OA (BBOA) and cooking OA (COA) possible and confirmed the ubiquity and dominance of OOA in ambient aerosol, as shown in Fig. 5 by a compilation of European AMS-PMF datasets (Lanz et al., 2010).
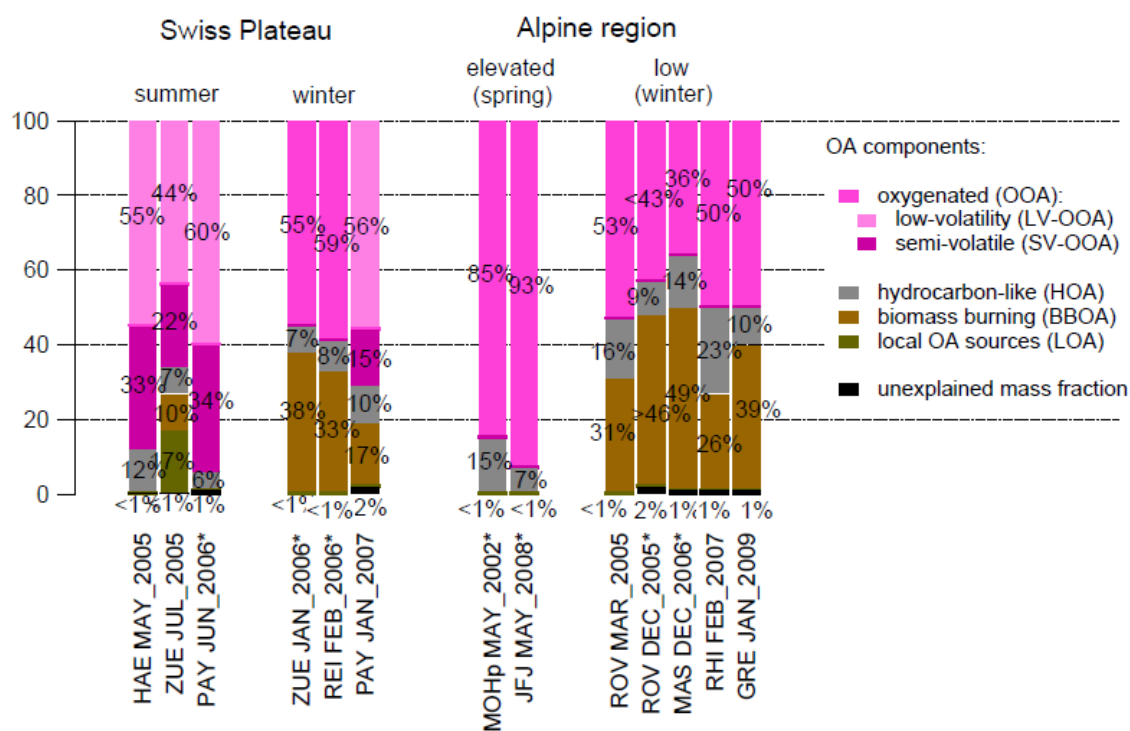

Figure 5: Relative composition of OA measured by AMS, determined by PMF, in several European locations and in different seasons (Lanz et al., 2010).

PMF analysis of OA measured by AMS also allowed the differentiation between two OA types, a low-volatility and a semi-volatile OA (LV- and SV-OOA, Lanz et al., 2007, Fig 5). They differ in volatility and atomic oxygen to carbon (O:C) ratio and represent heavily aged, regional OA and less photochemically aged OA, respectively. This implies that the evolution of OA in the atmosphere is dynamic, which has been studied in numerous field studies and laboratory experiments (Jimenez et al., 2009): Photochemical aging of VOCs, but also biomass burning emissions and diesel exhaust leads to a build up of OA mass; the evolution of the plume downwind a major city also exhibits an increase in OA mass (if accounted for the dilution). Photochemical processes and SOA formation can be parameterized by the degree of oxidation and the volatility of the organic components: Oxidation of gas phase species generates products with added functionality, higher polarity, and thus lower volatility, which then partition into the particle phase (Donahue et al., 2011). However, fragmentation can also generate highly oxidized products that are more volatile (Jimenez et al., 2009).

Photochemical aging causes the OOA spectra measured by AMS to become progressively similar and lose their source fingerprint (Andreae, 2009; Capes et al., 2008). Simultaneously, f_{44}, the fraction of m/z 44 (CO_2^+), mostly from the decarboxylation of carboxylic acids, increases, indicating the importance of acid formation in OOA evolution, while the fraction of m/z 43, mostly $C_2H_3O^+$ from non-acid oxygenates (f_{43}), approaches a low value of ~0.05 (Ng et al., 2010, Fig. 6).
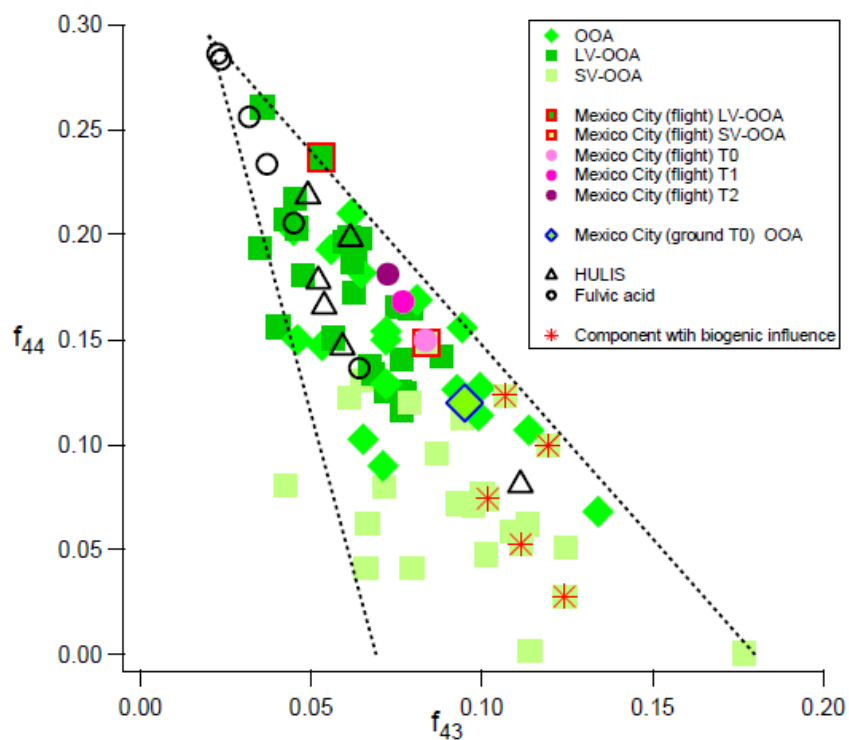
Figure 6: f_{44} vs. f_{43} for all the OOA components from different sites as well as various HULIS (humic-like substances) and fulvic acid samples. The dotted lines are added to guide the eye and define the triangular space where ambient OOA components fall (Ng et al., 2010).

f_{44} can be used as a surrogate of the O:C ratio. Atmospheric aging of OA was also parameterized in the space of a Van Krevelen diagram, which cross plots the hydrogen to carbon (H:C) ratio and the O:C ratio (Heald et al., 2011). Data from different laboratory and field measurements exhibited a movement along a line with a slope of ~-1 during the aging process, indicating carboxylic acid addition. Transforming the data from Fig. 6 to the ΔH:C/ΔO:C space revealed a slope of ~-0.5, suggesting that the net changes in chemical composition of ambient OOA aging are equivalent to not only the addition of acid, but also alcohol/peroxide functional groups (Ng et al., 2011a).

1.2.2 Measurements

The complexity of the atmospheric aerosol system places great demands on measurement techniques and instrumentation (Hallquist et al., 2009). Aerosol mass spectrometers (AMS) have become a widely applied tool because they allow chemical speciation, sizing and mass detection of submicron non-refractory PM at very high time resolution (Baltensperger et al., 2010; Canagaratna et al., 2007).

Infrastructure requirements of aerosol and gas-phase instrumentation put restrictions on ambient air quality measurements, which often lead to a fixed installation of instruments at a designated place with sufficient power and protection. However, in addition to temporal evolution, the spatial variation of the parameters of interest can be of importance for explaining particular atmospheric processes. Previous studies either featured the same type of instruments at various sites simultaneously (e. g. Mejia et al., 2008; Xie et al., 2008), or a set of various instruments mounted on a mobile platform.

Many mobile measurements have been performed using aircraft (e. g. Schneider et al., 2006; Bahreini et al., 2003; DeCarlo et al., 2010), or, if ground-based, focused on vehicle exhaust (e. g. Canagaratna et al., 2004; Zavala et al., 2009; Thornhill et al., 2010). Only few studies covered ground-based spatially resolved particle characterization or source apportionment (Bukowiecki et al., 2002; Bukowiecki et al., 2003; Weimer et al., 2009).

1.3 Thesis motivation

The high uncertainties related to sources and formation pathways of organic aerosol bear the need for further laboratory and field experiments in diverse environments. This thesis investigates sources of ambient submicron aerosol using mobile and stationary aerosol mass spectrometer (AMS) measurements in two European cities and analyzing the data of the organic fraction with positive matrix factorization (PMF).

Chapter 3 describes results from mobile AMS measurements in Zurich (Switzerland). Based on the spatial variation of particulate matter (PM) chemical species and organic source components, a new method is developed which allows the separation and quantification of the local and regional fraction of PM measured in downtown Zurich, information of great importance to local and national policymakers occupied with air pollution.

Chapter 4 presents results from stationary AMS measurements in the city of Barcelona (Spain). A high-resolution time-of-flight AMS and additional instrumentation were deployed during a month-long campaign in March 2009 to investigate sources of organic aerosol in the Western Mediterranean Basin.

Results from mobile measurements in the Barcelona region (during the same period as the stationary measurements described in chapter 4) are presented in chapter 5. The additional dimension of space allows the characterization of the spatial variation of emissions and organic source components in the Barcelona region and the investigation of the evolution of pollutants as they are dispersed from the city center.

2

METHODOLOGY

2.1   PSI mobile laboratory

The results presented in chapters 3 and 5 are based on measurements performed with the PSI mobile laboratory (Fig. 7). While the selection of instruments onboard the laboratory has changed over the years depending on the scope of the measurement campaigns or due to further instrument development (Bukowiecki et al., 2003; Weimer et al., 2009, and chapter 5), the basic setup of the van has not been modified since its first design described by Bukowiecki et al. (2002). The current model is an IVECO 35S14V Daily van (length 6 m; width 2 m; height 3 m; maximum gross weight 3.5 tons), equipped with a diesel particulate filter, which reduces particulate self-contamination during measurements. A second alternator built into the van engine system allows for a continuous operation of the complete set of instruments (power consumption: ~2.36 kW) while driving: 2.88 kW are delivered by the two alternators when the engine is running. The power is stored in two 12V/110Ah batteries, bridging short-time power interruptions (up to 30 min). Two sinus inverters (90% efficiency) connected to the batteries yield the necessary power with 220V to operate the instruments. The batteries are recharged, or in case of stationary measurements, externally fed with 380V from the electricity network via a voltage transformer.

The main inlet is located in front, at a height of 3.2 m above ground. It consists of a 4-cm inner diameter (i. d.) stainless steel tube. A heavy-duty blower provides a constant flow of 14 ms^{-1} (50 kmh^{-1}), eliminating the influence of driving speed. The flow is monitored with an anemometer AM-4203 (Lutron, Taiwan). The high flow velocity in this part of the inlet reduces particle losses in the size range of interest (50 – 700 nm, see next section) substantially ($\leq$ 0.23% for diffusion or gravitational losses, $\leq$ 0.3% for turbulent diffusion losses), despite the high Reynolds number of ~42 000.

Two smaller stainless steel tubes with an i. d. of 0.8 cm distribute the sample air to the instrument rack in the front and the instruments mounted in the back part of the van. They reach inside the main inlet tube in the flow direction, one in the front, 10 cm behind the main inlet entrance, the other one in the back, 250 cm behind the main inlet entrance. There is a reduction in

flow velocity from the main inlet tube to the tubes reaching the instruments by factors of 2 and 4 for the front and back branch, respectively. Such anisokinetic sampling can lead to an enrichment of larger particles. However, no such artifacts were observed during tests with the main inlet flow switched on and off, most likely due to the low size range of the particles measured for this thesis. From a common manifold for the front and for the back rack, respectively, copper (or Teflon, for the gas phase instruments) tubing with 0.4 cm i. d. leads to the different instruments (lengths: ~100 cm for particle phase instruments, 200-300 cm for gas phase instruments).
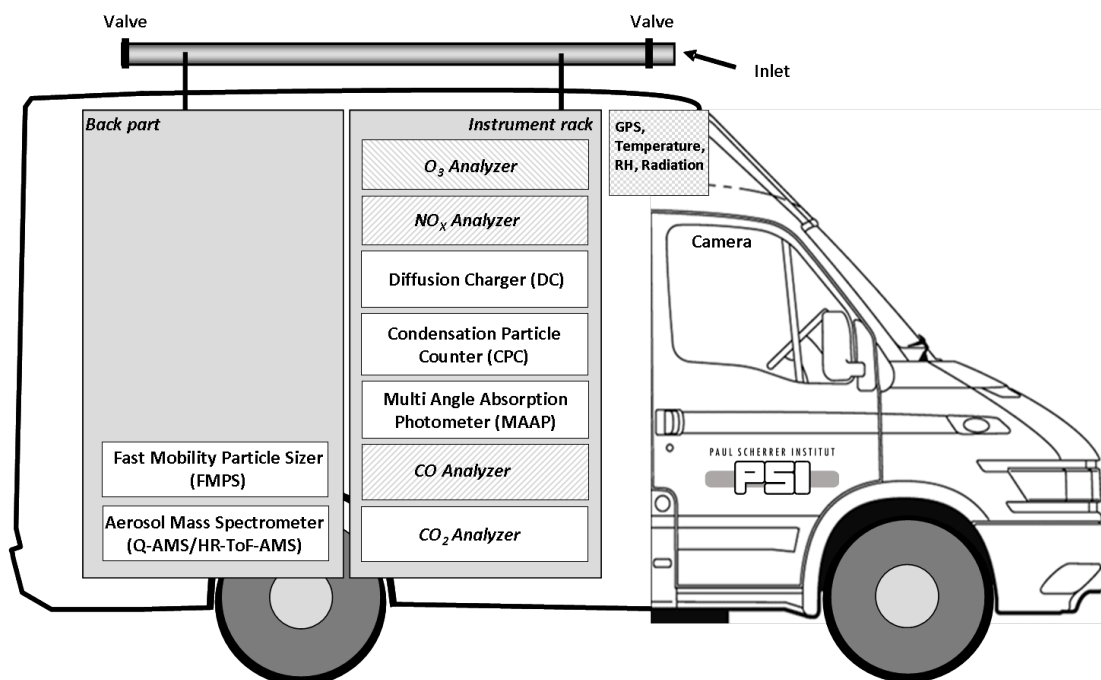
Figure 7: PSI mobile laboratory. NO_X analyzer and CO analyzer were only included in measurements performed after November 2008. For the Barcelona campaign (chapter 5), the Q-AMS (see main text) was upgraded to an HR-ToF-AMS and the ozone analyzer was added.

Residence time for the aerosol sample varies between 5 and 6 s, depending on the position of the instrument. Due to the high main inlet flow velocity, the difference in residence time between the front and the back branch is negligible (0.02 s). Shock absorbers installed between the rack shelves and the individual instruments prevent damage from vibration shocks while driving. Air conditioning in the instrument region of the van prevents the build-up of heat up due to instrument power consumption.

2.2   Instrumentation

Table 1 presents an overview of the instruments deployed in the mobile laboratory and at the urban background station in Barcelona (chapter 4). Except for both AMS, the values for the detection limits are those provided by the manufacturer.

Table 1: Overview of the instruments in the mobile laboratory and deployed during the stationary measurements in Barcelona (chapter 4). If not noted otherwise, the values for the detection limits are those as provided by the manufacturer.

INSTRUMENT	PARAMETER MEASURED	DETECTION LIMIT	TIME RESOLUTION	FLOW	REMARKS
Q-AMS, Aerodyne	Size-resolved non-refractory chemical composition of PM$_1$	32 - 470 ng m^{-3} *	6 s	0.1 l min^{-1}	Zurich campaign (chapter 3)
HR-ToF-AMS, Aerodyne	Size-resolved non-refractory chemical composition of PM$_1$	12 - 22 ng m^{-3}*	1 s	0.1 l min^{-1}	Barcelona campaign (chapters 4, 5)
FMPS, TSI	Size distribution, d_p = 5.6 - 560 nm	1 (at 560 nm) - 100 (at 5.6 nm) particles cm^{-3}	1 s	10 l min^{-1}	
SMPS (DMA, PSI; CPC 3022A, TSI)	Size distribution, d_p = 13 - 638 nm	not defined	5 min	0.3 l min^{-1}	Barcelona campaign (chapter 4)
CPC 3010, TSI	Particle number concentration, d_p > 10 nm	0.0001 cm^{-3}	1 s	1 l min^{-1}	
LQ1-DC, Matter Engineering	Particle active surface area	10 µm^2 cm^{-3}	1 s	1.5 l min^{-1}	
MAAP 5012, Thermo	Absorption (black carbon mass concentration)	2 min: < 100 ng m^{-3}	1 s	16.7 l min^{-1}	
Aethalometer AE31, Magee Scientific	Absorption (black carbon mass concentration)	0.1 µg m^{-3}	5 min	2.9 l min^{-1}	Barcelona campaign (chapter 4)
LI-7000 CO$_2$/H$_2$O analyzer	CO$_2$	0.1 ppm	1 s	1.2 l min^{-1}	
LMA-3 Luminox® Monitor, SCINTREX	NO$_x$	5 ppt	1 s	1.5 l min^{-1}	Added in December 2008
CO Analyzer AL5002, Aerolaser GmbH	CO	3 ppb	1 s	0.03 l min^{-1}	Added in December 2008
Ozone Monitor Dual Beam, Model 205, 2B Technologies, Inc.	O$_3$	2 s: 1 pbb	1 s	1.5 l min^{-1}	Added for Barcelona campaign (chapter 5)
GPS, Garmin IIplus	Longitude, latitude, altitude, driving speed	common standard	2 s		
Thermilinear thermistor network, YSI 44203	Temperature	common standard	1 s		
Pressure device, PSI	Pressure	common standard	1 s		
HUMICAP sensor, Vaisala HMP 31UT	Relative humidity	common standard	1 s		
Pyranometer "Solarimeter" CM10, Kipp & Zonen,	Global radiation	common standard	1s		

* Measured 1-min detection limits in MS mode (V mode) (DeCarlo et al., 2006)

2.2.1 Aerosol mass spectrometer

Aerosol mass spectrometers (AMS) provide size-resolved information on the non-refractory chemical components of PM_1 such as ammonium, nitrate, sulfate, chloride, and organics. Figure 8 shows a schematic of the two versions of AMS used to collect data for the present thesis: a quadrupole AMS (Q-AMS, Aerodyne Research Inc., a) and a high-resolution time-of-flight AMS (HR-ToF-AMS, Aerodyne Research Inc., b).
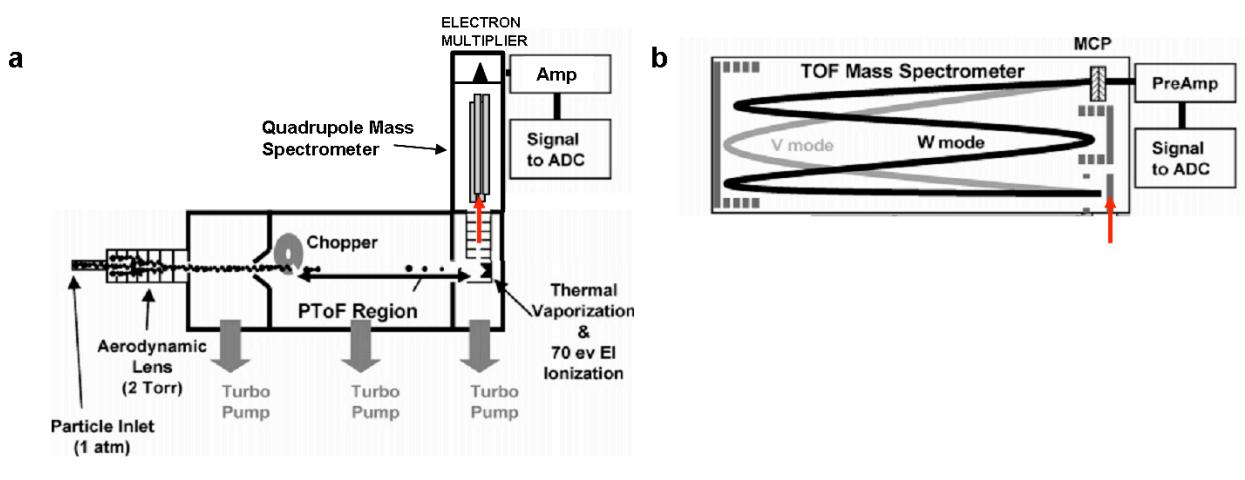

Figure 8: Schematic of a Q-AMS (a) and the TOF mass spectrometer (b) which replaces the quadrupole in the HR-ToF-AMS. The red arrows show the ion flight direction. Particle inlet and PTOF region are the same for both instrument versions. Schematic adapted from DeCarlo et al. (2006), and Canagaratna et al. (2007).

The instrument consists of three main sections: a particle beam generation region, an aerodynamic sizing region, and a mass analyzer where the particle composition is determined. The aerosol sample enters the instrument through the particle inlet where a 100 μm diameter orifice reduces the flow to ~0.1 1 min^{-1}. The particles are then focused into a narrow beam in the aerodynamic lens, which has a transmission efficiency close to 100% for particles with a diameter between 50 and 700 and lower but still substantial transmission in the 30 - 70 nm and 500 nm - 1 μm ranges (Liu et al., 2007).

At the exit of the lens, the particles enter the aerodynamic sizing region where they are accelerated by a supersonic expansion due to a pressure drop to ~10^{-5} Torr. Depending on their vacuum aerodynamic properties, they acquire different terminal velocities. In the particle time-of-flight (PTOF) mode, size-resolved mass spectra are acquired. The time of flight of the particles between a rotating chopper (frequency ~150 Hz, 2% slit area) and the detector is used to determine the particle vacuum aerodynamic diameter d_{va}. For the urban background measurements in Barcelona (chapter 4), the HR-ToF-AMS was calibrated for particle sizing using polystyrene latex

(PSL) spheres with known sizes at the beginning of the campaign. During mobile measurements no PTOF data were acquired due to time resolution constraints. In the mass spectrum (MS) mode, mass spectra are acquired continuously with the chopper either in the "closed" position, blocking the particle beam to measure background mass spectra, or in the "open" position to acquire sample mass spectra.

Throughout the vacuum chamber, between the aerodynamic lens and the vaporizer, the particle mass is concentrated by a factor of 10^7 compared to the ambient air (Allan et al., 2003) by means of a skimmer cone at the exit of the lens removing gas from the sample flow and the differentially pumping turbomolecular pumps (see Fig. 8).

A resistively heated surface (600 °C) flash vaporizes the particles. The gas-phase molecules are ionized by electron impact (70 eV) from an electron emitting tungsten filament. Since only ~10 eV would be needed to ionize the molecules, they are fragmented by the excess energy. The positive ions are extracted from the ionizer and led into the mass analyzer, either a quadrupole (QMS, Balzers QMG 422, Fig. 8 a) or a time-of-flight (TOF) mass spectrometer (H-TOF, Tofwerk, Fig 8 b).

The quadrupole mass analyzer consists of two metal rod pairs with a radio frequency voltage applied between them and a direct current voltage superimposed. A given ratio of voltages will only allow ions with a certain mass-to-charge ratio (m/z) to reach the detector, thus quantifying only ions of one m/z at a time. The quadrupole in the AMS described here scans the range of m/z-values 1 – 300 in 300 ms by continuously varying the applied voltages.

The TOF mass spectrometer allows the simultaneous categorization of ions of the whole m/z range (usually ~10 – 500, depending on the timing settings). The ions are orthogonally extracted into the TOF mass analyzer by a high-voltage pulser and accelerated by an electric potential. The velocity of the ion leaving the extractor and thus its time of flight through the mass spectrometer is a function of its m/z. The TOF mass spectrometer features two ion optical modes, a single reflection mode with higher sensitivity and lower resolving power referred to as V-mode, and a so-called W mode with a two-reflectron configuration that yields higher resolving power but lower sensitivity. The mass resolving power defined as the nominal m/z divided by the full width at half-maximum (m/Δm) was measured to be 220, 2100, and 4300 for the Q-AMS, HR-ToF AMS V-mode, and W-mode, respectively (DeCarlo et al., 2006). The much higher resolution of the HR-ToF-AMS allows the separation of ions at the same nominal mass (HR data). Figure 9 (DeCarlo et al., 2006) shows the different levels of information for the AMS versions used here.
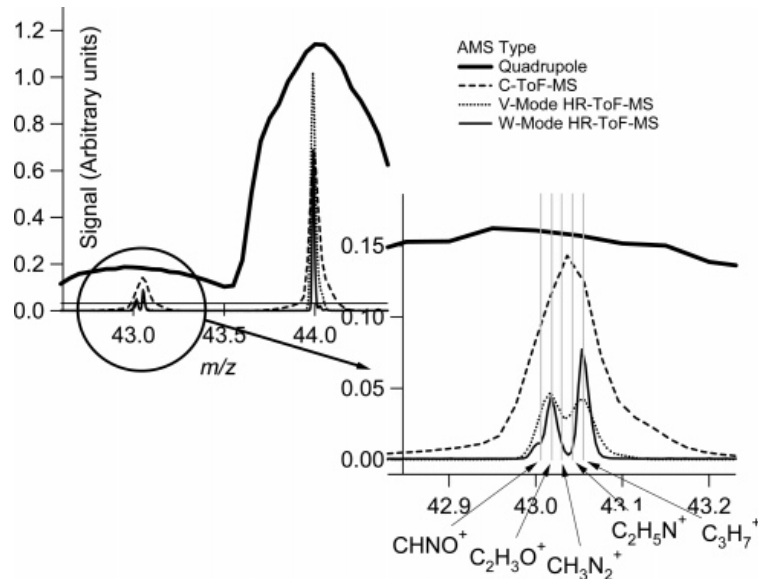
Figure 9: Raw data of Q-AMS (Quadrupole) and HR-ToF-AMS, V- and W-mode, around *m/z*'s 43 and 44. The C-ToF-AMS shown here was not used in the present thesis. Figure copied from DeCarlo et al. (2006).

The signals from the detectors, an electron multiplier in the Q-AMS, a multichannel plate detector (MCP) in the HR-ToF-AMS, are amplified and sampled with a 12-bit (Q-AMS) or 8-bit (HR-ToF-AMS) analog-to-digital converter. Further details of the AMS instruments configuration and functioning can be found in e. g. Jimenez et al. (2003), DeCarlo et al. (2006), or Canagaratna et al. (2007).

The raw data in the form of continuous mass spectra are then converted into mass spectra with discrete *m/z* channels in order to be interpreted. In the Q-AMS, the averaged height of a distinct raw peak with a plateau of ~0.4 amu width at a certain *m/z* is taken to be the detected ion rate at this *m/z* (Allan, 2004). In the HR-ToF-AMS, it is the peak area around a certain *m/z* that defines the ion rate for unit mass resolution (UMR) data. Peak areas for individual ions at one *m/z* (HR data) are determined by means of a custom peak-fitting routine (DeCarlo et al., 2006). During a measurement campaign, *m/z* calibrations as well as baseline and single ion signal checks are performed on a once-per-week basis. This information is used to calculate the total ion rate signal I_{sf} of all fragments *f* of a species *s* which is then converted to a mass concentration C_s using the following formula (Jimenez et al., 2003):

$$C_{\mathrm{s}} = \mathrm{R}_t \, \frac{1}{Q} \frac{1}{N_A} \frac{\mathrm{MW}_{\mathrm{NO}_3}}{\mathrm{IE}_{\mathrm{NO}_3}} \sum_f I_{sf} \qquad\qquad (1)$$

Where Q is the air volume sampling rate, N_A the Avogadro's number, MW_{NO3} the molecular weight of nitrate, IE_{NO3} the ionization efficiency (the number of ions detected per molecule vaporized) of nitrate and R_t a response factor of *s* relative to nitrate. Nitrate is chosen as a reference

because ammonium nitrate particles are easy to generate at low costs and vaporize at nearly 100% efficiency, leaving little residue (Alfarra, 2004). The ionization efficiency of a molecule is directly proportional to its electron ionization impact cross section which in turn is proportional to the number of electrons in a molecule and thus of the molecular weight of the molecule. Therefore, the relationship MW_{NO3}/IE_{NO3} can be used to derive mass concentrations for other species than nitrate if their chemical nature is known by introducing the empirically determined, species-specific factor R_t (Jimenez et al., 2003). Ammonium nitrate IE calibrations were performed ~once a week during measurement campaigns.

As ionization by electron impact causes excessive fragmentation of the molecules, the signal at one *m/z* can have contributions from various species and from air. For UMR data analysis, species separation and quantification of mass spectral data from the AMS is done using a so-called fragmentation table (Allan et al., 2004) based on known fragmentation patterns. For the data analyzed in the present thesis, the initial fragmentation table was modified according to Aiken et al. (2008), who empirically determined relationships between the CO_2^+ fragment and the fragments CO^+, H_2O^+, OH^+ and O^+. Contributions from air were quantified measuring particle filtered air for a few minutes after mass calibrations.

Since particle losses occur in the AMS during the transmission through the instrument and due to bouncing off the vaporizer (Middlebrook et al., 2012), a collection efficiency (CE) has to be determined when establishing mass concentrations. For the CE applied to the data sets presented in this thesis, the reader is referred to the respective chapters.

Q-AMS data were analyzed using the standard algorithm developed by Allan et al. (2004) (AMS Analysis Toolkit 1.41), and HR-ToF-AMS data using the standard analysis software SQUIRREL v1.51B and PIKA v1.10B within Igor Pro 6 (Wavemetrics).

2.2.2 Instruments to measure particle physical properties

The particle number concentration was measured with a condensation particle counter (CPC 3010s, TSI) with a time resolution of 1 s. The CPC detects particles with an optical particle detector after they have grown into droplets by condensing butanol vapor. A dilution flow of 9 l min^{-1} was used to extend the upper limit of the concentration range (0.0001 to 10 000 particles cm^{-3}) by a factor of 10.

A diffusion charger (LQ1-DC, Matter Engineering) was used to measure the particle active surface area, which is proportional to the attachment rate of positively or negatively charged air ions attaching to the particle surface by Brownian diffusion (Baltensperger et al., 2001). The DC

was continuously measuring during mobile measurements; however active surface data were only used for comparison reasons and will not be further discussed throughout this thesis.

Particle size distributions were measured onboard the mobile laboratory with a fast mobility particle sizer (FMPS, TSI). Its setup allows the acquisition of size distributions with a very high time resolution (1 s): The measurement column contains a high-voltage electrode with multiple electrical sections of different voltages and column diameters, making the simultaneous classification of particles with different electrical mobilities (and thus size) possible (Johanson et al., 2004).

At the urban background site in Barcelona (chapter 4), a scanning mobility particle sizer (SMPS, homebuilt by PSI, Gysel et al., 2007), consisting of a neutralizer with a ^{85}Kr source, a differential mobility analyzer DMA, and a condensation particle counter (CPC 3022A, TSI) was operated in parallel to the AMS. It measured submicron particle number size distributions between 13 and 638 nm electrical mobility diameter with a time resolution of 5 min.

2.2.3 Black carbon instruments

Onboard the mobile laboratory, a multi angle absorption photometer (MAAP 5012, Thermo) was deployed for information on black carbon (BC) mass concentrations based on light absorption measurements (Petzold et al., 2002). Particles are accumulated on a glass-fiber filter in the detection chamber. A light source emits light with a wavelength of 630 nm that is either transmitted, absorbed, or reflected by the deposited aerosol and filter tape matrix. A series of photo-detectors measures both the reflected and the transmitted light at different angles. This information is used together with the area of the dust collecting spot, the volumetric flow rate, and a mass specific absorption cross section σ_{abs} of 6.6 m^2g^{-1} to estimate the BC mass concentration based on the Lambert-Beer law.

During the Barcelona campaign (chapter 4), BC mass concentrations at the urban background station were derived from particle light attenuation *(b$_{ATN}$)* measurements at a wavelength of 880 nm by an aethalometer, Model AE31 (Magee Scientific). In contrast to the MAAP, the aethalometer does not take artifacts caused by the aerosol-light-scattering fraction into account; however it measures the absorption over a broad region of the visible spectrum of wavelengths (at λ = 450, 590, 615, 660, 880, and 950 nm). For the determination of ambient BC concentrations usually only the measurement at the near-infrared channel (λ = 880 nm) is used, since lower wavelengths have too high contributions by compounds other than BC (Weingartner et al., 2003). *b$_{ATN}$* measured at 880 nm by the aethalometer was corrected for multiple scattering of the light beam within the unloaded filter matrix (C = 2.81, Collaud Coen et al., 2010) and for the

"shadowing" caused by the deposited particles (f = 1.2) following the procedure by Weingartner et al. (2003), yielding the aerosol absorption coefficient b_{abs} (using an attenuation cross-section σ_{ATN} of 16.6 m^2 g^{-1}). b_{abs} and an absorption cross-section $\sigma_{abs} = \sigma_{ATN}/C$ of 5.91 m^2 g^{-1} were then used to calculate BC mass concentration at 880 nm..

2.2.4 Gas phase instruments

CO_2 was measured during all mobile measurement campaigns using a LI-7000 CO_2/H_2O analyzer (LICOR). The dual optical path analyzer determines the absorptance of infrared radiation by CO_2 and H_2O in a sample cell and a reference cell. The comparison of the measured transmitted radiant power in both cells is used to calculate the ambient gas concentration. During mobile measurement campaigns (chapters 3 and 5), zero air and 560 ppm CO_2 were introduced into the instrument twice a day, measured for a few minutes and averaged to one data point each. The resulting calibration curve applied to the acquired data is a linear equation with the offset being the median of all zero air data points and the slope being the ratio of 560 to the median of all 560 ppm data points minus the zero air value.

The carbon monoxide (CO) analyzer AL5002 (Aerolaser GmbH) was installed in the mobile laboratory in December 2008. Thus CO data were not acquired during part 1 of the Zurich campaign (chapter 3). CO is measured based on its resonance fluorescence in vacuum ultra-violet (VUV) at 150 nm, which is detected using a VUV-photomultiplier tube and a fast counter (Gerbig et al., 1999). During measurement campaigns, three subsequent automatic calibrations with zero-air and a known CO concentration were performed twice a day.

Also in December 2008, a LMA-3 Luminox[®] Monitor (SCINTREX) was additionally set up in the mobile laboratory, detecting the presence of NO_2 via chemiluminescence (using a luminol solution). To measure NO_x concentrations, a chromium trioxide converter was added, oxidizing NO to NO_2 by CrO_3 with an average effectiveness of ~80%.

During the Barcelona campaign (chapter 5), O_3 was measured with an ozone monitor (Dual Beam, Model 205, 2B Technologies, Inc.) based on its strong absorption of UV light at 254 nm. The instrument estimates interferences from other gases such as SO_2 and aromatic compounds using an ozone scrubber.

All gas phase measurements were performed with a time resolution of 1 s.

2.3   Statistical analysis: Positive Matrix Factorization (PMF)

The observed quantities measured by the AMS were related to organic aerosol sources by means of factor analysis. Factor analysis is a statistical method to explain a number of observed variables by a (lower) number of unobserved variables called factors. In other words, it reduces the dimensionality of the measured data by finding features or hidden variables corresponding to a few, important factors, in our case organic aerosol sources (Backhaus et al., 2003).

Here, the factor analytical tool Positive Matrix Factorization (PMF, Paatero and Tapper, 1993, 1994) was applied to the organic mass fraction of PM_1 collected by the AMS and the results were interpreted with the support of the ancillary data. Within the ensemble of air quality models, PMF falls into the category of receptor models: it starts from m observations of n measured quantities x_{ij} at a receptor site from which it derives p individual source components f and their time-dependent intensities g plus a residual term e_{ij} (Henry et al., 1984):

$$x_{ij} = \sum_k g_{ik} f_{kj} + e_{ij} \qquad\qquad i = 1...m; \; j = 1...n; \; k = 1...p, \qquad\qquad (2)$$

or in matrix form

$$\mathbf{X = GF + E} \qquad\qquad\qquad (3)$$

Based on Eq. (2-3), PMF assumes that the measured $m \times n$ organic data matrix $\mathbf{X}$ can be modeled as a linear combination of p factor profiles (the $p \times n$ matrix $\mathbf{F}$) and their respective mass contributions (the $m \times p$ matrix $\mathbf{G}$), plus the $m \times n$ residual matrix $\mathbf{E (E = X - GF)}$. The solution is a weighted iterative least squares fit minimizing Q as in Eq. (4), where the known measurement uncertainties σ_{ij} for the values x_{ij} are used for determining the weights of the residuals e_{ij}:

$$Q = \sum_{i=1}^{m} \sum_{j=1}^{n} \left(e_{ij} / \sigma_{ij} \right)^2 \qquad\qquad\qquad (4)$$

The measurement uncertainty or error ΔI associated with a signal I is the standard deviation of the Poisson distribution describing the modeled distribution of I, convolved with the Gaussian distribution of the signal from a single ion, plus a term for electronic noise, per sampling time. The errors are calculated independently for the "open" and the "closed" signal (ΔI_o, ΔI_c, compare also section 2.2.1) and must be summed in quadrature (Allan et al., 2003):

$$\Delta I = \sqrt{\Delta I_o^2 + \Delta I_c^2} \qquad\qquad\qquad (5)$$

ΔI is then converted to µg m^{-3} according to Eq. (1), and the following corrections are applied to the uncertainties matrix (Ulbrich et al., 2009):

- The minimum error is set to 1 ion per sampling time.

- Columns (*m/z*'s) with a signal-to-noise (SNR) ratio below 0.2 are removed from the matrix; columns with an SNR between 0.2 and 2 are downweighted by a factor of 3.

- In order not to overestimate the importance of *m/z* 44, all *m/z*'s directly proportional to that mass fragment (Aiken et al., 2008) are downweighted by the square root of their number.

PMF is a functional linear unmixing model, i. e. it does not require *a priori* information to solve the bilinear problem in Eq. (3). This is in contrast to chemical mass balance (CMB) models, also receptor models and the first source apportionment technique applied to ambient particles (Henry, 1997). However, all of the above approaches are based on the assumption that factor profiles **F** do not change over time. Compared to Principal Component Analysis (PCA), a widely applied dimensionality reduction technique and in some fields used synonymously for factor analysis (Paatero and Tapper, 1993), PMF has several advantages which make it more suitable for real world problems :

- Individual data points in the data matrix **X** are weighted by their analytical uncertainty, allowing proper handling of missing or below detection limit data.

- **G** and **F** are constrained to have non-negative values.

- There is no orthogonality imposed on **F**.

However, PMF-results are not unique due to rotational ambiguity: Linear transformations ("rotations") still conserving the non-negativity constraint can result in an identical fit to the data, such that

$$\mathbf{GF} = \mathbf{GTT^{-1}F}$$ (6)

where **T** is a transformation matrix and $\mathbf{T^{-1}}$ its inverse.

Although PMF is a mathematical concept, the choice of the number of factors *p* cannot purely be based on mathematical criteria. PMF solutions of ambient datasets also must be meaningful in that context, and it is the task of the modeler to subjectively choose the best solution. The following points usually are considered when investigating possible PMF solutions:

- The *Q*-value in Eq. (4) is one mathematical criterion for the quality of the fit. If the model is appropriate for the problem at hand and the data uncertainties estimations are accurate, $(e_{ij} / \sigma_{ij})^2$ is ~1 and the expected Q (Q_{exp}) = $mn - p\ (m+n) \approx mn$, the degrees of freedom of the fitted data (Paatero et al., 2002). Q / Q_{exp} >>1 indicates an underestimation in p or the uncertainties, while Q / Q_{exp} << 1 indicates an overestimation in one or both of these quantities. Each added factor introduces more degrees of freedom allowing more data to be fit and hence decreases *Q*. Possible multiple local minima of the *Q* function (Paatero, 2007) can be explored by starting the algorithm from different pseudorandom values (*SEEDS*).

- Another parameter to explore the quality of the PMF fit is *max(rotmat)*, the largest element in **RotMat**, a matrix where the standard deviation of possible values of the transformation matrix **T** are reported. Generally, the best fit demands a minimal *max(rotmat)*, since larger values in **T** imply greater rotational freedom of a solution; however, *max(rotmat)* is not considered to be a suitable criterion for the determination of the number of factors (Lanz et al., 2007).

- The rotational freedom of a solution may be explored through a non-zero valued user-specified rotational parameter *fpeak*. *Fpeak* > 0 tries to impose rotations on the emerging solutions using positive coefficients *r* in **T**, *fpeak* < 0 vice versa. *Fpeak* = 0 produces the most central solution.

- Generally high mass loadings in the residuals or, more specifically, structures in the residuals can indicate solutions that do not explain the measurements well.

- A too high number of *p* can often lead to the split-up of a factor of a solution with a lower number of *p*, indicated by high similarities of factor profiles or time series within a solution.

- Usually superimposed on the mathematical criteria to determine a solution are the comparisons of the resulting mass spectra and their time series with ancillary data and reference spectra (e. g. Ulbrich et al., 2007).

The model was solved with the PMF2 algorithm v.4.2. (Paatero, 2007) in the robust mode without modification of the convergence criteria, and results were analyzed using the PMF evaluation tool (PET 2.03A, Ulbrich et al., 2009).

3

SPATIAL VARIATION OF CHEMICAL COMPOSITION AND SOURCES OF SUBMICRON AEROSOL IN ZURICH DURING WINTERTIME

3.1   Abstract

Mobile measurements of PM_1 (particulate matter with an aerodynamic diameter < 1 μm) chemical composition using a quadrupole aerosol mass spectrometer and a multi-angle absorption photometer were performed using the PSI mobile laboratory during winter 2007/2008 and December 2008 in the metropolitan area of Zurich, Switzerland. Positive matrix factorization (PMF) applied to the organic fraction of PM_1 yielded 3 factors: Hydrocarbon-like organic aerosol (HOA) related to traffic emissions; organic aerosol from wood burning for domestic heating purposes (WBOA); and oxygenated organic aerosol (OOA), assigned to secondary organic aerosol formed by oxidation of volatile precursors. The chemical composition of PM_1 was assessed for an urban background site and various sites throughout the city. The background site is dominated by secondary inorganic and organic species (57%), BC, HOA, and WBOA account for 15%, 6%, and 12%, respectively. As for the other sites, HOA is important along major roads (varying between 7 and 14% of PM_1 for different sites within the city, average all sites 8%), domestic wood burning makes up between 8 − 15% of PM_1 for different sites within the city (average all sites 10.5%). OOA makes up the largest fraction of organic aerosol (44% on average).

A new method allows for the separation and quantification of the local fraction of PM_1 emitted or rapidly formed in the city, and the fraction of PM_1 originating from the urban background. The method is based on simultaneous on-road mobile and stationary background measurements and the correction of small-scale meteorological effects using the ratio of on-road sulfate to stationary sulfate. Especially during thermal inversions over the Swiss plateau, urban background concentrations contribute substantially to particulate number concentrations (between 40 and 80% depending on meteorological conditions and emissions, 60% on average) as well as to the mass concentrations of PM_1 components measured on road in downtown Zurich (between 30 and 90%, on average 60% for black carbon and HOA, and between 90 and 100% for WBOA, OOA, and the measured inorganic components). The results emphasize, on a scientific level, the advantage of mobile measurements for distinguishing local from regional air pollution research, and on a political level, the importance of regional collaboration for mitigating air pollution issues.

3.2   Introduction

Health effects of particulate matter (PM) are especially important in highly populated areas. A growing portion of the world's population lives in cities and megacities, being exposed to an increased risk of morbidity and pre-mature mortality due to poor air quality (Baldasano et al., 2003; Molina and Molina, 2004; Gurjar et al., 2010). Therefore, field campaigns in urban centers (e. g., Milan, Italy, Mexico City, Mexico, Barcelona, Spain), addressing emissions from urban anthropogenic activities as well as the evolution of the city's pollution plume to surrounding areas, are an important and widely applied part of aerosol research (e. g. Baltensperger et al., 2002; Zhang et al., 2004; Molina et al., 2010; Pandolfi et al., 2012). The city of Zurich, Switzerland, with ~400 000 inhabitants, has been the focus of previous field studies, e. g. investigations on the contribution of road traffic to ambient levels of fine particles (Gehrig et al., 2001), non-exhaust particles generated by road traffic (Bukowiecki et al., 2010), the chemical composition of PM (Hueglin et al., 2005), sources of organic aerosol by means of factor analytical modeling of mass spectrometer data (Lanz et al., 2007), or the fossil and non-fossil fraction of carbonaceous aerosol (Szidat et al., 2006). Especially high PM concentrations (up to 120 μg m^{-3}) can be observed during winter time due to thermal inversions preventing dilution of emissions, and increased emissions from wood burning for domestic heating purposes (Lanz et al., 2008).

The present study combines ground-based mobile aerosol mass spectrometer (AMS) measurements with positive matrix factorization (PMF) source apportionment. It was our goal to explore the spatial variation of the chemical composition of PM_1 (particulate matter with an aerodynamic diameter $d_a < 1$ μm) for winter time in the city of Zurich. A new method to

distinguish the local fraction of PM_1 from the fraction related to the urban background will be presented. This differentiation is of high importance for local policy makers concerned with air quality.

3.3 Methods

3.3.1 Zurich mobile measurement campaigns

For 10 days between 27 November 2007 and 16 December 2008 on-road mobile measurements were performed in the city of Zurich, Switzerland (400 m a.s.l.), representing 66 hours of data. Measurements of the PM_1 chemical composition, size distribution and number concentration, trace gas concentrations (NO_X, CO, CO_2), and meteorological and geographical parameters (temperature, relative humidity, solar radiation, altitude, longitude, latitude) were conducted. Figure 10 gives an overview of the dates and times of measurement and the number of loops driven along the chosen route. The route was chosen such that major traffic arteries, residential areas, suburbs, and surrounding hills were covered. After each loop, stationary data were acquired at the urban background site "Kaserne" for a few minutes. Zurich Kaserne has been characterized in previous studies as "urban background" for PM_{10}, $PM_{2.5}$, and PM_1 and additional air quality parameters (Gehrig and Buchmann, 2003; Hueglin et al., 2005; Szidat et al., 2006; Bukowiecki et al., 2010; Lanz et al., 2008). It is a courtyard shielded from direct emissions by its surrounding walls. In addition, the roads in its vicinity belong to residential areas with only minor traffic density. The site is part of the Swiss National Air Pollution Monitoring Network (NABEL).

Mobile measurements were usually performed during morning and evening periods, when traffic and domestic heating emissions are at their maximum (Lanz et al., 2008; Krecl et al., 2008), for about 3-4 hours each, and normally included 3 loops per half-day. The elevated areas (Buchegg Square – Limmattal Station, 550 m a.s.l., and Üetliberg, 800 m a.s.l.) were covered once per half-day. The section leading up to Üetliberg and the one from the main train station to Selnau were only made in December 2008.

3.3.2 Mobile laboratory and instrumentation

Measurements were performed with the PSI mobile laboratory and instrumentation as described in chapter 2. The majority of data presented in this chapter was collected with the Q-AMS, providing information on the non-refractory chemical components with a vacuum aerodynamic diameter ≤ 1 µm, including ammonium (NH_4^+, further denoted as NH_4), nitrate (NO_3^-,

in the following denoted as NO_3), sulfate (SO_4^{2-}, denoted as SO_4), chloride (Cl^-, denoted as Chl), and organics. Polycyclic aromatic hydrocarbons (PAHs, formed during burning or pyrolysis of organic matter in incomplete combustion (Dzepina et al., 2007)) were included in total organic mass loadings unless specified differently. The instrument was operated in the mass spectrum (MS) mode only, with an averaging time of 6 s (50 % open/closed), scanning an *m/z* range from 1 - 300. No drier was used prior to Q-AMS sampling, as is generally recommended in order to control RH and particulate phase water. This is an important parameter influencing the collection efficiency of the instrument after the lens (Cross et al., 2009). However, the temperature difference between outside and inside the mobile laboratory has a (varying) drying effect on the sample air, as it reduces relative humidity (RH) inside the van (e. g. for campaign average values from 79% RH at 2 °C outside to 33% RH at ~15 °C inside).

3.3.3 Data Analysis

Source components of the organic fraction measured by Q-AMS were defined using PMF (Paatero and Tapper, 1993; Paatero and Tapper, 1994; Lanz et al., 2007; Ulbrich et al., 2009)). Q-AMS data were analyzed using the standard algorithm developed by Allan et al. (2004) (AMS Analysis Toolkit 1.41) within Igor Pro 6. The fragmentation table for organics was modified according to Aiken et al. (2008). The CE of the Q-AMS was determined to be 0.85, based on a comparison of the mass concentrations of the sum of Q-AMS and MAAP data (non-refractory PM_1 plus BC) with a tapered element oscillating microbalance (TEOM) monitor (Thermo). This comparison was performed in the time period of 27 November 2007 to 10 January 2008. An Aerodyne high-resolution time-of-flight (HR-ToF-AMS) was measuring at the background site during December 2008. The CE of the HR-ToF-AMS was determined to be 1 (Richard et al., 2011). Q-AMS (CE = 0.85) and HR-ToF-AMS (CE = 1) agreed very well (maximum difference 10% for all comparison periods). A high ammonium nitrate fraction (42% of total PM_1 mass on average) and possible high aerosol water content due to a lack of a specific drying unit in the sample air (see section 3.3.2) support the relatively high Q-AMS CE. Comparisons of various AMS datasets from all over Europe within the EUCAARI/EMEP project show that ammonium nitrate fractions of > 0.25 can already lead to a CE above 0.5 (Nemitz et al., 2012, in preparation). Interestingly, Hildebrandt et al. (2010) found, based on the method by Kostenidou et al. (2007), exactly the same CE for this instrument, when it was operated in Crete.

All data including gas phase species were averaged to 1 min to match the averaging time chosen for the Q-AMS data. The quadrupole mass spectrometer scans consecutively through mass-to-charge ratios (*m/z*'s) 1 - 300, spending a finite time at each *m/z*. As described in Bahreini et al.

(2003), particle counting statistics hence impose additional limitation on the signal-to-noise ratio. Assuming that at least 10 particles are required to be detected at each *m/z* for a relevant representative average of the ambient chemical composition, and an aerosol number concentration of ~30 000 (rounded median of all CPC measurements), it takes 0.3 s (14 s) to measure 10 particles (10 "high-mass particles" (Jimenez et al., 2003)) at a given *m/z* in MS mode. Hence 1 min averaging time corresponds to a temporal resolution sufficiently low to get a representative sample of the ambient PM_1 chemical composition but still high enough in terms of spatial resolution (225 m with a campaign average driving speed of 13.5 km h^{-1}).

AMS data uncertainties were calculated using the algorithm developed by Allan et al. (2003). Further modification steps of the elements σ_{ij} of the uncertainties matrix were done according to the protocol detailed in Ulbrich et al. (2009). *m/z*'s directly proportional to *m/z* 44 (*m/z*'s 16, 17, 18, and 28) were not downweighted, since downweighting of those variables led to no feasible PMF solution (see supplementary information SI, Fig. 19). As stated in Lanz et al. (2007), meteorology plays a dominant role in aerosol mass concentrations during Swiss plateau winters, governing the diurnal pattern of emissions, which makes it difficult for PMF to differentiate between the different factors. Increasing the weight of *m/z* 44 by a factor of 2.24 (the square root of the number of m/z 44-related ions, Ulbrich et al., 2009) relative to normally calculated errors was just sufficient a priori information to yield an atmospherically relevant PMF solution. Richard et al. (2011) observed the same for their dataset obtained from stationary measurements in Zurich Kaserne in December 2008.

Due to the time gap between the measurements in winter 2007 and December 2008 and thus varying instrument performance (with an especially bad resolution of the quadrupole mass spectrometer during December 2008 measurements, compare section 3.4.2), the organic dataset had to be split into two parts for the application of PMF (part 1: measurements days November 2007 – February 2008; part 2: December 2008). PMF2 was run in the robust mode (outliers $|e_{ij}/\sigma_{ij}| > 4$ were dynamically reweighted during fitting to not pull the fit excessively). The model error (term in the uncertainties estimation proportional to the signal), which is intended to decrease the *Q*-value for points that do not fit the model, was set to 0 (Ulbrich et al., 2009).

3.4   Results

3.4.1 Overview of measurements

Figure 10 gives information on dates and times of measurements, the number of loops on the measurement route in the corresponding time interval, the mean temperature, as well as an overview on the parameters measured and their variability. The importance of meteorological conditions for the day-to-day variation of the pollutant concentrations becomes evident looking at concentration trends of all measured parameters, all of which follow a roughly similar temporal pattern. Zurich lies on the Swiss plateau, a densely populated region wedged in between the Jura mountains in the north and the Alps in the south. In winter, frequent thermal inversions lead to an entrapment and hence accumulation of emissions and subsequently formed secondary components, resulting in a rather uniform distribution of pollution throughout the whole Swiss plateau region (Lanz et al., 2010).

Figure 20 in the SI shows such a situation for 29 November 2007, where air masses had been residing over Switzerland for 3 days before arriving at the receptor site. Consequently, the 3 measurement days in November 2007 were characteristic of a gradual accumulation of pollutants, e. g PM_1, PAHs, and CO_2. The decrease in number concentration at the same time could be due to processing of air masses, leading to particle growth through coagulation/condensation.

The Sunday of 16 December 2007 showed low concentrations for all parameters due to fewer emissions (Sunday ban of heavy-duty traffic). 08 January 2008 was the first day after a rainy period, hence particle mass concentrations were low since there was only little time for processing of the air masses and accumulation of pollutants. On 15 February 2008, *m/z* 39 (a wood smoke marker with contributions from K and $C_3H_3^+$ ions), and PAH concentrations were particularly low compared to total PM_1, most likely due to the fact that measurements were only performed during the morning, and evening emissions from wood burning for domestic heating purposes are usually higher than morning emissions. The highest PM_1 concentrations (median 50 μg m^{-3}, equal to the Swiss 24h-legal limit that must not be exceeded more than once a year) were recorded on 19 February 2008, a day during a period of stable temperature inversion and subsequent accumulation of pollutants.

Stagnant air masses due to thermal inversion also led to an accumulation of pollutants from 14 – 15 December 2008. NO_X, in Switzerland mostly emitted from fossil fuel combustion from traffic (58 %), but also from households (7 %), industry (25 %), and agriculture (10 %) (BAFU, 2009), showed concentrations up to 100 ppb (median) and 140 ppb (upper quartile) on 15 December, far above the mean value of 30 ppb for December 2008 – February 2009 measured at Zurich Kaserne by NABEL. However, it must be taken into account that measurements were

performed on road and hence there was a substantial influence by local tailpipe emissions. The median of the CO concentration, a byproduct of incomplete combustion, were within the range of the annual mean of 0.36 mg m^{-3} (~315 ppb) (BAFU and EMPA, 2009). Rather high wind speed (up to 4 m s^{-1}) on 14 December 2008 and a change in meteorological conditions (start of a frontal passage) including breakup of the inversion in the late afternoon of 16 December 2008 led to PM$_1$, *m/z* 39, PAHs, and number concentrations that were at the lower end of the concentration range for part 2 compared to the other days.

Since mobile measurements are only point measurements, the question of representativeness arises. Figure 21 in the SI presents a frequency plot of PM$_{10}$ daily averages of the periods 01 November 2007 – 28 February 2008 and 01 December 2008 – 31 December 2008 at the urban background site Kaserne, with the values corresponding to the days of mobile measurements colored in black. The distribution of the mobile measurement days covers the full range of PM$_{10}$ mean values, indicating that the chosen days gave a reasonable overview of the concentration range observed in these two winters.
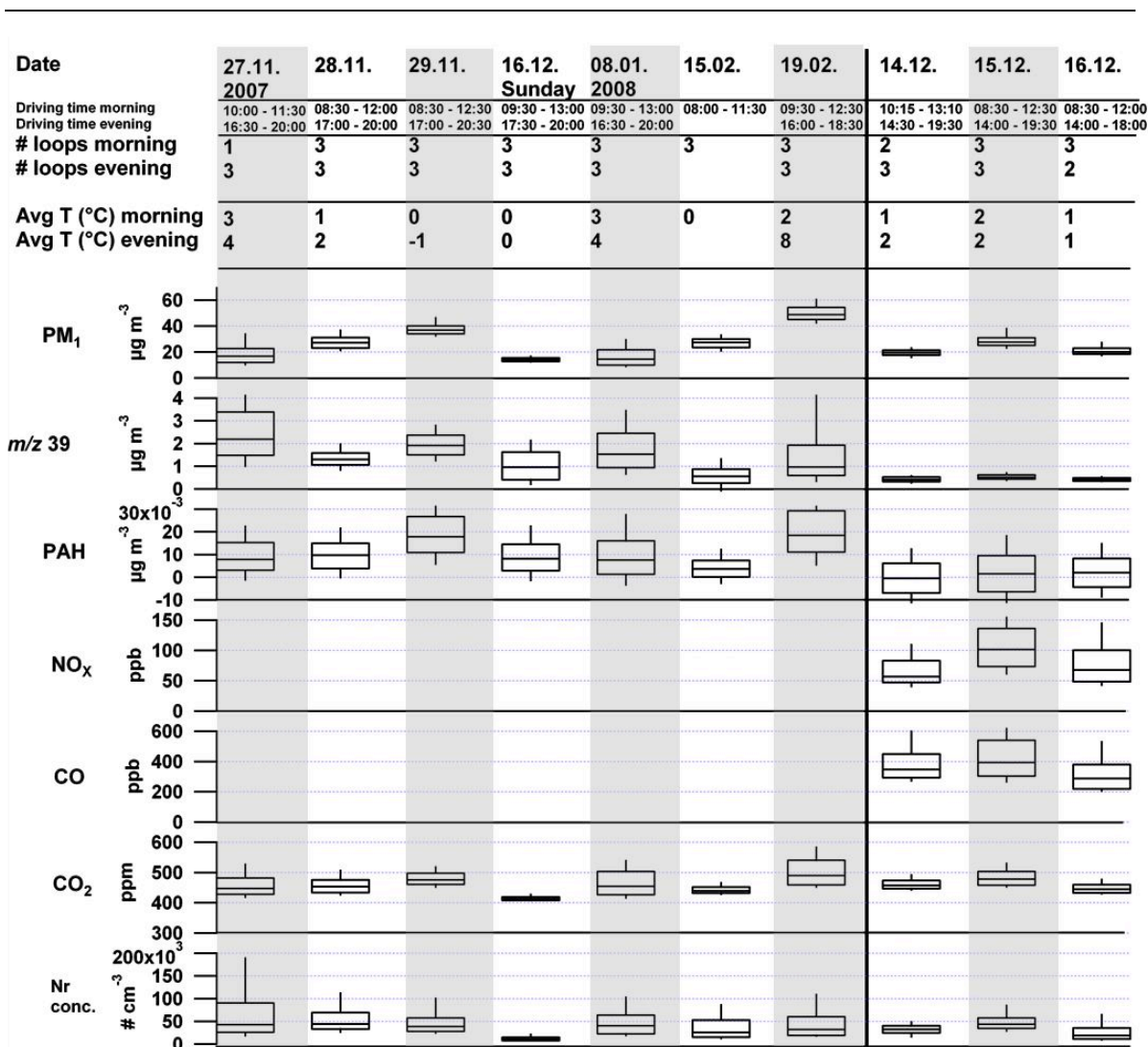
Figure 10: Overview of drives. Number of loops states how many times the measurement route in Fig. 14 was driven in the given time interval. PM_1 includes AMS and MAAP measurements; m/z 39 and PAH mass concentrations were measured by Q-AMS. Boxes represent upper and lower quartiles, horizontal lines correspond to the median, and whiskers denote 10%- and 90%-percentiles. The vertical line shows the division of the dataset into part 1 and part 2. 16 December 2007 is the only Sunday measured, all other days are weekdays.

3.4.2 PMF results: Organic source components

For both part 1 and part 2 of the organic data matrix measured in Zurich by Q-AMS, three factors were found, attributed to the following components: Hydrocarbon-like organic aerosol (HOA) representing the fraction of organics related to primary traffic emissions; wood burning organic aerosol (WBOA) from wood burning for domestic heating purposes; and oxygenated organic aerosol (OOA), which represents secondary organic aerosol formed by oxidation and condensation of volatile organic precursors (Fig. 11). The mass spectral profiles found independently for the two parts are well correlated: Using the full spectra for the correlation

yielded R^2 values of 0.97, 0.97, and 0.93 for OOA, HOA, and WBOA, respectively; and slopes of 1.04, 1.18, and 1.04 for OOA, HOA, and WBOA, respectively. When correlating the OOA spectra of part 1 and part 2 without the peaks related to *m/z* 44 (i.e., removing *m/z*'s 16, 17, 18, and 28), the same R^2 of 0.97 was found.

The HOA factors show high signals of the ion series $C_nH_{2n+1}^+$ (*m/z* 29, 43, 57, 71, ...) from saturated alkanes, and $C_nH_{2n-1}^+$ (*m/z* 41, 55, 69,...) from alkenes plus cycloalkanes. Diesel exhaust is typically dominated by recondensed engine lubricating oil and consists mainly of n-alkanes, branched alkanes, cycloalkanes, and aromatics (Canagaratna et al., 2004). Correlation of the HOA factors found here with the standard HOA mass spectral profile from Ng et al. (2011b) yields R^2 values of 0.98 and 0.9 for part 1 and part 2, respectively, showing their high similarity. The factors identified as OOA have their dominant signal at *m/z* 44, which mostly represents CO_2^+ from the thermal decomposition of organic acids (Alfarra, 2004). This is in accordance with previous findings suggesting that the fraction of *m/z* 44 in the organic spectra increases with photochemical aging (Ng et al., 2010). Comparisons with the standard OOA spectrum from Ng et al. (2011b) show high similarity (R^2 of 0.96 and 0.83 for part 1 and part 2, respectively). *m/z*'s 17, 18, and 28 were removed from the fit due to differences in the frag table used here (Aiken et al., 2008). The presence of significant signal at *m/z* 60 in the WBOA spectra helped identify their origin, since *m/z* 60 is attributed to $C_2H_4O_2^+$, a fragment of levoglucosan which in turn is a pyrolysis product of cellulose (Alfarra et al., 2007). R^2 of 0.83 and 0.63 were found for the correlations of the WBOA factors with the standard biomass burning (BBOA) spectrum from Ng et al. (2011b) for part 1 and part 2, respectively.

Rotational ambiguity leads to non-unique solutions still fulfilling the non-negativity constraint (Paatero et al., 2002). The rotational freedom of the chosen solution can be explored through a user-specified rotational parameter *fpeak* and was chosen to be -0.1 for part 1, and 0 for part 2. DeCarlo et al. (2010) explored the solution space for the chosen *fpeak* running PMF with 50 random initial values *(SEED)* at iteration start. For the present dataset, *SEED* values between 0 and 50 yielded two solution groups. For the group not representing the present solution corresponding to *SEED* = 0, WBOA and OOA were less clearly separated (Pearson's R value of 0.77, compared to 0.44 for the present solution). For further detailed discussion of parameters chosen and mathematical criteria for the number of factors determined we refer the reader to section 3.7.4.

For part 2, *m/z* 29 was removed from the matrix before running PMF due to exceptionally low resolution of the quadrupole mass spectrometer making the separation of neighboring peaks such as *m/z* 28 and *m/z* 29 difficult. *m/z* 29 was then reintegrated as a linear combination of fractions of the PMF solutions HOA, OOA, and WBOA, respectively, of part 2: The measured time series of *m/z* 29 was fit using Eq. (7), where $G_1 - G_3$ represent the time series of factors 1 -3 (OOA,

HOA, and WBOA) of the PMF solution, and the resulting a, b, and c the fractions of m/z 29 of each factor. e denotes an error term.

$$f(G_1, G_2, G_3) = G_1 * a + G_2 * b + G_3 * c + e$$

(7)

In addition, part 2 comprises fewer data with an overall lower signal-to-noise ratio (SNR) than part 1 (not shown), from 3 days of relatively stable meteorological conditions, making the differentiation of factors more difficult. Especially HOA and WBOA can potentially be difficult for PMF to be separated perfectly, as has been observed by e .g. Aiken et al. (2010) and DeCarlo et al. (2010). For WBOA, the solution chosen for part 2 has lower signal at m/z's 41, 43, 55, and 57 than the part 1 solution. However, choosing an *fpeak* with a higher fraction of m/z 57 (*fpeak* < 0) would lead to a solution with lower signal at m/z 60, a marker of biomass burning emissions (see above). For *fpeak* = 0.1, m/z 60 in WBOA would be at a maximum, but for *fpeak* ≥ 0.1 the contribution from m/z 44 in WBOA becomes zero (Fig. 29 in the SI), which is not in accordance with wood burning emission studies (e. g. Heringa et al., 2011).

The results found here are in good agreement (R^2 of 0.99 (0.98), 0.99 (0.97), and 0.85 (0.66) for OOA, HOA, and WBOA part 1 (part 2), respectively) with the factors found for stationary measurements at the urban background site Kaserne in January 2006 by Lanz et al. (2008), who used a hybrid receptor model solved by the multilinear engine (ME-2) which incorporates a priori known source composition. The same three PMF factors (with R^2 of 0.98 (0.97), 0.87 (0.86), and 0.87 (0.79) for OOA, HOA, WBOA part 1 (part 2), respectively) were also found by Richard et al. (2011) for a unit mass resolution (UMR) organic dataset again from Zurich Kaserne, measured by a high-resolution time-of-flight AMS in December 2008.

Additional quality assurance of PMF results was done by comparing the time traces of factors 1 to 3 with measured marker mass fragments, inorganic components, and ancillary data (Fig. 33 – 36 in the SI). Least squares estimates are very sensitive to outliers (non-robust method), and especially the BC data, but also the PMF factor time series of part 2 and gases time series exhibited many spikes. The beforehand mentioned low resolution of the Q-AMS during part 2 measurements led to rather noisy data. In addition, since the data were acquired while moving, short-time concentration peaks could partially be missed due to Q-AMS-specific particle counting statistics (compare section 3.3.3). Hence, the regression analysis of the corresponding time series proved to yield too low R^2 values to confirm a correlation even though they showed similar behavior when plotting the time traces on top of each other. Consequently, data for these comparisons were cleared of outliers (the upper 1st percentile of data was removed) and smoothed using a moving average of 5 data points. Figures 37 and 38 in the SI show the correlations for the

corrected and the uncorrected data, respectively. In the following, R^2 values calculated using smoothed data are in bold.

For part1 (part 2), the OOA time trend followed the time series of organic mass fragment 44 (CO_2^+), $R^2 = 0.99$ (**0.80**), HOA showed the same time trends as organic mass fragment 57 (mostly $C_4H_7^+$, also $C_3H_5O^+$), $R^2 = 0.92$ (**0.88**), and the WBOA time series followed organic mass fragment 60 ($C_2H_4O_2^+$), $R^2 = 0.51$ (**0.42**). Temporal trends of BC are more similar to those of HOA ($R^2 = $ **0.65** (0.67) for part 1 (part 2)) than WBOA ($R^2 = $ **0.18** (**0.19**) for part 1 (part 2)). This suggests that traffic emissions contribute more to PM_1 BC than wood burning emissions. This is supported by ^{14}C measurements in winter 2002/2003 in Zurich by Szidat et al. (2009): Fossil fuel usage contributed 75% and biomass burning 25% to elemental carbon (EC). For CO and NO_X, available only for part 2, R^2 values with HOA of **0.42** and **0.73**, respectively, were found, again confirming the relation of HOA to traffic emissions. As observed by Lanz et al. (2008), the OOA time series was correlated with NH_4 ($R^2 = 0.73$ (**0.35**) for part 1 (part 2)) and the sum of NO_3 and SO_4 ($R^2 = 0.77$ (**0.39**) for part 1 (part 2)) rather than with NO_3 and SO_4 individually, supporting the interpretation of OOA as being mostly secondary. Ambient temperature shows a slight anti-correlation with OOA for part 1 (27 November 2007 – 08 January 2008: slope = -0.4, $R^2 = 0.3$, see Fig. 34 and 36 in the SI), indicating the importance of thermal inversions (with low boundary layer temperatures) for the build-up of secondary particle mass.
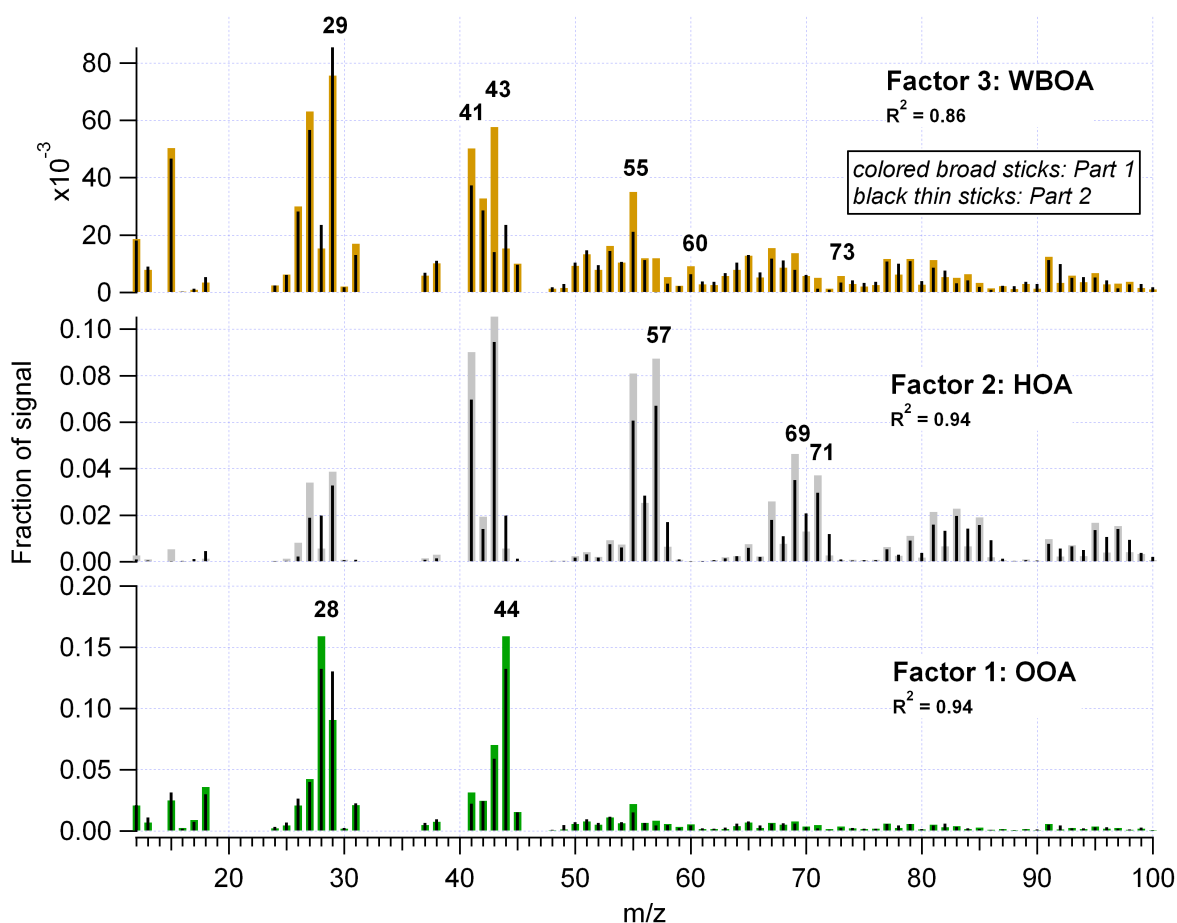
Figure 11: Normalized mass spectral signatures of factors 1 (OOA), 2 (HOA), 3 (WBOA) of the chosen PMF solution. Colored sticks and black sticks denote results for part 1 and 2, respectively. R^2 values quantify similarity of spectra from part 1 and 2.

3.4.3 PM$_1$ chemical composition

The chemical composition of PM$_1$ (mean per measurement day) is shown as absolute (A) and relative (B) values in Fig. 12, where the dotted black line separates the primary and secondary components. Generally, the ratio of primary to secondary components decreases when total concentrations increase, due to stagnant conditions inhibiting the exchange of air masses and thus allowing for their aging and accumulation of secondary aerosol. Note the difference in relative composition of 16 December 2007 and 08 January 2008, 2 days with similar total concentrations (14 and 17 ug m^{-3}, respectively) but different distribution of compounds. On 16 December 2007, a Sunday, traffic emissions were much lower compared to weekdays, due to the dominical ban of heavy-duty trucks, thus the fraction of primary compounds, especially HOA, was very low. In contrast, primary components dominated on 08 January 2008, since there had been only little time

to build up secondary aerosol mass following washout from precipitation in the preceding days (this is similar for the 27 November 2007 measurements).

Generally, the BC fraction made up ~22% of total PM_1, but this fraction increased substantially for days when primary emissions dominated PM_1 composition. OOA constituted the biggest organic fraction (on average 44% of total organics), as has been found in other places (Jimenez et al., 2009), and WBOA and HOA were less important (32% and 24%, respectively).

The meteorological conditions during the measurements did not allow for a separation of OOA into a low-volatility and a semi-volatile fraction, OOA-I/LV-OOA and OOA-II/SV-OOA, respectively, (Lanz et al., 2007; Hildebrandt et al., 2010) due to relatively small variations in daily temperature and diurnal patterns. However, the degree of oxygenation of OOA can be estimated by plotting the normalized signal at m/z 44 (f_{44}) vs. the normalized signal at m/z 43 (f_{43}) from PMF-OOA spectra (Ng et al., 2010). The PMF-OOA f_{44} and f_{43} values of various datasets acquired all over the world form a triangle (black dotted lines in Fig. 13). The OOA found here lies in the middle of this triangle, and can thus be interpreted as moderately processed OOA with a degree of oxygenation that does not correspond to highly aged air masses. For comparison reasons, the f_{44}/f_{43} values for HOA and WBOA are included as well. In addition, Fig. 13 shows f_{44}/f_{43} values of the measured spectra (where f_{44} and f_{43} also have contributions from HOA and BBOA and thus do not fall fully into the triangle shape). Nevertheless it can be shown that the previously discussed day of 08 January 2008 sticks out (light green), with lower f_{44} and slightly higher f_{43} than the average campaign data, again consistent with this day being dominated by fresh emissions and less aged air masses.

The inorganic fraction is dominated by nitrate, as is common in Swiss winters, when cold temperatures favor ammonium nitrate partitioning into the particle phase (ammonium nitrate formation is unlikely to be limited by ammonia (Andreani-Aksoyoglu et al., 2008)).
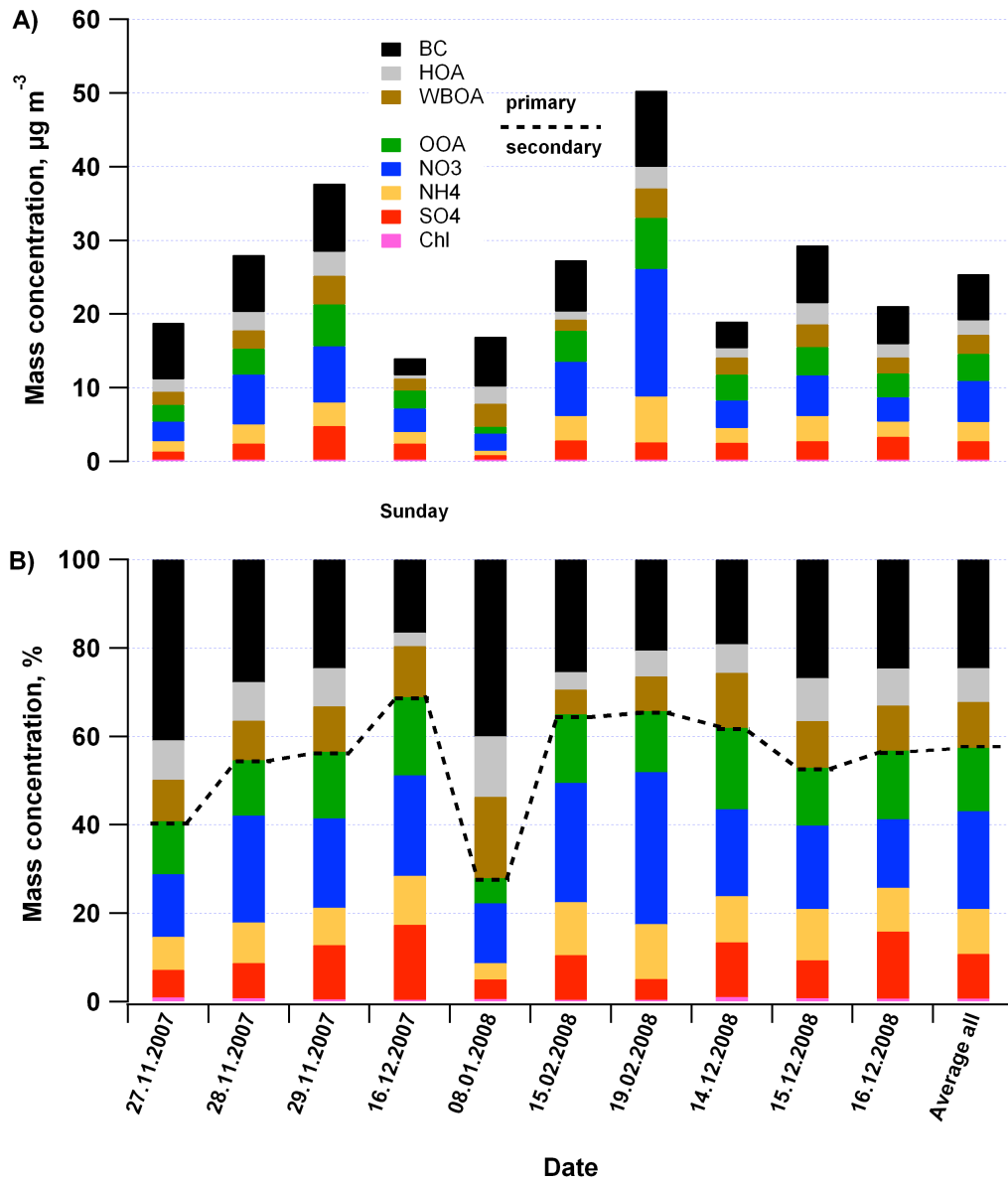
Figure 12: Absolute (A) and relative (B) composition of PM1, average values per measurement day (complete drive including stops at background station) and average over whole dataset ("average all"). The dashed line shows the proportions of primary and secondary components.
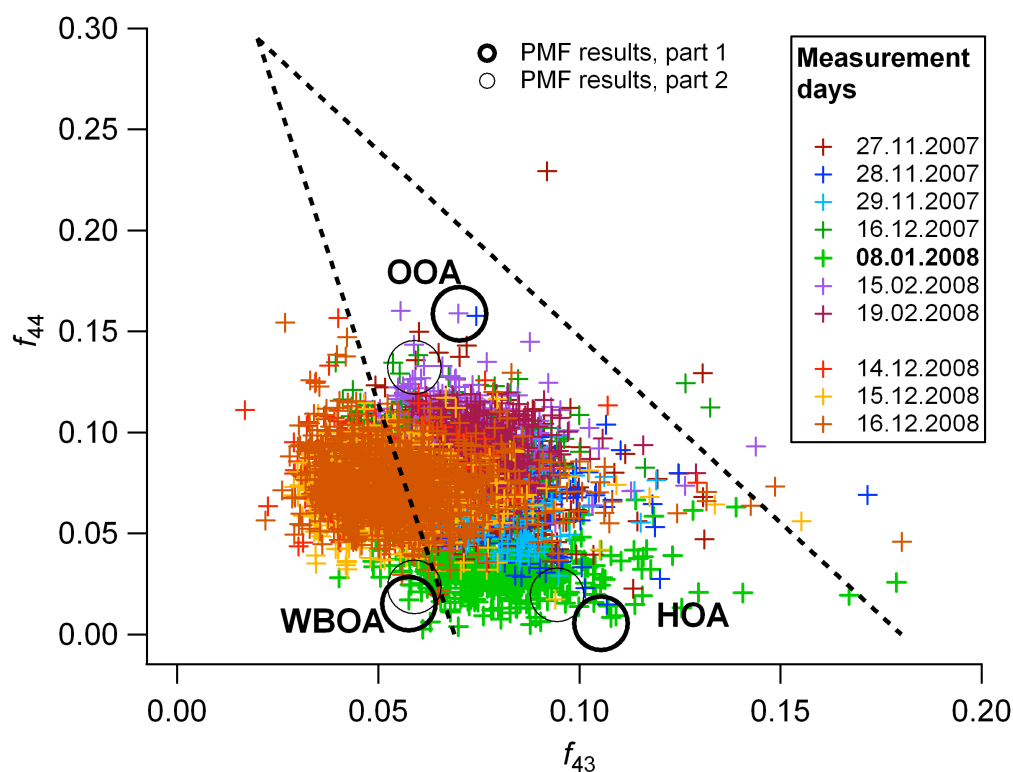
Figure 13: Fractions of organic mass fragments 44 (f_{44}) and 43 (f_{43}) in the Ng triangle (Ng et al., 2010), measured. Black circles show the fractions for the resulting spectra from PMF. The measurement day of 08 January 2008 (light green dots) with a low secondary contribution (Fig. 12) shows a lower degree of oxygenation than the other data.

3.4.4 Spatial variation of chemical composition

Mobile measurements add an additional dimension of space to a dataset. Mapping the spatial variation of PM_1 concentration and composition as measured by AMS and MAAP (including the results from the PMF analysis) in Zurich yields a rather consistent picture, with small differences depending on present local primary emission sources or altitude (Fig. 14). On average, the highest mass concentrations were measured on main traffic arteries within city limits (e. g. Rosengarten Street with 47 μg m^{-3}). Elevated areas such as Höngg (26 μg m^{-3}) experience enhanced dilution, or, as Üetliberg, can lie outside the boundary layer and are thus less influenced by emissions from the city. Residential areas and lower traffic roads show similar concentrations throughout the city area between 22 μg m^{-3} (Triemli) and 32 μg m^{-3} (Meierhof Square).

In addition to the homogeneity of overall PM_1 concentration, the equally uniform spatial distribution of the chemical composition again confirms the influence of meteorology on air pollution levels as mentioned above. However, a clear distinction can be made between the urban background site "Zurich Kaserne" and the sites covered during mobile measurements. At the background station, 50% of PM_1 are comprised of secondary inorganic compounds such as

ammonium nitrate and ammonium sulfate, BC makes up 15%, and the organic fraction is dominated by OOA (49% of organics), followed by WBOA (34%) and HOA (17%). Lanz et al. (2008) found in their analysis of Zurich Kaserne data 3 - 13% HOA, 52 - 57% OOA, and 35 - 40% WBOA for winter 2006. The differences to the average organic composition measured throughout the city as described in the previous section can be explained by the different setup of measurements – the contribution of HOA is expected to be larger on-road than for stationary measurements at the urban background site. Interestingly, the WBOA fraction was very similar for both the urban background site (34%) and on-road (32%), implying that the WBOA source is either regional, or well mixed on the local scale due to its emission typically from chimneys and subsequent downmixing. Richard et al. (2011) found a much lower ratio WBOA/HOA (17%/22%) for Zurich Kaserne, 01 - 18 December 2008, and a higher OOA percentage (60%). During December 2008, homeless people were regularly lighting fires in the late afternoon close to the measurement station. We hypothesize that this led to a local WBOA factor in the solution of Richard et al. (2011), explaining less of the variation of PM_1 and ignoring the regional WBOA contribution due to its similar temporal pattern with regional OOA, at least to some extent. To better compare the data from Richard et al. (2011) to our results, the PMF2 algorithm was run on the last part of their dataset only (15 -18 December 2008, the period of part 2 of the mobile measurements), when the open fires were banned from the site. The variation of the 3 factor contributions became much more congruent with the results found for this study: HOA 15%, OOA 50%, WBOA 32% (plus 3% in the residual).
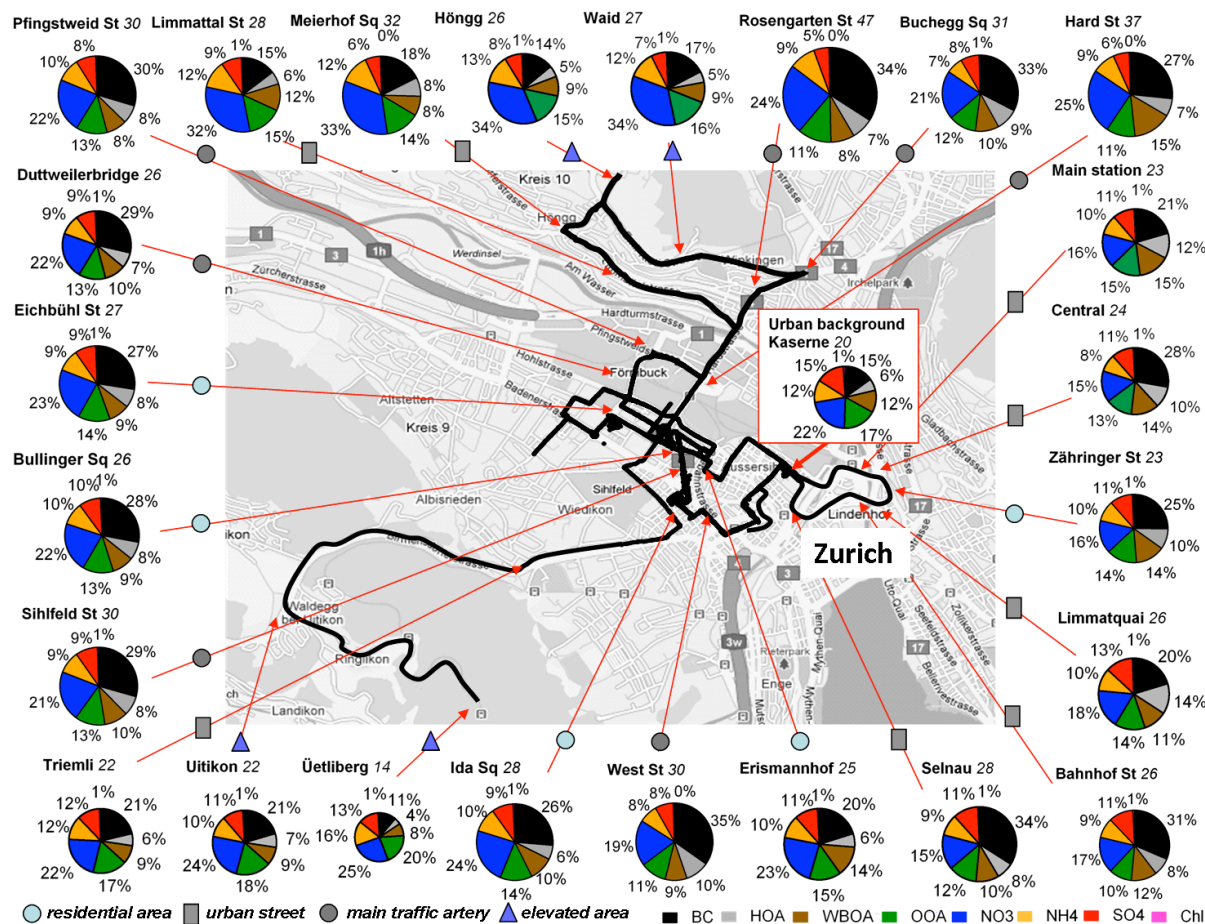
Figure 14: Spatial variation of the PM_1 chemical composition as measured by Q-AMS and MAAP, PMF results included, in the area of Zurich city. Pie areas are relative to total average concentrations from all measurements, absolute concentrations are given in μg m^{-3} (numbers in italics behind site names). Sites are categorized according to residential areas, urban streets, main traffic arteries, and elevated areas.

For the other sites, carbonaceous material (BC, HOA, WBOA, and OOA) makes up the biggest fraction with up to 60%, except for the elevated areas (without Uitikon) where inorganic constituents such as ammonium nitrate and ammonium sulfate constitute more than half of PM_1 mass. BC is the most abundant component, contributing to up to 35% of PM_1 mass on major traffic arteries such as West Street or Rosengarten Street. OOA is the organic compound with the highest concentrations for almost all sites throughout the city. Interestingly, for many sites WBOA concentrations exceed HOA concentrations. The importance of wood burning emissions in Zurich has already been described by Lanz et al. (2008). Many houses in Zurich feature a fireplace or use exclusively wood for heating purposes, e.g. at the residential area "Erismannhof" where WBOA accounts for 14% of PM_1. The fact that even on major traffic arteries, higher contributions from wood burning than from traffic emissions are often measured, can be explained by wood burning emissions being part of a regional air pollution problem. Switzerland is a country with many rural areas, where wood burning for domestic heating purposes is abundant, and contributes substantially

to the overall PM concentrations in the Swiss plateau region during these winter periods. In addition, it has to be taken into account that wood burning as well as traffic emissions have a high potential for the formation of secondary organic aerosol (Chirico et al., 2010; Heringa et al., 2011), possibly doubling or even tripling the primarily emitted organic aerosol mass. Thus, both wood burning and traffic emissions contribute not only with primary emissions to organic PM_1 measured in Zurich, but also via OOA on a regional scale.

3.4.5 Background versus local contributions

Concept

The distinction and quantification of the fraction of PM_1 emitted or formed locally within the city limits, and the fraction of PM_1 from the background is of high importance, especially for policy makers implementing mitigation activities. The unique setup of the Zurich mobile measurements campaign featuring an urban background site (Zurich Kaserne) in combination with mobile measurements makes this task possible. As stated earlier, Zurich Kaserne lies in the middle of downtown Zurich but is shielded from direct traffic emissions: Its PM_1 chemical composition is different from that measured on-road (see Fig. 14) and representative of the urban background pollution. Lenschow et al. (2001) and Querol et al. (2004) showed that in a city area, the background PM concentration ("urban background") is elevated compared to the regional background PM concentration. However, Baltensperger et al. (2002) also showed that this enhancement is more pronounced for primary components (like BC) than for secondary components (like sulfate). When the meteorological conditions favor the build-up of secondary components and a uniform distribution of pollutants throughout the Swiss plateau (as was the case during our mobile measurements) a quite homogenous distribution over rural and background sites may be found also for PM_{10} or $PM_{2.5}$. Figure 39 in the SI presents the time series of PM_{10} (NABEL data) measured at Zurich Kaserne, in Payerne (a rural station ~100 km southwest of Zurich), and Tänikon (another rural station ~25 km northeast of Zurich) for the same time intervals as the mobile measurement drives (panel A) and their mean values (panel B, error bars denote ± one standard deviation). The urban background site shows very similar PM_{10} concentrations (31 µg m^{-3}) as the two rural stations Payerne (31 µg m^{-3}) and Tänikon (33 µg m^{-3}) on the Swiss plateau. Concerning $PM_{2.5}$, average values for 14 – 16 December 2008 (the days of mobile measurements) were 24.3 µg m^{-3} in Payerne and 25.5 µg m^{-3} at Zurich Kaserne.

Local contributions can be estimated by subtracting the background concentration of component S measured at Kaserne from the on-road concentration of component S measured at the same time. Methodological and dynamic-meteorological constraints impose further modifications

of this simple approach. Stationary measurements were always performed at Zurich Kaserne with the mobile laboratory a few minutes before and after a roundtrip of ~1 hour. Data acquired during a Kaserne visit were averaged and these mean values were linearly interpolated for the times when measuring on-road. The differences in concentration of components between the background and on-road measurements can be due to either local emissions, immediate formation of secondary components or to small-scale dilution and concentration effects of open squares compared to street canyons (inhomogeneities in the boundary layer). Numerous studies show that street canyons can be characterized by poor ventilation conditions, which in turn lead to high levels of air pollution (Vardoulakis et al., 2003). To assess the latter, a SO_4 scaling was introduced. The formation of secondary sulfate is rather slow, the oxidation rate of gaseous SO_2 by OH being lower by a factor of ~10 compared to NO_2 (Sander et al., 2003). The formation of OOA is also more rapid and effective than the sulfate formation. Chirico et al. (2010) and Heringa et al. (2011) have shown in their smog chamber experiments that diesel or wood burning emissions start to form OOA on very short time scales (primary concentrations were more than doubled within 1 hour for a diesel vehicle without aftertreatment, and the organic matter enhancement ratio for wood burning can be up to a factor of 2 after 1 hour). In addition, SO_2 concentrations in Switzerland are very low (mean value in January 2009: 8 μg m^{-3} (BAFU and EMPA, 2009)). There are no big point sources of SO_2 on the Swiss plateau, as there are no refineries and no SO_2 emitting power plants. Most important emitters are domestic heating appliances in winter, local small industries, or also emissions from traffic well distributed throughout the region.

The local concentration S_l of component S_m measured at time t at position p is then calculated using Eq. (8), making the following assumptions:

- Secondary formation and primary emissions of SO_4 are negligible during the course of one roundtrip (~1 hour).

- Differences in SO_4 between Kaserne and measurement point p are purely due to small-scale meteorological effects.

- The concept is valid only for measurements within the boundary layer.

$$S_{l,t,p} = S_{m,t,p} - \frac{SO_{4m,t,p}}{SO_{4b,t}} * S_{b,t} \qquad (8)$$

Subscript $_b$ refers to background (urban background site Kaserne).

In contrast to most other studies investigating urban emissions and their downwind plume (e. g. DeCarlo et al., 2010), our goal was not to assess emissions of the city and their fate downwind, but to assess the differences between local emissions and urban background. The city's emissions of course also contribute to the background but downwind of the city plume. The fraction of secondary components formed during one hour will be counted as local, whereas the fraction formed on a longer timescale will be quantified as urban background.

Confirming assumption 3, dilution effects (i.e., intrusion of air masses from above the boundary layer with a different relative composition) in open spaces (as opposed to street canyons) or elevated areas such as Meierhof Square and Üetliberg can lead to concentrations of S at position p that are lower than at the background site. Thus, the calculated local contribution becomes negative, showing also the limitations of the method presented here. As an alternative approach, local concentrations were also calculated without the SO_4 scaling factor (see Fig. 40 in the SI), e.g.

$$S_{l,t,p} = S_{m,t,p} - S_{b,t} \qquad (9)$$

Here, the S_b values were not averaged as above, but rather, the interpolated median value of 2 subsequent Kaserne visits was used for the S_b time series. This method decreases the negative local contributions, but also overestimates the local contributions by neglecting the meteorological effects and was thus discarded. Qualitatively, both methods yield similar results, with BC and HOA dominating the local contributions (see Fig. 40). Bukowiecki et al. (2002) estimated the background of CO and particle number concentrations using a moving 5-min 5%-percentile. A similar approach (using a moving 20-min lower 5%-percentile of each PM_1 component as background estimate) was also tested for the present dataset, but did not yield meaningful results. Just taking the lowest concentration of individual PM_1 components assumes that background and local aerosol compositions are the same, an implication contradicting the observations made here.

Local contribution of PM_1 components: Spatial variation

Figure 15 shows the results for the estimation of local contributions with the SO_4 normalization method for different places throughout the city and the mean value for all data in absolute (upper panel A) and relative values (lower panel B). BC concentrations dominate the composition of the local fraction of PM_1 measured in Zurich (1 – 12 µg m^{-3}, making up between ~30 and 80%). HOA also exhibits high local concentrations, adding another 0.5 – 2.5 µg m^{-3} or ~10 – 30% to the local PM_1 fraction. It can thus be concluded that traffic is the most important local contributor to PM_1 measured on road in Zurich. Concerning WBOA, substantial local contributions can be seen at the residential area "Erismannhof" (1 µg m^{-3} or 30 % of local PM_1) where wood is exclusively used for heating purposes. Surprisingly, also Bahnhof Street and

Hard Street, both busy roads, show enhanced local contributions of WBOA (1 - 2 μg m⁻³, or 15-20% of local PM₁, respectively). Residential areas in the vicinity of these roads seem to contribute more to primary organic aerosol (WBOA) than the emissions from traffic (HOA). Overall, compared to the high fractions of WBOA measured in Zurich, its local contributions are rather small. NO_3 is the secondary component with the highest local contributions, especially in areas dominated by traffic emissions (up to 1.5 μg m⁻³ or 10%, at Hard Street). This could either be due to the local NH_3 emissions of catalyst cars, or due to rapid oxidation of NO_2 to HNO_3 followed by neutralization with excess NH_3, both leading to enhanced NH_4NO_3 concentrations measured on road. Overall, mostly primary emissions contribute to local PM₁, while secondary aerosol, requiring processing and formation time, is generally part of the background air. For an explanation of negative values we refer to the previous section.
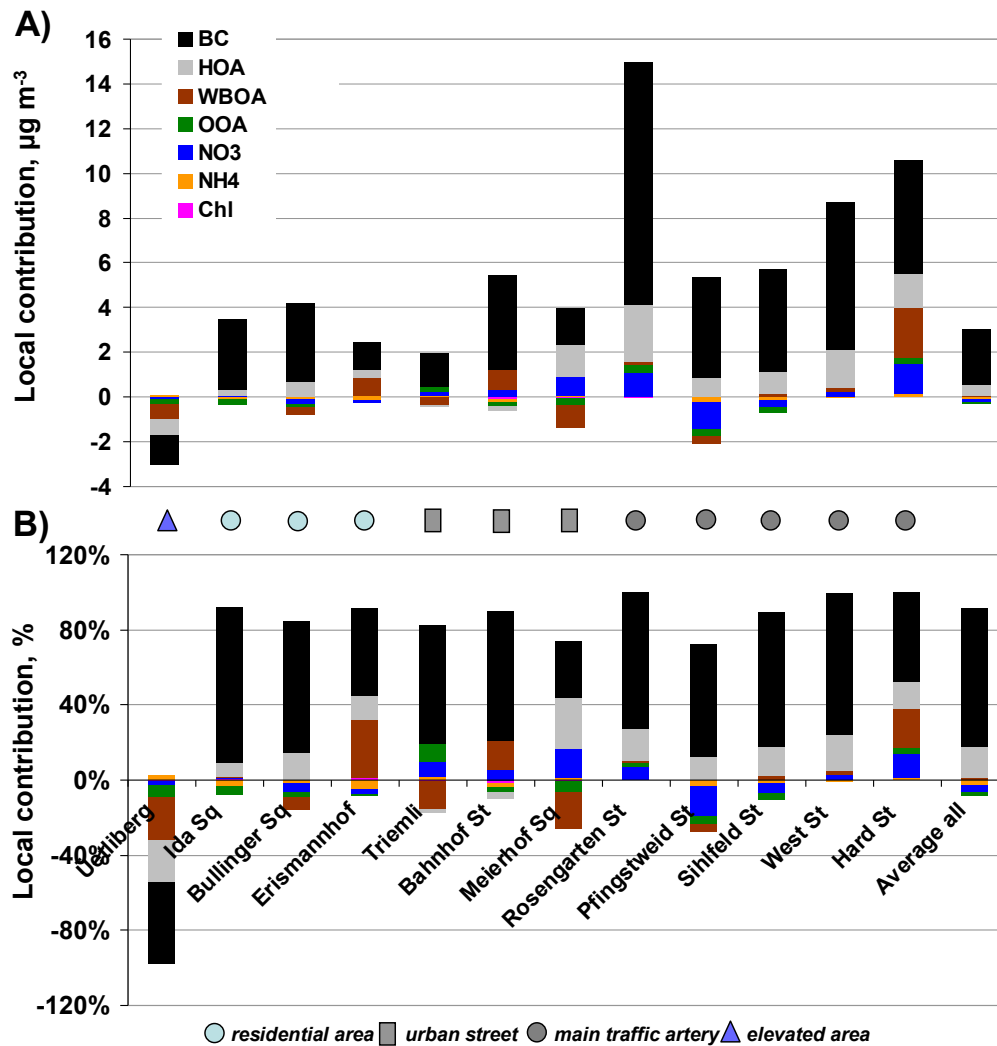
Figure 15: Local contributions of PM₁ components for different sites (absolute values panel A, relative values panel B), averages for the whole campaign are shown. The "average all" bar represents the mean value of the local contribution of all data.

A more general conclusion can be drawn from looking at the percentage of local contributions to measured concentrations for a defined component, or in other words the fraction of a specific aerosol component that is locally emitted or rapidly formed at a specific site. Figure 16 presents the values of these local contributions, averaged over the sites shown in Fig. 15 (the error bars denote ± standard deviation and show the day-to-day variability of the local contribution fraction, see next paragraph). As stated earlier, primary components from traffic such as BC and HOA exhibit on average (top panel) high local contributions (around 40%); a similar value (39%) was obtained for particulate PAHs but is not shown here because of large error bars due to very low loadings. In contrast, secondary components such as OOA are almost entirely part of the background pollution. The number concentration (measured by the CPC) shows the same high fraction of local contribution (40%) as BC and HOA, and can thus also to a great extent be related to traffic emissions. Interestingly, WBOA, also a primary component, has only very little local contribution in Zurich (~2% on average), and is mostly part of the background (see also Richard et al., 2011). Overall, more than half of primary PM_1 measured in Zurich during winter cannot be directly related to local emissions. For secondary inorganic components the local portion is even below 6%. This fraction is part of the Swiss plateau wide background air pollution trapped by thermal inversions. Nevertheless, it has to be taken into account that the time intervals considered for the calculation of the background concentration were short (see section 3.4.5, concept, ~1 hour) and thus secondary aerosol formation time was limited; and that Zurich contributes a large portion, which cannot be quantified, to the background pollution as well (compare section 3.4.5, concept). For the gas phase species (not shown), the local contributions amount to 20 and 10% for NO_X and CO, respectively. These values are lower than the local fractions of the traffic-related particulate emissions, but above the WBOA and OOA contributions. For CO_2, the method did not produce valid results, most likely due to the high background level. The alternative background estimation without SO_4 scaling yielded a similar pattern, but with 5 – 10% higher local contributions, in accordance to the statements made above.
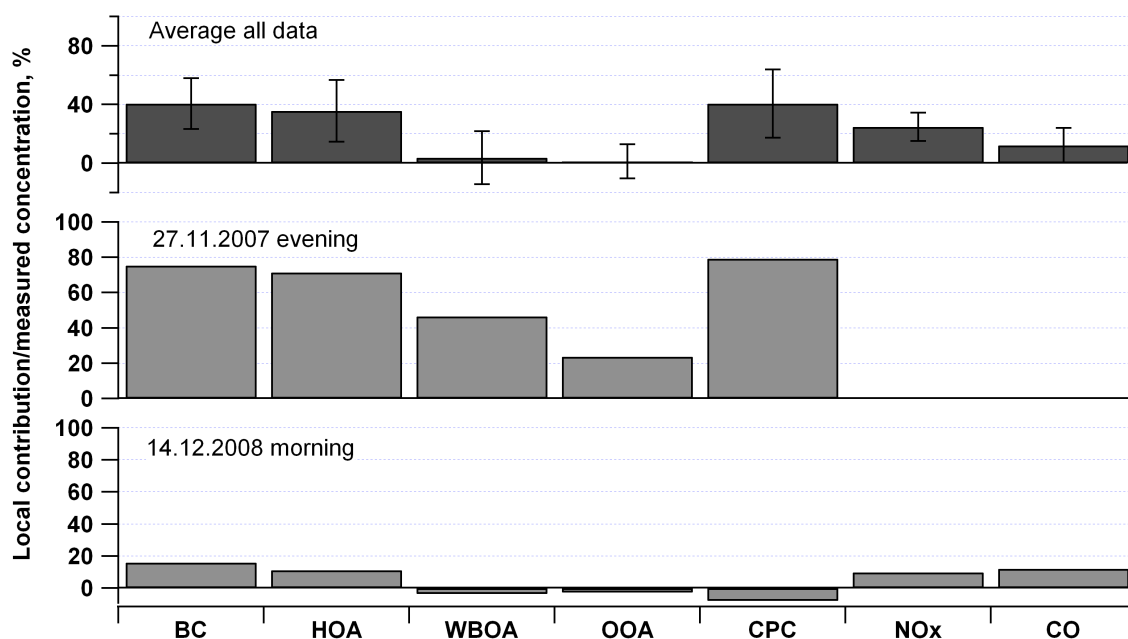
Figure 16: Percentage of local contributions to total measured concentrations for different components (average of all data ± 1 standard deviation, top panel) and 2 measurement drives. Note that for NO_X and CO (top panel) only part 2 data were included in the average (not measured for part 1). The percentage of background contributions to total measured concentrations can be derived from this plot by subtracting the value denoted by the bars from 100%: ~60% for BC, HOA, and CPC, close to 100% for WBOA and OOA, ~90% for NOX and CO.

Figure 16 also compares the magnitude of the local relative contribution for two different days (and scenarios). The middle panel shows the day of 27 November 2007, where the ratio of local contributions to measured concentrations was particularly high, even for the secondary organic fraction (OOA). In contrast, the lowest panel presents the situation for 14 December 2008 where the local contributions are almost non-existent except for the primary, traffic related compounds BC and HOA. Since neither of the two days was a Sunday, a weekday effect can be ruled out for this example. In Fig. 17, the time series of BC, HOA, WBOA, and OOA background and measured concentration are displayed. The day with low local PM_1 fractions (right panel) exhibits higher background concentrations (bold lines) than the day with high local contributions (left panel), but also has generally lower total concentrations of components (thin lines), resulting in low local contribution levels. The lower measured concentrations of 14 December 2008 can be explained by higher wind speed than on 27 November 2007 (3 ms^{-1} compared to 1.3 ms^{-1}) causing dispersion of primary emissions and by significantly less traffic since rush hour was mostly over when the measurements started.
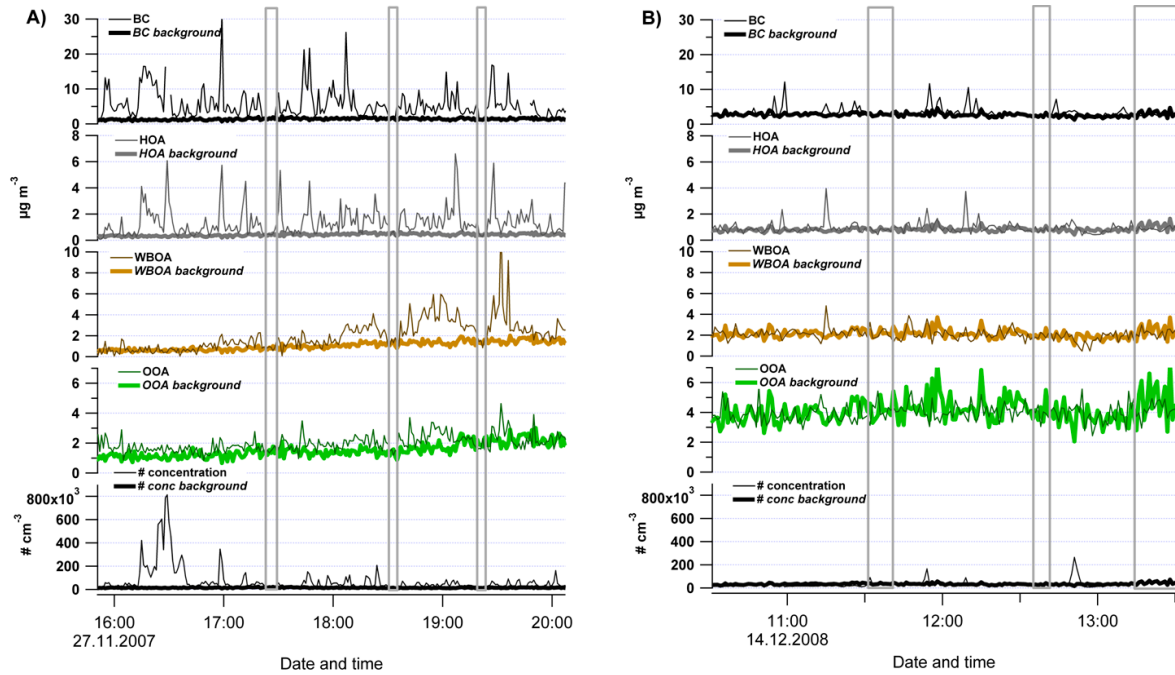
Figure 17: Time series of measured components and their calculated background concentrations. Panel A shows an example drive with high local contributions (big difference between background and measured concentrations), panel B an example drive with low local contributions. Grey bars denote periods when measuring at the background station Kaserne.

The influence of meteorological parameters such as temperature and wind speed on the magnitude of local contributions is explored in Fig. 18. No conclusive pattern could be observed for the ratio of local/measured concentrations (mean values per drive, primary components only) versus temperature, wind speed, or wind direction measured at Kaserne (NABEL data), nor versus temperature differences between Kaserne and Üetliberg (not shown). The weak, slightly positive correlation with temperature and very weak, slightly negative correlation with wind speed of local percentages still points to the link between background concentration levels as seen in Fig. 17 and thermal inversions: As stated earlier, during such conditions, temperatures are low and stagnant air masses (with low wind speeds prevailing) allow for processing of primary PM_1 and a build-up of secondary aerosol, thus increasing the background concentrations measured in Zurich and across the Swiss plateau and lowering the ratio local/measured. Hence, the higher the temperature, or the less pronounced the thermal inversion, the higher the ratio of the local/measured concentration.
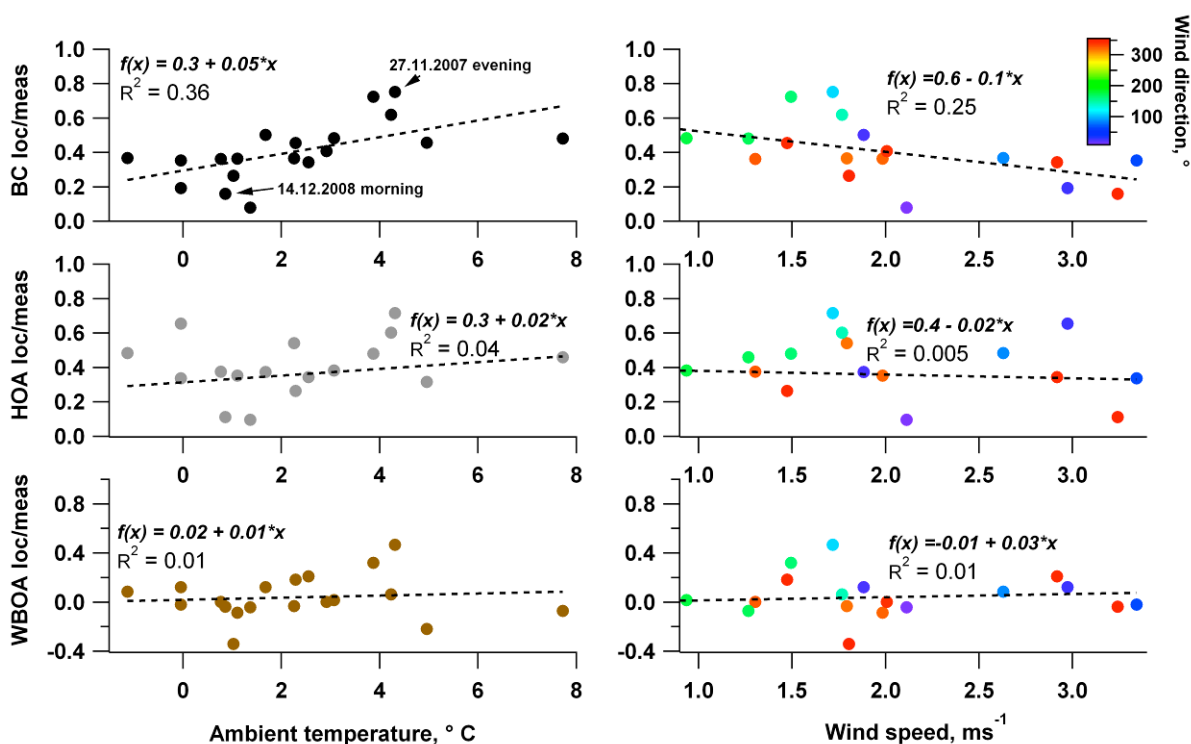
Figure 18: Ratios of local contributions to measured concentrations of different components as a function of ambient temperature (left) and wind speed (right). Data points are average values per measurement drive. Wind speed data are colored according to wind direction.

3.5   Conclusions

On-road mobile measurements of PM_1 chemical composition were performed with a Q-AMS and additional instrumentation deployed in the PSI mobile laboratory during winter 2007/2008 and December 2008 in the metropolitan area of Zurich, Switzerland. PMF applied to the organic fraction of PM_1 yielded 3 different factors assigned to the following sources: Traffic emissions (HOA), emissions from wood burning for domestic heating purposes (WBOA), and an oxygenated fraction (OOA), related to secondary formation of organic aerosol from volatile precursors. On average, OOA made up the biggest organic fraction, followed by WBOA and HOA. Concerning primary emissions, traffic emissions were responsible for high loadings of organic aerosol along major roads and contributed substantially to BC mass loadings, however, domestic wood burning was in general more important than traffic in Zurich during these winter campaigns. The inorganic fraction was dominated by nitrate, as the formation of particulate ammonium nitrate is favored by low temperatures.

Meteorology also plays a major role for the overall total concentration and chemical composition of PM_1 as well as the spatial distribution of its constituents. Swiss winters often see thermal inversions over the Swiss plateau between the Jura mountains and the Alps, with emissions

being trapped, processed, and accumulating. This leads to a quite uniform distribution of the chemical components in PM_1 throughout the region, with small variations throughout the city of Zurich depending on elevated areas (dilution), major traffic arteries (high BC, HOA contributions) or residential areas with wood burning emissions. An important question in this context is the separation of the PM_1 fraction assigned to very local emissions from the background aerosol, as a help for local authorities in designing mitigation strategies. For this purpose, a method was developed that is based on the particular setup of this campaign, featuring mobile on-road and stationary urban background measurements at the same time. Normalizing the differences between background and on-road measurements to their SO_4 ratio accounts for dilution effects due to small-scale meteorology. Results show that BC and HOA have a substantial local fraction of around 40%. Consequently, traffic related emissions are a large local contributor to PM_1 measured on road in Zurich and thus of importance concerning abatement strategies. In contrast, emissions from wood burning have high very local contributions, but are, together with secondary components, to a great extent part of the background. Hence, the reduction of these components requires a regional approach.

Meteorology and especially thermal inversions greatly influence the ratio of local to measured concentrations. Long-lasting stagnant conditions lead to an accumulation of PM_1 which can dominate the aerosol levels measured in downtown Zurich despite the high anthropogenic activity and the related emissions of air pollutants.

Highly time-resolved mobile measurements of air pollutants provide additional information on the spatial variation of the parameter of interest, here PM_1, and hence enable new insights into the distribution, evolution in the atmosphere, and source emission strengths of atmospheric aerosol. Further mobile measurements with the new generation of aerosol mass spectrometers are thus of interest for our understanding of ambient aerosol concentration and composition patterns.

3.6   Acknowledgements

3.7   Supplementary information

3.7.1 Preparatory data analysis
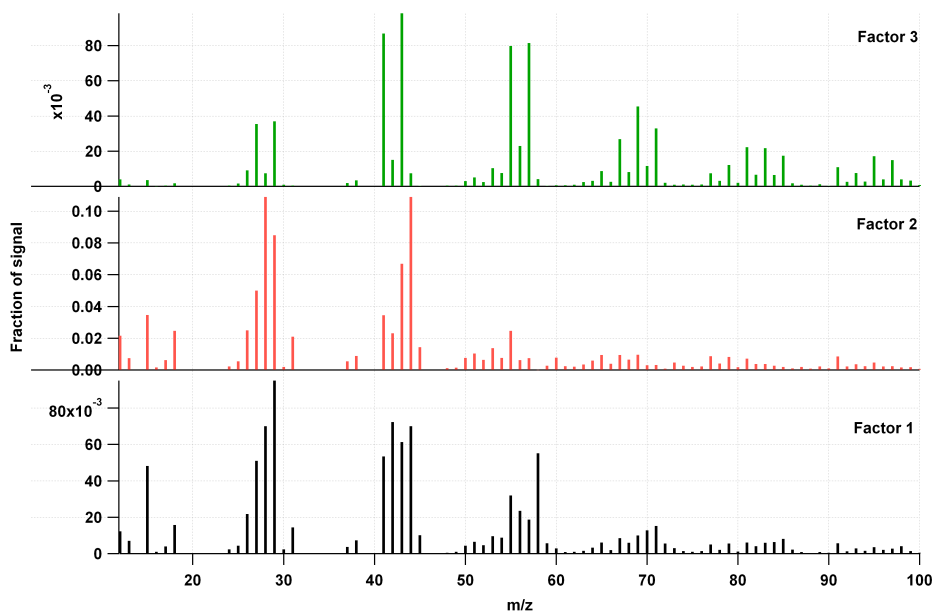
Figure 19: 3-factorial solution of running the PMF2 algorithm on the organic data matrix where the *m/z*'s directly proportional to *m/z* 44 were downweighted.

When downweighting *m/z*'s directly proportional to *m/z* 44, the PMF solution does not fully separate OOA and WBOA. *m/z*'s 60 and 73, markers for BBOA (Alfarra et al., 2007), show up in Factor 2, which resembles OOA with the dominating signal at *m/z* 44 (see also section 3.4.2 in the manuscript). As for the corresponding time series (not shown), both Factor 1 and Factor 2 follow periodically the time series of inorganic secondary components, but no consistent comparison can be done.

3.7.2 Air mass back trajectories

Four-day backward trajectories were calculated based on 3-dimensional wind fields of the regional weather prediction model COSMO using the trajectory model TRAJ (Fay et al., 1995). The fields were taken from hourly "analyses" operationally generated by the Swiss weather service MeteoSwiss at a resolution of 7 km x 7 km x 60 vertical levels for a domain covering large parts of Europe.
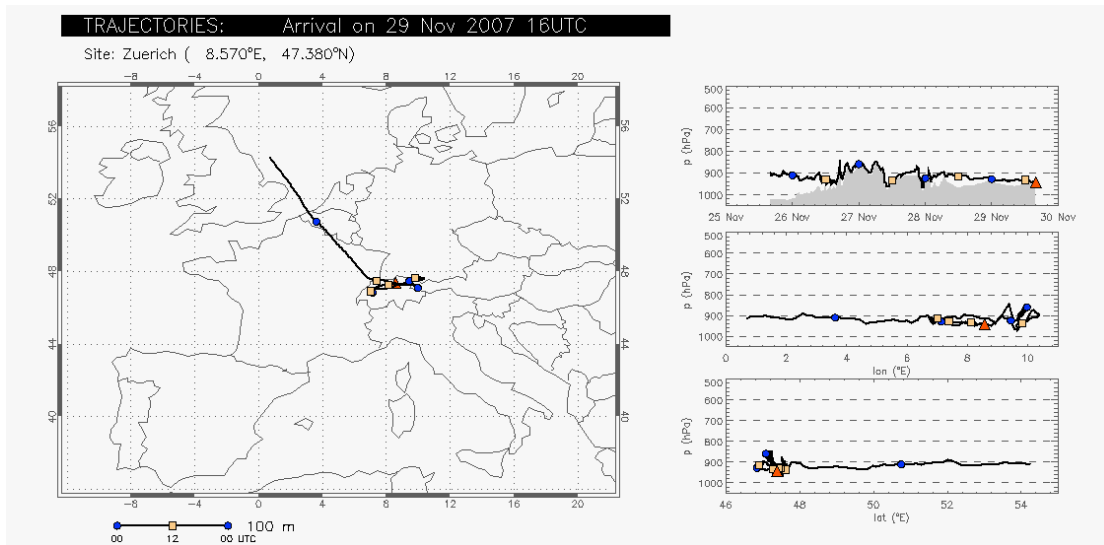
Figure 20: Air mass back trajectories for 29 November 2007. Air masses moved from Belgium/Germany to Switzerland and stagnated over the Swiss plateau, residing there for about 3 days prior to reaching the receptor site Zurich Kaserne (red triangle).

3.7.3 Representativeness plot of mobile measurements
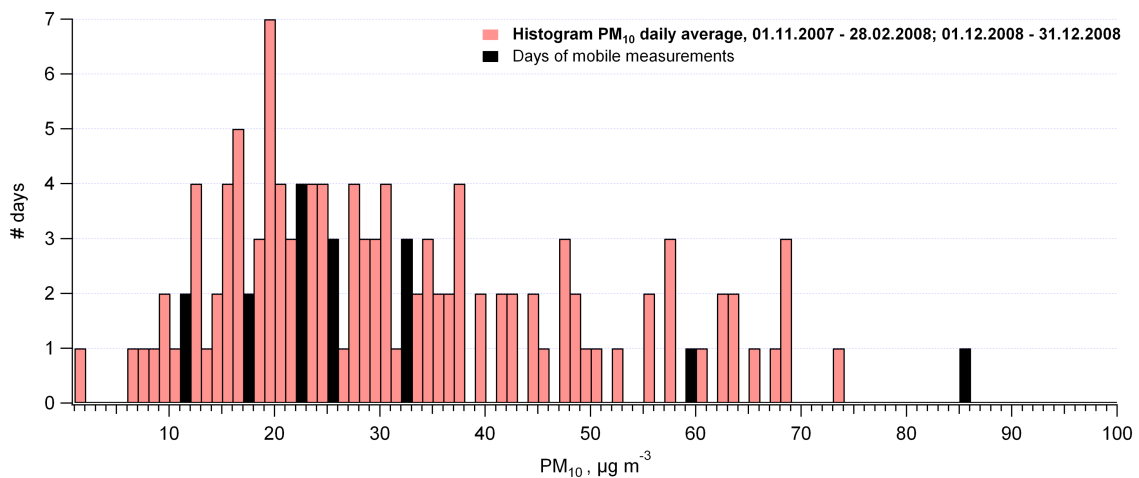
Figure 21: Histogram of PM10 daily mean values for the periods of 01 November 2007 – 31 February 2008 and 01 December 2008 – 31 December 2008. Values of days when mobile measurements were performed are colored in black.

3.7.4 PMF diagnostics
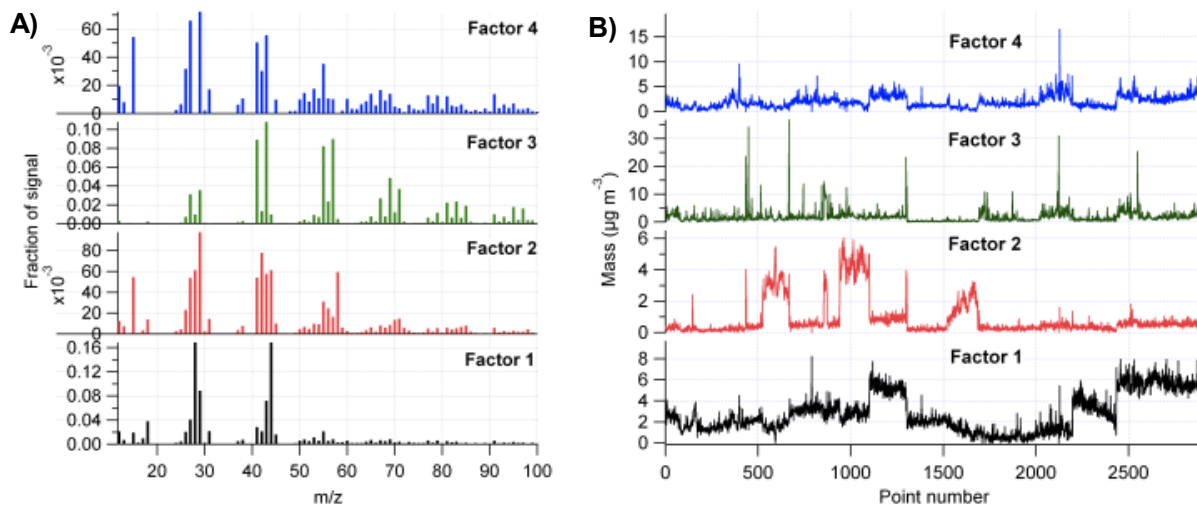
Figure 22: 4-factor solution for part 1, source spectra (F, panel A), and time series (G, panel B).

Choosing $p > 3$ did not yield meaningful results. For part 1, $p \geq 4$ resulted in an additional factor similar to BBOA and OOA and a prominent peak at m/z 58 related to amines, most likely an artifact of inlet contamination during overnight parking of the mobile laboratory at a garage of public transport buses. This amine factor was persistent also for an increasing number of p with no meaningful factors. Adding an additional factor for part 2 led to a split of the HOA factor (Fig. 23), with 2 factors featuring a high signal at m/z 43.

For part 1, $p = 4$, the resulting additional factor 2 (Fig. 22) shows high similarity with factor 1 (Pearson's $R = 0.74$) and factor 4 (Pearson's $R = 0.77$) and can be interpreted as a recombination of OOA and BBOA. Interestingly, it features a few distinct peaks relating to the ion series ($C_nH_{2n+2}N$) characteristic for amines, e. g. m/z 58 (Silva et al., 2008). As shown by the time series of factor 2 in panel B), there were 3 measurement drives with substantial factor 2 mass loadings – drives following a night when the mobile laboratory had been parked in a garage of public transport buses in Zurich. The punctual occurrence of this factor and the missing analogies in volatile organic compounds (VOC) time series measured at Zurich Kaserne (not shown) lead to the hypothesis that the amine signal could be explained by emissions related to SCR (selective catalytic reduction, a NO_X abatement technology using an aqueous urea solution (Koebel et al., 2000)) systems the buses are equipped with to meet the EURO V legal emission standards (implemented in Switzerland on 1 September 2009).

Running PMF excluding the amine-influenced periods yielded the same 3 factors as for the complete part 1 dataset ($R^2 > 0.99$ for all 3 factors). The 3-factorial solution of the full part 1

dataset exhibits elevated total residual masses for those 3 measurement drives (Fig. 31), mostly due to *m/z* 58 (compare non-normally distributed scaled residuals for *m/z* 58 in the inset of Fig. 32).
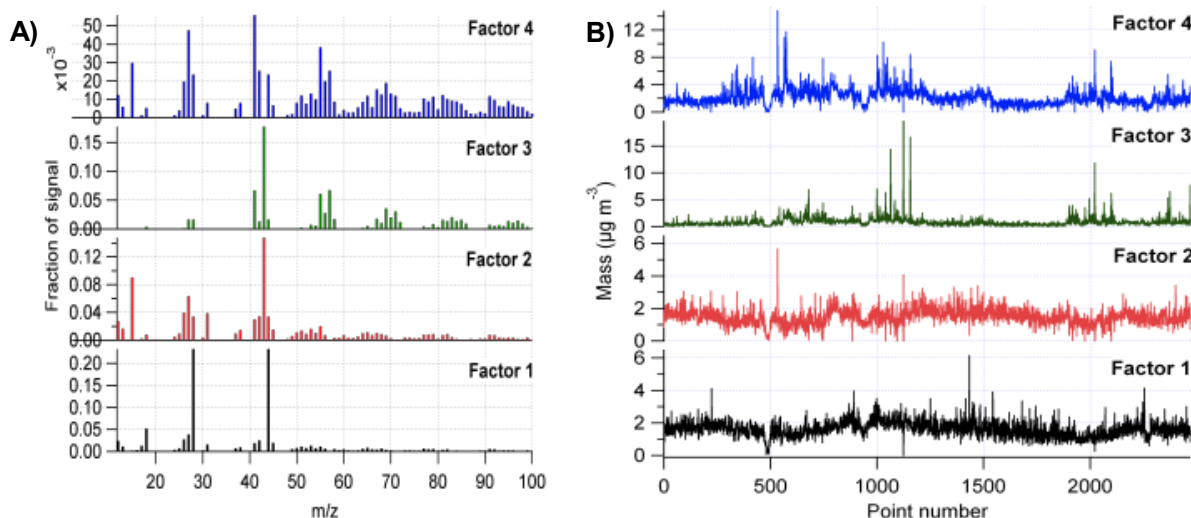
Figure 23: 4-factor solution for part 2, source spectra (F, panel A), and time series (G, panel B).

fpeak was chosen to be -0.1 for part 1, and 0 for part 2, based on a trade-off between "high" signal at *m/z* 60 ($C_2H_4O_2^+$, among others a fragment of levoglucosan which in turn is a pyrolysis product of cellulose an hence a marker of biomass burning emissions (Alfarra et al., 2007)), and non-zero signal at *m/z* 44 (predominantly non-gaseous CO_2^+) in the BBOA spectrum.
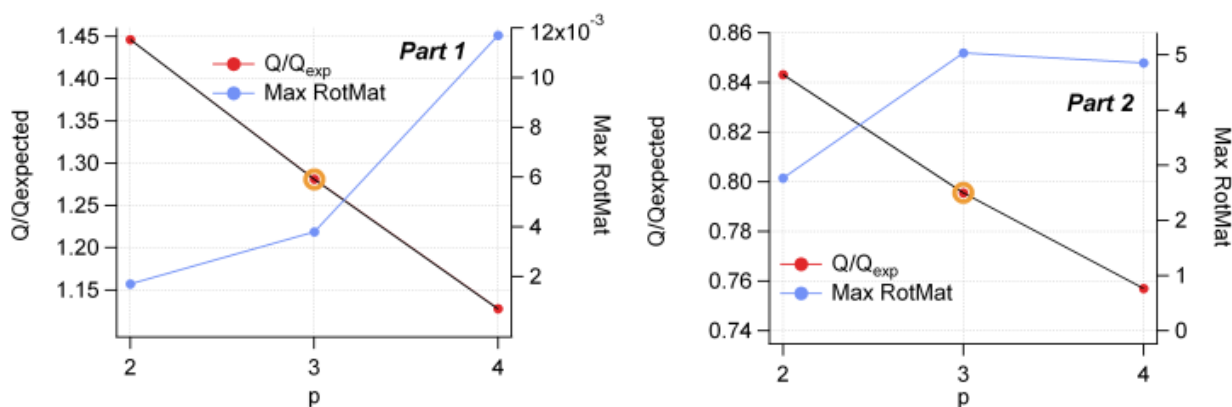
Figure 24: Q / Q_{exp} and the maximum value of the rotational matrix versus the number of factors for part 1 and part 2. The chosen solution is denoted by the orange circle.
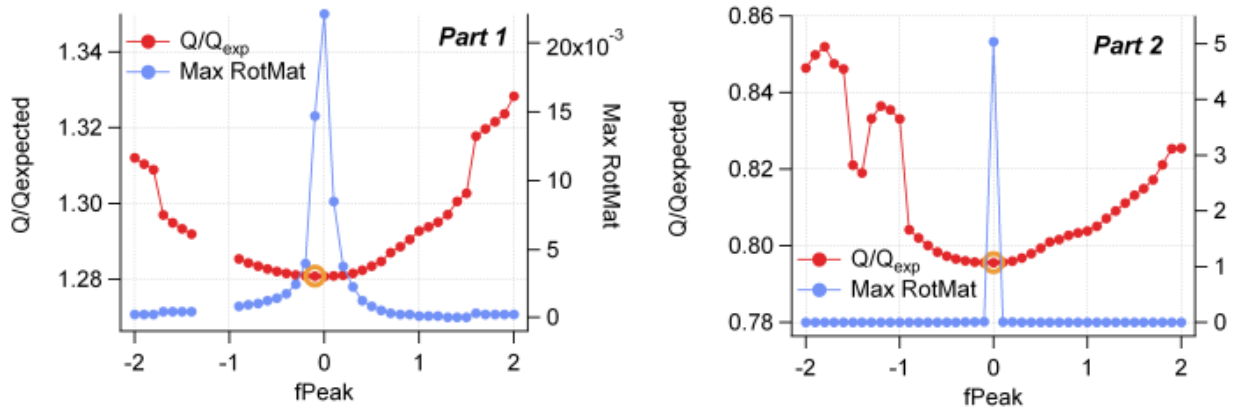
Figure 25: Q / Q_{exp} and the maximum value of the rotational matrix versus *fpeak* for part 1 and part 2. The chosen solution is denoted by the orange circle.
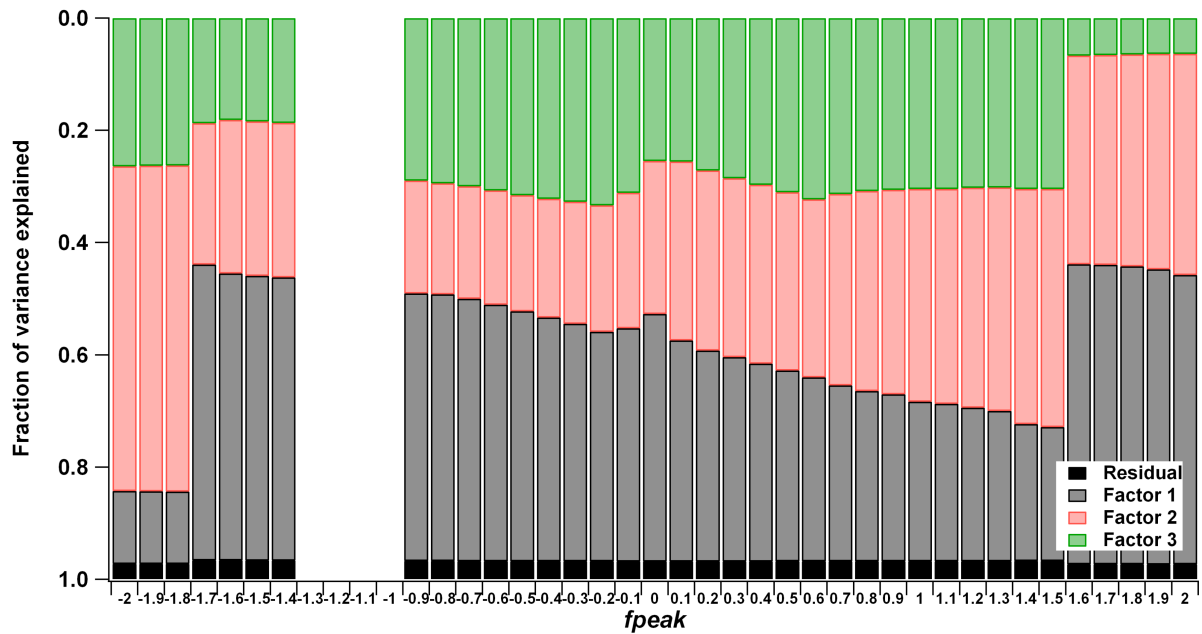
Figure 26: Part 1 (data from 27 November 2007 – 19 February 2008) - variance explained by $p = 3$ as a function of rotational parameter *fpeak*. *Fpeak* was chosen to be -0.1 for this part of the campaign.
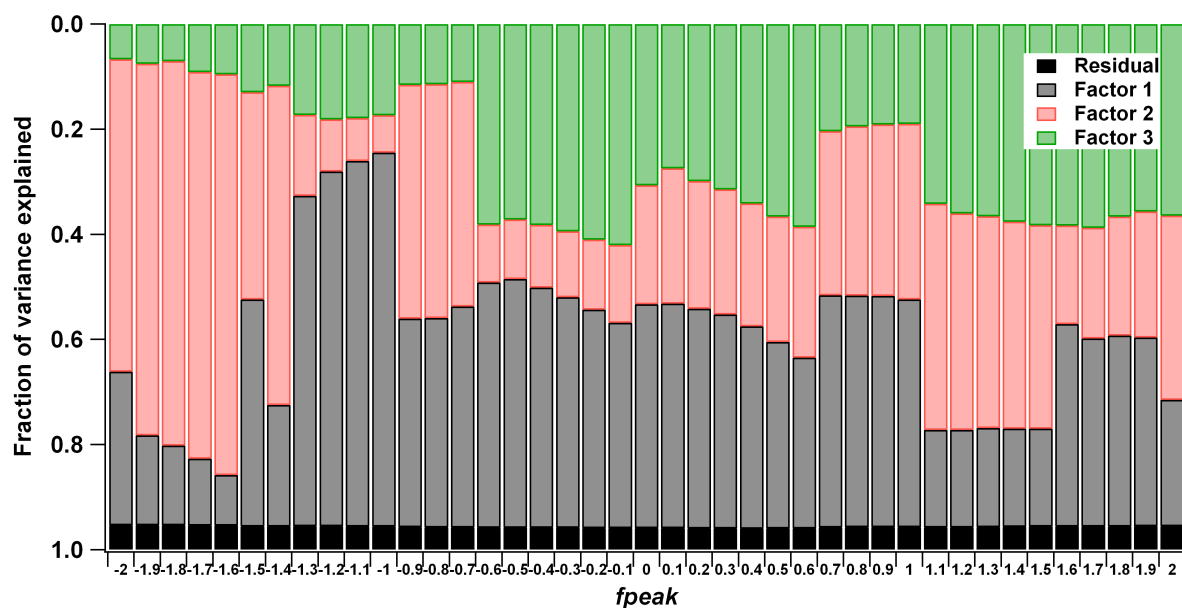
Figure 27: Part 2 (data from 14 December 2008 – 16 December 2008) - variance explained by $p = 3$ as a function of rotational parameter *fpeak*. *Fpeak* was chosen to be 0 for this part of the campaign.
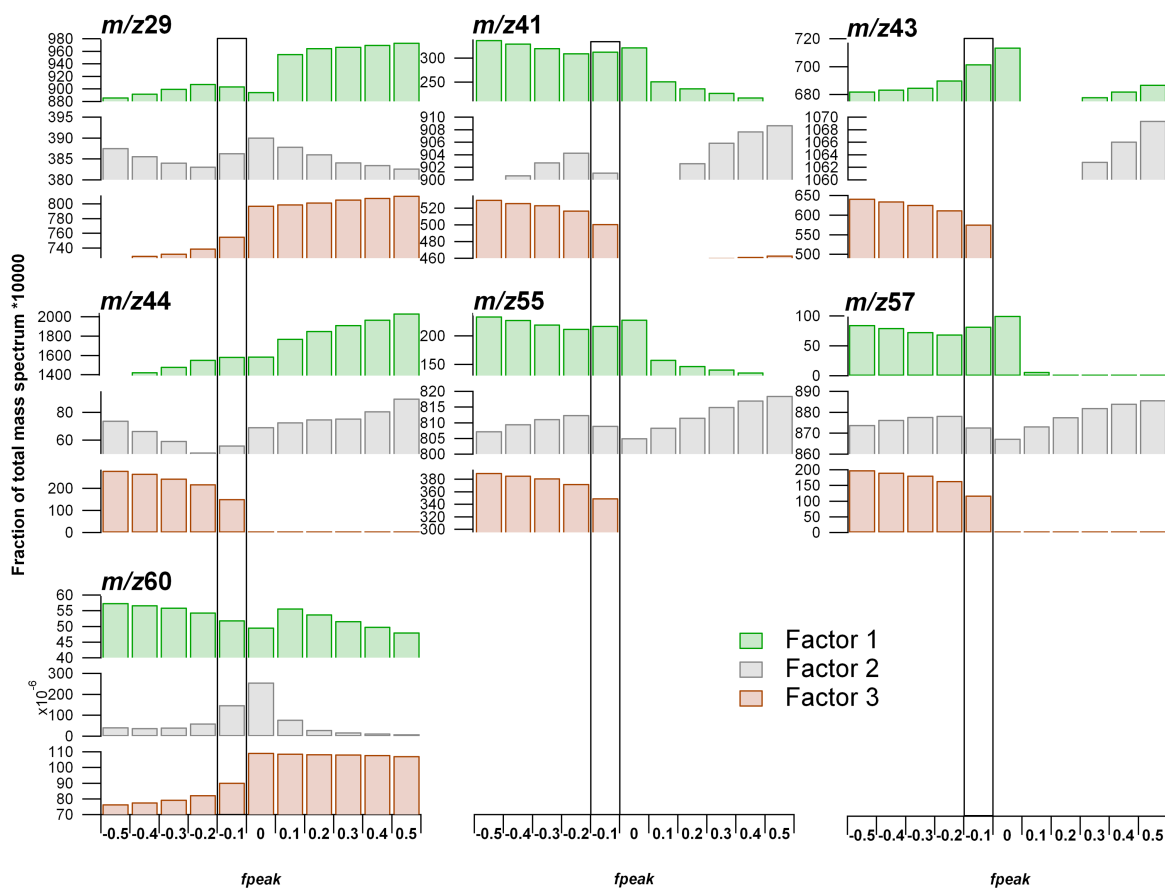
Figure 28: Part 1 (data from 27 November 2007 – 19 February 2008) - fraction of organic *m/z*'s 29 (CHO^+, $C_2H_5^+$), 41 (pre-dominantly $C_3H_5^+$), 43 ($C_2H_3O^+$, $C_3H_7^+$), 44 (pre-dominantly CO_2^+, also $C_2H_4O^+$, C_2H_8+), 55 (pre-dominantly $C_4H_7^+$), 57 ($C_3H_5O^+$, $C_4H_9^+$), and 60 ($C_2H_4O_2^+$) as a function of *fpeak* [-0.5,0.5] for the 3-factorial solution. Note the different scaling of the y-axes. The boxes frame the chosen *fpeak* of -0.1.

Figure 29: Part 2 (data from 14 December 2008 – 16 December 2008) - fraction of organic *m/z*'s 29 (CHO^+, $C_2H_5^+$), 41 (pre-dominantly $C_3H_5^+$), 43 ($C_2H_3O^+$, $C_3H_7^+$), 44 (pre-dominantly CO_2^+, also $C_2H_4O^+$, $C_2H_8^+$), 55 (pre-dominantly $C_4H_7^+$), 57 ($C_3H_5O^+$, $C_4H_9^+$), and 60 ($C_2H_4O_2^+$) as a function of *fpeak* [-0.5,0.5] for the 3-factorial solution. Note the different scaling of the y-axes. The boxes frame the chosen *fpeak* of 0.

Figure 30: Boxplots of scaled residuals (only median and 25%-percentiles shown) as a function of *m/z*.
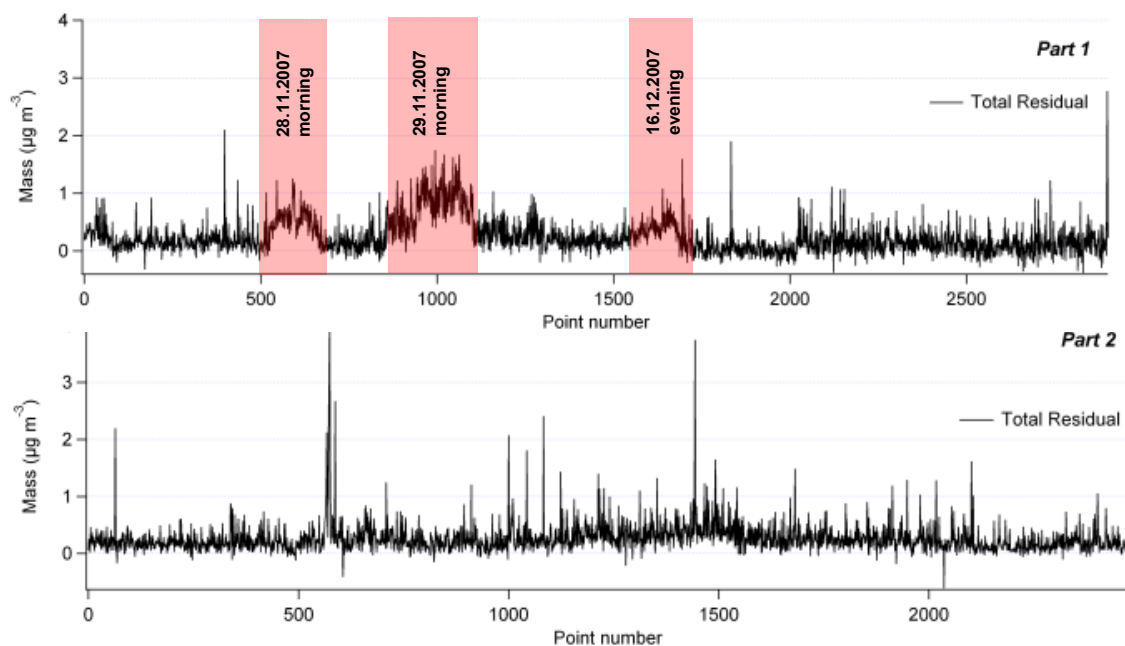
Figure 31: Time series of summed total residuals. Red bars in part 1 panel denote periods influenced by amine-like factor.
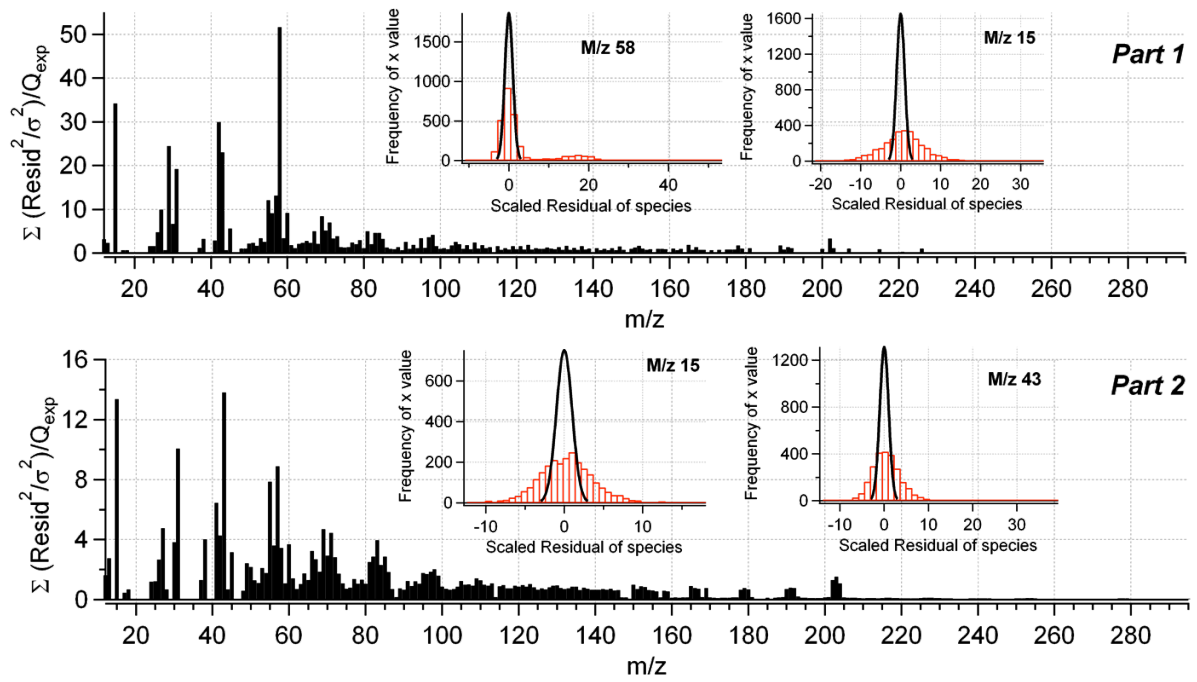
Figure 32: Q / Q_{exp} as a function of *m/z*. Insets show normal distribution of scaled residuals for individual peaks. Note positive bias of distribution of residuals of *m/z* 58 for part 1.
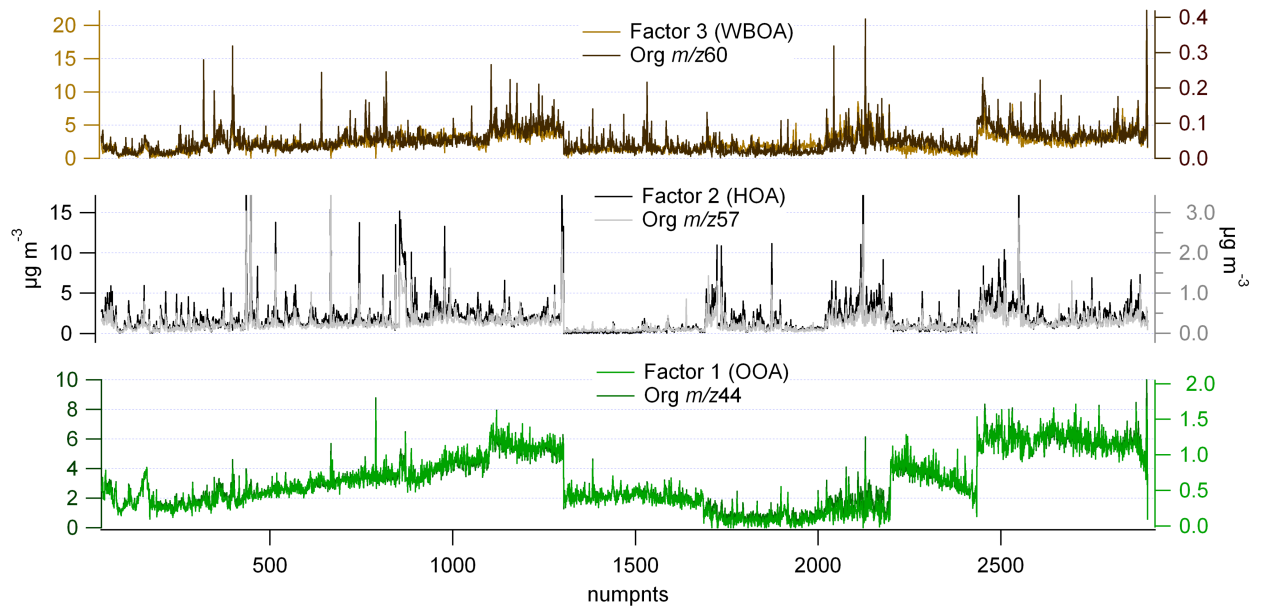
Figure 33: Part 1 – time series of factors and organic marker masses 60, 57, 44.
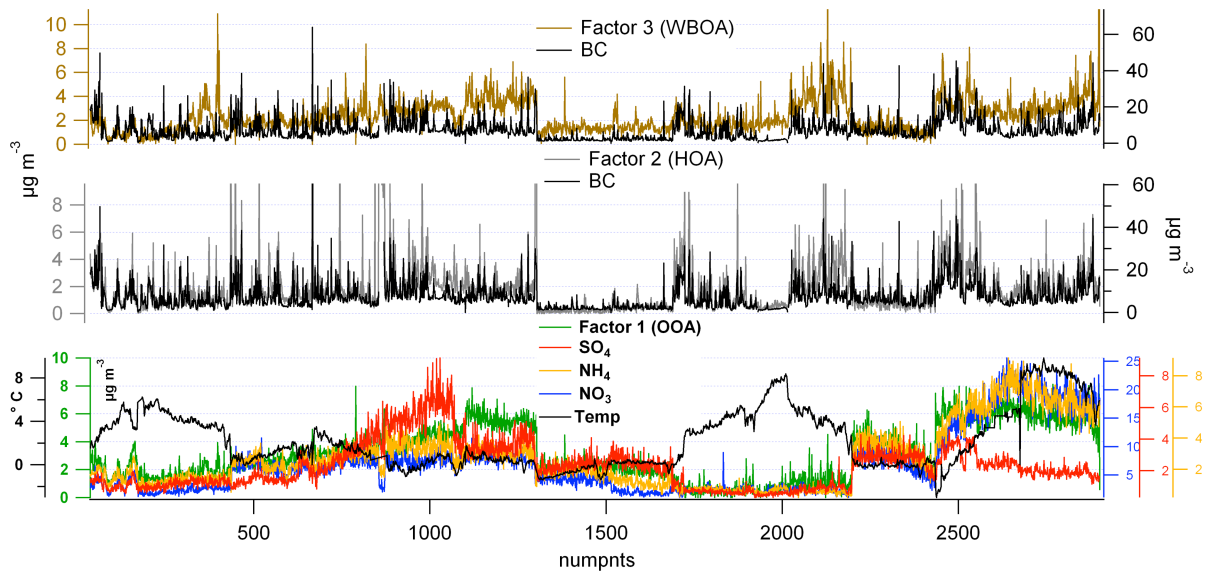
Figure 34: Part 1 – time series of factors and ancillary data.
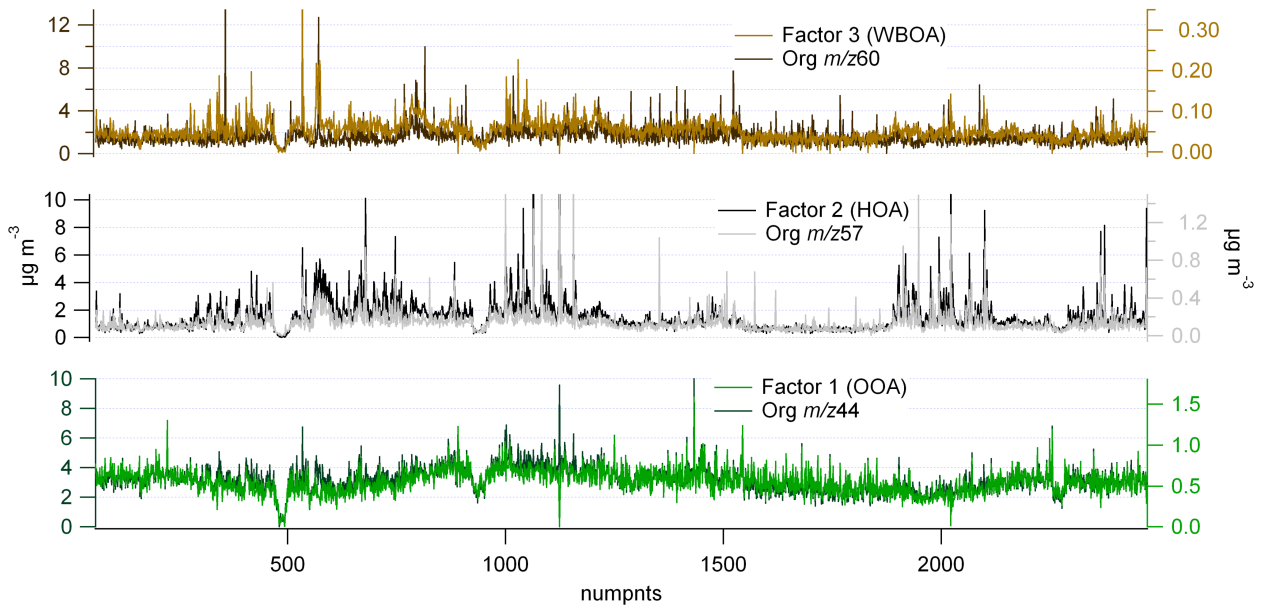
Figure 35: Part 2 - time series of factors and organic marker masses 60, 57, 44.
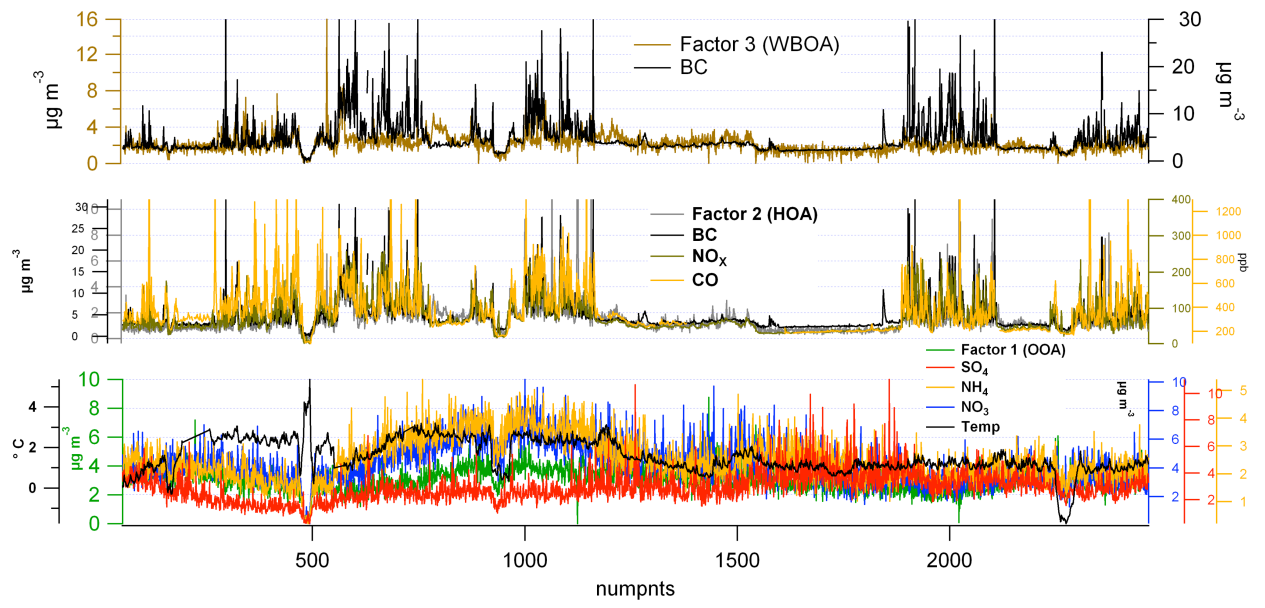
Figure 36: Part 2 - series of factors and ancillary data.
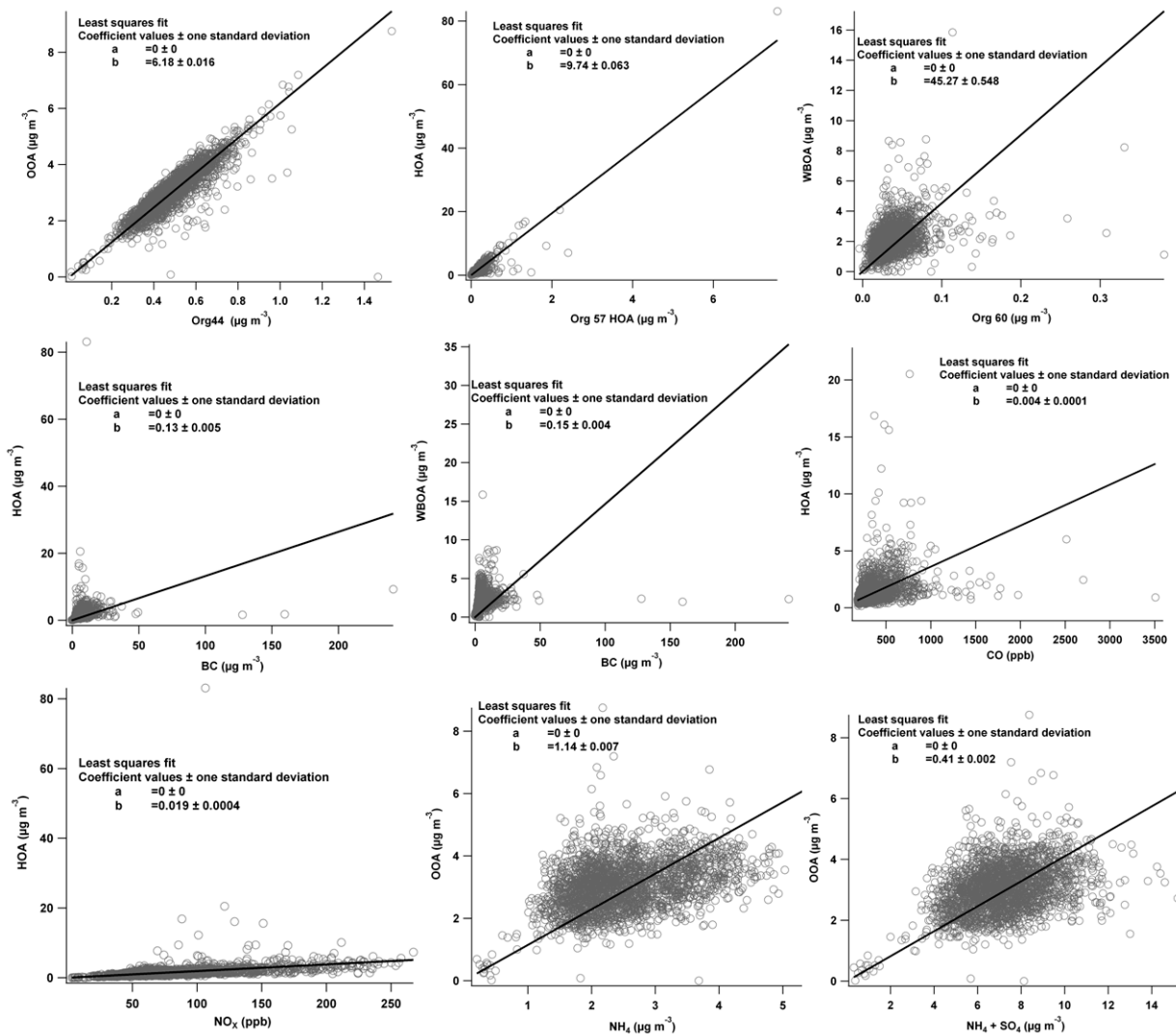
Figure 37: Regression analysis of PMF factor time series and ancillary data, no corrections applied.
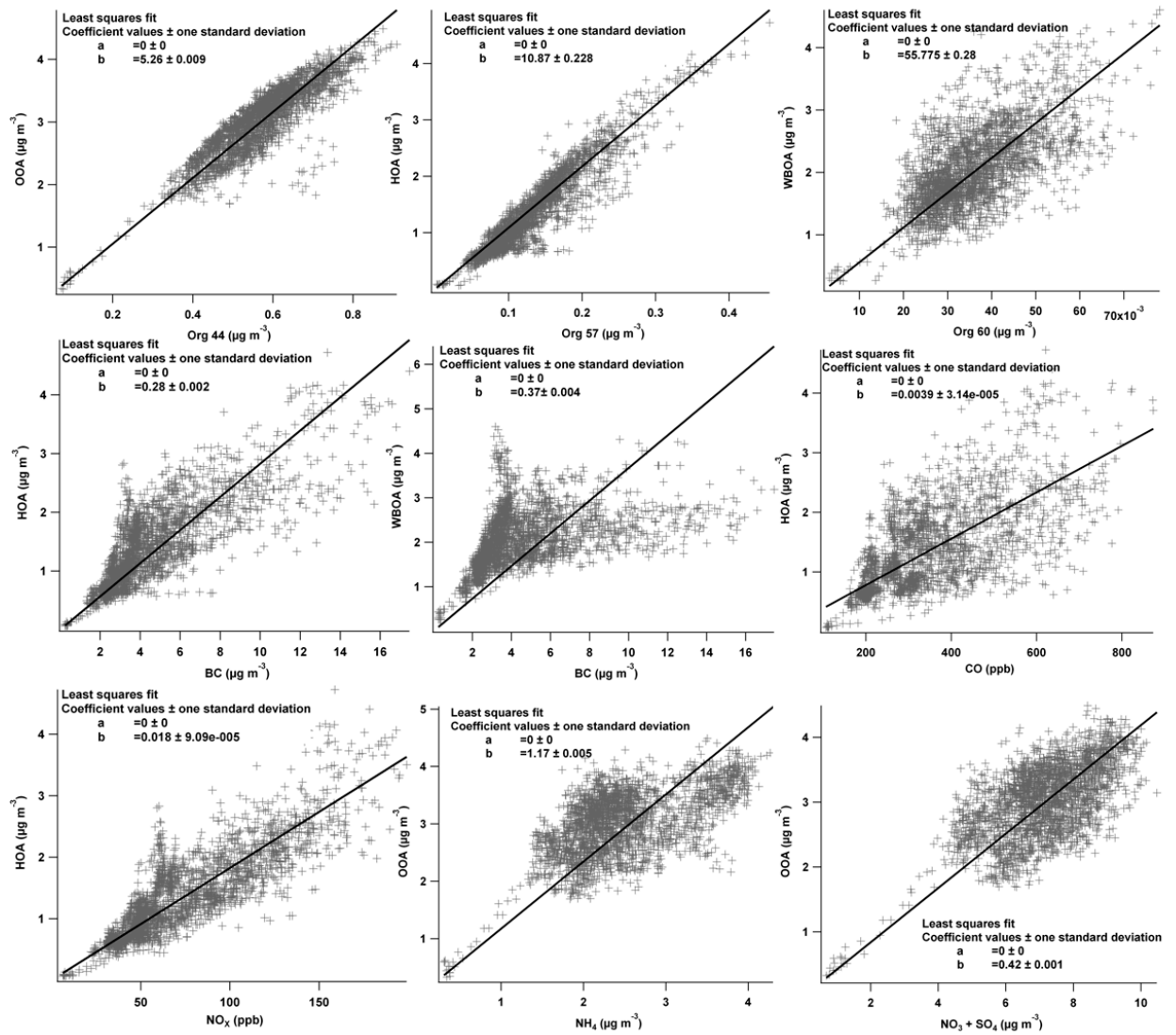
Figure 38: Regression analysis of PMF factor time series and ancillary data, after removing the upper 1st percentile of data points and applying a moving average over 5 data points.

3.7.5 Estimation of local contribution
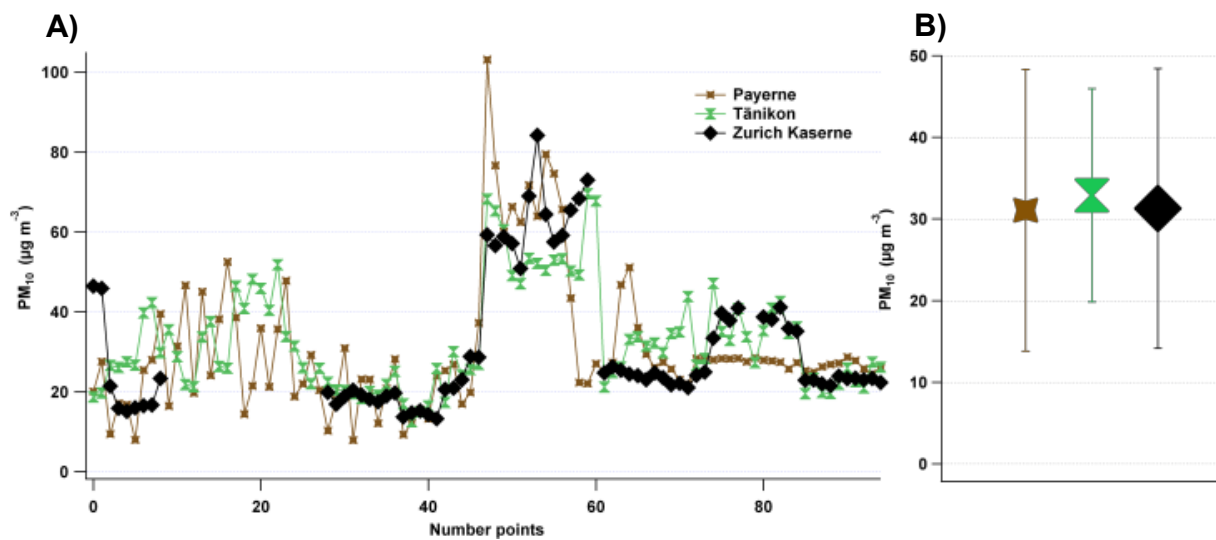
Figure 39: Time series of PM_{10} at Payerne (rural station), Tänikon (rural station), and Zurich Kaserne (urban background station) (panel A) during the same time intervals as the mobile measurements. Panel B shows the mean value and standard deviation of the time series in panel A.
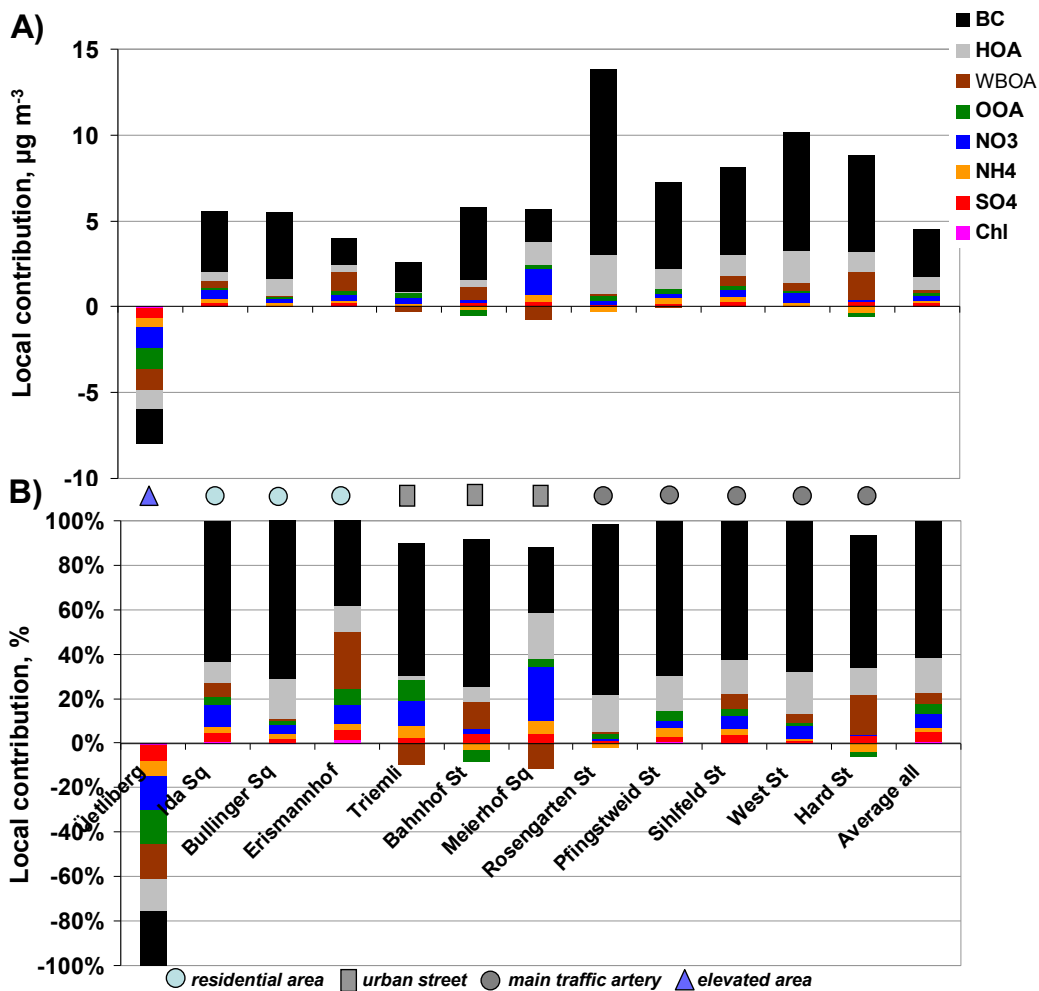
Figure 40: Local concentrations calculated by subtracting the concentration of component *S* measured at Kaserne from the concentration of component *S* measured on-road at the same time (panel A, relative values panel B). For the time series of Kaserne data, the interpolated median value of 2 subsequent Kaserne visits was used. The "average all" bar is the mean value of the local contribution of all data.

4

ORGANIC AEROSOL FROM COOKING AND OTHER SOURCES IN BARCELONA

4.1   Abstract

PM_1 (particulate matter with an aerodynamic diameter < 1 μm) non-refractory components and black carbon were measured continuously together with additional parameters at an urban background site in Barcelona, Spain, during March 2009 (campaign DAURE, Determination of the sources of atmospheric Aerosols in Urban and Rural Environments in the western Mediterranean). Positive matrix factorization (PMF) was conducted on the organic aerosol (OA) data matrix measured by an aerosol mass spectrometer, on both unit mass (UMR) and high resolution (HR) data. Five factors or sources could be identified: LV-OOA (low-volatility oxygenated OA), related to regional, aged secondary OA; SV-OOA (semi-volatile oxygenated OA), a fresher oxygenated OA; HOA (hydrocarbon-like OA, related to traffic emissions); BBOA (biomass burning OA) from domestic heating or agricultural biomass burning activities; and COA (cooking OA). LV-OOA contributed 28% to OA, SV-OOA 27%, COA 17%, HOA 16%, and BBOA 11%. The COA HR spectrum contained substantial signal from oxygenated ions (O:C: 0.21) whereas the HR HOA spectrum had almost exclusively contributions from chemically reduced ions (O:C: 0.03). If we

assume that the carbon in HOA is fossil while that in COA and BBOA is modern, primary OA in Barcelona contains a surprisingly high fraction (59%) of non-fossil carbon.

This paper presents a method for estimating cooking organic aerosol in ambient datasets based on the fractions of organic mass fragments at *m/z* 55 and 57: their data points fall into a V-shape in a scatter plot, with strongly HOA influenced data aligned to the right arm and strongly COA influenced data points aligned to the left arm. HR data show that this differentiation is mainly driven by the oxygen-containing ions $C_3H_3O^+$ and $C_3H_5O^+$, even though their contributions to *m/z* 55 and 57 are low compared to the reduced ions $C_4H_7^+$ and $C_4H_9^+$. A simple estimation method based on the markers *m/z* 55, 57, and 44 is developed here and allows for a first-order-estimation of COA in urban air. This study emphasizes the importance of cooking activities for ambient air quality and confirms the importance of chemical composition measurements with a high mass and time resolution.

4.2   Introduction

An OA factor recently reported in ambient air in several AMS studies is cooking organic aerosol (COA, Allan et al., 2010; Huang et al., 2010; Sun et al., 2011). Emissions from cooking activities had been identified as a potentially important source of PM much earlier (Gray, 1986). To a great extent an indoor air pollution problem (Fortmann et al., 2001), cooking aerosol can also contribute substantially to ambient PM concentrations: e. g. meat charbroiling and frying were estimated to account for about 16% of fine organic carbon emissions or 6% of total fine PM concentration in the Los Angeles area (Hildemann et al., 1991; Schauer et al., 1996). Most studies focused on meat cooking emissions when investigating cooking aerosol; numerous compounds were identified in meat cooking OA, among which palmitic acid, stearic acid, oleic acid, and cholesterol are the most prominent (Cass, 1998; Schauer et al., 1999). Charbroiling OA was also identified in ambient air by AMS-PMF analyses (Lanz et al., 2007; Slowik et al., 2010). Schauer et al. (2001) extended the research on cooking PM to emissions from cooking vegetables with seed oils; studies on Chinese food cooking emissions further broadened the range of emissions investigated (He et al., 2004; Zhao et al., 2006; He et al., 2010). Fatty acids are the dominant group of compounds emitted by all cooking types; they differ in fractions of saturated, unsaturated, and polyunsaturated fats depending on the type of oil or meat fat (Zhao et al., 2006). Mohr et al. (2009) characterized primary OA from cooking various types of meat with an AMS and found that the unit mass resolution (UMR) spectral signature is very similar to HOA. The differences in the high resolution (HR) spectra are larger due to the oxygen present in the fatty acids; however, the similarity of UMR spectra from HOA and COA might be one of the reasons for the relatively small

number of locations where COA was detected with an AMS, despite its potential importance as a contributor to urban aerosol concentrations.

This paper provides a characterization of the chemical composition and organic aerosol sources of PM_1 in Barcelona during winter. In addition, a new method for identifying COA in ambient air and estimating cooking contributions to organic aerosol is presented. These techniques are demonstrated within the framework of the DAURE (Determination of the sources of atmospheric Aerosols in Urban and Rural Environments in the western Mediterranean) campaign in Barcelona, Spain. The intense and varied sources of primary emissions in this region provide an ideal test case for the feasibility of identifying cooking emissions and determining their importance relative to other OA sources.

4.3   Method

4.3.1   DAURE Campaign, Barcelona (Spain)

Data for this study were acquired during the intensive field campaign DAURE in Barcelona, Spain, from 25 February to 26 March 2009. The DAURE campaign was set up to study the aerosol formation processes during the winter anticyclonic episodes, when the highest PM_1 levels are recorded both at urban and regional scale in the Western Mediterranean (Pey et al., 2010). Thus, the aerosol sampled during this period is characterized by higher ambient concentrations, specially of nitrate and carbonaceous components, when compared with the urban background mean annual average in Barcelona (Pérez et al., 2008b). A detailed overview of the campaign, its objectives, the groups involved, the measurements performed, and a summary of the results are presented in Pandolfi et al. (2012).

The city of Barcelona is situated on the shore of the western Mediterranean basin, wedged in between the sea and the Catalan coastal ranges running parallel to the coastline NE-SW. The Besos and the Llobregat river valleys perpendicular to the coast limit the city area to the NE and SW. The warm and dry Mediterranean climate, intense solar radiation and low dispersive conditions favor high levels of regional aerosol (Pérez et al., 2008a); additionally, high anthropogenic emissions lead to intense pollution episodes. Barcelona is one of the cities in Europe with the highest number of cars per km^2 (Ajuntament de Barcelona, 2007). Emissions from the Barcelona harbor, an expanded industrial zone in the river valley and the densely populated pre-coastal depression behind the coastal range all add additional PM to the Barcelona area aerosol concentrations (Querol et al., 2001). Outbreaks of Saharan dust events can affect the Barcelona air quality (Pérez et al., 2006). The daily cycle of nocturnal offshore flows and diurnal sea breeze

(Jorba et al., 2011) plays an important role for the pollution dispersion in Barcelona. The sea breeze advects (polluted) coastal air masses inland, while nocturnal land breeze and mountain down slope flows transport air masses from the surrounding valleys to the city of Barcelona.

The measurement site was situated at the northwestern corner of the city centre in a small park (elevation 80 m a. s. l.) surrounded by residential areas. At a distance of ~300 m is Diagonal Avenue, one of the main traffic arteries crossing Barcelona with 100 000 vehicles per day (Ajuntament de Barcelona, 2007), while the Mediterranean Sea is ~6 km away.

4.3.2 Instrumentation and sampling

A complete list of instruments deployed during DAURE is given in Pandolfi et al. (2012). A brief discussion of the instruments used for the present analysis is included in chapter 2. Non-refractory PM_1 chemical composition was measured with the Aerodyne high-resolution time-of-flight aerosol mass spectrometer (HR-ToF-AMS, abbreviated as AMS hereafter). During DAURE the AMS was operated alternately in V and W mode (150 s each). In W mode, 15 cycles of 5 s open and 5 s closed data in the mass spectrum (MS) mode were acquired before saving. In V mode, 5 cycles of 15 s in MS mode (50% open) plus 30 s in particle time-of-flight (PToF) mode yielded the size distribution of PM_1 components.

The scanning mobility particle sizer (SMPS, homebuilt by PSI, consisting of a neutralizer with a ^{85}Kr source, a differential mobility analyzer DMA, and a condensation particle counter CPC 3022A, TSI) was operated in parallel to the AMS. It measured submicron particle number size distributions between 13 and 638 nm mobility diameter with a time resolution of 5 min.

Aerosol black carbon (BC) mass concentrations were derived from particle light attenuation (b_{ATN}) measurements (time resolution 5 min) at a wavelength of 880 nm by an aethalometer, Model AE31 (Magee Scientific).

In addition to the instruments described in chapter 2, an optical counter (Grimm Labortechnik GmbH & Co. KG; model 1.107) provided continuous measurements of PM_1 (and $PM_{2.5}$ and PM_{10}, not shown) with a time resolution of 1 h. The Grimm mass loadings were corrected using PM_1 samples collected on filters as discussed by Reche et al. (2011), using the following parameters: Grimm $PM_1 = (PM_1[uncorrected]-(-0.0024))/0.8236$.

The above instruments were deployed on a common sample inlet with a $PM_{2.5}$ cyclone (SCC 1.829, BGI Incorporated), requiring a flow rate of 5 l min^{-1}. The inlet was situated on the roof of the trailer containing the instruments, at a height of ~4 m above ground. A ½ inch outer diameter (o. d.) stainless steel tube led inside the trailer (length 2.3 m) to a manifold. From there the sample

air flowed (flow rate 0.4 l min^{-1}) through a Nafion dryer (Perma-Pure, length 100 cm) and 40 cm of ¼ inch o. d. stainless steel tube to the inlet of the AMS. The SMPS inlet was connected to the Nafion drier with a 120 cm long copper tube, 6 mm o. d. Copper tubing with 105 cm of 6 mm o. d. and 10 cm of 10 mm o. d. led to the aethalometer. The total inlet residence time was 14 s for the AMS and 10 s for the SMPS under laminar flow, and 3.5 s for the aethalometer, whose last part of the inlet flow was slightly turbulent (Reynolds Number *Re* = 2160).

4.3.3 Data analysis

AMS data were analyzed using the standard AMS data analysis software SQUIRREL v1.51B and PIKA v1.10B (Sueper, 2008) within Igor Pro 6.22A (Wavemetrics). A collection efficiency (CE) dependent on the nitrate fraction f_{NO3} was applied to the entire dataset, with CE = 0.5 for $f_{NO3} \leq 0.25$, CE = 1 for $f_{NO3} \geq 0.78$ and a linear increase of CE between these values for $0.25 \leq f_{NO3} \leq 0.78$. This relationship was empirically determined by comparisons of AMS and ancillary data from various field campaigns conducted within the *European integrated project on aerosol cloud climate air quality interactions* (EUCAARI) and the *European monitoring and evaluation programme* (EMEP) all over Europe (Nemitz et al., 2012). DAURE data were included in that collection of data sets. A very similar dependence of CE on f_{NO3} was recently reported by Middlebrook et al. (2012) for studies in the US. The time series of the estimated CE can be found in Fig. 49 in the supplementary information (SI) in section 4.7.1.

Positive matrix factorization (Paatero and Tapper, 1994; Lanz et al., 2007) was applied to both unit mass resolution (UMR) and high resolution (HR) organic spectra measured by AMS to investigate factors or sources contributing to the organic mass loadings. The UMR input matrices were prepared according to the protocol outlined in Ulbrich et al. (2009) and comprised *m/z*'s 12 – 300. The HR data and error matrices were generated as outlined in DeCarlo et al. (2010). Ions from *m/z*'s 12 – 115 were included in the data matrix; isotopes whose signal was constrained as the appropriate fraction of the peak area of their parent ion were removed. Elemental analysis of the HR data and PMF factors was done using the software APES v1.05 (Sueper, 2008) within Igor Pro 6.22A. SMPS data were analyzed and corrected for multiply charged particles using the PSI inversion routine (Wiedensohler et al., 2011).

All data are reported at local pressure and temperature conditions in local standard time (UTC+1).

4.4   Results

4.4.1   PM$_1$ time series and bulk chemical composition

Figure 41 shows the time series of the cumulative mass of organics (Org), nitrate (NO$_3$), chloride (Chl), ammonium (NH$_4$), sulfate (SO$_4$), and BC for the duration of the DAURE campaign. Charges are omitted for AMS nominally inorganic species, because non-ionic organosulfates and organonitrates also contribute to their concentrations (Farmer et al., 2010). The beginning of the campaign (25 February 2009 – 04 March 2009) and the second part (08 – 25 March 2009) were influenced by typical winter anti-cyclonic conditions in the Western Mediterranean Basin (WMB) which favor the accumulation of pollutants within the planetary boundary layer (PBL). Peak PM$_1$ concentrations of more than 60 μg m^{-3} were measured. The land/sea breeze cycle strongly influenced the daily evolution of pollutant concentrations during these episodes. The period from 04 - 08 March 2009 was characterized by Atlantic advection, with strong winds and precipitation on 05 March 2009. Clean air masses coming from the Atlantic renewed the polluted PBL and lowered concentrations (5 – 15 μg m^{-3} of PM$_1$). The meteorological diurnal cycle was less distinct. Further details on meteorological and dispersion conditions during DAURE can be found in Jorba et al. (2011) and Pandolfi et al. (2012). Since the SMPS was used to estimate the AMS CE, Grimm PM$_1$ data were added for comparison purposes. The campaign average concentration value of 18.5 μg m^{-3} of PM$_1$ compares well to 20 μg m^{-3} of PM$_1$ measured by combined AMS and aethalometer data. The coefficients of a least orthogonal distance fit shown in Fig. 50 in the SI (*intercept* = -3.60, *slope* = 0.99) confirm the good agreement of AMS plus aethalometer vs. Grimm data.

The campaign average dry chemical composition of PM$_1$ is shown in the pie chart inset in Fig. 41. The organic fraction makes up the largest part with 43%, followed by nitrate (18%), sulfate (16%), BC (12%), and ammonium (9%). Molar ratios of the inorganic species indicate a neutralized aerosol throughout the campaign and low mass fractions of organosulfate and organonitrates compared to the inorganic forms, consistent with results at other locations (Docherty et al., 2011). Similar results were found by Pandolfi et al. (2012) using 12-h chemically speciated filter data (PM$_1$): Excluding the crustal, marine and unidentified fractions from the filter data, organic matter (OM) accounts for 40%, NO$_3^-$ for 15%, NH$_4^+$ and SO$_4^{2-}$ for 16% each, and elemental carbon (EC) makes up 14%. Comparisons of AMS nitrate to PM$_{2.5}$ nitrate measured by an R&P ambient particulate nitrate monitor (8400N, Rupprecht and Patashnick Co., Inc.) show good agreement (R^2 = 0.92), with the PM$_{2.5}$ nitrate being 30% higher (not shown).
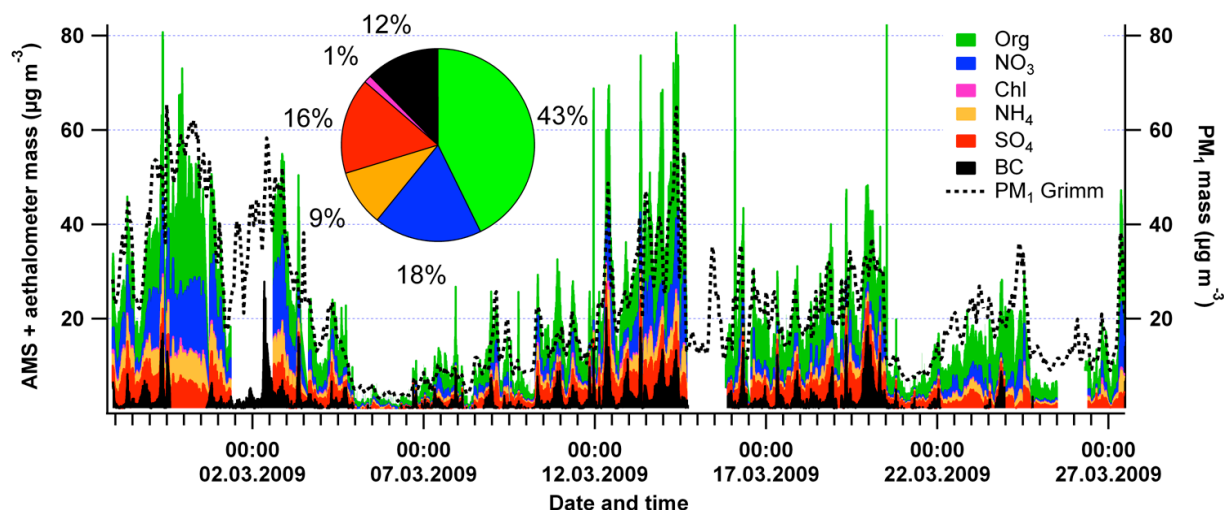
Figure 41: Stacked time series of AMS species (Org, NO_3, NH_4, SO_4, and Chl), BC measured by the aethalometer. PM_1 data from the Grimm laser-spectrometer (corrected using PM_1 samples collected on filters) are plotted on the right axis. The pie chart shows the campaign average relative contributions of AMS species and BC to PM_1 (campaign average concentration: 18.5 µg m^{-3}).

4.4.2 PMF: Identification of sources/components of organic aerosol (OA)

Factor profiles and time series

For both the UMR and HR organic data matrix, 5 factors could be identified using PMF: low-volatility and semi-volatile oxygenated OA (LV-OOA and SV-OOA, the latter is a recombination of two individual factors, see section below), hydrocarbon-like OA (HOA), biomass burning OA (BBOA), and cooking OA (COA). Since the HR data matrix provides an increased level of information (individual ion signal) compared to the UMR data, factor profiles, time series, and main conclusions are based on the HR PMF solution. However, as there are versions of the AMS that only provide UMR data (aerosol chemical speciation monitor ACSM, Ng et al., 2011c; C-ToF-AMS, Drewnick et al., 2005; quadrupole-AMS, Canagaratna et al., 2007), the UMR PMF solution and a comparison of the UMR and HR PMF solution are presented in the SI, section 4.7.3. For a discussion of the number of factors chosen and the criteria used to select the best UMR solution, we again refer the reader to the SI, section 4.7.3. HR solution criteria are briefly outlined here, figures can be found in the SI, section 4.7.3.
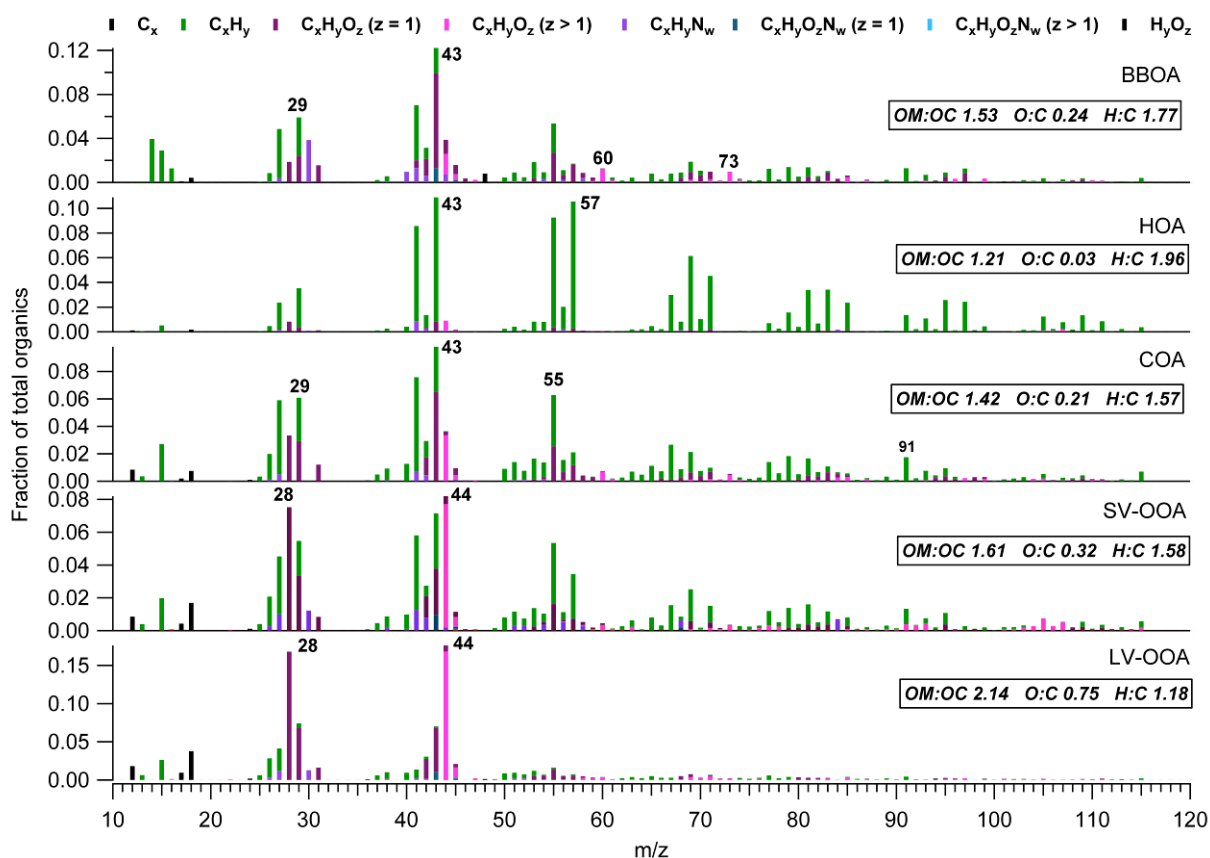
Figure 42: Mass spectra of the 5-factor-PMF solution. The elemental ratios of the different factors are shown in boxes.

The chosen 6-factor solution for the HR dataset is presented in Fig. 63. The two SV-OOA factors were recombined into a single SV-OOA factor using the sum of the time series and the loadings-weighted average of the spectra. The 5-factor solution (Fig. 64) was discarded due to the high similarity of two factors (spectra and time series). The 7-factor solution (Fig. 65) features three LV-OOA spectra: PMF seems to assign an individual LV-OOA factor to three different sections in the time series, which can be due to small variations in instrument tuning with time. As the variation in the solution space $p = 6$ as a function of *fpeak* is negligible (Figs 66 – 67), the most central solution (*fpeak* = 0) was chosen and different *SEED* values were explored (Figs. 68 – 69). *SEED* = 46 was chosen as the best solution due to correlations with reference spectra, even though it exhibits the highest Q / Q_{exp} value (12.75 compared to ~12.55 for SEED ≠ 46) and is thus not the mathematically optimal solution (see section 4.7.3). A boxplot of the scaled residuals (boxes are ± 25% of points) per *m/z* is shown in Fig. 70, time series of the residuals and Q / Q_{exp} are shown in Fig. 71. $Q / Q_{exp} \gg 1$ (12.75) indicates an underestimation of the number of factors or of the errors in the input data, possibly due to fitting errors in the HR data which are currently not included in the total error estimation. In addition to $p > 6$ (which was explored and not shown to give a more plausible solution, see above), the introduction of a "model error term" might also reduce Q / Q_{exp},

however, as discussed in Ulbrich et al. (2009), this is usually not applied in AMS datasets. Q / Q_{exp} values >> 1 for HR-ToF-AMS data have been shown recently by other authors, e. g. Allan et al. (2010) published a Q / Q_{exp} value of 10.5.

Figure 42 shows the HR mass spectra of the 5 factors. OOA is generally dominated by secondary organic aerosol formed in the atmosphere from gas-to-particle conversion processes of the oxidation products of volatile organic compounds (VOCs, Hallquist et al., 2009). Numerous sources emitting a large number of different organic species (Goldstein and Galbally, 2007) contribute to OOA formation. However, photochemical aging causes the OOA UMR spectra to become progressively similar and lose their source fingerprint (Andreae, 2009; Capes et al., 2008). Simultaneously, the fraction of m/z 44 (CO_2^+), mostly from the decarboxylation of carboxylic acids, increases (Ng et al., 2010). LV-OOA and SV-OOA factors serve as a basis set for describing the range of physicochemical properties occurring in the dynamic evolution of OOA (Jimenez et al., 2009). The LV-OOA spectrum found here features dominant signals at m/z 44 (with the signal at m/z 28 assumed equal to m/z 44, Aiken et al., 2008). The R^2 of its correlation with the standard UMR LV-OOA spectrum from Ng et al. (2011b) is 0.96. The dominant ion families are C_xH_yO and $C_xH_yO_z$ (z > 1); the O:C atomic ratio of 0.75 confirms the high degree of oxygenation. This value lies in the middle of the LV-OOA O:C range spanned by the 2D framework of OA aging (where the oxidation state approximated by the O:C ratio is plotted against the saturation vapor pressure, Jimenez et al., 2009). It is in between the O:C ratios of 0.6 of the OOA spectrum found for Mexico City, where no separation of LV-OOA and SV-OOA was possible (Aiken et al., 2010), and 1.02 found for LV-OOA in aircraft measurements in the Mexico city region (DeCarlo et al., 2010). As also found by e.g. Lanz et al. (2007) and DeCarlo et al. (2010), the LV-OOA time series correlates with that of non-volatile, regionally-transported SO_4 (see Fig. 43, R^2 = 0.43 for HR). Taken together with the high O:C ratio, this confirms LV-OOA as characteristic of aged, regional aerosol.

Investigation of the PMF factors' diurnal patterns helps greatly in their identification. Apart from varying emission sources and strengths during the course of a day, temperature-driven phenomena such as the sea breeze circulation and boundary layer heights play a very important role for the diurnal evolution of OA components. Figure 44 presents the hourly concentration median and the range spanned by the 1st and the 3rd quartile (shaded area). Consistent with its regional character, LV-OOA does not display a pronounced diurnal pattern.

The SV-OOA spectrum was calculated by recombining two individual factors found by PMF, as described in the supplementary material. Correlation with the standard SV-OOA mass spectrum from Ng et al. (2011b) yields an R^2 of 0.86. High signal at m/z 44 (and m/z 28) identifies it as OOA; the O:C (0.32) ratio is lower than for LV-OOA due to substantial contributions from the non-oxygen-containing ions at e. g. m/z 29, 43, and 55. The substantial signal at the ion series

$C_nH_{2n+1}^+$ (m/z 29, 43, 57, 71,...) from saturated alkanes and $C_nH_{2n-1}^+$ (m/z 41, 55, 69,...) from alkenes and cycloalkanes and the diurnal cycle exhibiting the typical rush-hour peaks around 09:00 and 22:00 (further increased later due to the decrease in boundary layer height) indicate an influence from vehicle emissions. The highest concentrations are measured around 11:00, linked to rapid SOA formation from primary emissions (Reche et al., 2011). A small peak in the late afternoon, when the photochemical activity is very high, corresponds to the daily maximum of O_3 concentrations (Pandolfi et al., 2012). The time series of SV-OOA shows a similar trend as the time series of the semi-volatile nitrate (see Fig. 3, $R^2 = 0.22$) also seen in other locations (Lanz et al., 2007; DeCarlo et al., 2010); the diurnal patterns of both SV-OOA and NO_3 (not shown) indicate that the temporal evolution of both components is rather driven by similar processes such as primary emissions, rapid chemical formation, and the diurnal cycles of land/sea breeze and boundary layer height than gas-to-particle partitioning based on volatility characteristics. SV-OOA can thus be described as of more local origin, less processed than LV-OOA.
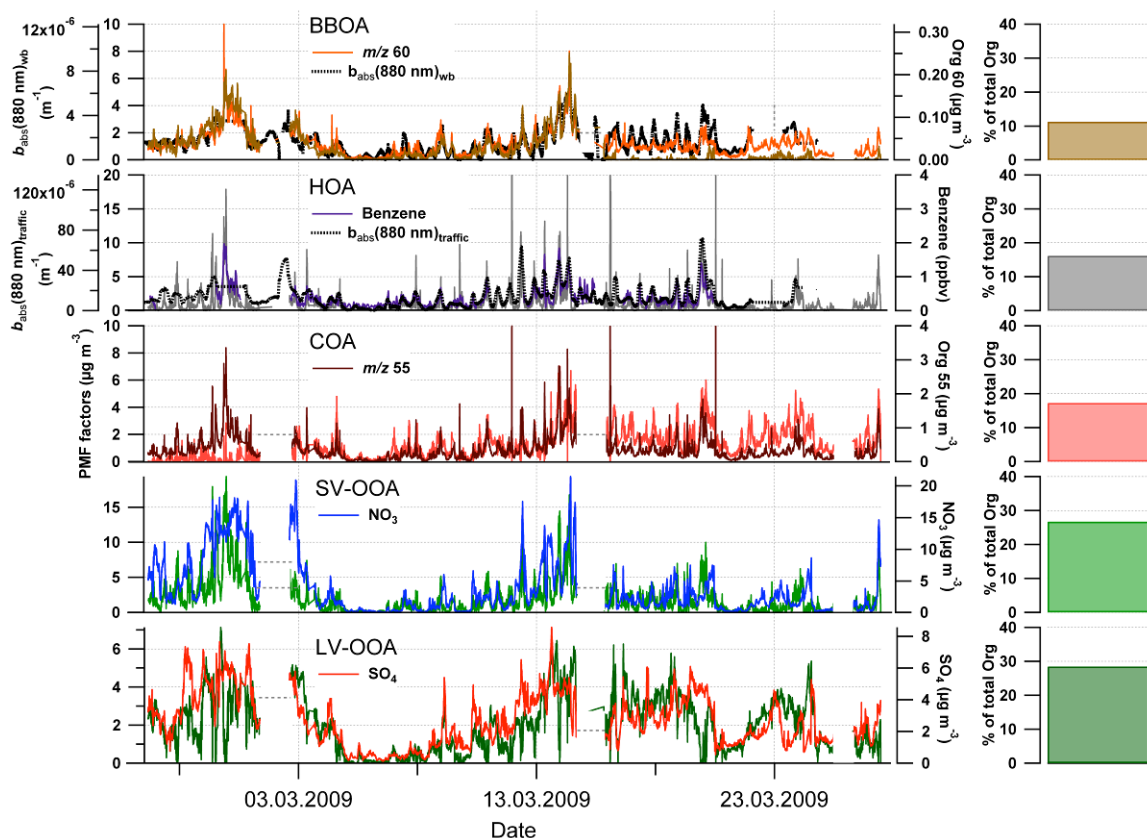
Figure 43: Time series of the 5-factor-PMF solution and ancillary data. The right panels show the relative contributions of the respective factors to OA.

The HOA factor is related to fossil fuel combustion. Diesel exhaust is typically dominated by recondensed engine lubricating oil and consists mainly of n-alkanes, branched alkanes, cycloalkanes, and aromatics (Canagaratna et al., 2004; Chirico et al., 2010), leading to high signal at the ion series $C_nH_{2n+1}^+$ and $C_nH_{2n-1}^+$. Especially *m/z* 57 is a major mass fragment and often used as a tracer for HOA (Zhang et al., 2005a). Given the high number of diesel cars in Barcelona (> 45% of the vehicle fleet, Reche et al., 2011) and proximity to the harbor, both vehicle and ship traffic could contribute to HOA (Murphy et al., 2009). However, the two distinct peaks in the morning and evening hours of the HOA diurnal cycle (Fig. 44) suggest traffic emissions as the main source; the sea breeze during the afternoon hours and the increase in boundary layer height have a diluting effect on the primary emissions. BC, particle number, toluene, benzene, and NO_x peak at the same time of the day (Pandolfi et al., 2012). Correlation of the HOA factor found here with the standard HOA mass spectral profile from Ng et al. (2011b) yields an R^2 value of 0.94. Consistent with the dominance of the reduced hydrocarbon ions (C_xH_y), the O:C ratio is very low (0.03), comparable to Mexico City (0.06, DeCarlo et al., 2010). The H:C elemental ratio (1.96) is the highest among the PMF factors. The HOA time series (Fig. 43) correlates with benzene (measured by a proton transfer reaction-mass spectrometer PTR-MS, Ionicon Analytik), a natural constituent of gasoline and also formed by combustion ($R^2 = 0.66$), supporting the identification of traffic as a major HOA source. The fraction of black carbon from traffic emissions was approximated by calculating b_{abs} at 880 nm of PM from vehicle exhaust (b_{abs} (880 nm) $_{traffic}$) using the model developed by Sandradewi et al. (2008), with an Ångstrom exponent $\alpha_{traffic} = 0.9$ (Herich et al., 2011). The time series b_{abs} (880 nm) $_{traffic}$ and the HOA time series show a similar trend. However, the R^2 value of 0.17 is too low to confirm correlation. There are spikes in the HOA time series not caught by the aethalometer model. This can be due to a lower time resolution of the aethalometer compared to the AMS or peaks in the organics time series assigned to HOA without or with lower concurrent BC emissions (i. e. possible variations in HOA/BC emission ratios of various vehicles or other fossil sources in the area). Removing 18 data points from spikes in the HOA time series (see Fig. 72 in the SI) increases the R^2 value to 0.52.

BBOA in the Barcelona region can be emitted by regional agricultural open fires or due to long-range transported pollutants from forest or agricultural fires, and possibly also from wood-combustion heating systems in suburban and rural areas (Reche et al., 2012). Characteristic mass fragments of BBOA spectra are *m/z* 60 and 73, attributed to $C_2H_4O_2^+$ and $C_3H_5O_2^+$, respectively. The ions are fragments of anhydrosugars such as levoglucosan, which are produced during cellulose pyrolysis (Alfarra et al., 2007). The BBOA time series closely follows the time series of the organic mass fragment 60 (Fig. 43). Contributions from *m/z* 29, 43, and 44 exceed the signals at *m/z* 60 and 73 – however, as they are abundant in almost all PMF spectra, they cannot be used as tracer mass fragments for BBOA (Alfarra et al., 2007). Comparison of the BBOA factor found here

with the standard BBOA spectrum from Ng et al. (2011b) yields an R^2 value of 0.8. BBOA contains high contributions from the oxygen-containing ion families. The O:C ratio of 0.24 is also higher than for the other primary sources, in accordance with findings by e. g. Alfarra et al. (2007) and Aiken et al (2010). The time series of BBOA shows a similar trend as the b_{abs}(880 nm) from wood burning (b_{abs}(880 nm)$_{wb}$), a surrogate for the BC fraction from biomass burning determined with the same method as b_{abs}(880 nm)$_{traffic}$ and using α_{wb} = 1.9 (Herich et al., 2011; Sandradewi et al., 2008). As the BBOA time series exhibits less spiky data than the HOA time series, the R^2 value (0.31) is higher than for b_{abs}(880 nm)$_{traffic}$ and HOA without removing the spikes from the fit. The low contribution of wood burning to BC measured in Barcelona (~10% according to the aethalometer model) and related to that the uncertainties of (b_{abs} (880 nm) $_{wb}$) as a function of α_{wb} probably lead to the weak correlation. BBOA exhibits a much smoother diurnal cycle than the other primary sources with no big peaks, which suggests that its sources are mainly outside of the city. As observed by Reche et al. (2012), concentrations during the night are slightly elevated due to smoke from open agricultural burning and heating systems in the surrounding valleys brought into the city by the land and downslope breezes.

COA has recently been identified as a major contributor to OA in several environments (Allan et al., 2010; Huang et al., 2010; Crippa et al., 2011). The COA spectrum exhibits signal from the same hydrocarbon ion series as the HOA spectrum; however, the oxygen-containing ions substantially contribute to e.g. *m/z*'s 43, 55, and 57, consistent with the high degree of oxygenation of fatty acids, which are a major constituent of COA (Mohr et al., 2009; He et al., 2010). Consequently the elemental O:C ratio is higher (0.21) and the H:C ratio lower (1.57) than for HOA. An important mass fragment of COA UMR spectra is *m/z* 55 (Lanz et al., 2007; Mohr et al., 2009; Allan et al., 2010). This is also shown by the similarity of the time series of COA and *m/z* 55 (Fig. 43). However, while the regression analysis of the UMR COA and *m/z* 55 yields an R^2 of 0.59, the R^2 of 0.13 for HR COA and *m/z* 55 is too low to confirm correlation due to the varying ratios of HR COA to *m/z* 55. During the first part of the campaign (until 02 March 2009), HR COA is lower relative to *m/z* 55, after 15 March 2009 it is higher. Comparison of the COA factor found here with the COA factor from Manchester (Allan et al., 2010) results in an R^2 of 0.88. The diurnal cycle (Fig. 44) shows that COA concentrations already start to rise during the late morning hours and peak around 15:00 (shortly after Spanish lunch times), when the sea breeze is at a maximum and transports the COA from downtown to the measurement site, and later in the evening around 22:00, shortly after Spanish dinner time, due to the lower nocturnal boundary layer height. The COA diurnal cycle is consistent with those reported in previous studies (Allan et al., 2010; Huang et al., 2010; Sun et al., 2011), with peaks during midday (depending on lunch times of the different countries) and in the later evening.

The right panel in Fig. 43 shows the mass of OA explained by the PMF factors. LV-OOA makes up 28% of the OA. SV-OOA contributes 27% to OA. Together, the secondary fraction accounts for 55% of OA. This dominance of OOA is consistent with previous findings for various locations in Northern hemisphere midlatitudes and in central Europe (Jimenez et al., 2009; Lanz et al., 2010). For the primary components, COA makes up 17%, HOA 16%, and BBOA 11%.

The comparatively small fraction of HOA for Barcelona is surprising given its high traffic density. However, this finding is supported by Minguillón et al. (2011), who showed that for this specific winter period, 40% of the organic carbon (OC) of PM_1 was fossil and 60% non-fossil. Considering the three primary-dominated components and their OM:OC ratios displayed in Fig. 42, we can estimate that 59% of the carbon in POA in Barcelona is non-fossil while 41% is fossil. The dominance of non-fossil carbon in urban POA is important for the interpretation of modern carbon measurements. Interestingly, the OM:OC ratios of the PMF spectra presented here and the results from Minguillón et al. (2011) also suggest a modern carbon fraction of 60% for all oxygenated OC (LV and SV). The COA fraction is roughly the same as HOA; cooking emissions, for which no control strategies have been implemented so far, appear to play a very important role for air quality under current conditions. Similar results were reported by Allan et al. (2010) and Crippa et al.(2011), who presented even higher COA fractions in two UK cities and Paris, respectively. The BBOA fraction found here (absolute mean value 0.8 µg m^{-3} for the whole campaign) is slightly lower than the biomass burning OM estimated from non-fossil EC and typical EC/OC ratios for biomass burning sources (Minguillón et al., 2011) or the Multilinear Engine (ME) receptor model applied on filter measurements (Reche et al., 2012) and slightly above the BBOA concentration determined by levoglucosan measurements (Minguillón et al., 2011). However, compared to the Mexico City region during the dry season when frequent forest fires contribute significantly to PM_1 with a mean value of 2.5 µg m^{-3} for March 2006 (Aiken et al., 2009), or Swiss Zurich winters when wood is burned for domestic heating purposes, with BBOA concentrations of 2.4 and 3.5 µg m^{-3} (Mohr et al., 2011; Lanz et al., 2008), biomass burning is a less important source of OA in Barcelona during winter time.
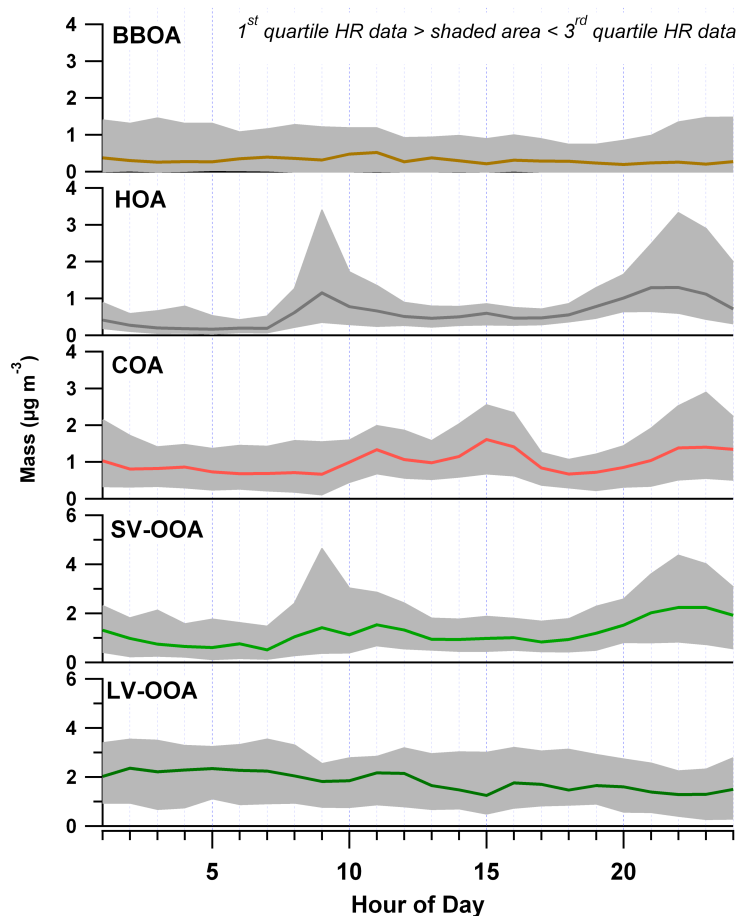
Figure 44: Diurnal cycles of the 5-factor-PMF solution. The colored lines represent the median per hour of day, and the shaded area the range between the 1st and the 3rd quartile of the data.

Size distributions

Figure 45 shows the mean mass size distributions of PM$_1$ components for all periods when the percentage of total organics of either LV-OOA, SV-OOA, COA, HOA or BBOA was above its upper 95%-percentile and, at the same time, all other PMF factors' fractions of total organics were below their upper 75%-percentile. The number of points used in the average and the organic mass fractions of the corresponding factors during those periods is included in the figure. Total AMS mass and SMPS data of the same time periods were added for comparison. The SMPS mass was calculated using an average particle density based on the chemical composition determined by the AMS. The following densities ρ (g cm^{-3}) were used (Duplissy et al., 2011): for Org, $\rho = 1.27$; for SO$_4$, $\rho = 1.78$; for NO$_3$, $\rho = 1.72$; for NH$_4$, $\rho = 1.75$; and for Chl, $\rho = 1.4$. The SMPS mobility diameter was converted to the vacuum aerodynamic diameter (d_{va}) (DeCarlo et al., 2004) using these densities and assuming spherical particles.

Periods with a larger impact of LV-OOA show a single-mode distribution peaking at 400 nm d_{va} (accumulation mode), consistent with its identification as aged, regionally influenced aerosol (Zhang et al., 2005b). The total AMS and SMPS mass size distributions show very good agreement, indicating negligible concentrations of BC during high LV-OOA periods and sphericity of particles (DeCarlo et al., 2004; Slowik et al., 2004). During high SV-OOA episodes, the size distribution exhibits both a strong accumulation mode and a smaller mode with d_{va} < 100 nm. This is most likely due to condensation of fresh secondary OA (Zhang et al., 2005b). Compared to the AMS total mass, the SMPS mass distribution is much broader with a lower accumulation mode peak height, indicating the potential role of non-spherical particles at higher sizes. Potential evaporative losses of semi-volatile species such as ammonium nitrate and SV-OOA in the DMA-CPC system (Gysel et al., 2007) could also lead to this underestimation (the ammonium nitrate fraction is larger during SV-OOA dominated periods than when LV-OOA concentrations are high). The AMS size distribution during high HOA episodes features a bimodal distribution with contributions from particles with d_{va} < 100 nm, comparable to the HOA size distribution found by 3D-factorization of mass spectra from Mexico City (Ulbrich et al., 2011) or based on tracer *m/z* (Nemitz et al., 2008).
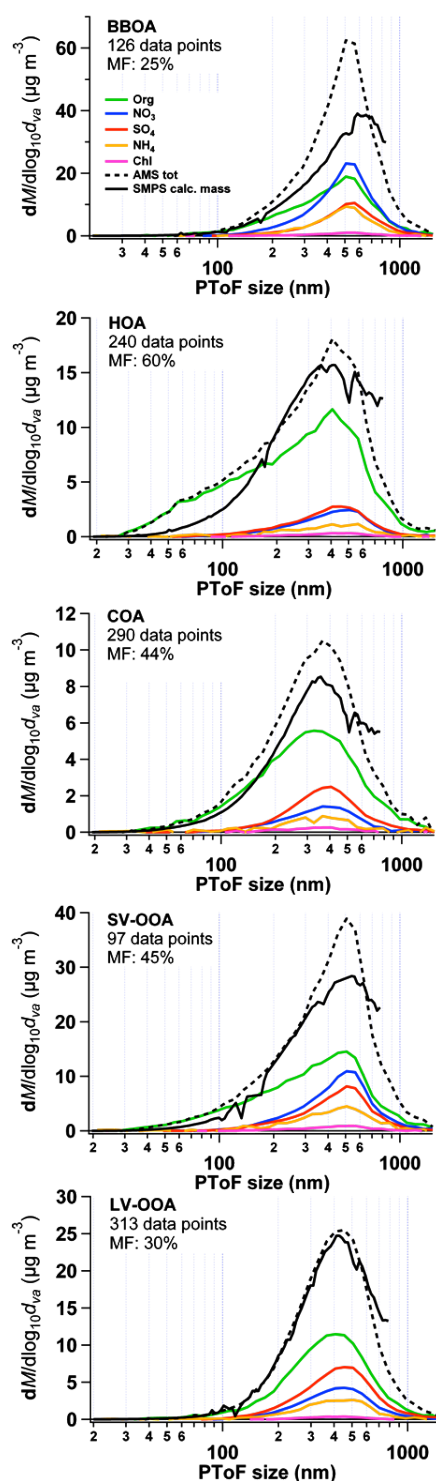
Figure 45: Size distributions of PM$_1$ components for periods with high LV-OOA, SV-OOA, COA, HOA or BBOA. The number of data points averaged and the organic mass fraction (MF) of the respective factor during those data points are given. Total AMS mass and SMPS data of the same time periods were added for comparison.

The discrepancy between AMS and SMPS size distributions at small particle sizes is characteristic of fractal particles (Slowik et al., 2004; DeCarlo et al., 2004), which are produced by

combustion sources such as traffic emissions. Different sizing of fractal particles by the SMPS leads to an overestimation of the mass of these particles (DeCarlo et al., 2004). The size distribution during high COA periods resembles more the size distribution of particles during periods dominated by secondary OA, peaking at ~350 nm d_{va}.

A similar single-mode distribution was previously observed by Hildemann et al. (1991) for meat cooking aerosol, with the peak center at around 200 nm mobility diameter. Rogge et al. (1991) explained the formation of PM from (meat) cooking activities by nucleation and growth of evaporated grease, which most likely yields spherical particles. For periods when BBOA dominates the organic composition, also ammonium nitrate concentrations are rather high. As shown in Fig. 4, BBOA is slightly increased during nighttime, when lower temperatures favor partitioning of semi-volatile species such as nitrate into the particle phase. Consequently, the difference between SMPS and total AMS mass size distribution is especially distinct for BBOA episodes. The AMS size distribution peaks at ~500 nm, contributions from particles with a d_{va} of ~ 200 nm can be observed as well.

4.4.3 Cooking organic aerosol

As described in section 4.4.2, COA and the HOA show clear differences in the ratio of oxygen-containing ions to reduced ions and thus in their degree of oxygenation. However, if only AMS UMR data is available, the detection of COA in ambient air can be difficult due to the similarity of its UMR spectrum with HOA (Mohr et al., 2009). This spectral similarity complicates efforts to resolve distinct HOA and COA factors by PMF and is a likely cause of the scarcity of COA factors resolved from urban AMS datasets (Lanz et al., 2007; Allan et al., 2010; Huang et al., 2010; Slowik et al., 2010; Crippa et al., 2011). However, the substantial contributions of COA to total organic PM_1 suggest the importance of this anthropogenic activity to urban air quality. Here the spectral characteristics of HOA and COA discussed above are used to develop an approach for distinguishing and quantifying the contributions of HOA and COA to ambient aerosol.

Organic mass fragments 55 and 57

As stated earlier, the organic mass fragments 55 (*m/z* 55) and 57 (*m/z* 57) are crucial for the identification of COA and HOA, respectively. However, these fragments cannot directly serve as tracers because (1) each strongly appears in both factor mass spectra and (2) interferences from LV- and SV-OOA are present, which have to be subtracted (denoted by the subscript $_{OOAsub}$). We therefore define the following quantities:

$$f_{55,OOAsub} = \left(m/z55 - m/z55_{LV-OOA} - m/z55_{SV-OOA} \right)/Org \qquad (10a)$$

$$f_{57,OOAsub} = \left(m/z57 - m/z57_{LV-OOA} - m/z57_{SV-OOA} \right)/Org \qquad (10b)$$

Contributions from LV- and SV-OOA are calculated as the product of the factor time series and the mass fraction of the selected m/z in the factor mass spectrum. Figure 46a shows $f_{55, OOA\,sub}$ as a function of $f_{57, OOA\,sub}$ for the whole Barcelona dataset. The data points fall into a V-shape in the scatter plot; subtraction of the LV- and SV-OOA interferences changed the intercept to 0 (compare Fig. 73 in the SI) but did not otherwise alter the result. Data points are colored by time of day. The $f_{55, OOA\,sub} / f_{57, OOA\,sub}$ slope is steepest in the afternoon, corresponding to the peak in the COA diurnal pattern (see Fig. 44). In contrast, the shallowest slopes are found in the traffic-dominated morning and evening hours.

Figure 46a also includes F_{55} (defined as *m/z* 55 / Org) and F_{57} (*m/z* 57 / Org) from PMF HOA and COA factors (bold symbols), as well as from emission spectra of cooking and traffic sources (thin symbols). These factors/sources were grouped as "cooking-like" or "traffic-like", and a linear fit was applied to each group. Point #1, Zurich Summer PMF-HOA (Lanz et al., 2007), was excluded as an outlier. Fits to the cooking-like (red solid and dotted lines) and traffic-like (black solid and dotted lines) follow the higher and lower edges of the Barcelona data in Fig. 46a, which correspond to cooking- and traffic-influenced data, respectively. This supports the use of the $f_{55, OOA\,sub} / f_{57, OOA\,sub}$ ratio as a metric for identifying COA.
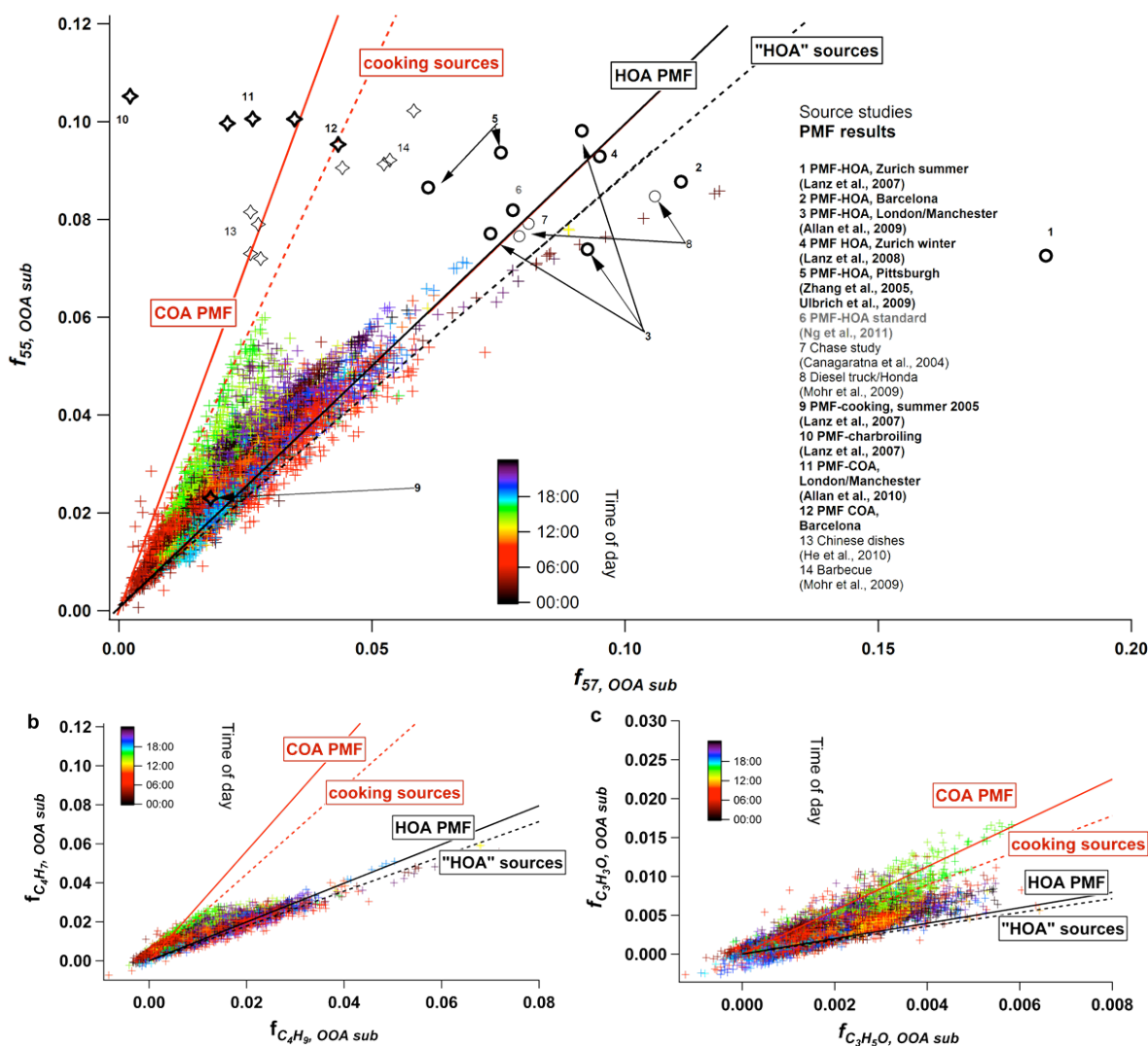
Figure 46: $f_{55, OOA\ sub}$ (see text) plotted against $f_{57, OOA\ sub}$ (a), $f_{C4H7+, OOA\ sub}$ plotted against $f_{C4H9+, OOA\ sub}$ and $f_{C3H3O+, OOA\ sub}$ against $f_{C3H5O+,OOA\ sub}$ (c) for the whole Barcelona dataset. Data points are colored according to time of day. Included in (a) are F_{55} and F_{57} extracted from various PMF HOA and COA factors (bold symbols), as well as from cooking and traffic source emission studies (thin symbols), the lines represent the linear fits applied to each group. Note that axes are scaled differently for clarity reasons.

Figure 42 shows that m/z 55 for HOA is composed mostly of a different ion ($C_4H_7^+$) than COA ($C_4H_7^+$ and $C_3H_3O^+$). High resolution source spectra show consistent results; see Fig. 74 in the SI. Similarly, for HOA m/z 57 is composed of $C_4H_9^+$ while COA m/z 57 includes both $C_4H_9^+$ and $C_3H_5O^+$. A simplified apportionment of these ions is assessed in Figs 46b and 46c, where $C_3H_3O^+$ and $C_3H_5O^+$ are apportioned to COA, with $C_4H_7^+$ and $C_4H_9^+$ apportioned entirely to HOA. These Figures are similar to Fig. 46a, with $f_{55, OOA\ sub}$ and $f_{57, OOA\ sub}$ replaced by $f_{C4H7+, OOA\ sub}$ and $f_{C4H9+, OOA\ sub}$ in Fig. 46b, and by $f_{C3H3O+, OOA\ sub}$ and $f_{C3H5O+, OOA\ sub}$ in Fig. 46c. Solid and dashed lines are the same as in Fig. 46a. HOA and COA are much less distinguishable in Fig. 46b than for the UMR data (Fig. 46a), with the data points mostly aligned to the HOA fit line. This results from the low ratio of $f_{C4H7+, OOA\ sub}$ to $f_{C4H9+, OOA\ sub}$. In contrast, Fig. 46c shows that $f_{C3H3O+, OOA\ sub}$ and $f_{C3H5O+,}$

$_{OOA\ sub}$ are comparable to the UMR data in their ability to distinguish HOA and COA, indicating that the spectral differences are driven by the oxygen-containing ions. The fractional contribution of each PMF factor to *m/z* 55, $C_4H_7^+$, and $C_3H_3O^+$ is shown in Fig. 47 as a stacked diurnal cycle. The top panel (a) shows only small contributions from LV-OOA and BBOA to *m/z* 55. Although SV-OOA contributions are larger, SV-OOA is readily distinguished by high *m/z* 44 allowing the SV-OOA contribution to *m/z* 55 to be subtracted as done above. HOA has significant signal at *m/z* 55, however, as discussed above, HOA and COA can be distinguished by the oxygen-containing organic ions of *m/z* 55 and 57. This is shown in Figs 47b and 47c: $C_3H_3O^+$ shows lower signal than $C_4H_7^+$, but that signal is dominated by COA emissions and is thus a more useful tracer.
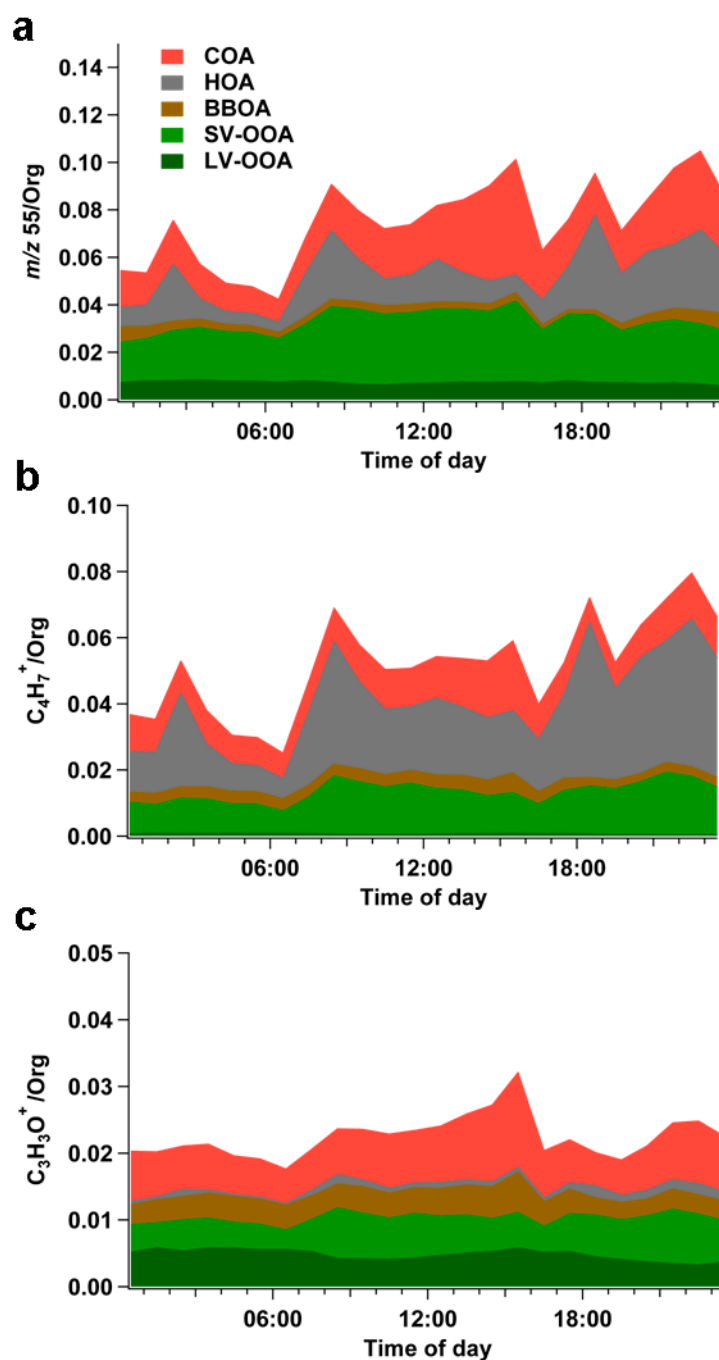
Figure 47: Stacked diurnal cycle of the time series of the fractions of *m/z* 55 (a), $C_4H_7^+$(b), and $C_3H_3O^+$ (c) of LV-OOA, SV-OOA, HOA, COA, and BBOA, respectively, normalized to total organics.

Estimation of COA from *m/z* 55

In this section a simple approximation to estimate the COA concentration based on the time series of the organic mass fragments 55, 57, and 44 is provided. Similar methods to estimate HOA, BBOA, and OOA concentrations have been given by Aiken et al. (Aiken et al., 2009). As

described in the previous section, *m/z* 55 can be used as a tracer for COA, even though its signal also has contributions from the other factors, mostly HOA and OOA (Eq. (11)). BBOA can contribute as well to *m/z* 55; however, due to the high variability wood burning spectra (Weimer et al., 2008) and the low BBOA concentrations in Barcelona it was not considered in the estimation.

$$m/z55 = m/z55(COA) + m/z55(HOA) + m/z55(OOA) \qquad (11)$$

Consequently, the contributions from the other factors have to be subtracted and the remaining *m/z55(COA)* has to be scaled up by a factor *q* to yield the estimated COA concentration COA_{est},

$$COA_{est} = q * m/z55(COA) \qquad (12)$$

The contribution from OOA to *m/z* 55 is linear with *m/z* 44,

$$m/z55(OOA) = b * m/z44 \qquad (13)$$

where

$$b = \frac{F_{55,OOA}}{F_{44,OOA}} \qquad (14)$$

$F_{55,OOA}$ denotes the signal at *m/z* 55 in the OOA mass spectrum normalized to the sum of the spectrum.

The contribution from HOA to *m/z* 55 is linear with *m/z* 57,

$$m/z55(HOA) = a * m/z57(HOA) \qquad (15)$$

where

$$a = \frac{F_{55,HOA}}{F_{57,HOA}} \qquad (16)$$

m/z 57 can have contributions not only from HOA, but also from COA and OOA; thus:

$$m/z57(HOA) = m/z57 - m/z57(COA) - m/z57(OOA) \qquad (17)$$

The last term in Eq. (17) is again linear with *m/z* 44, with the coefficient

$$c = \frac{F_{57,OOA}}{F_{44,OOA}} \qquad (18)$$

With

$$m/z57(COA) = \frac{1}{d} * m/z55(COA) \qquad (19)$$

$$d = \frac{F_{55,COA}}{F_{57,COA}} \qquad (20)$$

Eq. (12) can be solved as

$$COA_{est} = q * \left[\frac{\frac{1}{a}m/z55 - m/z57 + \left(c - \frac{b}{a}\right)m/z44}{\frac{1}{a} - \frac{1}{d}} \right] \qquad (21)$$

with

$$q = \frac{1}{F_{55,COA}} \qquad (22)$$

The coefficients a, b, c, d, and q were estimated using the PMF factor mass spectra from this study and those published in Allan et al. (2010), and Crippa et al. (2011): $q = 11 \pm 2$; $a = 0.9 \pm 0.2$; $b = 0.15 \pm 0.1$; $c = 0.07 \pm 0.07$; and $d = 3.0 \pm 0.7$. The approach was tested with the present data set. Figure 48 shows a comparison of PMF COA (both UMR and HR) found here with COA_{est} calculated using Eq. (21). Overall, the agreement is good: The correlation of the UMR PMF COA time series and COA_{est} yields an R^2 of 0.7; the R^2 of the correlation with the HR solution is lower (0.32) due to the period in the beginning, until 02 March 2009 (compare section 4.4.2). Removing the Barcelona data ($a = 0.8$, $b = 0.12$, $c = 0.03$, $d = 2.2$, and $q = 10$) from the average coefficients calculation did not change the values for a, b, c, d, and q; thus, the comparison between COA_{est} and PMF COA is not positively biased by the double use of the same data set. The application of this approach to other datasets will be of great interest to validate the coefficients found here.
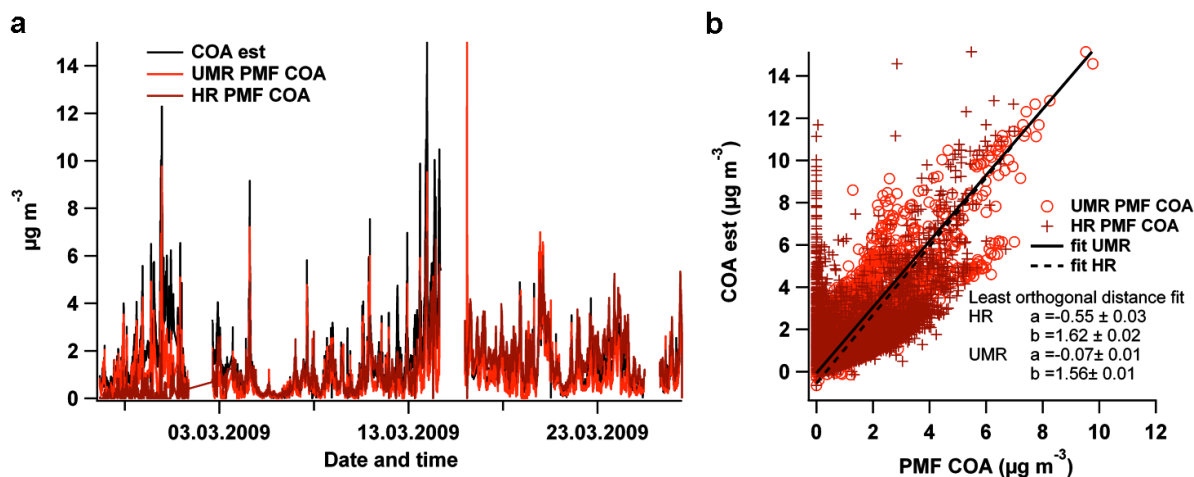
Figure 48: Comparison of PMF COA and COA estimated using organic mass fragments 55, 57, and 44 (COA est), time series (panel a) and scatterplot of time series (panel b).

4.5   Conclusions

Several studies confirm the possible importance of cooking activities as a major contributor to urban aerosol loadings; however, the number of urban environments where COA was detected and quantified is still very low. A reason for that might be the similarity of AMS UMR spectra of HOA and COA. This paper presents an approach to detect cooking organic aerosol (COA) in ambient datasets and a simple method based on organic mass fragments 55, 57, and 44 measured by AMS to estimate COA concentrations.

AMS data were acquired at an urban background site in Barcelona, Spain, during March 2009, in order to investigate the specific high PM winter anticyclone episodes. PMF analysis revealed 5 factors or sources contributing to OA: LV-OOA, related to regional, aged secondary OA; SV-OOA, a first-generation secondary OA with substantial contributions from immediately formed secondary or oxidized primary OA from vehicle emissions; HOA (primary hydrocarbon-like OA, again related to traffic and possibly ship emissions); BBOA from domestic heating or agricultural wood burning activities; and COA (cooking organic aerosol). From these results we estimate that POA in Barcelona has a non-fossil carbon fraction of about 59%, which helps explain the high non-fossil fraction of OC observed during DAURE.

The COA HR spectrum contains considerable signal from oxygenated ions whereas the HR HOA spectrum has almost exclusively contributions from chemically reduced ions, however, on a UMR basis, the spectral patterns are very similar. Plotting *m/z* 55 normalized to total organics against *m/z* 57 normalized to total organics helps identify COA in ambient datasets: The data points fall into a V-shape, with HOA-influenced data aligned to the lower arm, a line defined by fitting

F_{55} and F_{57} from various PMF HOA and vehicle emissions spectra; COA influenced data points lie on the upper arm of the V-shape denoted by a fit of F_{55} and F_{57} from PMF COA factors and cooking emissions spectra. HR data show that this differentiation is mainly driven by the oxygen-containing ions $C_3H_3O^+$ and C_3H_5O. $C_3H_3O^+$ shows lower signal than $C_4H_7^+$, but that signal is to a larger extent from COA emissions than that from $C_4H_7^+$ compared to the other factors, and thus helps identifying the COA factor much better than $C_4H_7^+$.

The agreement of COA estimated based on mass fragments 55, 57, and 44 and the PMF COA is satisfying for the present dataset. The application of this approach to other datasets will be of great interest to validate the coefficients determined in this study.

COA contributes 17% to organic PM in Barcelona during the winter anticyclonic pollution episodes, consistent with the high non-fossil fraction of carbonaceous PM_1 found by ^{14}C analysis. This is a significant fraction with consequences for human health; even more so since cooking is usually an indoor activity and what is being measured at an urban background site is already significantly diluted compared to the emissions site. The study emphasizes the significance of cooking activities for ambient air quality and confirms the importance of chemical composition measurements with a high mass and time resolution.

4.6   Acknowledgements

4.7   Supplementary information

4.7.1 Collection efficiency (CE)
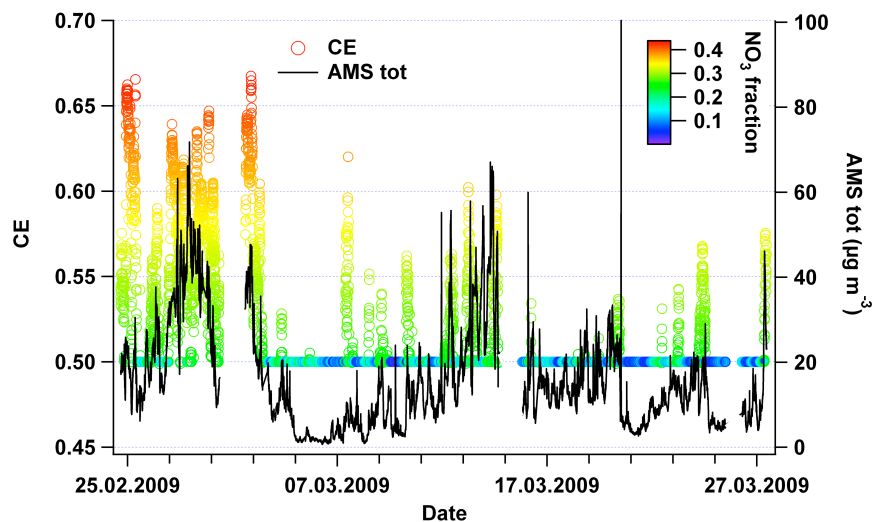
Figure 49: Time series of the collection efficiency (CE) used for the present dataset (left axis) and total concentration of species measured by AMS (right axis).

4.7.2 PM$_1$ time series
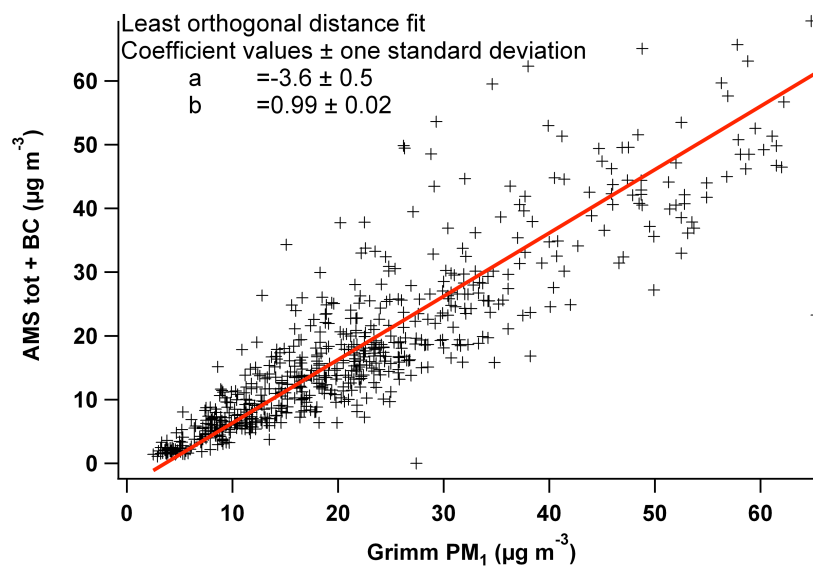
Figure 50: Scatterplot of combined time series of total AMS species (HR) and BC (y-axis) and Grimm PM$_1$. The data were fitted with a least orthogonal distance fit (red line).

4.7.3 PMF

UMR solution
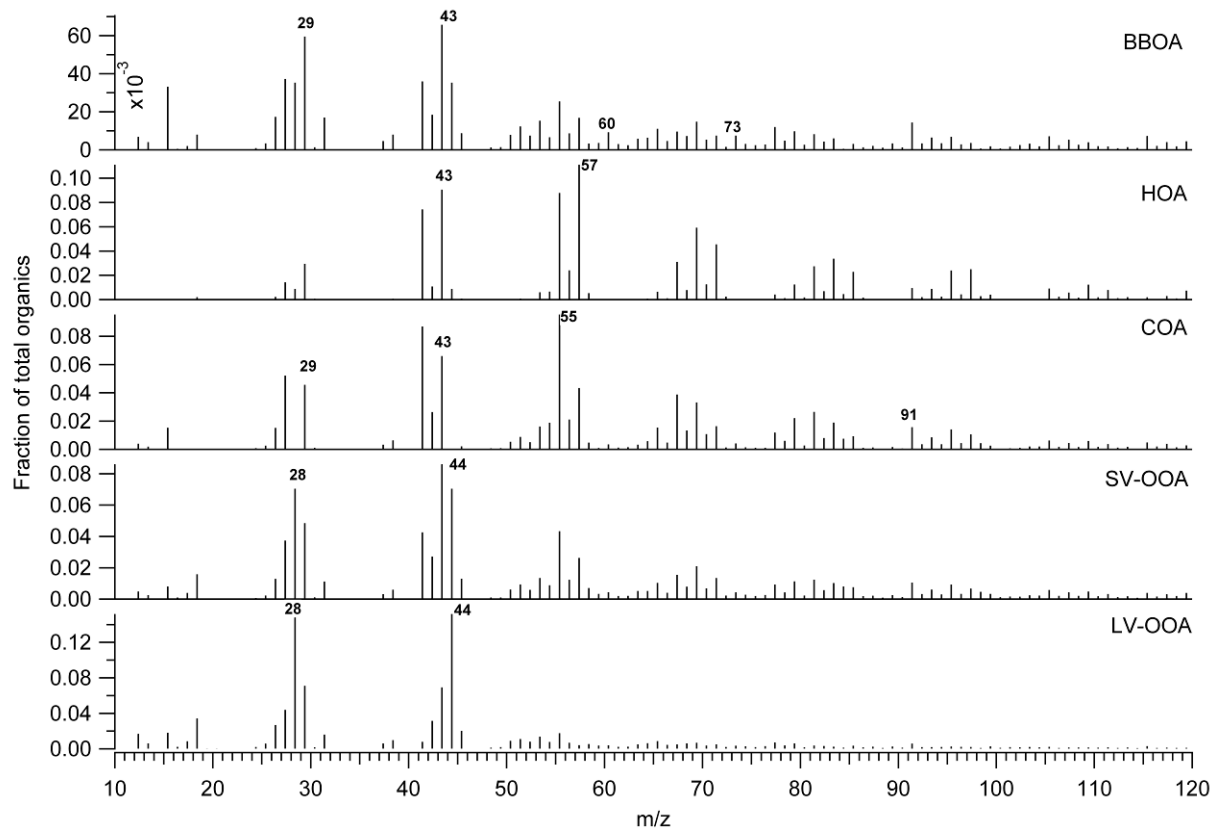
Figure 51: Mass spectra of the UMR 5-factor-PMF solution.
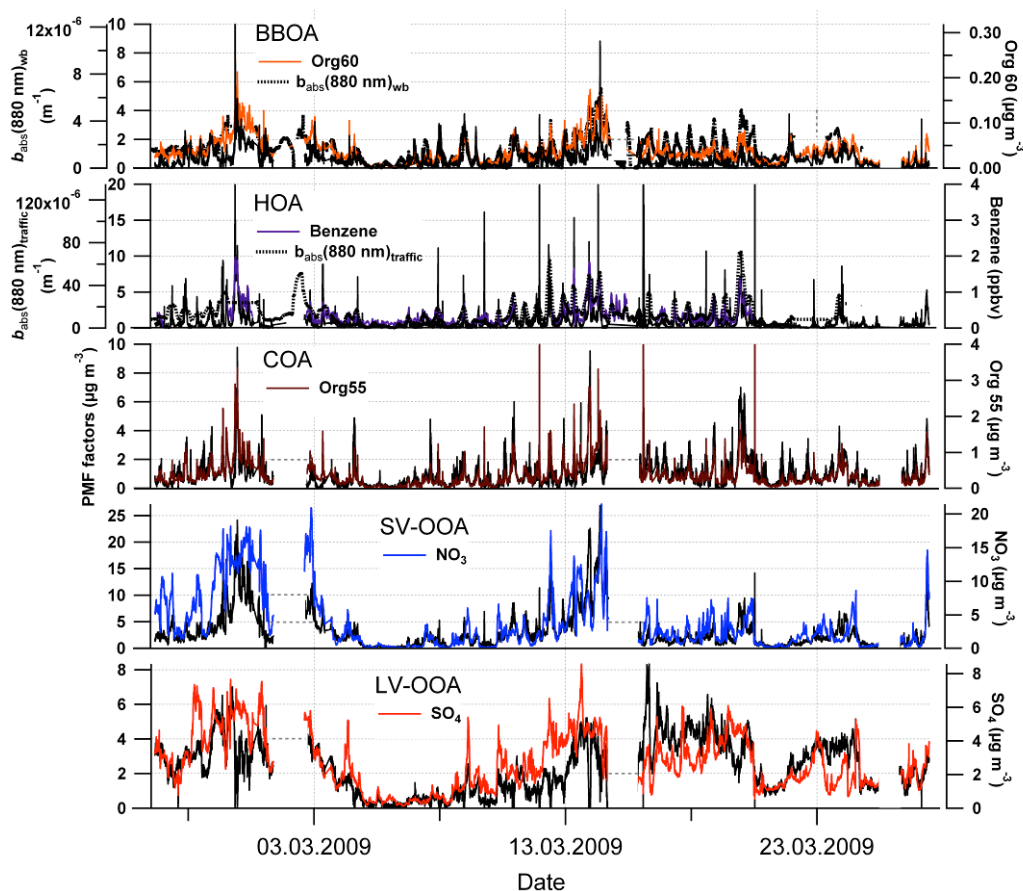
Figure 52: Time series of the UMR 5-factor-PMF solution and ancillary data.

Comparison of UMR and HR PMF solution

The R^2 of the correlation of the mass spectra of the UMR and HR PMF solution range from 0.80 (COA) to 0.99 (LV-OOA), confirming their similarities. Bigger differences can be seen in the time series of the corresponding factors. The COA time series show discrepancies in the total mass especially in the beginning of the campaign (until 02 March 2009), visualized in the data points with a much lower slope in Fig. 53h. For the BBOA, the UMR time series features peaks not inherent to the HR time series. Concerning the mass attribution to each factor, HR generally assigns more mass to the primary OA factors and less to the OOA factors. Here the higher resolution and, relied to that, the signal on an individual ion basis of the HR data matrix adds additional information to the HR data matrix and thus allows for a better quantification of primary and secondary OA.
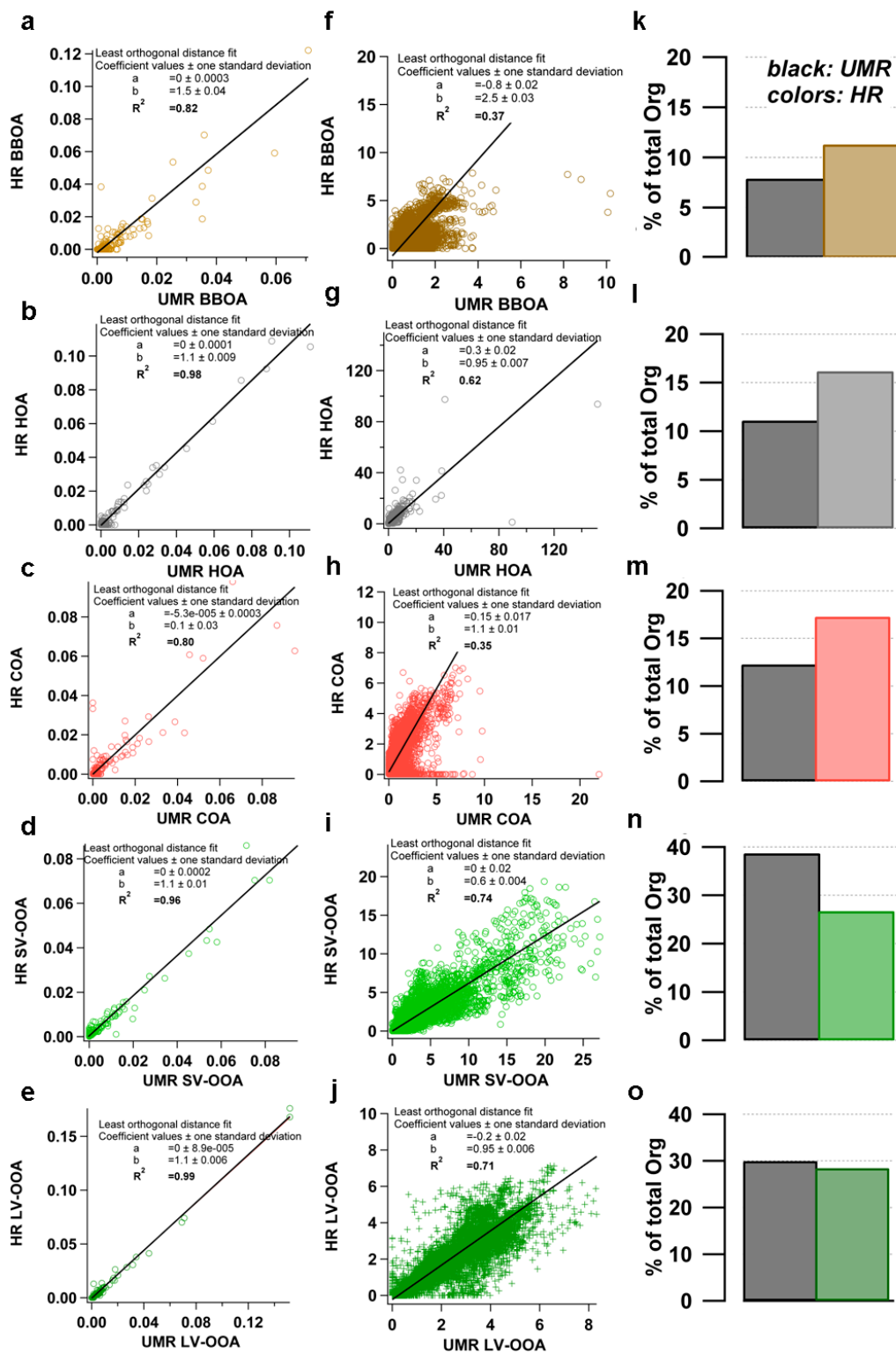
Figure 53: Scatter plots of UMR and HR PMF spectra (a-e), time series (f-j) and a comparison of the mass attributed to each factor relative to OA (k-o).

UMR solution criteria

The number of factors p was chosen to be 6 for the UMR dataset (Fig. 54). In the solution with $p = 5$ (Fig. 55a), the spectra of BBOA, HOA, and COA are less clearly separated (e. g. high signal at m/z 57 in the top factor resembling BBOA, but very little signal at m/z 57 in the red factor resembling COA). Figure 55b shows the time series of the 5-factor solution – they are less clearly distinct than those of the 6-factor solution. The 7-factor solution (Fig. 56a) features a factor consisting mostly of signal at m/z 43 and a factor (orange) with single, isolated peaks inconsistent with regular ion series. The time series show a more similar evolution (Fig. 56b), indicating a split of factors.

For the PMF solution presented in the manuscript, the 6-factor solution was chosen and the two factors assigned to SV-OOA (black and purple) regrouped to one SV-OOA, using the sum for the time series and the loadings-weighted average of the spectra.

Figure 58 presents the explained variance of the organics as a function of *fpeak* for the chosen 6-factor solution. *Fpeak* was chosen to be -0.7 based on correlations of the corresponding factors with reference spectra.

A boxplot of the scaled residuals (boxes are +/- 25% of points) per m/z is shown in Fig. 59, time series of the residuals and Q / Q_{exp} are shown in Fig. 60. On 16 March 2009, a power failure led to a breakdown of the instrument and a subsequent pumping down effect (Fig. 60). Downweighting this period in the input for PMF did not alter the solution.

The solution space for the chosen $p = 6$ (central rotation) was explored by running PMF with 50 random initial values (*SEED)* at iteration start (Figs 61 – 62). Roughly three solution groups can be identified (numbers in Fig. 62). Groups 1 and 2 feature a factor spectrum predominantly consisting of m/z 43 and two spectra that are basically identical. The spectrum with BBOA-like features shows no contributions at m/z 44, which is inconsistent with previous studies. For group 3, all spectra not assigned to OOA show very high similarities. The solution with a central rotation (*fpeak* = 0) was thus discarded regardless of *SEED* values. Similar information was also published in the supplementary information in the previous chapter.
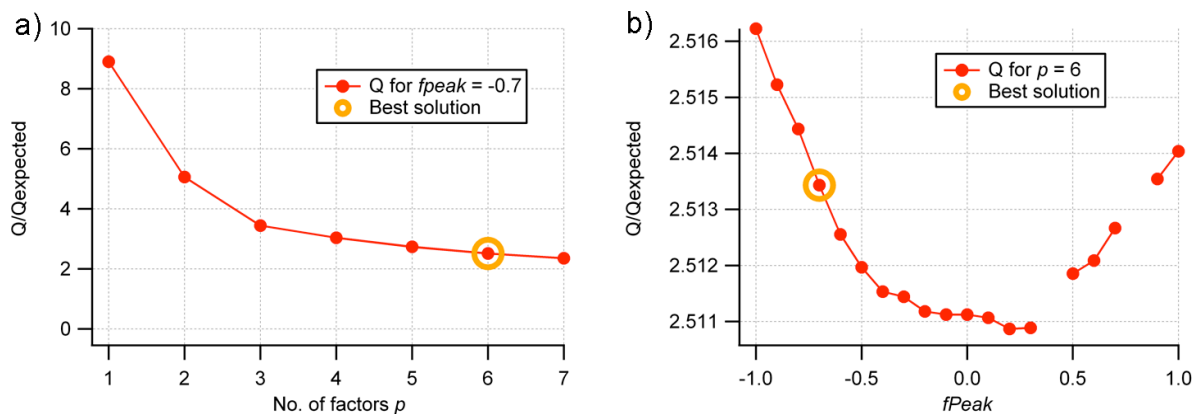
Figure 54: Q/Q_{exp} versus the number of factors p (a) or *fpeak* (b). The orange circle denotes the chosen UMR solution.
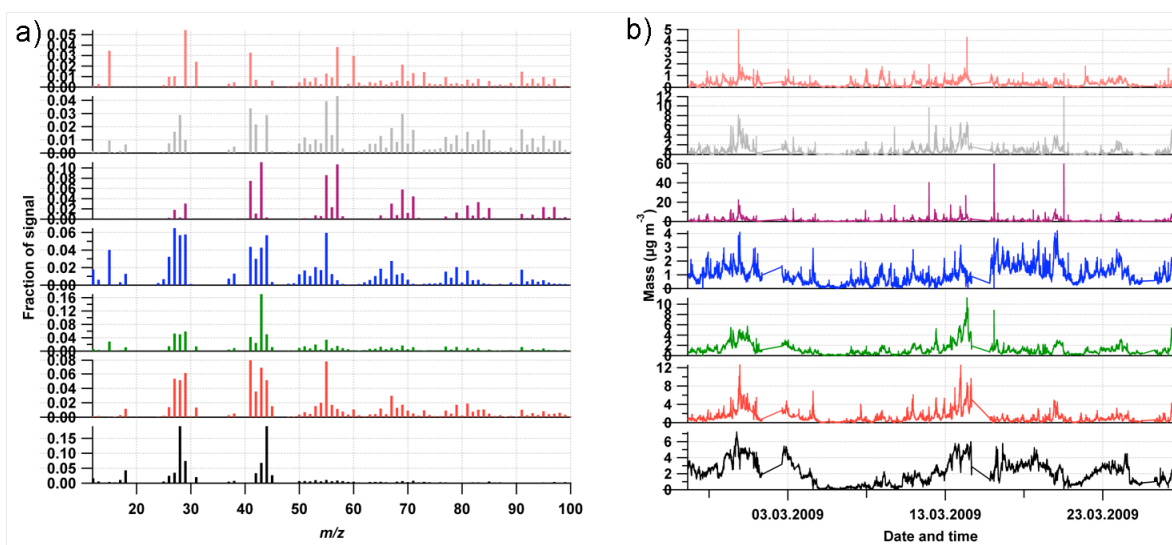
Figure 55: 6-factor UMR solution chosen, mass spectra (a) and time series (b). The black and the purple factor (SV-OOA 1 and 2) were regrouped to SV-OOA.
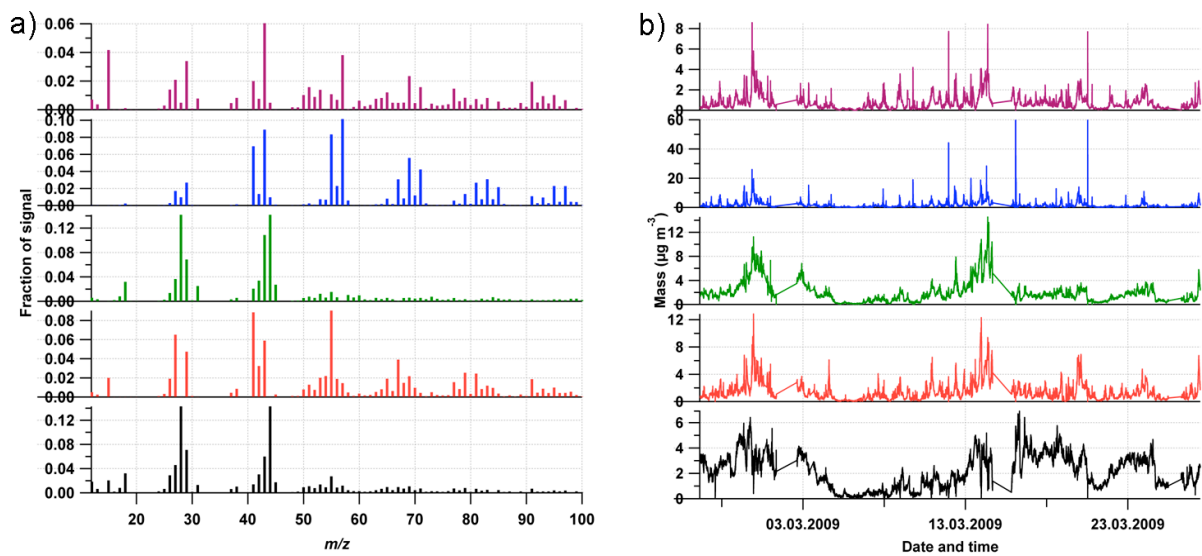
Figure 56: 5-factor UMR solution, mass spectra (a) and time series (b).
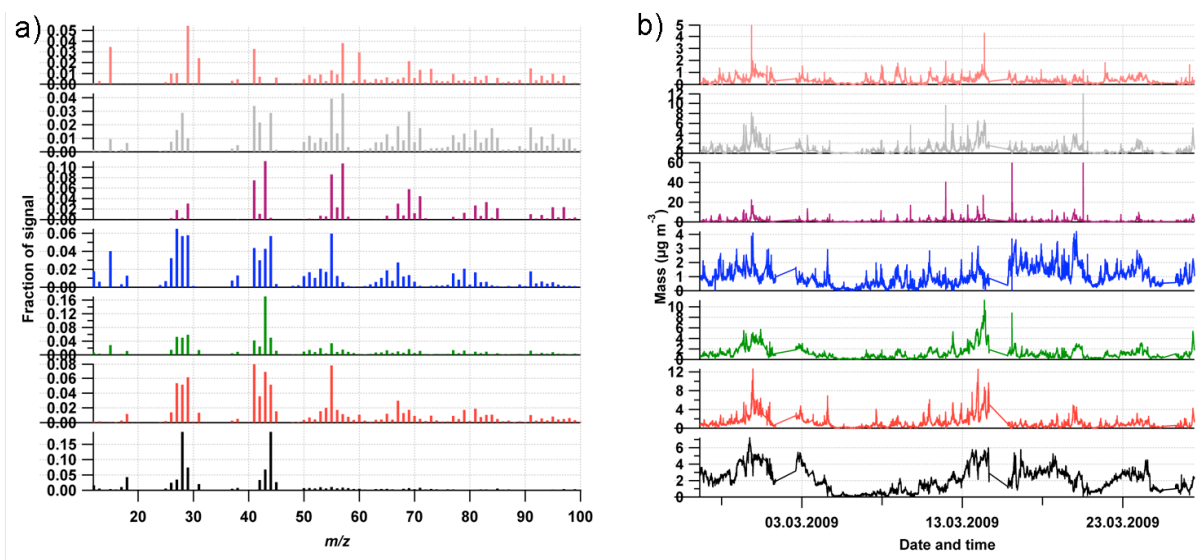
Figure 57: 7-factor UMR solution, mass spectra (a) and time series (b).
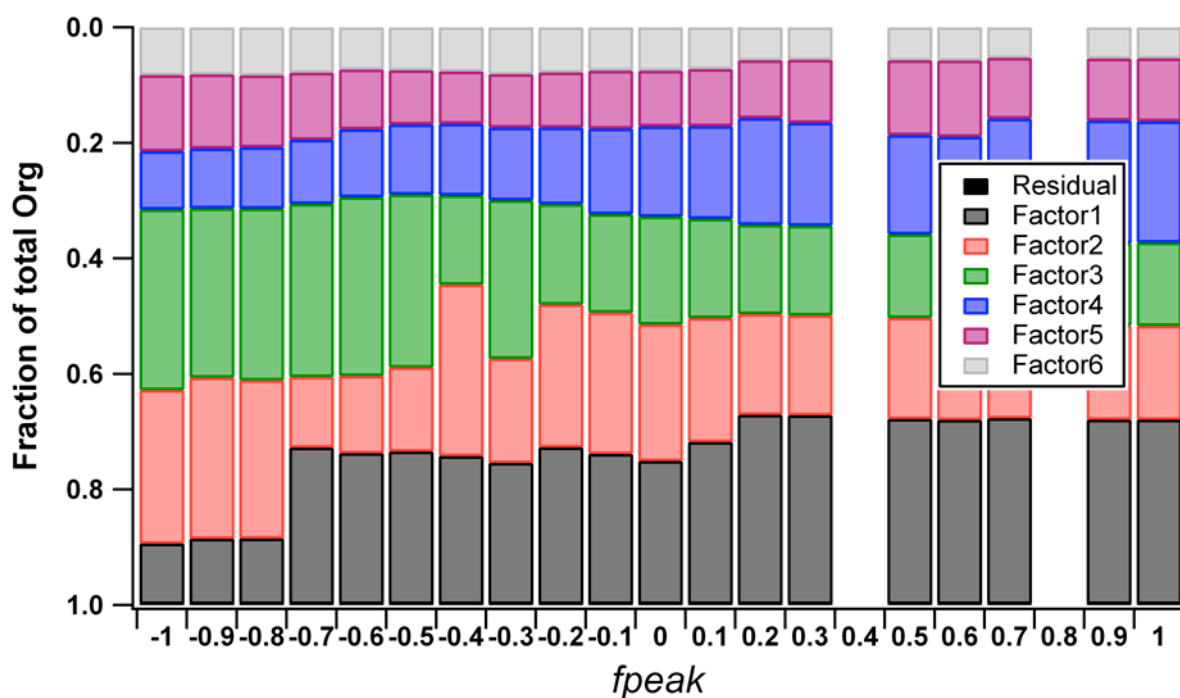
Figure 58: Variance explained by PMF due to the 6-factor UMR solution as a function of *fpeak*. For the solution presented, **f***peak* =-0.7.
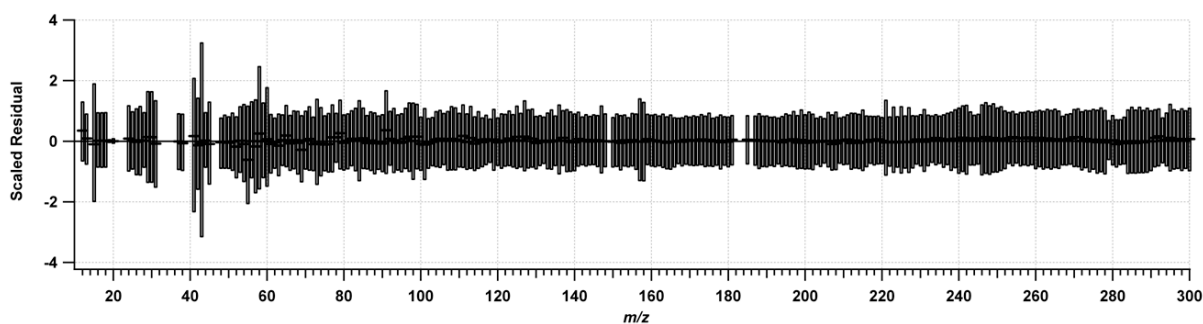
Figure 59: Median black strokes and lower/upper quartiles (boxes) of the scaled residuals per *m/z*.
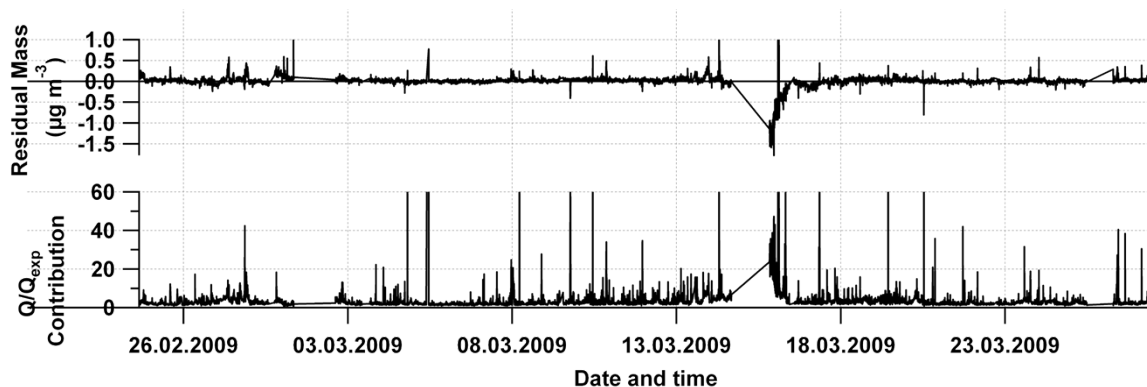
Figure 60: Time series of scaled residuals (top panel) and *Q* / *Q*_*exp* (lower panel).
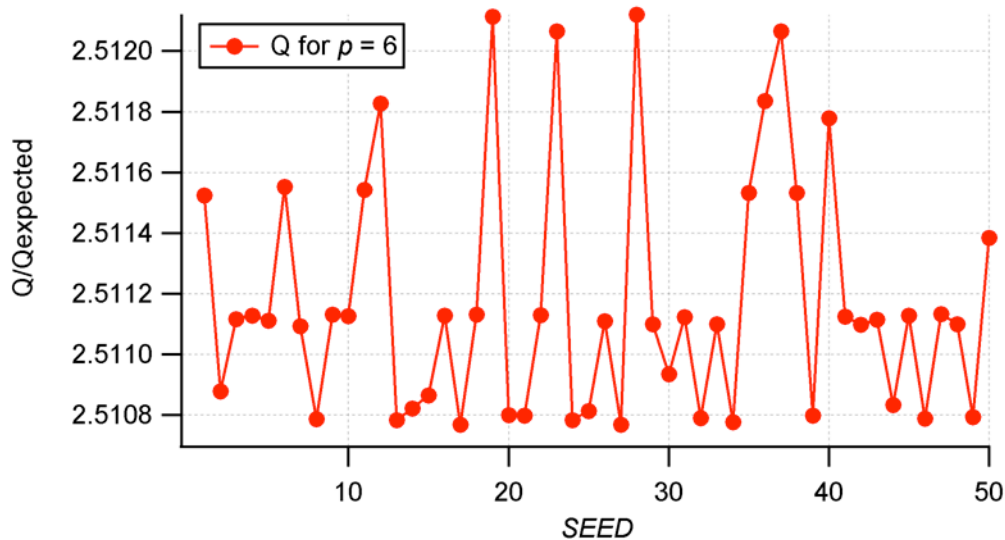
Figure 61: Q / Q_{exp} as a function of different *SEED* values.
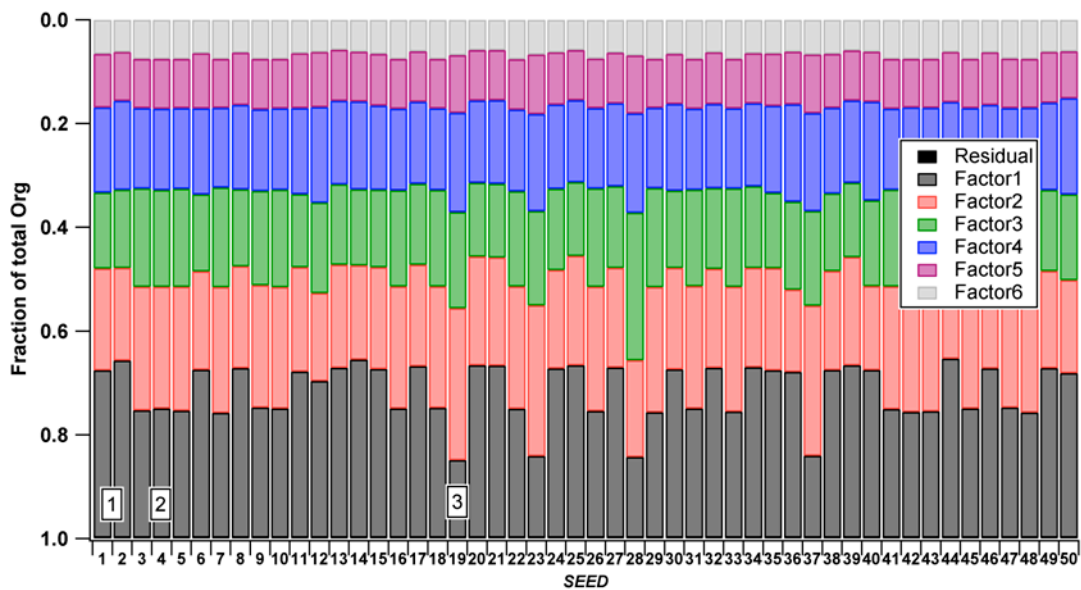
Figure 62: Variance explained by PMF due to the 6-factor UMR solution as a function of *SEED*. The numbers 1, 2 and 3 denote the three solution groups identified.

HR solution criteria
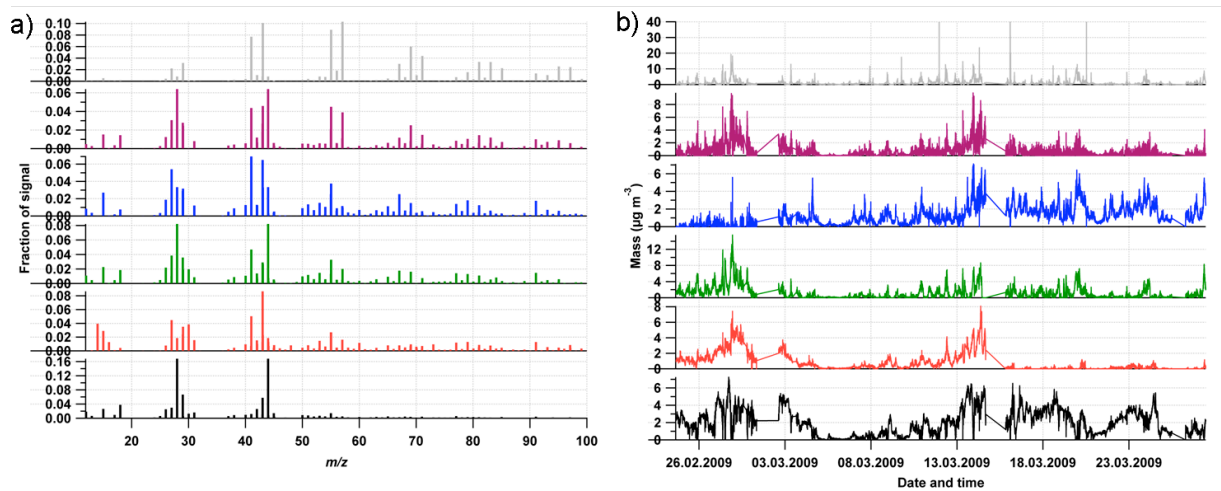
Figure 63: Chosen 6-factor solution of the HR dataset, mass spectra (a) and time series (b).
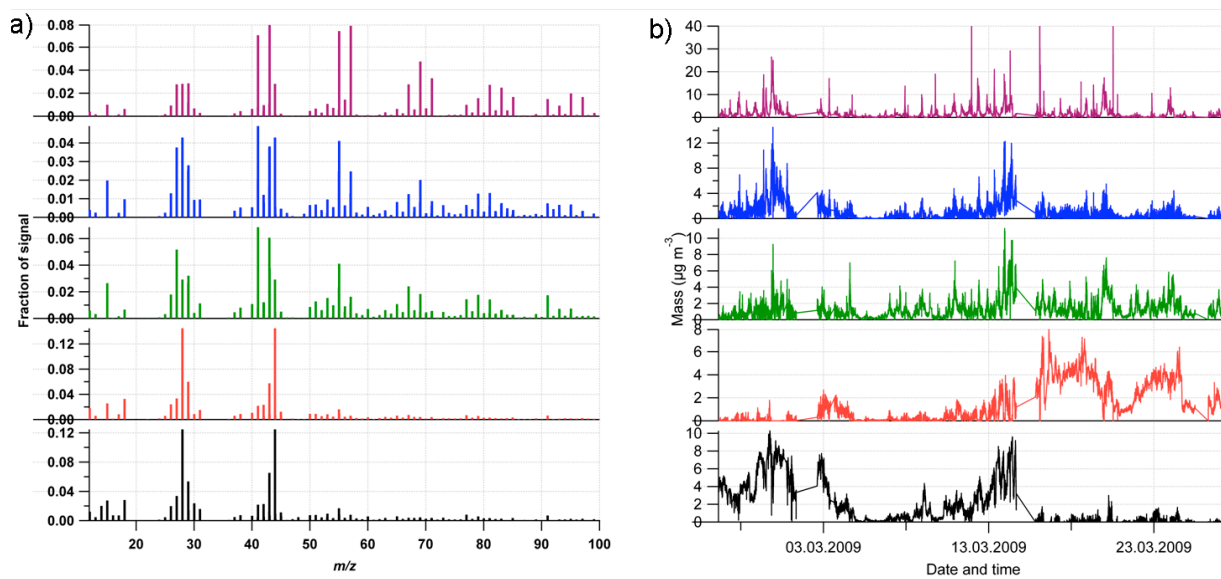
Figure 64: 5-factor solution for the HR dataset, mass spectra (a) and time series (b).
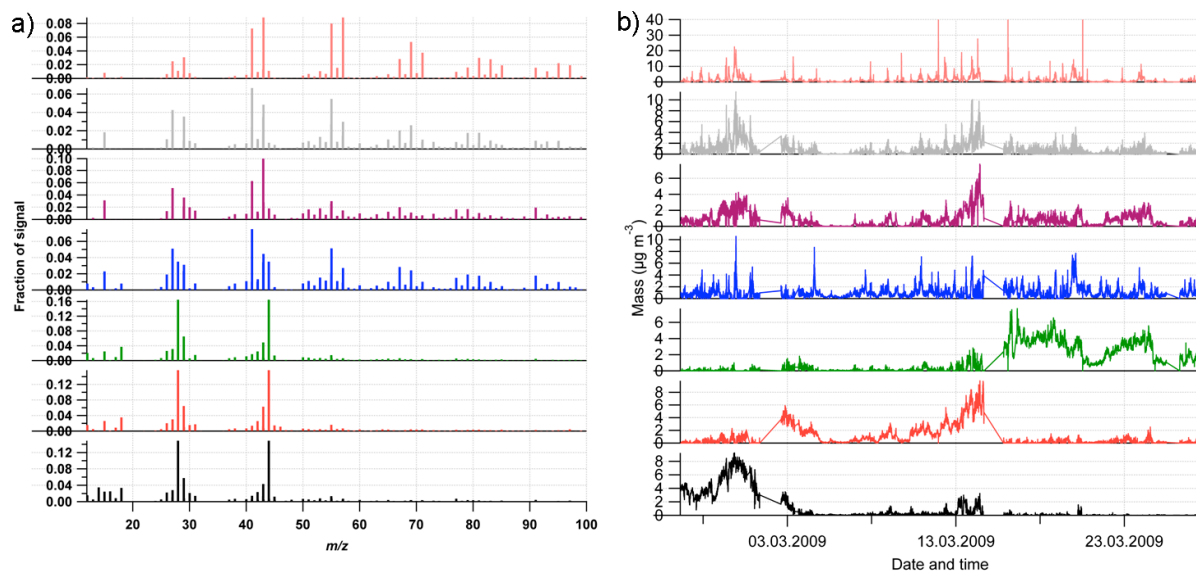
Figure 65: 7-factor solution for the HR dataset, mass spectra (a) and time series (b).
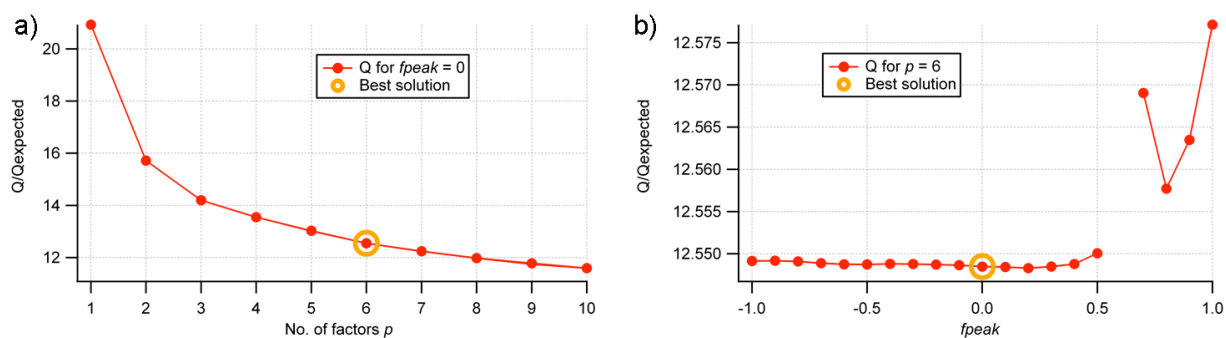
Figure 66: Q / Q_{exp} versus the number of factors p (a) or *fpeak* (b), HR PMF. The orange circle denotes the chosen solution.
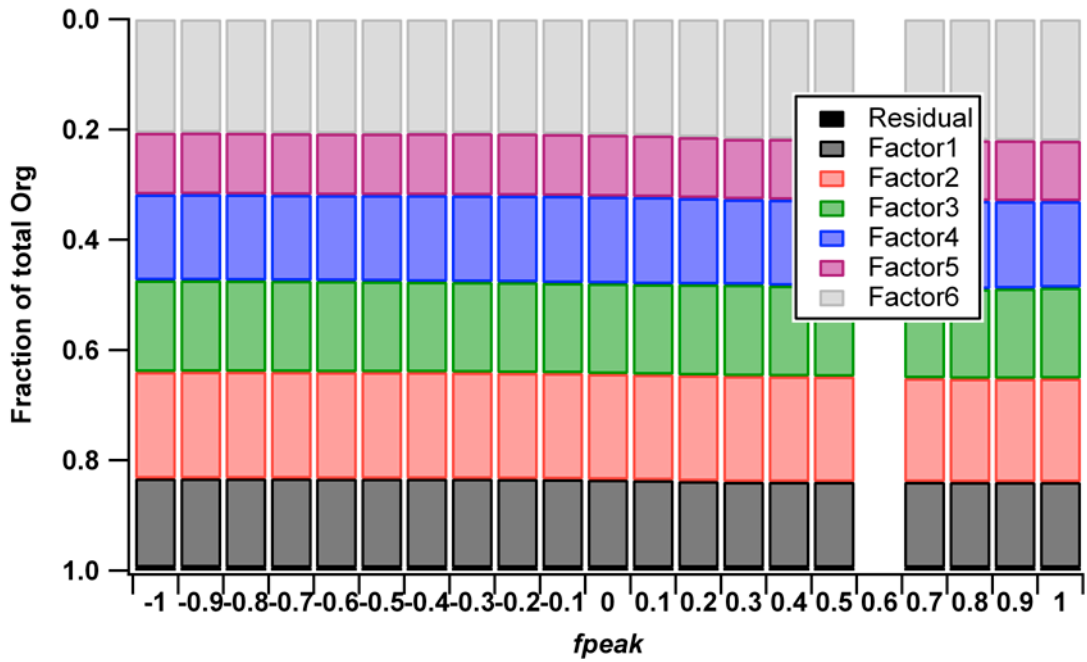
Figure 67: Variance explained by PMF due to the 6-factor HR solution as a function of *fpeak*. For the solution presented, *fpeak* =0.
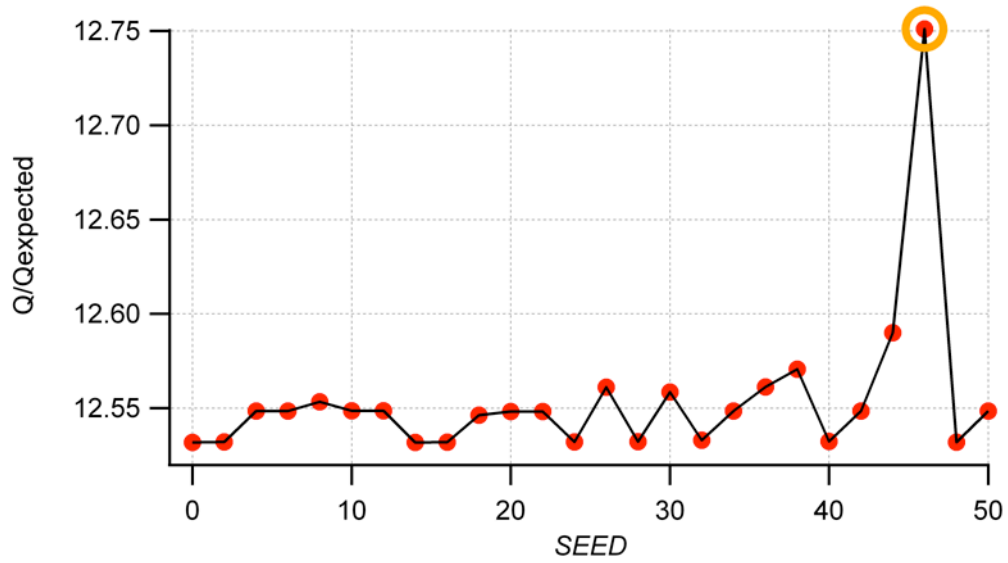
Figure 68: Q / Q_{exp} versus *SEED* for the HR solution.
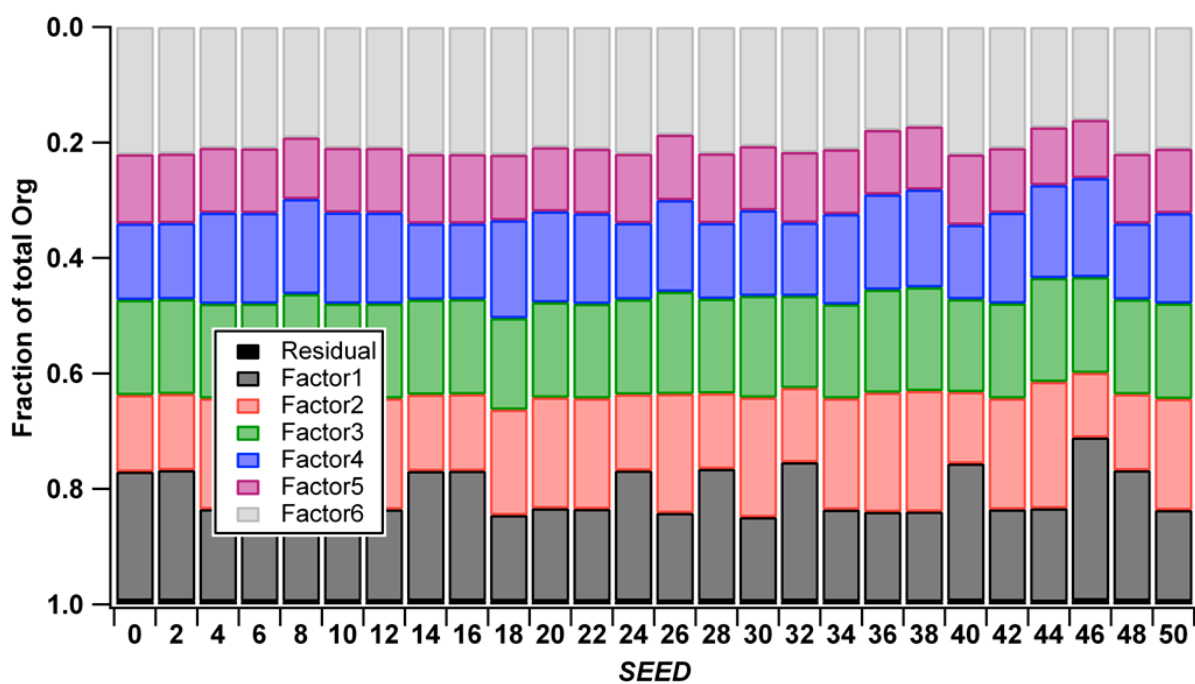
Figure 69: Variance explained by PMF due to the 6-factor HR solution as a function of *SEED*.
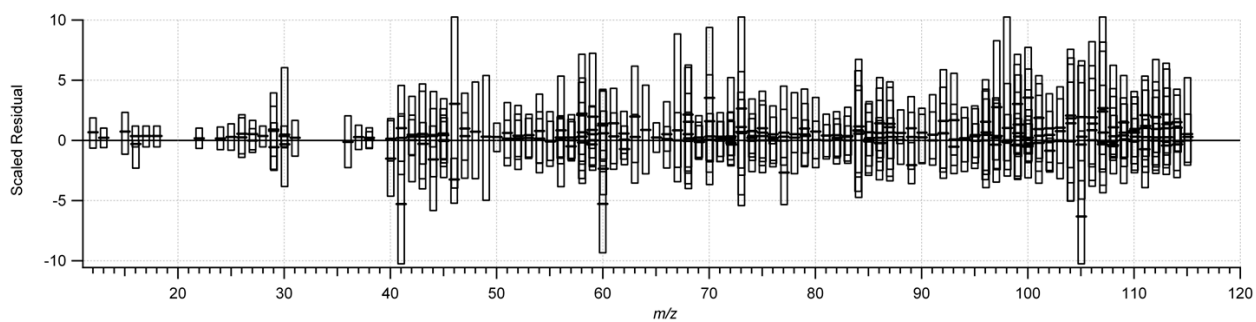
Figure 70: Median (black strokes) and lower/upper quartiles (boxes) of the scaled residuals per *m/z* (HR solution).
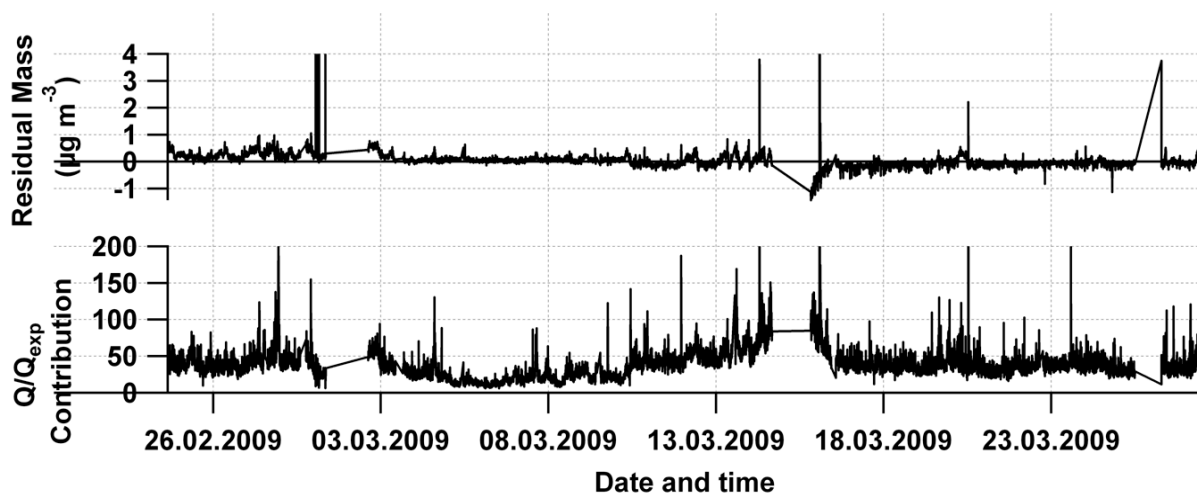
Figure 71: Time series of scaled residuals (top panel) and Q / Q_{exp} (lower panel) for the HR solution.
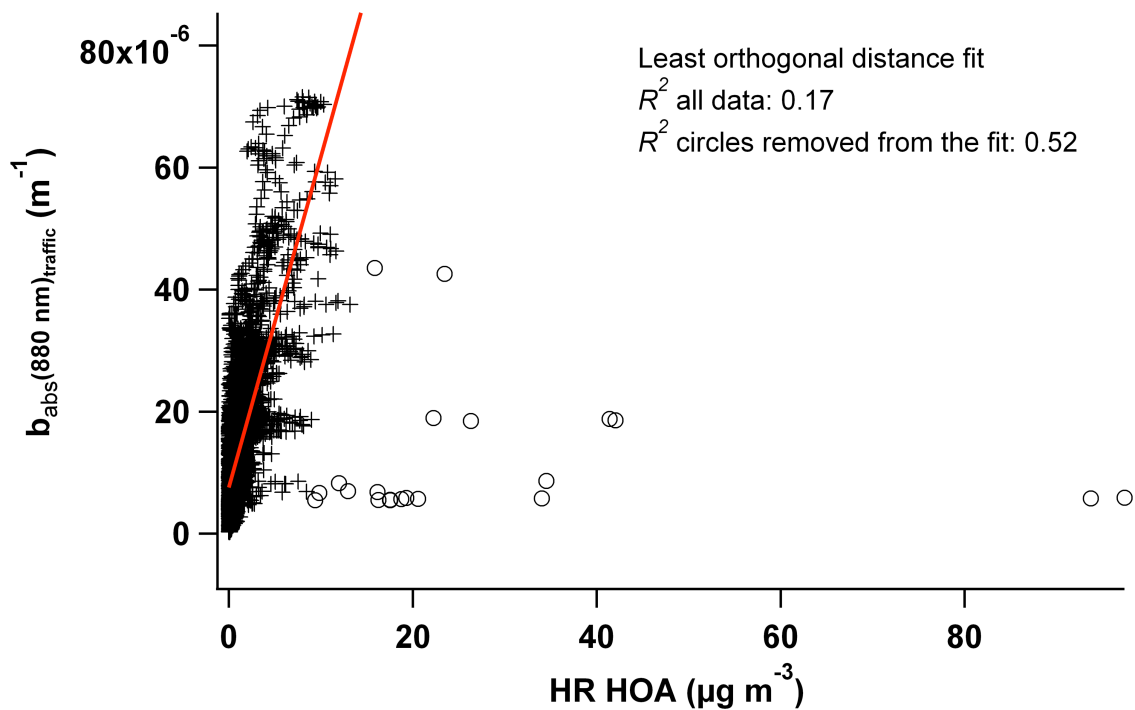
Figure 72: Scatter plot of the time series of b_{abs}(880 nm)traffic and HOA. The red line is the least orthogonal distance fit where the circle data points were removed.
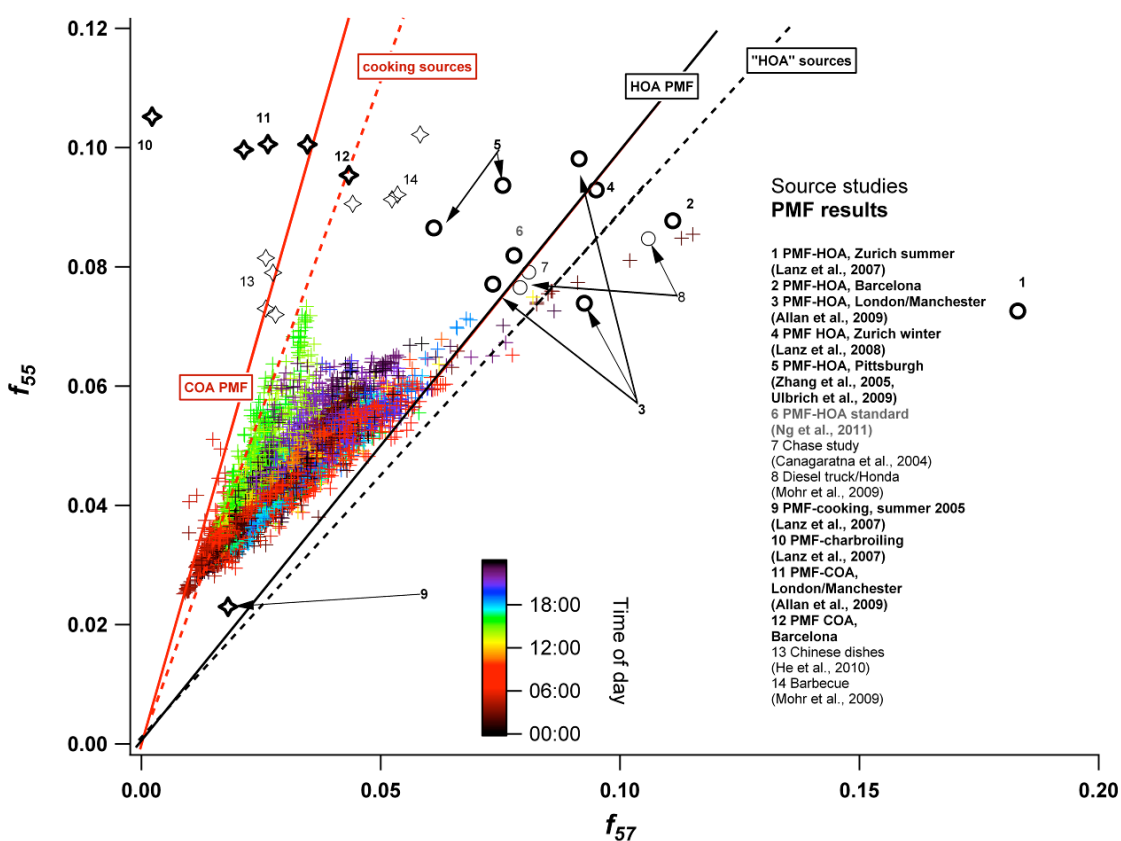
Figure 73: *m/z* 55/Org (f_{55}) plotted against *m/z* 57/Org (f_{57}).
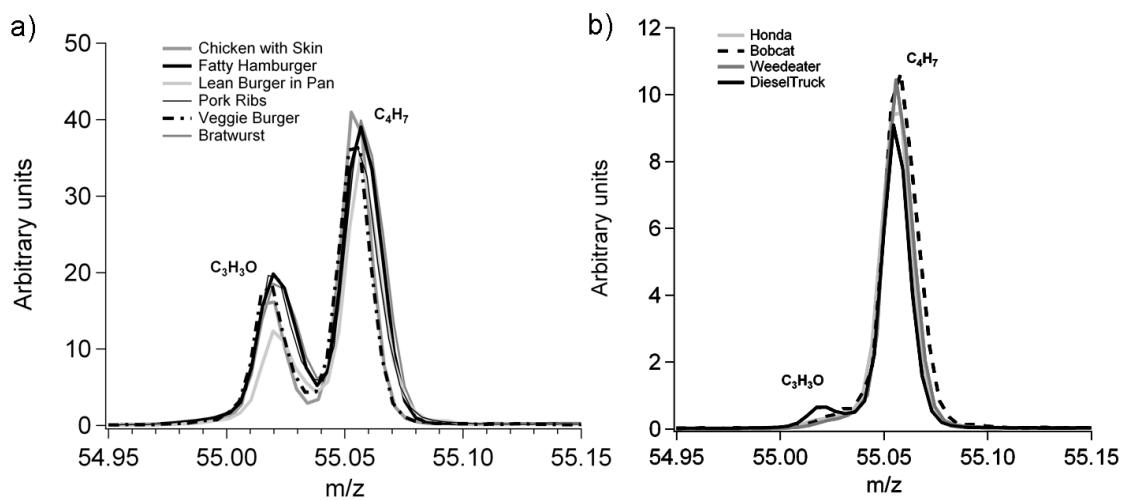
Figure 74: Signal at *m/z* 55 in the HR spectra of meat cooking sources (a) and vehicle engine sources (b). In the engine exhaust spectra, the signal is almost entirely due to the reduced hydrocarbon ion $C_4H_7^+$, whereas in the cooking spectra there is also substantial contribution from the oxygen-containing ion $C_3H_3O^+$. Reprinted from Mohr et al. (2009).

5

SPATIAL VARIATION OF AEROSOL CHEMICAL COMPOSITION AND ORGANIC COMPONENTS IN THE BARCELONA REGION

5.1 Abstract

Mobile measurements of atmospheric particle and gas-phase components were conducted during the DAURE campaign (Determination of the sources of atmospheric Aerosols in urban and rural Environments in the western Mediterranean) in February – March 2009 in the Barcelona region. Positive matrix factorization (PMF) was applied to the organic aerosol (OA) data measured by a high-resolution time-of-flight aerosol mass spectrometer (AMS). Five factors were found: hydrocarbon-like OA (HOA, 18 – 36% of OA), cooking OA (COA, 11 – 18% of OA), biomass burning OA (BBOA, 8 – 14% of OA), and low volatility/semi-volatile oxygenated OA (LV-OOA, 25 – 42%, and SV-OOA, 12 – 15% of OA). Emissions, regional topography, and meteorological conditions influence the spatial distribution of the pollutants of interest. High concentrations of HOA (2.8 μg m-3 or 36% of OA) and other traffic-related species were found in the city center. In the harbor area upwind of the city center, substantial contributions from secondary aerosol components advected by the sea breeze were found. Downwind of the city center, photochemical aging of the air masses and additional primary aerosol sources (industrial areas, the airport, and agricultural open fires) influence the evolution of the pollutants in the city plume.

5.2 Introduction

In this chapter results of the mobile aerosol and gas-phase measurements in Barcelona, Spain are presented. The goal was the investigation of the evolution of the pollutants in the plume of Barcelona and the characterization of the sources and processes of atmospheric pollutants in the region. The city of Barcelona and the surrounding region, as described in chapter 4, feature a unique topography greatly influencing the meteorology and the distribution of air pollutants (Pérez et al., 2008a). The Mediterranean climate and high anthropogenic emissions mutually reinforce the high levels of regional aerosol concentrations (Pérez et al., 2008a); winter cyclonic episodes can further increase them (Pérez et al., 2008b).

The mobile measurements were performed within the framework of the international DAURE campaign (Determination of the sources of atmospheric Aerosols in Urban and Rural Environments in the western Mediterranean, see chapter 4). Based on stationary measurements of various particle- and gas-phase parameters at an urban background site (Pandolfi et al., 2012), sources of PM such as road traffic, construction-demolition works, shipping emissions, and photochemical processes (Reche et al., 2011) were investigated and quantified. Contributions of activities such as biomass burning (Reche et al., 2012) or cooking (chapter 4 and Mohr et al., 2012) to organic aerosols, the fossil and non-fossil fractions of organic carbon (Minguillón et al., 2011), and the particulate trace metal content (Moreno et al., 2011) were assessed, among others. The results presented here complement these findings by adding information on the evolution of the Barcelona city plume and the emissions in the regions surrounding the city.

5.3 Experimental Section

5.3.1 Mobile measurements

16 days of mobile measurements resulting in 61 hours of data were performed during the DAURE campaign with the PSI mobile laboratory, an IVECO Daily van equipped with several gas- and particle-phase instruments which acquired data continuously while driving. A detailed description of the van and its setup can be found in chapter 2. Figure 75 presents a map of the Barcelona region and the route driven. The whole region was divided into 4 parts for the measurement drives: City center (zone 1 in Fig. 75, four morning and four afternoon drives), harbor (zone 2, one morning, two afternoon drives), the industrialized Llobregat valley (zone 3, two morning, one afternoon drives) and the mountain ranges and Vallés (zone 4 – 6, four afternoon drives).

Table 1 summarizes the instruments deployed in the mobile laboratory and gives information on the parameters measured, the detection limits and the time resolution of the data acquisition. Details are to be found in chapter 2. Data acquisition with the high-resolution time-of-flight aerosol mass spectrometer (AMS) during the measurement drives was performed in the V-mode only, which has a higher sensitivity, but a lower resolution than the W-mode, with a time resolution of 6 s.
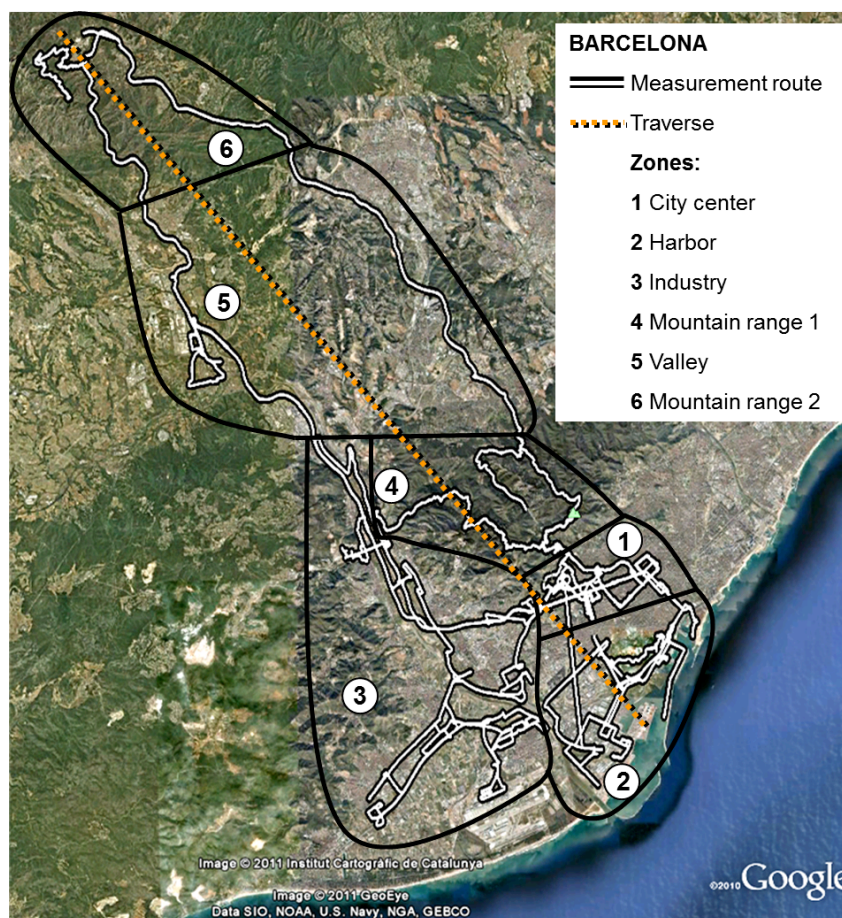
Figure 75: Route driven for the mobile measurements, and zoness defined for the analysis. The traverse shows the split in the dataset for the analysis of the pollutant concentrations as a function of distance to the sea.

5.3.2 Data Analysis

AMS data were processed using the software SQUIRREL v.1.51B and PIKA v1.1.10B based on the algorithms by Allan et al. (2003) within Igor Pro 6.22A. The fragmentation table was modified according to Aiken et al. (2008). The collection efficiency (CE) was determined based on a) the nitrate fraction f_{NO3} of the species measured by AMS (Nemitz et al., 2012; Middlebrook et

al., 2012) and b) comparison of the AMS when the mobile laboratory was measuring at the urban background site with the SMPS, the stationary AMS, and PM_1 measured by a laser spectrometer (Grimm Labortechnik GmbH & Co. KG) and corrected with PM_1 sample loadings collected on filters (section 4.3.2., Mohr et al., 2012). This resulted in a CE = 0.7 for $f_{NO3} \leq 0.25$, CE = 1 for $f_{NO3} \geq 0.78$, and a linear increase between those values for $0.25 \leq f_{NO3} \leq 0.78$.

PMF was applied to organic high resolution (HR) data (time resolution of 6 s). The input matrices, comprising the complete mobile data set, were prepared as outlined in chapter 4, section 4.3.3. The signals of the ions C_7H_7 and C_2H_7N were downweighted by a factor 100 due to higher fitting uncertainties of these two ions. All data are in local standard time (UTC + 1) and at local pressure and temperature conditions (10 - 25 ° C and 943 - 1048 hPa).

5.4 Results and Discussion

5.4.1 Regional overview

Figure 76 gives an overview of the mean concentrations of the parameters measured per zone defined in Fig. 75 (a), and the mean chemical composition of PM_1 (b). Highest concentrations of all particle components except black carbon (BC) and chloride (Chl) are found in the harbor area due to a combination of high primary emissions from ships, trucks and delivery vans and the influence of aged, processed air masses advected by the sea breeze. Especially the SO_4 concentrations are higher in the harbor area than anywhere else in the region and can, to some extent, be related to oxidation of SO_2 or direct emissions of H2SO4 from diesel fuel combustion in ship engines (Pandolfi et al., 2011). In addition, the ratio of secondary inorganic components to (primary) BC in the harbor area is the highest of all regions, confirming the aged characteristics of the aerosol here.

The mean concentrations in the city center are slightly lower than in the harbor area and dominated by (primary) traffic emissions, shown by the high concentrations of BC, NO_2, CO, and particle number. The contributions of secondary inorganics such as NO_3, NH_4, and SO_4 are considerably lower than in the harbor area; however, the Chl concentrations are almost as high as in the industrialized area, possibly through reaction of HNO_3 with sea salt NaCl and subsequent formation of ammonium chloride by the reaction of NH_3 with HCl.

Zone 3 comprises in addition to industrial areas the Barcelona airport, an extensive highway network and agricultural areas, where during the measurements several open fires were observed. Consequently, the concentrations of all primary gas-phase and particle-phase components are nearly as high as in the city center. Chl concentrations are the highest here of all zones, most likely due to HCl emissions from industries or waste incinerators (Querol et al., 2001).

The concentrations of the secondary inorganic components are slightly higher than in the city center. The geographical orientation of the Llobregat valley (perpendicular to the sea) allows the inflow of the land and sea breezes, thus advecting processed air masses with a higher fraction of secondary components.

The mountain ranges (zones 4 and 6) are characterized by lower concentrations of all species. Depending on the time of day and the meteorological situation, this can be due to a) boundary layer heights below their altitude (the first mountain range was usually crossed in the early afternoon), or b) less direct emissions: both mountain ranges are covered by forests and are only sparsely populated. Even though at a higher altitude, the concentrations of PM_1 species (except BC) in zone 6 are higher than in zone 4. This can be assigned to the fact that this zone was usually reached in the late afternoon, when the diurnal sea breeze was advecting the pollutants from the city and the valley in between the mountain ranges to this area. Low BC but higher secondary inorganics/organics concentrations indicate oxidation processes and formation of secondary PM during the transport of the air masses from zone 1 to zone 6.

The valley in between the mountain ranges, a mostly residential area, exhibits similar concentrations as the Llobregat valley, except for the lower Chl concentrations. The organic fraction of PM_1 is ~35% for all zones.
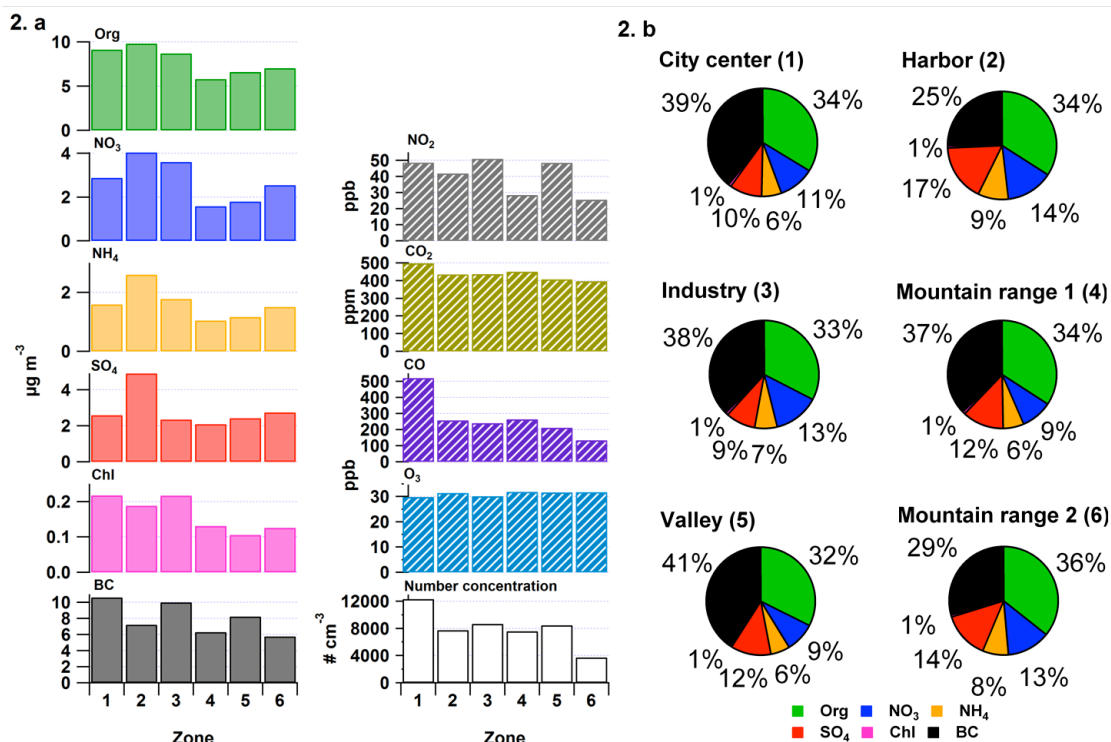
Figure 76: Average concentrations for parameters measured per region (a) and mean relative composition of PM_1 per region measured by MAAP and AMS (b).

5.4.2 PMF results

The same five OA factors as found for the parallel stationary AMS measurements at the urban background site (section 4.4.2.) were identified for the mobile OA data (Fig. 77): Hydrocarbon-like OA (HOA) from traffic (mostly diesel) emissions; biomass burning OA (BBOA) mostly from open agricultural fires (Reche et al., 2012); cooking OA (COA); and two different oxygenated OA, related to secondary OA: Low-volatility OOA (LV-OOA), and a semi-volatile OOA (SV-OOA). The R^2 values of the correlations of the stationary factor profiles and the mobile factor profiles are shown in Table 2, as well as the factors' atomic oxygen to carbon (O:C) ratios and the ratios of organic matter (OM) to organic carbon (OC) for both solutions. The noisy characteristics of the 6 s mobile data and different magnitudes of the peaks resulted in high scatter in the correlations, thus 5-min averages were used for most of the time series correlations (numbers in italics).
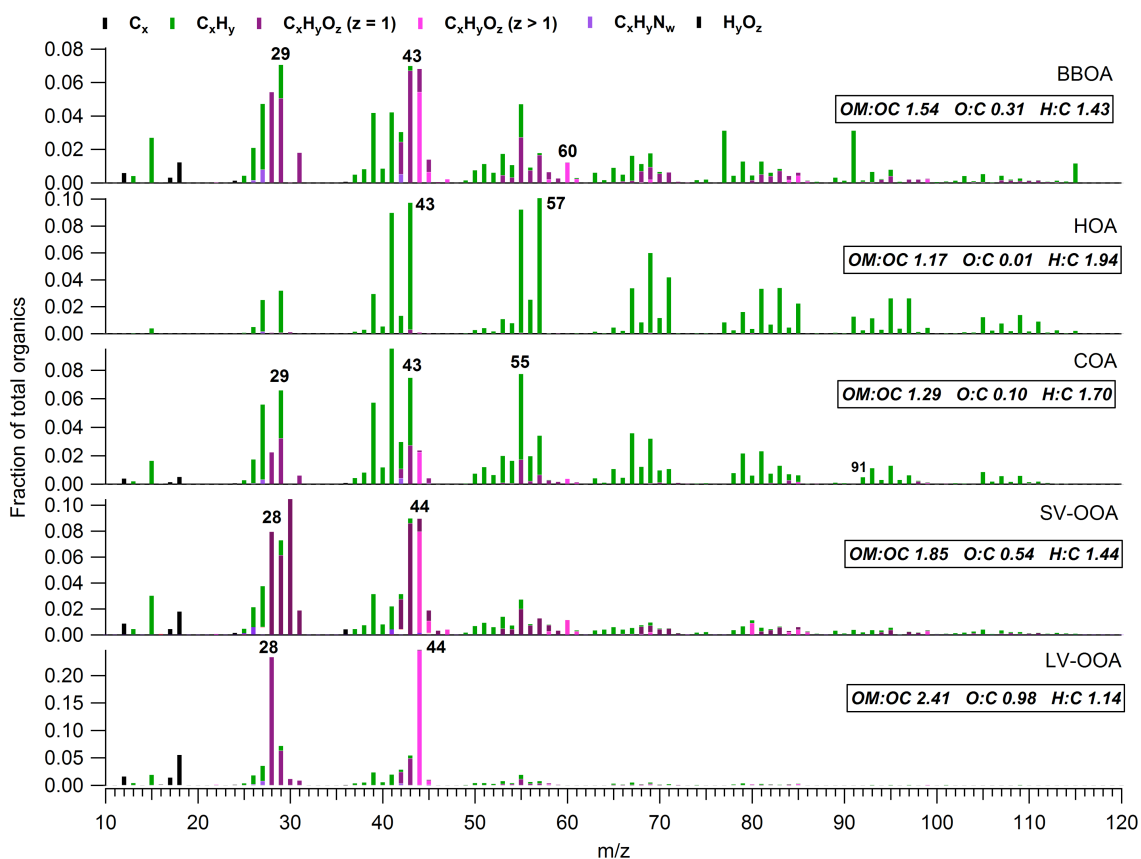
Figure 77: Factor profiles of the 5-factor high resolution PMF solution found for the organic data matrix measured by AMS.

The PMF solution was analyzed as outlined in the supplementary information in Mohr et al. (2012). Based on the correlations displayed in Table 2, the 5-factor-solution with the most central rotation (fpeak = 0; tested values from -1 to 1 with 0.2 intervals) and a pseudorandom start value SEED = 23 (tested values from 0 to 50, 2.0 intervals) was chosen. The ratio of the Q-value (the

parameter to be minimized by the PMF algorithm when fitting the data (Paatero and Tapper, 1994) to the expected Q-value which equals the degree of freedom of the fitted data (Q/Qexp) is 1.18, indicating a good estimation of the values in the input error matrix (Ulbrich et al., 2008; Paatero et al., 2002). The 4-factor solution was discarded due to one factor being a combination of COA and BBOA; the 6-factor solution yielded a "residual" factor.

Concerning profile factors, mobile and stationary HOA, COA and LV-OOA correlate well with R^2 values of 0.99, 0.92, and 0.96, respectively. The O:C ratios of the mobile and stationary HOA factors are similarly low (0.01 and 0.03, respectively). For the COA, the stationary factor exhibits a higher O:C ratio (0.21) than the mobile factor (0.1), indicating measurements closer to the source while on-road compared to the urban background station. The inclusion of air masses that had more time to undergo aging processes (areas distant from the city center) in the mobile measurements explains the higher degree of oxygenation of the mobile LV-OOA factor (O:C: 0.98 vs 0.75 for stationary LV-OOA). The BBOA spectra ($R^2 = 0.77$) exhibit differences in the signals at m/z 44 (and 28), which are higher in the mobile spectrum. This is also reflected in the O:C ratios (0.31 and 0.24 for the mobile and stationary factor profile, respectively). The SV-OOA spectra exhibit the least similarities ($R^2 = 0.69$), mostly due to the signal of the CHO ion ($R^2 = 0.86$ for the linear regression fit excluding CHO). Again, the O:C ratio of the mobile factor is higher than that of the stationary factor (0.54 and 0.32, respectively).

Correlating BC with the time series of both HOA ($R^2 = 0.63$) and BBOA ($R^2 = 0.24$) shows its origin in fossil fuel combustion (supported by the $R^2 = 0.71$ of the correlation of HOA and CO, and $R^2 = 0.52$ for HOA and NO_2). Minguillón et al. (2011) showed by means of ^{14}C analysis that 87% of elemental carbon is fossil during the period of this study. Due to the influence of ship emissions on the SO4 concentrations, their temporal evolution is less well correlated ($R^2 = 0.30$) with LV-OOA as usually observed in ambient datasets (Lanz et al., 2008). LV-OOA exhibits a similar temporal evolution ($R^2 = 0.40$) as e.g. the organic fraction of m/z 44 (f_{44}), a surrogate for the degree of oxidation and thus photochemical age of the air mass (Ng et al., 2010). SV-OOA correlates well with NO_3 ($R^2 = 0.74$) due to its volatile nature, as observed in other datasets (Lanz et al., 2008).

Table 2: O:C and OM:OC ratios, and R^2 values of the correlations of the PMF factors found here and the PMF solution of concurrent stationary measurements.

	R^2	O:C		OM:OC	
		mob.	stat.	mob.	stat.
BBOA	0.77	0.31	0.24	1.54	1.53
HOA	0.99	0.01	0.03	1.17	1.21
COA	0.92	0.10	0.21	1.29	1.42
SV-OOA	0.69	0.54	0.32	1.85	1.61
LV-OOA	0.96	0.98	0.75	2.41	2.14

5.4.3 Spatial variation of OA factors

Figure 78 shows the spatial variation of OA and the relative contributions of the PMF factor loadings to OA for the 6 zones. As expected by the proximity to the primary sources, HOA exhibits the highest percentage of OA in the city center (36% of OA). Except for zones 6 (Montserrat, 12%), and 2 (harbor, 11%), the COA relative contributions to OA exhibit a uniform pattern throughout the densely populated areas of the city of Barcelona and Vallés/Llobregat (17 – 18%). The relatively high number of open agricultural fires observed during drives in the Llobregat valley (zone 3) and the Montserrat region (zone 6) is reflected in the slightly higher BBOA contribution there (12-14%, 0.8 – 0.9 µg m^{-3}) compared to downtown Barcelona (8%, 0.6 µg m^{-3}). Except for the city center area, the OOA fraction dominates OA, as observed in other locations (both urban and rural) in the northern hemisphere (Zhang et al., 2007), with 25 – 42% LV-OOA and 12 – 15% SV-OOA. The importance of secondary components in the harbor area and in the zone of the prelitoral mountain range, mentioned earlier, is also reflected in the OA fraction of PM$_1$: Very high OOA contributions (57 and 53%, respectively) are found in both zones. Biogenic or in general non-fossil emissions might contribute substantially to OOA (Minguillón et al., 2011). At the urban background site, LV-OOA contributes 28%, SV-OOA 27%, COA 17%, HOA 16%, and BBOA 11% to OA (Mohr et al., 2011).
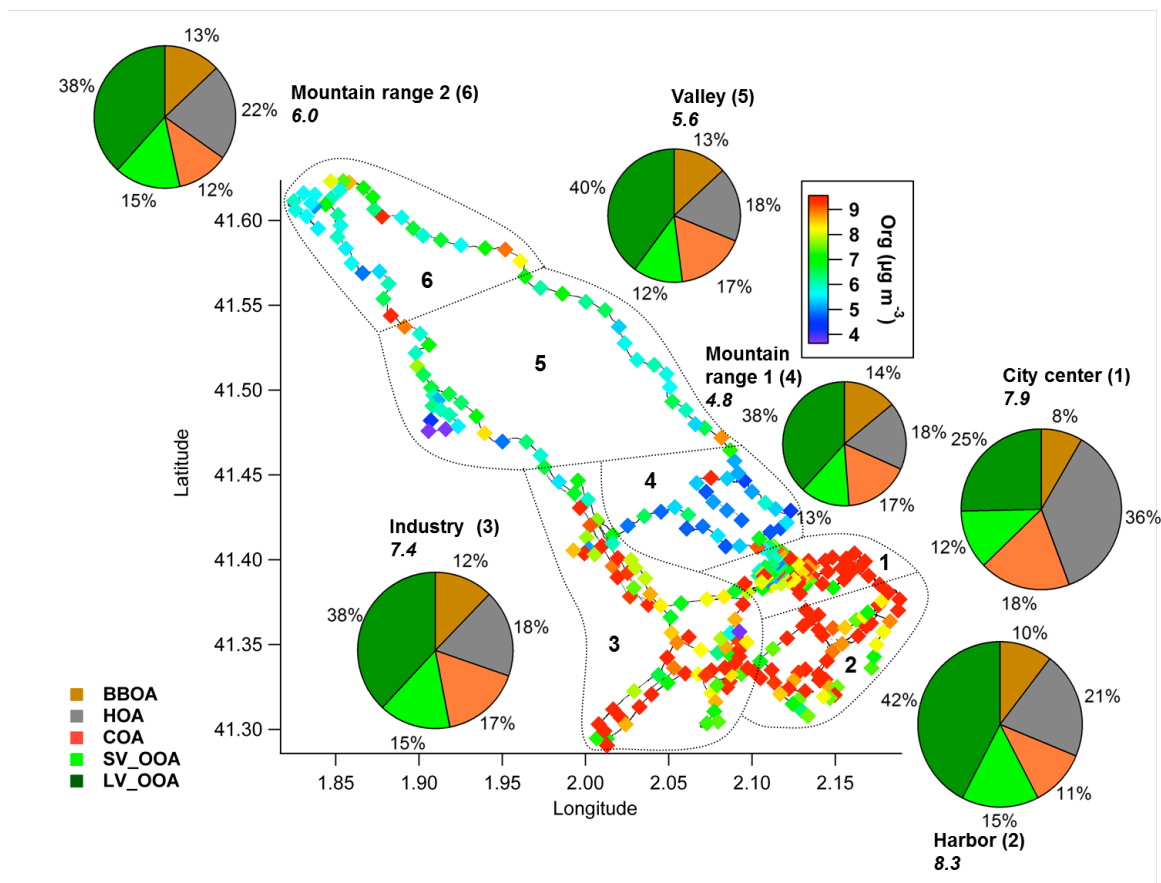
Figure 78: Spatial variation of the OA (Org) concentration and average relative composition of OA per region. The ratios of the areas of the pies are relative to the average OA mass concentrations of the regions, denoted by the numbers in italics.

5.4.4 Evolution of pollutant concentrations with distance to the sea

For the investigation of the evolution of pollutant concentrations as a function of the distance to the sea, the data were sorted according to their rectangular distance to a line parallel to the shore and binned into 50 equally sized distances. In addition, the data were separated by the line called traverse in Fig. 75 to investigate the western and the eastern parts of the mobile measurement route separately. Figure 79 summarizes the findings (the data were normalized to the value at their first bin in order to be displayed on the same axis). The species related to traffic emissions (a – b) exhibit maximum concentrations in the city center, in the valley between the mountain ranges, and the industrial valley (the altitude transect is shown in panels o – p). Generally, the concentrations in the western part are higher due to emissions in the industrial valley. The CO_2 concentrations (c – d) show a similar evolution as the traffic-related parameters; however, their peak is much lower in the valleys, especially on the eastern traverse. For BBOA (e – f), evolution shows a less distinct pattern than the traffic-related species; the concentrations stay more or less constant. This indicates

significant sources outside the city center of Barcelona throughout the region covered by mobile measurements. COA (e - f) features a distinct peak in the city center (most likely enhanced due to the fact that all measurement drives in the city center include rush hour times) on the East traverse and relatively uniform concentrations on the west traverse after the minimum at the seaside. The concentrations of the semi-volatile aerosol components (ammonium nitrate and SV-OOA, g - h) decrease with distance to the city center and increase again on the prelitoral mountain range, possibly influenced also by the lower temperatures at the higher altitudes. The concentrations of the semi-volatile aerosol components (ammonium nitrate and SV-OOA, g - h) decrease with distance to the city center and increase again on the second mountain range, in accordance with previous statements.

The formation of secondary OA can be investigated by the ratio of OA to ΔCO, i. e. the CO concentrations minus a background value (DeCarlo et al., 2010) to account for dilution effects. This concept, however, cannot easily be applied to the Barcelona region and the measurements presented here: Along one traverse, the measurement route crosses two mountain ranges with CO concentrations down to 70 ppb and thus lower than the average CO concentration at the urban background site immediately before and after the drives (110 ± 15 ppb). In addition, depending on the time of day and the extent of the sea breeze, the CO concentrations upwind of the city can be higher than at the (downwind) background station due to the sea breeze advecting polluted, processed air masses to the city. The CO background concentration for this dataset was set equal to the lowest values measured along the traverse (70 ppb), leading to a general overestimation of ΔCO und thus an underestimation of secondary OA (compare to LV-OOA traverses, i-j). The time series of this ratio can thus only be interpreted qualitatively: With increasing distance to the city center, the processing of the air masses leads to a slow increase in OA mass (and SO_4, usually formed slowly and thus regionally With increasing distance to the city center, the processing of the air masses leads to a slow increase in OA mass (and SO_4, usually formed slowly and thus regionally (Mohr et al., 2011)). However, the highest concentrations of SO_4 and secondary OA are found at the harbor area, confirming the influence of highly aged air masses advected by the sea breeze.
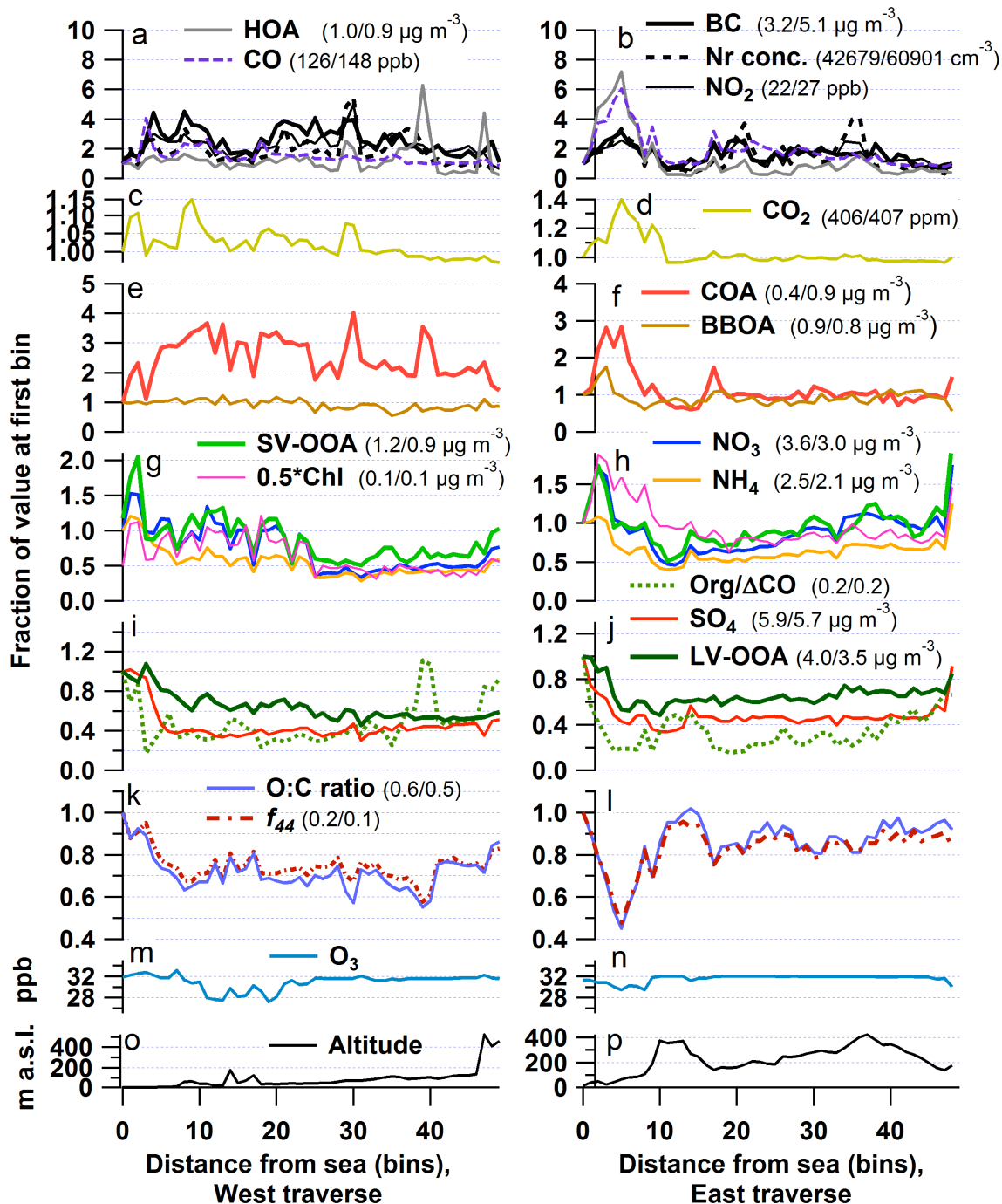
Figure 79: Binned concentration of components as a function of distance to the sea (normalized to the value at the first bin, except for altitude). The numbers in brackets denote the absolute value in the first bin for the West and East traverse, respectively.

The aging of air masses, consisting of photochemical oxidation processes of gas-phase components which (re-) condense onto the particles or processes within the particles do not only lead to an increase in particle mass (e. g. LV-OOA and SV-OOA), but also in the O:C ratio (panels k – l) (Jimenez et al., 2009). A surrogate for the degree of oxidation of OA is the ratio of the

organic mass fragment at *m/z* 44 (CO_2^+), mostly from the decarboxylation of organic acids, to total OA (f_{44}) (Ng et al., 2010). Both O:C and f_{44} are high at the shore, pass through a minimum and then increase again with distance to the sea. Plotting f_{44} from Fig. 79k vs f_{43} (the ratio of the organic mass fragment at *m/z* 43 - mostly $C_2H_3O^+$ from non-acid oxygenates - to total OA), binned as well according to the distance from the sea, the data fall into a well defined shape found for many ambient datasets (Ng et al., 2010) (Fig. 80a). The "final" f_{44} for the point furthest away from the sea is reached from the top (high f_{44}) for the western traverse due to the high degree of oxidation of the harbor air masses, and from the bottom (low f_{44}) for the eastern traverse where the data of the chemically reduced air masses of the city center prevail, corresponding to OOA with a rather low degree of oxidation. However, it has to be taken into account that f_{44} comprises all organic data and not just SV- and LV-OOA, unlike in Ng et al (2010). The Van Krevelen plot (Fig. 80b) shows another aspect of the aging processes of bulk OA: A slope of -1 in the H:C-O:C space corresponds to an addition of a carboxylic acid group to the bulk OA (Heald et al., 2011), and a slope of -0.5 to the addition of both carboxylic acid and alcohol/peroxide functional groups (Ng et al., 2010). The H:C and O:C data of the present dataset (binned according to the distance to sea) fall on the same line for both West and the East traverse with a slope of ~-0.8, again with different starting points (harbor or city center).
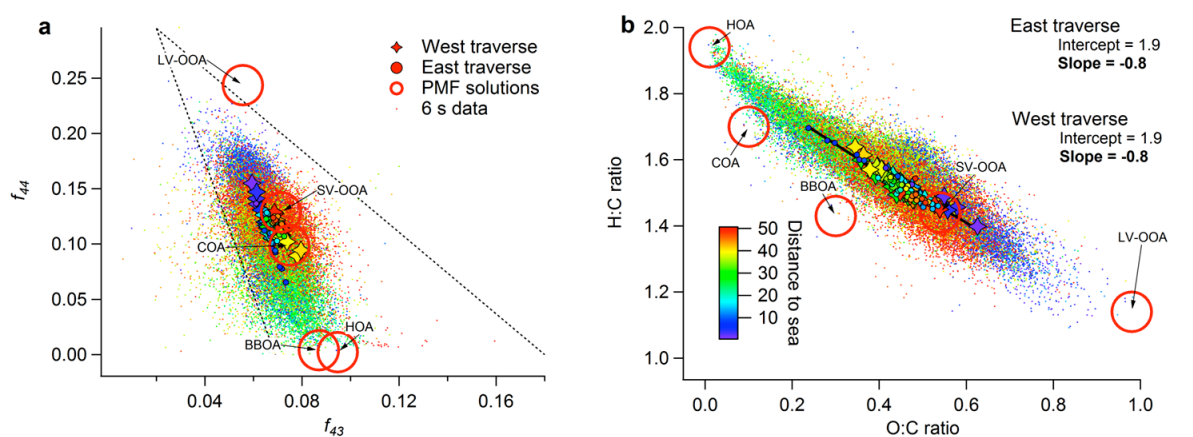
Figure 80: f_{44} plotted versus f_{43} for the data binned according to the distance to the sea (a) and H:C ratio plotted versus O:C ratio for the data binned according to the distance to the sea (b) for both the eastern and the western traverse.

5.4.5 Acknowledgement

6

CONCLUSIONS AND OUTLOOK

The chemical composition of particulate matter (PM) influences the effects on human health, the climate, physical properties, chemical reaction pathways in the atmosphere and the lifetime of atmospheric aerosols. In addition, information about PM chemical composition can help determine the identity and magnitude of particle sources; such source apportionment is in turn the basis of all mitigation activities. Knowledge is especially limited for the organic fraction of PM, a dynamic system of primary and secondary components which often dominates the PM composition.

This thesis improves on previous organic aerosol (OA) source identification/quantification efforts through the improved identification of hard-to-resolves sources (e.g. cooking aerosol) and development of methods for quantitatively comparing local vs. regional air quality influences. This is achieved through analysis of highly time-resolved measurements of submicron aerosol chemical composition in Zurich and Barcelona using an aerosol mass spectrometer (AMS). The positive matrix factorization (PMF) factor analytical model is applied to the organic fraction and shown to be a powerful tool to investigate OA sources. With the instruments deployed in a mobile laboratory, chemical composition can be determined as a function of both time and space.

The particular combination of AMS, PMF, and mobile measurements allowed the separation and quantification of the fraction of PM emitted or formed locally in the city of Zurich and the fraction of PM originating from the urban, regionally-influenced background. Both secondary OA and primary OA such as biomass burning OA, observed in high concentrations in Zurich during winter time inversions, are mainly part of the regional background aerosol. This information is of great importance for local and national authorities planning and implementing mitigation strategies. In Barcelona, mobile AMS measurements allowed PM concentrations to be assessed in terms of influences from the sea breeze, regional topography, and emission patterns in the Barcelona area.

Mobile measurements require a higher temporal resolution of data acquisition than do stationary measurements because of the constant changes in measurement location. This results in

two drawbacks. First, AMS raw data are noisier than for longer averaging times, which introduces higher uncertainties in the peak fitting process of the high-resolution analysis. Second, the high time resolution leads to a larger dataset, which in turn requires additional computational power for analysis. If datasets must be divided into several parts for analysis, this can be very time consuming and may introduce additional uncertainties. The design of further mobile measurement campaigns should thus carefully address the trade-offs between temporal and spatial resolution.

There is also a trade-off between the additional level of information provided by mobile measurements concerning space and the often-limited temporal information. The proximity of sources and the possibility of acquiring almost pure spectra of a certain source (e. g. the plume of a diesel car or a fire) enabled by mobile measurements often help PMF to detect a certain factor. On the other hand, the differences in the temporal evolution of factors are crucial for their identification by PMF. Especially for secondary factors such SV-OOA, where the temporal variation is determined more by day-night cycles rather than peaks of a few seconds or minutes, the constrained time periods of mobile measurements can make its identification difficult. Mobile measurements should be conducted during different times of the day to mitigate this issue.

The deployment of a high-resolution time-of-flight AMS in the city of Barcelona during a month-long campaign led to the identification and quantification of an additional primary OA source compared to Zurich: cooking OA (COA). This factor had not been previously identified in that region, despite its substantial contribution to OA of ~17%. It is a possible explanation for the surprisingly high fraction of modern carbon identified by other methods in the same campaign. A possible reason for the scarcity of COA factors resolved in previous datasets is the similarity of the unit mass resolution spectra from hydrocarbon-like OA and COA. Only with the increasing availability of high-resolution AMS measurements is the significance of cooking activities for ambient urban air quality starting to be assessed. This highlights the importance of chemical composition measurements with high mass and time resolution for insights into atmospheric aerosol processes.

Future work investigating OA sources should proceed in two directions: (1) studying primary aerosol sources; and (2) exploring secondary OA, its sources, components, and their fate in the atmosphere. Both paths will profit substantially from developments in the instrumental sector, especially in the field of mass spectrometry. Next generation instruments such as the Thermal Desorption Aerosol Gas Chromatograph AMS (TAG-AMS), which combines mass spectral analysis of the total organic aerosol with molecular identification capability and volatility profiles, the Atmospheric Pressure Interface Time-of-Flight mass spectrometer (API-TOF) which is able to measure the composition of aerosol particles smaller than two nm and thus gives insights into nucleation processes, and the Micro-Orifice Volatilization Impactor Chemical Ionization mass

spectrometer (MOVI-CIMS), which measures concentrations of oxygenated gas and particle-phase species, e.g. organic acids, will greatly enhance our ability to resolve distinct source profiles for primary emissions and formation pathways of secondary components. Application of this instrumentation in both laboratory studies and ambient measurements, both mobile and stationary, will bring further advances in our understanding of the sources of atmospheric aerosols.

7

REFERENCES

Aiken, A. C., DeCarlo, P. F., Kroll, J. H., Worsnop, D. R., Huffman, J. A., Docherty, K. S., Ulbrich, I. M., Mohr, C., Kimmel, J. R., Sueper, D., Sun, Y., Zhang, Q., Trimborn, A., Northway, M., Ziemann, P. J., Canagaratna, M. R., Onasch, T. B., Alfarra, M. R., Prevot, A. S. H., Dommen, J., Duplissy, J., Metzger, A., Baltensperger, U., and Jimenez, J. L.: O/C and OM/OC ratios of primary, secondary, and ambient organic aerosols with high-resolution time-of-flight aerosol mass spectrometry, Environ. Sci. Technol., 42, 4478-4485, doi 10.1021/Es703009q, 2008.

Aiken, A. C., Salcedo, D., Cubison, M. J., Huffman, J. A., DeCarlo, P. F., Ulbrich, I. M., Docherty, K. S., Sueper, D., Kimmel, J. R., Worsnop, D. R., Trimborn, A., Northway, M., Stone, E. A., Schauer, J. J., Volkamer, R. M., Fortner, E., de Foy, B., Wang, J., Laskin, A., Shutthanandan, V., Zheng, J., Zhang, R., Gaffney, J., Marley, N. A., Paredes-Miranda, G., Arnott, W. P., Molina, L. T., Sosa, G., and Jimenez, J. L.: Mexico City aerosol analysis during MILAGRO using high resolution aerosol mass spectrometry at the urban supersite (T0) - Part 1: Fine particle composition and organic source apportionment, Atmos. Chem. Phys., 9, 6633-6653, 2009.

Aiken, A. C., de Foy, B., Wiedinmyer, C., DeCarlo, P. F., Ulbrich, I. M., Wehrli, M. N., Szidat, S., Prevot, A. S. H., Noda, J., Wacker, L., Volkamer, R., Fortner, E., Wang, J., Laskin, A., Shutthanandan, V., Zheng, J., Zhang, R., Paredes-Miranda, G., Arnott, W. P., Molina, L. T., Sosa, G., Querol, X., and Jimenez, J. L.: Mexico city aerosol analysis during MILAGRO using high resolution aerosol mass spectrometry at the urban supersite (T0) - Part 2: Analysis of the biomass burning contribution and the non-fossil carbon fraction, Atmos. Chem. Phys., 10, 5315-5341, 10.5194/acp-10-5315-2010, 2010.

Ajuntament de Barcelona: Dades bàsiques 2006, Direcció de serveis de mobilitat, Barcelona, 2007.

Alfarra, M. R.: Insights into Atmospheric Organic Aerosols using an Aerosol Mass Spectrometer, PhD, Institute of Science and Technology, University of Manchester, Manchester, 2004.

Alfarra, M. R., Prevot, A. S. H., Szidat, S., Sandradewi, J., Weimer, S., Lanz, V. A., Schreiber, D., Mohr, M., and Baltensperger, U.: Identification of the mass spectral signature of organic aerosols from wood burning emissions, Environ. Sci. Technol., 41, 5770 - 5777, 2007.

Allan, J. D., Jimenez, J. L., Williams, P. I., Alfarra, M. R., Bower, K. N., Jayne, J. T., Coe, H., and Worsnop, D. R.: Quantitative sampling using an Aerodyne aerosol mass spectrometer: 1. Techniques of data interpretation and error analysis, J. Geophys. Res-Atmos., 108, D34090, doi:10.1029/2002JD002358, 2003.

Allan, J. D.: Aerosol mass spectrometer: Instrument development, data analysis techniques and quantitative atmospheric particulate measurements, Phd, Department of Physics, University of Manchester, Manchester, 2004.

Allan, J. D., Delia, A. E., Coe, H., Bower, K. N., Alfarra, M. R., Jimenez, J. L., Middlebrook, A. M., Drewnick, F., Onasch, T. B., Canagaratna, M. R., Jayne, J. T., and Worsnop, D. R.: A generalised method for the extraction of chemically resolved mass spectra from Aerodyne aerosol mass spectrometer data, J. Aerosol. Sci., 35, 909-922, 2004.

Allan, J. D., Williams, P. I., Morgan, W. T., Martin, C. L., Flynn, M. J., Lee, J., Nemitz, E., Phillips, G. J., Gallagher, M. W., and Coe, H.: Contributions from transport, solid fuel burning and cooking to primary organic aerosols in two UK cities, Atmos. Chem. Phys., 10, 647-668, 2010.

Andreae, M. O.: A new look at aging aerosols, Science, 326, 1493-1494, 10.1126/science.1183158, 2009.

Andreani-Aksoyoglu, S., Keller, J., Prévôt, A. S. H., Baltensperger, U., and Flemming, J.: Secondary aerosols in Switzerland and northern Italy: Modeling and sensitivity studies for summer 2003, J. Geophys. Res., 113, D06303, doi:10.1029/2007JD009053, 2008.

Backhaus, K., Erichson, B., Plinke, W., and Weiber, R.: Multivariate Analysemethoden. Eine anwendungsorientierte Einführung, Springer Verlag, Berlin/Heidelberg, 818 pp., 2003.

BAFU, and EMPA: NABEL Luftbelastung 2008. Messresultate des nationalen Beobachtungsnetzes für Luftfremdstoffe (NABEL), 2009.

BAFU, and UVEK: Feinstaub. Fragen und Antworten zu Eigenschaften, Emissionen, Immissionen, Auswirkungen und Massnahmen, 2011.

Bahreini, R., Jimenez, J. L., Wang, J., Flagan, R. C., Seinfeld, J. H., Jayne, J. T., and Worsnop, D. R.: Aircraft-based aerosol size and composition measurements during ACE-Asia using an Aerodyne aerosol mass spectrometer, J. Geophys. Res-Atmos., 108, D238645, doi 10.1029/2002jd003226, 2003.

Baldasano, J. M., Valera, E., and Jiménez, P.: Air quality data from large cities, The Science of The Total Environment, 307, 141-165, 2003.

Baltensperger, U., Weingartner, E., Burtscher, H., and Keskinen, J.: Dynamic mass and surface area measurements, in: Aerosol measurement. Principles, techniques, and applications, edited by: Baron, P. A., and Willeke, K., Wiley-Interscience, New York, 2001.

Baltensperger, U., Streit, N., Weingartner, E., Nyeki, S., Prévôt, A. S. H., Van Dingenen, R., Virkkula, A., Putaud, J. P., Even, A., ten Brink, H., Blatter, A., Neftel, A., and Gäggeler, H. W.: Urban and rural aerosol characterization of summer smog events during the PIPAPO field campaign in Milan, Italy, J. Geophys. Res., 107, D228193, doi:10.1029/2001JD001292, 2002.

Baltensperger, U., Dommen, J., Alfarra, M. R., Duplissy, J., Gaeggeler, K., Metzger, A., Facchini, M. C., Decesari, S., Finessi, E., Reinnig, C., Schott, M., Warnke, J., Hoffmann, T., Klatzer, B., Puxbaum, H., Geiser, M., Savi, M., Lang, D., Kalberer, M., and Geiser, T.: Combined determination of the chemical composition and of health effects of secondary organic aerosols: the POLYSOA project, Journal of aerosol medicine and pulmonary drug deliver, 21, 145-154, 10.1089/jamp.2007.0655, 2008.

Baltensperger, U., Chirico, R., DeCarlo, P. F., Dommen, J., Gaeggeler, K., Heringa, M. F., Li, M. L., Prevot, A. S. H., Alfarra, M. R., Gross, D. S., and Kalberer, M.: Recent developments in the mass spectrometry of atmospheric aerosols, Eur. J. Mass Spectrom., 16, 389-395, 2010.

Bouwman, A. F., Lee, D. S., Asman, W. A. H., Dentener, F. J., Van Der Hoek, K. W., and Olivier, J. G. J.: A global high-resolution emission inventory for ammonia, Global Biogeochem. Cycles, 11, 561-587, 1997.

Bowman, D. M. J. S., Balch, J. K., Artaxo, P., Bond, W. J., Carlson, J. M., Cochrane, M. A., D'Antonio, C. M., DeFries, R. S., Doyle, J. C., Harrison, S. P., Johnston, F. H., Keeley, J. E., Krawchuk, M. A., Kull, C. A., Marston, J. B., Moritz, M. A., Prentice, I. C., Roos, C. I., Scott, A. C., Swetnam, T. W., van der Werf, G. R., and Pyne, S. J.: Fire in the Earth system, Science, 324, 481-484, 10.1126/science.1163886, 2009.

Brimblecome, P.: The Big Smoke: A History of Air Pollution, Methuen & Co. Ltd., London, New York, 1987.

Brook, R. D., Franklin, B., Cascio, W., Hong, Y., Howard, G., Lipsett, M., Luepker, R., Mittleman, M., Samet, J., Smith, S. C., and Tager, I.: Air pollution and cardiovascular disease, Circulation, 109, 2655-2671, 10.1161/01.cir.0000128587.30041.c8, 2004.

Bukowiecki, N., Dommen, J., Prevot, A. S. H., Richter, R., Weingartner, E., and Baltensperger, U.: A mobile pollutant measurement laboratory-measuring gas phase and aerosol ambient concentrations with high spatial and temporal resolution, Atmos. Environ., 36, 5569-5579, 2002.

Bukowiecki, N., Dommen, J., Prevot, A. S. H., Weingartner, E., and Baltensperger, U.: Fine and ultrafine particles in the Zurich (Switzerland) area measured with a mobile laboratory: an assessment of the seasonal and regional variation throughout a year, Atmos. Chem. Phys., 3, 1477-1494, 2003.

Bukowiecki, N., Lienemann, P., Hill, M., Furger, M., Richard, A., Amato, F., Prevot, A. S. H., Baltensperger, U., Buchmann, B., and Gehrig, R.: PM10 emission factors for non-exhaust particles generated by road traffic in an urban street canyon and along a freeway in Switzerland, Atmos. Environ., 44, 2330-2340, 2010.

Canagaratna, M. R., Jayne, J. T., Ghertner, D. A., Herndon, S., Shi, Q., Jimenez, J. L., Silva, P. J., Williams, P., Lanni, T., Drewnick, F., Demerjian, K. L., Kolb, C. E., and Worsnop, D. R.: Chase studies of particulate emissions from in-use New York City vehicles, Aerosol. Sci. Technol., 38, 555-573, 2004.

Canagaratna, M. R., Jayne, J. T., Jimenez, J. L., Allan, J. D., Alfarra, M. R., Zhang, Q., Onasch, T. B., Drewnick, F., Coe, H., Middlebrook, A., Delia, A., Williams, L. R., Trimborn, A. M., Northway, M. J., DeCarlo, P. F., Kolb, C. E., Davidovits, P., and Worsnop, D. R.: Chemical and microphysical characterization of ambient aerosols with the Aerodyne aerosol mass spectrometer, Mass Spectrom. Rev., 26, 185-222, 2007.

Capes, G., Johnson, B., McFiggans, G., Williams, P. I., Haywood, J., and Coe, H.: Aging of biomass burning aerosols over West Africa: Aircraft measurements of chemical composition, microphysical properties, and emission ratios, J. Geophys. Res-Atmos., 113, D00C15, 10.1029/2008JD009845, 2008.

Cass, G. R.: Organic molecular tracers for particulate air pollution sources, TRAC-Trend. Anal. Chem., 17, 356-366, 1998.

Chirico, R., DeCarlo, P. F., Heringa, M. F., Tritscher, T., Richter, R., Prevot, A. S. H., Dommen, J., Weingartner, E., Wehrle, G., Gysel, M., Laborde, M., and Baltensperger, U.: Impact of aftertreatment devices on primary emissions and secondary organic aerosol formation potential from in-use diesel vehicles: results from smog chamber experiments, Atmos. Chem. Phys., 10, 11545 - 11563, 10.5194/acp-10-11545-2010, 2010.

Collaud Coen, M., Weingartner, E., Apituley, A., Ceburnis, D., Fierz-Schmidhauser, R., Flentje, H., Henzing, J. S., Jennings, S. G., Moerman, M., Petzold, A., Schmid, O., and Baltensperger, U.: Minimizing light absorption measurement artifacts of the aethalometer: evaluation of five correction algorithms, Atmos. Meas. Tech., 3, 457-474, 2010.

Crippa, M., DeCarlo, P. F., Mohr, C., Heringa, M. F., Chirico, R., Slowik, J. G., Poulain, L., Wiedensohler, A., Freutel, F., Drewnick, F., Schneider, J., Di Marco, C. F., Nemitz, E., Zimmermann, R., Elsässer, M., Prévôt, A. S. H., and Baltensperger, U.: Wintertime aerosols chemical composition and source apportionment in the metropolitan area of Paris, In prep., 2011.

Cross, E. S., Onasch, T. B., Canagaratna, M., Jayne, J. T., Kimmel, J., Yu, X. Y., Alexander, M. L., Worsnop, D. R., and Davidovits, P.: Single particle characterization using a light scattering module coupled to a time-of-flight aerosol mass spectrometer, Atmos. Chem. Phys., 9, 7769-7793, 2009.

DeCarlo, P. F., Slowik, J. G., Worsnop, D. R., Davidovits, P., and Jimenez, J. L.: Particle morphology and density characterization by combined mobility and aerodynamic diameter

measurements. Part 1: Theory Aerosol. Sci. Technol., 38, 1185-1205, 10.1080/027868290903907, 2004.

DeCarlo, P. F., Kimmel, J. R., Trimborn, A., Northway, M. J., Jayne, J. T., Aiken, A. C., Gonin, M., Fuhrer, K., Horvath, T., Docherty, K. S., Worsnop, D. R., and Jimenez, J. L.: Field-deployable, high-resolution, time-of-flight aerosol mass spectrometer, Anal. Chem., 78, 8281-8289, 2006.

DeCarlo, P. F., Ulbrich, I. M., Crounse, J., de Foy, B., Dunlea, E. J., Aiken, A. C., Knapp, D., Weinheimer, A. J., Campos, T., Wennberg, P. O., and Jimenez, J. L.: Investigation of the sources and processing of organic aerosol over the Central Mexican Plateau from aircraft measurements during MILAGRO, Atmos. Chem. Phys., 10, 5257-5280, 2010.

Docherty, K. S., Aiken, A. C., Huffman, J. A., Ulbrich, I. M., DeCarlo, P. F., Sueper, D., Worsnop, D. R., Snyder, D. C., Grover, B. D., Eatough, D. J., Goldstein, A. H., Ziemann, P. J., and Jimenez, J. L.: The 2005 study of organic aerosols at Riverside (SOAR-1): instrumental intercomparisons and fine particle composition, Atmos. Chem. Phys. Discuss., 11, 6301-6362, 2011.

Dockery, D. W., Pope, C. A., Xu, X., Spengler, J. D., Ware, J. H., Fay, M. E., Ferris, B. G., and Speizer, F. E.: An Association between air pollution and mortality in six U.S. cities, New England Journal of Medicine, 329, 1753-1759, doi:10.1056/NEJM199312093292401, 1993.

Donahue, N. M., Kroll, J. H., Pandis, S. N., and Robinson, A. L.: A two-dimensional volatility basis set - Part 2: Diagnostics of organic-aerosol evolution, Atmos. Chem. Phys. Discuss., 11, 24883-24931, 2011.

Drewnick, F., Hings, S. S., DeCarlo, P., Jayne, J. T., Gonin, M., Fuhrer, K., Weimer, S., Jimenez, J. L., Demerjian, K. L., Borrmann, S., and Worsnop, D. R.: A new time-of-flight aerosol mass spectrometer (TOF-AMS) - Instrument description and first field deployment, Aerosol. Sci. Technol., 39, 637-658, 2005.

Duplissy, J., DeCarlo, P. F., Dommen, J., Alfarra, M. R., Metzger, A., Barmpadimos, I., Prevot, A. S. H., Weingartner, E., Tritscher, T., Gysel, M., Aiken, A. C., Jimenez, J. L., Canagaratna, M. R., Worsnop, D. R., Collins, D. R., Tomlinson, J., and Baltensperger, U.: Relating hygroscopicity and composition of organic aerosol particulate matter, Atmos. Chem. Phys., 11, 1155-1165, 2011.

Dzepina, K., Arey, J., Marr, L. C., Worsnop, D. R., Salcedo, D., Zhang, Q., Onasch, T. B., Molina, L. T., Molina, M. J., and Jimenez, J. L.: Detection of particle-phase polycyclic aromatic hydrocarbons in Mexico City using an aerosol mass spectrometer, Int. J. Mass Spectrom., 263, 152-170, 2007.

Engelhart, G. J., Hildebrandt, L., Kostenidou, E., Mihalopoulos, N., Donahue, N. M., and Pandis, S. N.: Water content of aged aerosol, Atmos. Chem. Phys., 11, 911-920, 2011.

European Parliament and the Council: Directive 2008/50/EC of the European Parliament and of the Council of 21 May 2008 on ambient air quality and cleaner air for Europe, Official Journal of the European Union, L 152, 2008.

Farmer, D. K., Matsunaga, A., Docherty, K. S., Surratt, J. D., Seinfeld, J. H., Ziemann, P. J., and Jimenez, J. L.: Response of an aerosol mass spectrometer to organonitrates and organosulfates and implications for atmospheric chemistry, Proceedings of the National Academy of Sciences, 107, 6670-6675, 10.1073/pnas.0912340107, 2010.

Fay, B., Glaab, H., Jacobsen, I., and Schrodin, R.: Evaluation of Eulerian and Lagrangian atmospheric transport models at the Deutscher-Wetterdienst using Anatex surface tracer data, Atmos. Environ., 29, 2485-2497, 1995.

Finlayson-Pitts, B. J., and Pitts, J. N.: Chemistry of the Upper and Lower Troposphere, Academic Press, San Diego, London, 2000.

Fortmann, R., Kariher, P., and Clayton, R.: Indoor air quality: Residential cooking exposures. Final report., State of California Air Resources Board, Research Division, Sacramento, CA, 2001.

Gehrig, R., Hueglin, C., Devos, W., Hofer, P., Kobler, J., Stahel, W. A., Baltensperger, U., and Monn, C.: Contribution of road traffic to ambient fine particle concentrations (PM10) in Switzerland, 1-4, Inderscience, Geneva, SUISSE, 2001.

Gehrig, R., and Buchmann, B.: Characterising seasonal variations and spatial distribution of ambient PM10 and PM2.5 concentrations based on long-term Swiss monitoring data, Atmos. Environ., 37, 2571-2580, doi 10.1016/S1352-2310(03)00221-8, 2003.

Gerbig, C., Schmitgen, S., Kley, D., Volz-Thomas, A., Dewey, K., and Haaks, D.: An improved fast-response vacuum-UV resonance fluorescence CO instrument, J. Geophys. Res-Atmos., 104, 1699-1704, 1999.

Goldstein, A. H., and Galbally, I. E.: Known and unexplored organic constituents in the earth's atmosphere, Environ. Sci. Technol., 41, 1514-1521, 2007.

Grantz, D. A., Garner, J. H. B., and Johnson, D. W.: Ecological effects of particulate matter, Environ. Int., 29, 213-239, 10.1016/s0160-4120(02)00181-2, 2003.

Gray, H. A.: Control of atmospheric fine primary carbon particle concentrations. Final report for California Air Resources Board., Environmental Quality Laboratory, California Institute of Technology, Pasadena, 353 pp., 1986.

Gysel, M., Crosier, J., Topping, D. O., Whitehead, J. D., Bower, K. N., Cubison, M. J., Williams, P. I., Flynn, M. J., McFiggans, G. B., and Coe, H.: Closure study between chemical composition and hygroscopic growth of aerosol particles during TORCH2, Atmos. Chem. Phys., 7, 6131-6144, 2007.

Hallquist, M., Wenger, J. C., Baltensperger, U., Rudich, Y., Simpson, D., Claeys, M., Dommen, J., Donahue, N. M., George, C., Goldstein, A. H., Hamilton, J. F., Herrmann, H., Hoffmann, T., Iinuma, Y., Jang, M., Jenkin, M. E., Jimenez, J. L., Kiendler-Scharr, A., Maenhaut, W., McFiggans, G., Mentel, T. F., Monod, A., Prevot, A. S. H., Seinfeld, J. H., Surratt, J. D., Szmigielski, R., and Wildt, J.: The formation, properties and impact of secondary organic aerosol: current and emerging issues, Atmos. Chem. Phys., 9, 5155-5236, 2009.

Haywood, J., and Boucher, O.: Estimates of the direct and indirect radiative forcing due to tropospheric aerosols: A review, Rev. Geophys., 38, 513-543, 2000.

He, L.-Y., Hu, M., Huang, X.-F., Yu, B.-D., Zhang, Y.-H., and Liu, D.-Q.: Measurement of emissions of fine particulate organic matter from Chinese cooking, Atmos. Environ., 38, 6557-6564, 2004.

He, L. Y., Lin, Y., Huang, X. F., Guo, S., Xue, L., Su, Q., Hu, M., Luan, S. J., and Zhang, Y. H.: Characterization of high-resolution aerosol mass spectra of primary organic aerosol emissions from Chinese cooking and biomass burning, Atmos. Chem. Phys., 10, 11535-11543, 2010.

Heald, C. L., Kroll, J. H., Jimenez, J. L., Docherty, K. S., DeCarlo, P. F., Aiken, A. C., Chen, Q., Martin, S. T., Farmer, D. K., and Artaxo, P.: A simplified description of the evolution of organic aerosol composition in the atmosphere, Geophys. Res. Lett., 37, L08803, 2011.

Henry, R. C., Lewis, C. W., Hopke, P. K., and Williamson, H. J.: Review of receptor model fundamentals, Atmospheric Environment (1967), 18, 1507-1515, 1984.

Henry, R. C.: History and fundamentals of multivariate air quality receptor models, Chemometr. Intell. Lab., 37, 37-42, 1997.

Herich, H., Hueglin, C., and Buchmann, B.: A 2.5 year's source apportionment study of black carbon from wood burning and fossil fuel combustion at urban and rural sites in Switzerland, Atmos. Meas. Tech., 4, 1409-1420, 2011.

Heringa, M. F., DeCarlo, P. F., Chirico, R., Tritscher, T., Dommen, J., Weingartner, E., Richter, R., Wehrle, G., Prevot, A. S. H., and Baltensperger, U.: Investigations of primary and secondary particulate matter of different wood combustion appliances with a high-resolution time-of-flight

aerosol mass spectrometer, Atmos. Chem. Phys., 11, 5945 - 5957, 10.5194/acp-11-5945-2011, 2011.

Hildebrandt, L., Engelhart, G. J., Mohr, C., Kostenidou, E., Lanz, V. A., Bougiatioti, A., DeCarlo, P. F., Prevot, A. S. H., Baltensperger, U., Mihalopoulos, N., Donahue, N. M., and Pandis, S. N.: Aged organic aerosol in the Eastern Mediterranean: the Finokalia Aerosol Measurement Experiment-2008, Atmos. Chem. Phys., 10, 4167-4186, doi 10.5194/acp-10-4167-2010, 2010.

Hildemann, L. M., Markowski, G. R., and Cass, G. R.: Chemical composition of emissions from urban sources of fine organic aerosol, Environ. Sci. Technol., 25, 744-759, 1991.

Hinds, W. C.: Aerosol Technology. Properties, Behavior, and Measurement of Airborne Particles, Wiley, Hoboken, N.J., xx, 483 pp., 1999.

Hong, S., Candelone, J.-P., Patterson, C. C., and Boutron, C. F.: Greenland ice evidence of hemispheric lead pollution two millennia ago by Greek and Roman civilizations, Science, 265, 1841-1843, 10.1126/science.265.5180.1841, 1994.

Huang, X. F., He, L. Y., Hu, M., Canagaratna, M. R., Sun, Y., Zhang, Q., Zhu, T., Xue, L., Zeng, L. W., Liu, X. G., Zhang, Y. H., Jayne, J. T., Ng, N. L., and Worsnop, D. R.: Highly time-resolved chemical characterization of atmospheric submicron particles during 2008 Beijing Olympic Games using an Aerodyne high-resolution aerosol mass spectrometer, Atmos. Chem. Phys., 10, 8933-8945, 2010.

Hueglin, C., Gehrig, R., Baltensperger, U., Gysel, M., Monn, C., and Vonmont, H.: Chemical characterisation of PM2.5, PM10 and coarse particles at urban, near-city and rural sites in Switzerland, Atmos. Environ., 39, 637-651, 2005.

IPCC: Fourth Assessment Report: The Physical Science Basis, Working Group I, Final Report, Geneva, Switzerland, available at: http://www.ipcc.ch/ipccreports/ar4-wg1.htm, 2007.

Jacobson, M. C., Hansson, H. C., Noone, K. J., and Charlson, R. J.: Organic atmospheric aerosols: Review and state of the science, Reviews of Geophysics, 38, 267-294, 2000.

Jimenez, J. L., Jayne, J. T., Shi, Q., Kolb, C. E., Worsnop, D. R., Yourshaw, I., Seinfeld, J. H., Flagan, R. C., Zhang, X. F., Smith, K. A., Morris, J. W., and Davidovits, P.: Ambient aerosol sampling using the Aerodyne aerosol mass spectrometer, J. Geophys. Res-Atmos., 108, D78425, doi:10.1029/2001JD001213, 2003.

Jimenez, J. L., Canagaratna, M. R., Donahue, N. M., Prevot, A. S. H., Zhang, Q., Kroll, J. H., DeCarlo, P. F., Allan, J. D., Coe, H., Ng, N. L., Aiken, A. C., Docherty, K. S., Ulbrich, I. M., Grieshop, A. P., Robinson, A. L., Duplissy, J., Smith, J. D., Wilson, K. R., Lanz, V. A., Hueglin, C., Sun, Y. L., Tian, J., Laaksonen, A., Raatikainen, T., Rautiainen, J., Vaattovaara, P., Ehn, M., Kulmala, M., Tomlinson, J. M., Collins, D. R., Cubison, M. J., Dunlea, E. J., Huffman, J. A., Onasch, T. B., Alfarra, M. R., Williams, P. I., Bower, K., Kondo, Y., Schneider, J., Drewnick, F., Borrmann, S., Weimer, S., Demerjian, K., Salcedo, D., Cottrell, L., Griffin, R., Takami, A., Miyoshi, T., Hatakeyama, S., Shimono, A., Sun, J. Y., Zhang, Y. M., Dzepina, K., Kimmel, J. R., Sueper, D., Jayne, J. T., Herndon, S. C., Trimborn, A. M., Williams, L. R., Wood, E. C., Middlebrook, A. M., Kolb, C. E., Baltensperger, U., and Worsnop, D. R.: Evolution of organic aerosols in the atmosphere, Science, 326, 1525-1529, 2009.

Johanson, T., Caldow, R., Pöcher, A., Mirme, A., and Kittelson, D.: A new electrical mobility particle sizer spectrometer for engine exhaust particle measurements, Society of Automotive Engineers Technical Paper Series 2004-01-1341, 2004.

Jorba, O., Pandolfi, M., Spada, M., Baldasano, J. M., Pey, J., Alastuey, A., Arnold, D., Sicard, M., Artiñano, B., Revuelta, M. A., and Querol, X.: The DAURE field campaign: meteorological overview, Atmos. Chem. Phys. Discuss., 11, 4953-5001, 2011.

Koebel, M., Elsener, M., and Kleemann, M.: Urea-SCR: a promising technique to reduce NOx emissions from automotive diesel engines, Catal. Today, 59, 335-345, 2000.

Krecl, P., Strom, J., and Johansson, C.: Diurnal variation of atmospheric aerosol during the wood combustion season in Northern Sweden, Atmos. Environ., 42, 4113-4125, 2008.

Laden, F., Schwartz, J., Speizer, F. E., and Dockery, D. W.: Reduction in fine particulate air pollution and mortality - Extended follow-up of the Harvard six cities study, Am. J. Resp. Crit. Care, 173, 667-672, 10.1164/rccm.200503-443OC, 2006.

Lanz, V. A., Alfarra, M. R., Baltensperger, U., Buchmann, B., Hueglin, C., and Prevot, A. S. H.: Source apportionment of submicron organic aerosols at an urban site by factor analytical modelling of aerosol mass spectra, Atmos. Chem. Phys., 7, 1503-1522, 2007.

Lanz, V. A., Alfarra, M. R., Baltensperger, U., Buchmann, B., Hueglin, C., Szidat, S., Wehrli, M. N., Wacker, L., Weimer, S., Caseiro, A., Puxbaum, H., and Prevot, A. S. H.: Source attribution of submicron organic aerosols during wintertime inversions by advanced factor analysis of aerosol mass spectra, Environ. Sci. Technol., 42, 214-220, doi 10.1021/Es0707207, 2008.

Lanz, V. A., Prevot, A. S. H., Alfarra, M. R., Weimer, S., Mohr, C., DeCarlo, P. F., Gianini, M. F. D., Hueglin, C., Schneider, J., Favez, O., D'Anna, B., George, C., and Baltensperger, U.: Characterization of aerosol chemical composition with aerosol mass spectrometry in Central Europe: an overview, Atmos. Chem. Phys., 10, 10453-10471, 2010.

Lenschow, P., Abraham, H. J., Kutzner, K., Lutz, M., Preuß, J. D., and Reichenbächer, W.: Some ideas about the sources of PM10, Atmos. Environ., 35, 23-33, 2001.

Li, N., Sioutas, C., Cho, A., Schmitz, D., Misra, C., Sempf, J., Wang, M. Y., Oberley, T., Froines, J., and Nel, A.: Ultrafine particulate pollutants induce oxidative stress and mitochondrial damage, Environ. Health Perspect., 111, 455-460, 10.1289/ehp.6000, 2003.

Liu, P. S. K., Deng, R., Smith, K. A., Williams, L. R., Jayne, J. T., Canagaratna, M. R., Moore, K., Onasch, T. B., Worsnop, D. R., and Deshler, T.: Transmission efficiency of an aerodynamic focusing lens system: Comparison of model calculations and laboratory measurements for the Aerodyne aerosol mass spectrometer, Aerosol. Sci. Technol., 41, 721 - 733, 2007.

Lohmann, U., and Feichter, J.: Global indirect aerosol effects: a review, Atmos. Chem. Phys., 5, 715-737, 2005.

Maynard, A., and Kuempel, E.: Airborne nanostructured particles and occupational health, Journal of Nanoparticle Research, 7, 587-614, 2005.

Mejia, J. F., Morawska, L., and Mengersen, K.: Spatial variation in particle number size distributions in a large metropolitan area, Atmos. Chem. Phys., 8, 1127-1138, 2008.

Middlebrook, A. M., Bahreini, R., Jimenez, J. L., and Canagaratna, M. R.: Evaluation of composition-dependent collection efficiencies for the Aerodyne aerosol mass spectrometer using field data, Aerosol. Sci. Technol., 46, 258–271, 10.1080/02786826.2011.620041, 2012.

Middleton, J. T., Kendrick, J. B., Jr., and Schwalm, H. W.: Injury to herbaceous plants by smog or air pollution, Journal Name: Plant Dis.; (United States); Journal Volume: 34:9, Medium: X; Size: Pages: 245-252, 1950.

Minguillón, M. C., Perron, N., Querol, X., Szidat, S., Fahrni, S., Alastuey, A., Jimenez, J. L., Mohr, C., Ortega, A., Day, D. A., Lanz, V. A., Wacker, L., Reche, C., Cusack, M., Amato, F., Kiss, G., Hoffer, A., Decesari, S., Moretti, F., Hillamo, R., Teinilä, K., Seco, R., Peñuelas, J., Metzger, A., Schallhart, S., Müller, M., Hansel, A., Burkhart, J., Baltensperger, U., and Prevot, A. S. H.: Fossil versus contemporary sources of fine elemental and organic carbonaceous particulate matter during the DAURE campaign in Northeast Spain, Atmos. Chem. Phys., 11, 12067 - 12084, 10.5194/acp-11-12067-2011, 2011.

Mohr, C., Huffman, J. A., Cubison, M. J., Aiken, A. C., Docherty, K. S., Kimmel, J. R., Ulbrich, I. M., Hannigan, M., and Jimenez, J. L.: Characterization of primary organic aerosol emissions from meat cooking, trash burning, and motor vehicles with high-resolution aerosol mass spectrometry

and comparison with ambient and chamber observations, Environ. Sci. Technol., 43, 2443-2449, 2009.

Mohr, C., Richter, R., DeCarlo, P. F., Prévôt, A. S. H., and Baltensperger, U.: Spatial variation of chemical composition and sources of submicron aerosol in Zurich during wintertime using mobile aerosol mass spectrometer data, Atmos. Chem. Phys., 11, 7465-7482, 2011.

Mohr, C., DeCarlo, P. F., Heringa, M. F., Chirico, R., Slowik, J. G., Richter, R., Reche, C., Alastuey, A., Querol, X., Seco, R., Peñuelas, J., Jimenez, J. L., Crippa, M., Zimmermann, R., Baltensperger, U., and Prevot, A. S. H.: Identification and quantification of organic aerosol from cooking and other sources in Barcelona using aerosol mass spectrometer data, Atmos. Chem. Phys., 12, 1649 - 1665, 10.5194/acp-12-1649-2012, 2012.

Molina, L. T., Madronich, S., Gaffney, J. S., Apel, E., de Foy, B., Fast, J., Ferrare, R., Herndon, S., Jimenez, J. L., Lamb, B., Osornio-Vargas, A. R., Russell, P., Schauer, J. J., Stevens, P. S., and Zavala, M.: An overview of the MILAGRO 2006 campaign: Mexico City emissions and their transport and transformation, Atmos. Chem. Phys., 10, 8697 - 8760, 10.5194/acp-10-8697-2010, 2010.

Molina, M. J., and Molina, L. T.: Megacities and atmospheric pollution, J. Air Waste Manage., 54, 644-680, 2004.

Moreno, T., Querol, X., Alastuey, A., Reche, C., Cusack, M., Amato, F., Pandolfi, M., Pey, J., Richard, A., Prévôt, A. S. H., Furger, M., and Gibbons, W.: Variations in time and space of trace metal aerosol concentrations in urban areas and their surroundings, Atmos. Chem. Phys., 11, 9415-9430, 2011.

Murphy, S. M., Agrawal, H., Sorooshian, A., Padró, L. T., Gates, H., Hersey, S., Welch, W. A., Jung, H., Miller, J. W., Cocker, D. R., Nenes, A., Jonsson, H. H., Flagan, R. C., and Seinfeld, J. H.: Comprehensive simultaneous shipboard and airborne characterization of exhaust from a modern container ship at sea, Environ. Sci. Technol., 43, 4626-4640, 2009.

Nel, A.: Air pollution-related illness: Effects of particles, Science, 308, 804-806, 10.1126/science.1108752, 2005.

Nemitz, E., Jimenez, J. L., Huffman, J. A., Ulbrich, I. M., Canagaratna, M. R., Worsnop, D. R., and Guenther, A. B.: An Eddy-covariance system for the measurement of surface/atmosphere exchange fluxes of submicron aerosol chemical species - First application above an urban area, Aerosol. Sci. Technol., 42, 636-657, 2008.

Nemitz, E., Prevot, A. S. H., Äijälä, M., Allan, J. D., Berresheim, H., Carbone, S., Canagaratna, M. R., Capes, G., Ceburnis, D., Choularton, T., Coe, H., Cubison, M. J., Dall'Osto, M., Di Marco, C. F., DeCarlo, P. F., Ehn, M., Eriksson, A., Freney, E., Herrmann, H., Jimenez, J. L., Hildebrandt, L., Juninen, H., Kiendler-Scharr, A., Laaksonen, A., Lanz, V. A., McFiggans, G., Mensah, A., Mentel, T. F., Mohr, C., O'Dowd, C., Ortega, A., Ovadnevaite, J., Pagels, J., Pandis, S. N., Phillips, G. J., Poulain, L., Raatikainen, T., Saarikoski, S., Sellegri, K., Spindler, G., Sueper, D., Swietlicki, E., Tiitta, P., and Worsnop, D. R.: European submicron aerosol chemical composition derived from a campaign-based Aerosol Mass Spectrometer network, in prep., 2012.

Ng, N. L., Canagaratna, M. R., Zhang, Q., Jimenez, J. L., Tian, J., Ulbrich, I. M., Kroll, J. H., Docherty, K. S., Chhabra, P. S., Bahreini, R., Murphy, S. M., Seinfeld, J. H., Hildebrandt, L., Donahue, N. M., DeCarlo, P. F., Lanz, V. A., Prevot, A. S. H., Dinar, E., Rudich, Y., and Worsnop, D. R.: Organic aerosol components observed in northern hemispheric datasets from aerosol mass spectrometry, Atmos. Chem. Phys., 10, 4625-4641, doi 10.5194/acp-10-4625-2010, 2010.

Ng, N. L., Canagaratna, M. R., Jimenez, J. L., Chhabra, P. S., Seinfeld, J. H., and Worsnop, D. R.: Changes in organic aerosol composition with aging inferred from aerosol mass spectra, Atmos. Chem. Phys., 11, 6465-6474, 2011a.

Ng, N. L., Canagaratna, M. R., Jimenez, J. L., Zhang, Q., Ulbrich, I. M., and Worsnop, D. R.: Real-time methods for estimating organic component mass concentrations from aerosol mass spectrometer data, Environ. Sci. Technol., 45, 910-916, 2011b.

Ng, N. L., Herndon, S. C., Trimborn, A., Canagaratna, M. R., Croteau, P. L., Onasch, T. B., Sueper, D., Worsnop, D. R., Zhang, Q., Sun, Y. L., and Jayne, J. T.: An aerosol chemical speciation monitor (ACSM) for routine monitoring of the composition and mass concentrations of ambient aerosol, Aerosol. Sci. Technol., 45, 780-794, 2011c.

Nussbaumer, T., Klippel, N., and Oser, M.: Aerosol in biomass combustion: Health relevance of aerosols from biomass combustion in comparison to diesel soot indicated by cytotoxicity tests, Series Thermal Biomass Utilization, Graz University of Technology, 6, 45–54, 2005.

Paatero, P., and Tapper, U.: Analysis of different modes of factor-analysis as least-squares fit problems, Chemometr. Intell. Lab., 18, 183-194, 1993.

Paatero, P., and Tapper, U.: Positive matrix factorization - a nonnegative factor model with optimal utilization of error-estimates of data values, Environmetrics, 5, 111-126, 1994.

Paatero, P., Hopke, P. K., Song, X. H., and Ramadan, Z.: Understanding and controlling rotations in factor analytic models, Chemometr. Intell. Lab., 60, 253-264, 2002.

Paatero, P.: User's guidefor positive matrix factorization programs PMF2.EXE and PMF3.EXE, University of Helsinki, Finland, 2007.

Pandolfi, M., Gonzalez-Castanedo, Y., Alastuey, A., de la Rosa, J., Mantilla, E., de la Campa, A., Querol, X., Pey, J., Amato, F., and Moreno, T.: Source apportionment of PM10 and PM2.5 at multiple sites in the strait of Gibraltar by PMF: impact of shipping emissions, Environ. Sci. Pollut. R., 18, 260-269, 2011.

Pandolfi, M., Querol, X., Alastuey, A., Jimenez, J. L., Cusack, M., Reche, C., Pey, J., Mohr, C., DeCarlo, P. F., Ortega, A., Day, D., Prevot, A. S. H., Baltensperger, U., Artiñano, B., Baldasano, J. M., Jorba, O., Burkhart, J., Hansel, A., Schallhart, S., Müller, M., Metzger, M., Saarikoski, S., Cubison, M. J., Ng, S., Lorente, J., Nemitz, E., Di Marco, C., Peñuelas, J., Sicard, M., Comeron, A., Amato, F., Moreno, T., Viana , M., Pérez, N., Moreno, N., Seco, R., Filella, I., Llusià, J., Piot, M., and Pay, M. T.: Sources and origin of PM in the Western Mediterranean Basin: An overview of the DAURE campaign, in preparation, 2012.

Pérez, C., Nickovic, S., Baldasano, J. M., Sicard, M., Rocadenbosch, F., and Cachorro, V. E.: A long Saharan dust event over the western Mediterranean: Lidar, Sun photometer observations, and regional dust modeling, J. Geophys. Res., 111, D15214, 10.1029/2005JD006579, 2006.

Pérez, N., Pey, J., Castillo, S., Viana, M., Alastuey, A., and Querol, X.: Interpretation of the variability of levels of regional background aerosols in the Western Mediterranean, Sci. Total Environ., 407, 527-540, 2008a.

Pérez, N., Pey, J., Querol, X., Alastuey, A., López, J. M., and Viana, M.: Partitioning of major and trace components in PM10-PM2.5-PM1 at an urban site in Southern Europe, Atmos. Environ., 42, 1677-1691, 2008b.

Petzold, A., Kramer, H., and Schönlinner, M.: Continuous measurement of atmospheric black carbon using a multi-angle absorption photometer, Environ. Sci. Pollut. R., 4, 78 - 82, 2002.

Pey, J., Pérez, N., Querol, X., Alastuey, A., Cusack, M., and Reche, C.: Intense winter atmospheric pollution episodes affecting the Western Mediterranean, Sci. Total Environ., 408, 1951-1959, 2010.

Pope, C. A., Burnett, R. T., Thun, M. J., Calle, E. E., Krewski, D., Ito, K., and Thurston, G. D.: Lung cancer, cardiopulmonary mortality, and long-term exposure to fine particulate air pollution, JAMA: The Journal of the American Medical Association, 287, 1132-1141, 10.1001/jama.287.9.1132, 2002.

Querol, X., Alastuey, A., Rodriguez, S., Plana, F., Ruiz, C. R., Cots, N., Massagué, G., and Puig, O.: PM10 and PM2.5 source apportionment in the Barcelona Metropolitan area, Catalonia, Spain, Atmos. Environ., 35, 6407-6419, 2001.

Querol, X., Alastuey, A., Ruiz, C. R., Artiñano, B., Hansson, H. C., Harrison, R. M., Buringh, E., ten Brink, H. M., Lutz, M., Bruckmann, P., Straehl, P., and Schneider, J.: Speciation and origin of PM10 and PM2.5 in selected European cities, Atmos. Environ., 38, 6547-6555, 2004.

Reche, C., Viana, M., Moreno, T., Querol, X., Alastuey, A., Pey, J., Pandolfi, M., Prévôt, A., Mohr, C., Richard, A., Artiñano, B., Gomez-Moreno, F. J., and Cots, N.: Peculiarities in atmospheric particle number and size-resolved speciation in an urban area in the western Mediterranean: Results from the DAURE campaign, Atmos. Environ., 45, 5282-5293, 2011.

Reche, C., Viana , M., Amato, F., Querol, X., Moreno, T., Minguillón, M. C., Alastuey, A., Hillamo, R., Teinilä, K., Saarnio, K., Seco, R., and Mohr, C.: Biomass burning contributions to urban aerosols in a coastal Mediterranean city, in preparation, 2012.

Richard, A., Gianini, M. F. D., Mohr, C., Furger, M., Bukowiecki, N., Minguillón, M. C., Lienemann, P., Flechsig, U., Appel, K., DeCarlo, P. F., Heringa, M. F., Chirico, R., Baltensperger, U., and Prevot, A. S. H.: Source apportionment of size and time resolved trace elements and organic aerosols from an urban courtyard site in Switzerland, Atmos. Chem. Phys. Discuss., 11, 10.5194/acpd-11-3727-2011, 2011.

Rogge, W. F., Hildemann, L. M., Mazurek, M. A., Cass, G. R., and Simonelt, B. R. T.: Sources of fine organic aerosol .1. Charbroilers and meat cooking operations, Environ. Sci. Technol., 25, 1112-1125, 1991.

Samet, J. M., Dominici, F., Curriero, F. C., Coursac, I., and Zeger, S. L.: Fine particulate air pollution and mortality in 20 U.S. cities, 1987 - 1994, New England Journal of Medicine, 343, 1742-1749, doi:10.1056/NEJM200012143432401, 2000.

Sander, S. P., Golden, D. M., Kurylo, M. J., Huie, R. E., Orkin, V. L., Moortgat, G. K., Ravishankara, A. R., Kolb, C. E., Molina, M. J., and Finlayson-Pitts, B. J.: Chemical kinetics and photochemical data for use in atmospheric studies, Evaluation 14, Jet Propulsion Laboratory, Pasadena, CA (available at http://jpldataeval.jpl.nasa.gov), 2003.

Sandradewi, J., Prevot, A. S. H., Szidat, S., Perron, N., Alfarra, M. R., Lanz, V. A., Weingartner, E., and Baltensperger, U.: Using aerosol light absorption measurements for the quantitative determination of wood burning and traffic emission contributions to particulate matter, Environ. Sci. Technol., 42, 3316-3323, 2008.

Schauer, J. J., Rogge, W. F., Hildemann, L. M., Mazurek, M. A., and Cass, G. R.: Source apportionment of airborne particulate matter using organic compounds as tracers, Atmos. Environ., 30, 3837-3855, 1996.

Schauer, J. J., Kleeman, M. J., Cass, G. R., and Simoneit, B. R. T.: Measurement of emissions from air pollution sources. 1. C-1 through C-29 organic compounds from meat charbroiling, Environ. Sci. Technol., 33, 1566-1577, 1999.

Schauer, J. J., Kleeman, M. J., Cass, G. R., and Simoneit, B. R. T.: Measurement of emissions from air pollution sources. 4. C1-C27 organic compounds from cooking with seed oils, Environ. Sci. Technol., 36, 567-575, 2001.

Schneider, J., Hings, S. S., Hock, B. N., Weimer, S., Borrmann, S., Fiebig, M., Petzold, A., Busen, R., and Karcher, B.: Aircraft-based operation of an aerosol mass spectrometer: Measurements of tropospheric aerosol composition, J. Aerosol. Sci., 37, 839-857, 10.1016/j.jaerosci.2005.07.002, 2006.

Seinfeld, J. H., and Pandis, S. N.: Atmospheric Chemistry and Physics : From Air Pollution to Climate Change, 2nd ed., Wiley, Hoboken, N.J., xxviii, 1203 pp., 2006.

Silva, P. J., Erupe, M. E., Price, D., Elias, J., Malloy, Q. G. J., Li, Q., Warren, B., and Cocker, D. R.: Trimethylamine as precursor to secondary organic aerosol formation via nitrate radical reaction in the atmosphere, Environ. Sci. Technol., 42, 4689-4696, 10.1021/es703016v, 2008.

Slowik, J. G., Stainken, K., Davidovits, P., Williams, L. R., Jayne, J. T., Kolb, C. E., Worsnop, D. R., Rudich, Y., DeCarlo, P. F., and Jimenez, J. L.: Particle morphology and density characterization by combined mobility and aerodynamic diameter measurements. Part 2: Application to combustion-generated soot aerosols as a function of fuel equivalence ratio, Aerosol. Sci. Technol., 38, 1206-1222, 10.1080/027868290903916, 2004.

Slowik, J. G., Vlasenko, A., McGuire, M., Evans, G. J., and Abbatt, J. P. D.: Simultaneous factor analysis of organic particle and gas mass spectra: AMS and PTR-MS measurements at an urban site, Atmos. Chem. Phys., 10, 1969-1988, 2010.

Smolík, J., Zdímal, V., Schwarz, J., Lazaridis, M., Havárnek, V., Eleftheriadis, K., Mihalopoulos, N., Bryant, C., and Colbeck, I.: Size resolved mass concentration and elemental composition of atmospheric aerosols over the Eastern Mediterranean area, Atmos. Chem. Phys., 3, 2207-2216, 2003.

Sueper, D.: ToF-AMS High Resolution Analysis Software – Pika, online available at: http://cires.colorado.edu/jimenez-group/ToFAMSResources/ToFSoftware/PikaInfo/, 2008.

Sun, Y. L., Zhang, Q., Schwab, J. J., Demerjian, K. L., Chen, W. N., Bae, M. S., Hung, H. M., Hogrefe, O., Frank, B., Rattigan, O. V., and Lin, Y. C.: Characterization of the sources and processes of organic and inorganic aerosols in New York city with a high-resolution time-of-flight aerosol mass apectrometer, Atmos. Chem. Phys., 11, 1581-1602, 10.5194/acp-11-1581-2011, 2011.

Szidat, S., Jenk, T. M., Synal, H. A., Kalberer, M., Wacker, L., Hajdas, I., Kasper-Giebl, A., and Baltensperger, U.: Contributions of fossil fuel, biomass-burning, and biogenic emissions to carbonaceous aerosols in Zurich as traced by C-14, J. Geophys. Res-Atmos., 111, D07206, doi:10.1029/2005JD006590, 2006.

Szidat, S., Ruff, M., Perron, N., Wacker, L., Synal, H. A., Hallquist, M., Shannigrahi, A. S., Yttri, K. E., Dye, C., and Simpson, D.: Fossil and non-fossil sources of organic carbon (OC) and elemental carbon (EC) in Goteborg, Sweden, Atmos. Chem. Phys., 9, 1521-1535, 2009.

Thornhill, D. A., Williams, A. E., Onasch, T. B., Wood, E., Herndon, S. C., Kolb, C. E., Knighton, W. B., Zavala, M., Molina, L. T., and Marr, L. C.: Application of positive matrix factorization to on-road measurements for source apportionment of diesel- and gasoline-powered vehicle emissions in Mexico City, Atmos. Chem. Phys., 10, 3629 - 3644, 10.5194/acp-10-3629-2010, 2010.

UGZ: (Umwelt- und Gesundheitsschutz Zürich): Vordringen von PM10 in den Atemtrakt, 2004.

Ulbrich, I., Canagaratna, M. R., Zhang, Q., Worsnop, D. R., and Jimenez, J. L.: Interpretation of organic components from positive matrix factorization of aerosol mass spectrometric data, Atmospheric Chemistry and Physics discussion, 8, 6729-6791, 2008.

AMS Spectral Database. URL: http://cires.colorado.edu/jimenez-group/AMSsd/: http://cires.colorado.edu/jimenez-group/AMSsd/, 2007.

Ulbrich, I. M., Canagaratna, M. R., Zhang, Q., Worsnop, D. R., and Jimenez, J. L.: Interpretation of organic components from positive matrix factorization of aerosol mass spectrometric data, Atmos. Chem. Phys., 9, 2891-2918, 2009.

Ulbrich, I. M., Canagaratna, M. R., Cubison, M. J., Zhang, Q., Ng, N. L., Aiken, A. C., and Jimenez, J. L.: Three-dimensional factorization of size-resolved organic aerosol mass spectra from Mexico City, Atmos. Meas. Tech. Discuss., 4, 4561-4630, 2011.

Vardoulakis, S., Fisher, B. E. A., Pericleous, K., and Gonzalez-Flesca, N.: Modelling air quality in street canyons: a review, Atmos. Environ., 37, 155-182, 2003.

Volkamer, R., Jimenez, J. L., San Martini, F., Dzepina, K., Zhang, Q., Salcedo, D., Molina, L. T., Worsnop, D. R., and Molina, M. J.: Secondary organic aerosol formation from anthropogenic air pollution: Rapid and higher than expected, Geophys. Res. Lett., 33, -, 2006.

Watson, J. G.: Visibility: Science and regulation, J. Air Waste Manage., 52, 628-713, 2002.

Weimer, S., Alfarra, M. R., Schreiber, D., Mohr, M., Prévôt, A. S. H., and Baltensperger, U.: Organic aerosol mass spectral signatures from wood-burning emissions: Influence of burning conditions and wood type, J. Geophys. Res., 113, D10304, 10.1029/2007JD009309, 2008.

Weimer, S., Mohr, C., Richter, R., Keller, J., Mohr, M., Prévôt, A. S. H., and Baltensperger, U.: Mobile measurements of aerosol number and volume size distributions in an Alpine valley: Influence of traffic versus wood burning, Atmos. Environ., 43, 624-630, 2009.

Weingartner, E., Saathoff, H., Schnaiter, M., Streit, N., Bitnar, B., and Baltensperger, U.: Absorption of light by soot particles: determination of the absorption coefficient by means of aethalometers, J. Aerosol. Sci., 34, 1445-1463, 2003.

Wiedensohler, A., Birmili, W., Nowak, A., Sonntag, A., Weinhold, K., Merkel, M., Wehner, B., Tuch, T., Pfeifer, S., Fiebig, M., Fjäraa, A. M., Asmi, E., Sellegri, K., Depuy, R., Venzac, H., Villani, P., Laj, P., Aalto, P., Ogren, J. A., Swietlicki, E., Roldin, P., Williams, P., Quincey, P., Hüglin, C., Fierz-Schmidhauser, R., Gysel, M., Weingartner, E., Riccobono, F., Santos, S., Grüning, C., Faloon, K., Beddows, D., Harrison, R. M., Monahan, C., Jennings, S. G., O'Dowd, C. D., Marinoni, A., Horn, H. G., Keck, L., Jiang, J., Scheckman, J., McMurry, P. H., Deng, Z., Zhao, C. S., Moerman, M., Henzing, B., and de Leeuw, G.: Particle mobility size spectrometers: harmonization of technical standards and data structure to facilitate high quality long-term observations of atmospheric particle number size distributions, Atmos. Meas. Tech. Discuss., 3, 5521-5587, 2011.

Wilkins, E. T.: Air pollution aspects of the London fog of December 1952, Quarterly Journal of the Royal Meteorological Society, 80, 267-271, 1954.

Xie, S. D., Liu, Z., Chen, T., and Hua, L.: Spatiotemporal variations of ambient PM10 source contributions in Beijing in 2004 using positive matrix factorization, Atmos. Chem. Phys., 8, 2701-2716, 2008.

Zavala, M., Herndon, S. C., Wood, E. C., Onasch, T. B., Knighton, W. B., Marr, L. C., Kolb, C. E., and Molina, L. T.: Evaluation of mobile emissions contributions to Mexico City's emissions inventory using on-road and cross-road emission measurements and ambient data, Atmos. Chem. Phys., 9, 6305 - 6317, 10.5194/acp-9-6305-2009, 2009.

Zhang, Q., Stanier, C. O., Canagaratna, M. R., Jayne, J. T., Worsnop, D. R., Pandis, S. N., and Jimenez, J. L.: Insights into the chemistry of new particle formation and growth events in Pittsburgh based on aerosol mass spectrometry, Environ. Sci. Technol., 38, 4797-4809, 2004.

Zhang, Q., Alfarra, M. R., Worsnop, D. R., Allan, J. D., Coe, H., Canagaratna, M. R., and Jimenez, J. L.: Deconvolution and quantification of hydrocarbon-like and oxygenated organic aerosols based on aerosol mass spectrometry, Environ. Sci. Technol., 39, 4938-4952, 2005a.

Zhang, Q., Worsnop, D. R., Canagaratna, M. R., and Jimenez, J. L.: Hydrocarbon-like and oxygenated organic aerosols in Pittsburgh: insights into sources and processes of organic aerosols, Atmos. Chem. Phys., 5, 3289-3311, 2005b.

Zhang, Q., Jimenez, J. L., Canagaratna, M. R., Allan, J. D., Coe, H., Ulbrich, I., Alfarra, M. R., Takami, A., Middlebrook, A. M., Sun, Y. L., Dzepina, K., Dunlea, E., Docherty, K., DeCarlo, P. F., Salcedo, D., Onasch, T., Jayne, J. T., Miyoshi, T., Shimono, A., Hatakeyama, S., Takegawa, N., Kondo, Y., Schneider, J., Drewnick, F., Borrmann, S., Weimer, S., Demerjian, K., Williams, P., Bower, K., Bahreini, R., Cottrell, L., Griffin, R. J., Rautiainen, J., Sun, J. Y., Zhang, Y. M., and Worsnop, D. R.: Ubiquity and dominance of oxygenated species in organic aerosols in

anthropogenically-influenced Northern Hemisphere midlatitudes, Geophys. Res. Lett., 34, L13801, 2007.

Zhao, Y., Hu, M., Slanina, S., and Zhang, Y.: Chemical compositions of fine particulate organic matter emitted from Chinese cooking, Environ. Sci. Technol., 41, 99-105, 2006.

8

LIST OF TABLES AND FIGURES

ACKNOWLEDGEMENTS

The present thesis could not have been done without the support of many people to whom I'm deeply indebted.

First of all I would like to thank my doctor father, Prof. Urs Baltensperger, for providing the framework for this thesis with the inspiring research atmosphere of the LAC, and for his continuous support and overview. It would have been difficult to stay on track without his clear and focused advice.

Dr. André Prévôt is greatly thanked for his support and enthusiasm which never failed to motivate me. His advice led me from being an intern at PSI to a master thesis in Boulder, Colorado, and back to PSI for my PhD, experiences I'm very grateful for.

Prof. Ulrike Lohmann is thanked for her support of my work as my co-examiner and interesting discussions during IMBALANCE meetings. Thanks also go to Dr. Astrid Kiendler-Scharr for agreeing to act as my external co-examiner and entertaining discussions during AMS and EMEP/EUCAARI meeting dinners.

René Richter helped me with all the technical problems arising during my PhD. Without him, measuring, driving, and all the other things "academics'" are not so good at would have posed serious challenges. Merci, René, for all your patience and amicability! It was lots of fun to drive through the centers and suburbs of Zurich, Paris and Barcelona with you.

The friendly atmosphere at the LAC created by many wonderful colleagues makes it a nice place to work, thanks to all of you! Silke, it's actually your fault that I ventured into this PhD – my time as your "research assistant" was just too much fun! Thank you for your continuous support. Val, Nolwenn, Lisa and all the various crew members of OFLB/002 and OFLB/009 – a common office, many common meals and even more common fits of laughter greatly helped in pursuing this research. My thanks also go to Günther for his help for whatever problem and Bettina for the endurance of annoying computer questions, fun playing basketball in Berlin and organizing nice hikes. Thanks to Jay for reading whatever had to be correct English and scientifically sound.

Special thanks go to Maarten – those 4 years sharing an office, an instrument, stressful moments, ~2000 coffee breaks and quite a few jokes were a lot of fun!

The continuous effort and help of the AMS community, be it emergency help during campaigns, enlightening discussions or new software is greatly acknowledged. Especially the help and advice of Pete DeCarlo had a big influence on the quality of this work.

Last but not least I would like to thank my family and my friends. Your continuous support and encouragement kept me going and helped shifting the work-life balance when needed. Last but not least, my dearest thanks go to Matt: You've probably become an aerosol expert as well in those years from hearing all my talks and reading all my texts. Thank you for being my companion in good and in bad times.

CURRICULUM VITAE

Claudia Mohr, born on 21 April 1982 in Bern, Switzerland

Education and professional experience

Nov. 2007 –	PhD student at the Paul Scherrer Institut in Villigen (employer) and at the Institute for Atmospheric and Climate Science, ETH Zurich
	Supervisor: Prof. Dr. Urs Baltensperger
	Thesis topic: Source apportionment of ambient submicron aerosol using stationary and mobile aerosol mass spectrometer data
Oct. 2002 – Oct 2007	M.S. in Environmental Sciences, ETH Zurich
	Master Thesis (research conducted at University of Colorado at Boulder, Dept. of Chemistry and Biochemistry & CIRES): Analysis of primary organic emissions from meat cooking, trash burning, mobile sources, and biomass burning with high-resolution aerosol mass spectrometry
April – May 2006	Undergraduate Research Assistant, Forschungszentrum Karlsruhe in der Helmholtzgesellschaft, Institut für Meteorologie und Klimaforschung, Atmosphärische Umweltforschung, Karlsruhe, Germany

Formaldehyde measurements during the MILAGRO/MIRAGE-MEX field campaign in Mexico City, Mexico

Nov. 2005 – March 2006   Undergraduate Research Assistant, Paul Scherrer Institut, Laboratory of Atmospheric Chemistry, Villigen

Peer reviewed journal publications

Mohr, C., Richter, R., DeCarlo, P. F., Prévôt, A. S. H., and Baltensperger, U.: Spatial variation of chemical composition and sources of submicron aerosol in Zurich during wintertime using mobile aerosol mass spectrometer data, Atmos. Chem. Phys., 11, 7465-7482, 2011.

Mohr, C., Huffman, J. A., Cubison, M. J., Aiken, A. C., Docherty, K. S., Kimmel, J. R., Ulbrich, I. M., Hannigan, M., and Jimenez, J. L.: Characterization of primary organic aerosol emissions from meat cooking, trash burning, and motor vehicles with high-resolution aerosol mass spectrometry and comparison with ambient and chamber observations, Environ. Sci. Technol., 43, 2443-2449, 2009.

Richard, A., Gianini, M. F. D., **Mohr, C.**, Furger, M., Bukowiecki, N., Minguillón, M. C., Lienemann, P., Flechsig, U., Appel, K., DeCarlo, P. F., Heringa, M. F., Chirico, R., Baltensperger, U., and Prévôt, A. S. H.: Source apportionment of size and time resolved trace elements and organic aerosols from an urban courtyard site in Switzerland, Atmos. Chem. Phys., 11, 8945-8963, doi:10.5194/acp-11-8945-2011, 2011.

Reche, C., Viana, M., Moreno, T., Querol, X., Alastuey, A., Pey, J., Pandolfi, M., Prévôt, A., **Mohr, C.**, Richard, A., Artiñano, B., Gomez-Moreno, F. J., and Cots, N.: Peculiarities in atmospheric particle number and size-resolved speciation in an urban area in the western Mediterranean: Results from the DAURE campaign, Atmos. Environ., 45, 5282-5293, 2011.

Hildebrandt, L., Engelhart, G. J., **Mohr, C.**, Kostenidou, E., Lanz, V. A., Bougiatioti, A., DeCarlo, P. F., Prevot, A. S. H., Baltensperger, U., Mihalopoulos, N., Donahue, N. M., and Pandis, S. N.: Aged organic aerosol in the Eastern Mediterranean: the Finokalia Aerosol Measurement Experiment-2008, Atmos. Chem. Phys., 10, 4167-4186, doi 10.5194/acp-10-4167-2010, 2010.

Lanz, V. A., Prevot, A. S. H., Alfarra, M. R., Weimer, S., **Mohr, C.**, DeCarlo, P. F., Gianini, M. F. D., Hueglin, C., Schneider, J., Favez, O., D'Anna, B., George, C., and Baltensperger, U.: Characterization of aerosol chemical composition with aerosol mass spectrometry in Central Europe: an overview, Atmos. Chem. Phys., 10, 10453-10471, 2010.

Lee, B. H., Kostenidou, E., Hildebrandt, L., Riipinen, I., Engelhart, G. J., **Mohr, C.**, DeCarlo, P. F., Mihalopoulos, N., Prevot, A. S. H., Baltensperger, U., and Pandis, S. N.: Measurement of the ambient organic aerosol volatility distribution: application during the Finokalia Aerosol Measurement Experiment (FAME-2008), Atmos. Chem. Phys., 10, 12149-12160, 2010.

Pikridas, M., Bougiatioti, A., Hildebrandt, L., Engelhart, G. J., Kostenidou, E., **Mohr, C.**, Prevot, A. S. H., Kouvarakis, G., Zarmpas, P., Burkhart, J. F., Lee, B. H., Psichoudaki, M., Mihalopoulos, N., Pilinis, C., Stohl, A., Baltensperger, U., Kulmala, M., and Pandis, S. N.: The Finokalia Aerosol Measurement Experiment-2008 (FAME-08): an overview, Atmos. Chem. Phys., 10, 6793-6806, 2010.

Jimenez, J. L., Huffman, J. A., Docherty, K. S., **Mohr, C.**, Cubison, M. J., Ulbrich, I. M., Ziemann, P. J., and Onasch, T. B.: Chemically-resolved volatility measurements of organic aerosol from different sources, Environ. Sci. Technol., 43, 5351-5357, 2009.

Weimer, S., **Mohr, C.**, Richter, R., Keller, J., Mohr, M., Prévôt, A. S. H., and Baltensperger, U.: Mobile measurements of aerosol number and volume size distributions in an Alpine valley: Influence of traffic versus wood burning, Atmos. Environ., 43, 624-630, 2009.

Aiken, A. C., DeCarlo, P. F., Kroll, J. H., Worsnop, D. R., Huffman, J. A., Docherty, K. S., Ulbrich, I. M., **Mohr, C.**, Kimmel, J. R., Sueper, D., Sun, Y., Zhang, Q., Trimborn, A., Northway, M., Ziemann, P. J., Canagaratna, M. R., Onasch, T. B., Alfarra, M. R., Prevot, A. S. H., Dommen, J., Duplissy, J., Metzger, A., Baltensperger, U., and Jimenez, J. L.: O/C and OM/OC ratios of primary, secondary, and ambient organic aerosols with high-resolution time-of-flight aerosol mass spectrometry, Environ. Sci. Technol., 42, 4478-4485, doi 10.1021/Es703009q, 2008.

Bronnimann, S., Annis, J., Dann, W., Ewen, T., Grant, A. N., Griesser, T., Krahenmann, S., **Mohr, C.**, Scherer, M., and Vogler, C.: A guide for digitising manuscript climate data, Climate of the Past, 2, 137-144, 2006.

Articles under review

Mohr, C., DeCarlo, P. F., Heringa, M. F., Chirico, R., Slowik, J. G., Richter, R., Reche, C., Alastuey, A., Querol, X., Seco, R., Peñuelas, J., Jiménez, J. L., Crippa, M., Zimmermann, R., Baltensperger, U., and Prévôt, A. S. H.: Identification and quantification of organic aerosol from cooking and other sources in Barcelona using aerosol mass spectrometer data, Atmos. Chem. Phys. Discuss., 11, 27383-27420, doi:10.5194/acpd-11-27383-2011, 2011.

Knote, C., Brunner, D., Vogel, H., Allan, J., Asmi, A., Äijälä, M., Carbone, S., van der Gon, H. D., Jimenez, J. L., Kiendler-Scharr, A., **Mohr, C.**, Poulain, L., Prévôt, A. S. H., Swietlicki, E., and Vogel, B.: Towards an online-coupled chemistry-climate model: evaluation of COSMO-ART, Geosci. Model Dev. Discuss., 4, 1809-1874, doi:10.5194/gmdd-4-1809-2011, 2011.

Minguillón, M. C., Perron, N., Querol, X., Szidat, S., Fahrni, S., Alastuey, A., Jimenez, J. L., **Mohr, C.**, Ortega, A., Day, D. A., Lanz, V. A., Wacker, L., Reche, C., Cusack, M., Amato, F., Kiss, G., Hoffer, A., Decesari, S., Moretti, F., Hillamo, R., Teinilä, K., Seco, R., Peñuelas, J., Metzger, A., Schallhart, S., Müller, M., Hansel, A., Burkhart, J., Baltensperger, U., and Prevot, A. S. H.: Fossil versus contemporary sources of fine elemental and organic carbonaceous particulate matter during the DAURE campaign in Northeast Spain, Atmos. Chem. Phys. Discuss., 11, 23573 - 23618, 10.5194/acpd-11-23573-2011, 2011.

Articles in preparation

Mohr, C., DeCarlo, P. F., Heringa, M. F., Chirico, R., Richter, R., Crippa, M., Prévôt, A. S. H., and Baltensperger, U.: Spatial variation of organic aerosol components identified by positive matrix factorization in the Barcelona region, in prep., 2011.

Heringa, M. F., DeCarlo, P., Chirico, R., Tritscher, T., Clairotte, M., **Mohr, C.**, Crippa, M., Slowik, J. G., Dommen, J., Weingartner, E., Prévôt, A., and Baltensperger, U.: A new method to discriminate secondary organic aerosols from different sources using high-resolution aerosol mass spectra, in prep., 2011.

Reche, C., Viana , M., Amato, F., Querol, X., Moreno, T., Minguillón, M. C., Alastuey, A., Hillamo, R., Teinilä, K., Saarnio, K., Seco, R., and **Mohr, C.**: Biomass burning contributions to urban aerosols in a coastal Mediterranean city, in prep., 2011.

Nemitz, E., Prevot, A. S. H., Äijälä, M., Allan, J. D., Berresheim, H., Carbone, S., Canagaratna, M. R., Capes, G., Ceburnis, D., Choularton, T., Coe, H., Cubison, M. J., Dall'Osto, M., Di Marco, C.

F., DeCarlo, P. F., Ehn, M., Eriksson, A., Freney, E., Herrmann, H., Jimenez, J. L., Hildebrandt, L., Juninen, H., Kiendler-Scharr, A., Laaksonen, A., Lanz, V. A., McFiggans, G., Mensah, A., Mentel, T. F., **Mohr, C.**, O'Dowd, C., Ortega, A., Ovadnevaite, J., Pagels, J., Pandis, S. N., Phillips, G. J., Poulain, L., Raatikainen, T., Saarikoski, S., Sellegri, K., Spindler, G., Sueper, D., Swietlicki, E., Tiitta, P., and Worsnop, D. R.: European submicron aerosol chemical composition derived from a campaign-based Aerosol Mass Spectrometer network, in prep., 2011.

Crippa, M., DeCarlo, P. F., **Mohr, C.**, Heringa, M. F., Chirico, R., Slowik, J. G., Poulain, L., Wiedensohler, A., Freutel, F., Drewnick, F., Schneider, J., Di Marco, C. F., Nemitz, E., Zimmermann, R., Elsässer, M., Prévôt, A. S. H., and Baltensperger, U.: Wintertime aerosols chemical composition and source apportionment in the metropolitan area of Paris, in prep., 2011.

Pandolfi, M., Querol, X., Alastuey, A., Jimenez, J. L., Cusack, M., Reche, C., Pey, J., **Mohr, C.**, DeCarlo, P. F., Ortega, A., Day, D., Prevot, A. S. H., Baltensperger, U., Artiñano, B., Baldasano, J. M., Jorba, O., Burkhart, J., Hansel, A., Schallhart, S., Müller, M., Metzger, M., Saarikoski, S., Cubison, M. J., Ng, S., Lorente, J., Nemitz, E., Di Marco, C., Peñuelas, J., Sicard, M., Comeron, A., Amato, F., Moreno, T., Viana , M., Pérez, N., Moreno, N., Seco, R., Filella, I., Llusià, J., Piot, M., and Pay, M. T.: Sources and origin of PM in the Western Mediterranean Basin: An overview of the DAURE campaign, in prep., 2011.